L-Proline metabolism and the regulation of embryonic stem cell differentiation and programming

by

Van Thi Tuong Nguyen

BBiotech (Honours)

Submitted in fulfilment of the requirements for the degree of

Doctor of Philosophy

Menzies Institute for Medical Research

College of Health and Medicine

University of Tasmania

February 2019

Declaration by Author

I, Van Thi Tuong Nguyen, declare that this thesis is comprised of my original work, and to the best of my knowledge, no material contained herein has been previously submitted or accepted for a degree or qualification by the University or any other institution. All experimental work contributed by other researchers has been clearly stated and acknowledged within the text or list of contributions.

Date 18th February 2019

Van Thi Tuong Nguyen

Authority of access

This thesis may be made available for loan. Copying and communication of any part of this thesis is prohibited for one year from the date this statement was signed; after that time limited copying and communication is permitted in accordance with the Copyright Act 1968.

Date 18th February 2019

Van Thi Tuong Nguyen

List of contributions

This thesis consists of the contributive works done by other researchers, which is acknowledged here.

Chapter 3: Pilot study

Mr Peter Lu (PhD candidate) performed image analysis using Cellprofiler software and provided the coding workflow that were then applied to the analysis of this pilot study.

Chapter 4

Mr Patrick Lennard (Honours student) conducted the flow cytometry experiments, which provided the data used in Figure 4.2.6 and 4.2.8.

Date 18th February 2019

Van Thi Tuong Nguyen

Acknowledgement

"No man is an island"

– John Donne –

My PhD has been an incredible life experience that I will forever appreciate. No amount of words would ever be enough to express my gratitude to the people who have provided the invaluable assistance and support when I most needed it and which enabled me to complete this journey.

I sincerely would like to send my many thanks:

First and foremost, to my supervisory team, for their great support and patience to guide me all the way.

To Professor Alex Hewitt, for his willingness to take me on and to make me a part of what was a motivated and innovative group, and for helping me to become more independent in my research.

To Dr Jac Charlesworth, for being super caring and supportive, and for her readiness to provide helpful advice and suggestions whenever I needed it.

To Associate Professor Joy Rathjen, for the guidance and mentoring she provided, and for her knowledge and passion for science, which has taught me so much of how to become a better scientist and how to better perform during research work.

To the funding bodies of the University of Tasmania and the Menzies Institute for Medical Research, for making this project possible and ultimately successful. I am the recipient of *2015 Merle Weaver Postgraduate Scholarship* that was generously gifted from the estate of the late Merle White Weaver and managed by Tasmanian Perpetual Trustees Limited.

To the wonderful administration and the HDR team of College of Health and Medicine, for their basic kindness and support to my candidature, especially to Mark Bennett, who encouraged me to take on this challenge, and I am very grateful that this has happened.

To the beautiful people of office 502, who made it a lovely family situation and which I felt I was a member of, for taking care of my ups and downs, for sharing all the laughter and for being by my side during the harder times.

To my old friend, Donald, for his kindness and the precious time he spent reading my thesis and helping me with my English, without his generous help, this thesis would have been a struggle.

To all the other PhD fellows, researchers and laboratory staffs in the MSP building, for the lovely chats and for generously sharing their vast knowledge and experience, and for offering assistance whenever I met with the many difficulties.

Last but not least, to my family and friends, who fully believed in my abilities and who fully respected my life choices always, for their silent sacrifices that they will never tell, and for always being by my side to strengthen my every step.

Date 18th February 2018

Van Thi Tuong Nguyen

Abstract

Objective: Proline metabolism has been implied in cancer, with changes found to support the growth and metastasis of cancer cells. Based on this, proline metabolism has been proposed as a safe and specific target for cancer therapy. However, the mechanisms by which proline metabolism alters cell programming is not well-characterised. It is not known about the role of proline metabolism in normal cell growth and how proline metabolism regulates cellular programs. Embryonic stem (ES) cell differentiation is a non-pathological cell system, in which proline metabolism was suggested to play a role. Studying proline metabolism in ES cell differentiation will provide useful information about the metabolic control of cell programming and will identify potential targets for future research in cancers.

Background: Proline metabolism is an important node of a complex metabolic network that connects mitochondrial and cytoplasmic activities. Proline metabolism involves multiple reactions that are divided into three steps: proline uptake, catabolism and biosynthesis. The key reaction is the oxidation of proline, which is performed inside the mitochondria by a single enzyme: proline dehydrogenase (PRODH). PRODH oxidises proline to form pyrroline-5-carboxylate (P5C) and reactive oxygen species (ROS) as a by-product. In mouse ES cells, the primary transporter of proline, Snat2, was found to be involved in proline-induced differentiation. The use of amino acids to compete with proline transport via Snat2 was effective to prevent the formation of differentiated cells, suggesting that proline uptake via Snat2 is essential. In addition, the use of Prodh inhibitors and the neutralisation of ROS by antioxidants resulted in a decreased number of proline-induced differentiated cells. This evidence suggests that Prodh activity and the formation of ROS are required for ES cell differentiation. Furthermore, ROS-activated proteins, such as p38-MAPK and Src, were reported to be involved in proline-induced differentiation of ES cells. However, it is currently not known what connects proline metabolism and ROS production with ES cell differentiation. As a result, the precise mechanism of proline-induced ES cell differentiation is unclear. Taken together, it is hypothesised that ROS derived from proline metabolism play a role in ES cell differentiation.

Aims and Methods: To test this hypothesis, two lines of mouse ES cells: D3 and WA30 were investigated in three experiments. The first experiment aimed to examine the expression of the proline metabolic enzyme family to confirm potential proline metabolic reactions. The expression of proline transporter, Snat2, is differentially regulated in two different pluripotent states of ES cells: naïve and primed states. It was questioned if the regulation of Snat2 would affect proline metabolism and proline-induced differentiation in these ES cell states. Thus, the expression of the proline metabolic enzyme family was examined in different pluripotent states of ES cells. In the second experiment, the level of mitochondrial ROS production was used as an indicator of proline oxidation. The changes in ROS levels was also detected in different time courses to investigate the dynamics of proline response in naïve and primed ES cells. The third experiment aimed to correlate ROS production with proline metabolism and ES cell differentiation to examine the precise mechanism of proline-induced differentiation.

Results: The data showed that proline metabolic enzyme family is differentially expressed in different pluripotent states of ES cells. It was also found that naïve and primed ES cells have different distribution of the proline metabolic enzymes. The measurement of mitochondrial ROS production revealed heterogeneous populations of ES cells that produced different ROS levels. Up-regulated expression of proline metabolic enzyme, Prodh, in primed ES cells resulted in increased ROS production in the addition of proline, which is correlated with proline-induced differentiation. However, these mitochondrial ROS were not primarily required for the differentiation process. Proline-induced ROS production may not necessarily be correlated with proline metabolism and the role of Prodh needs further clarification.

Discussion: This is the first study to examine proline metabolism in ES cells following their pluripotent lineage specification and differentiation. The data suggest a proline metabolic switch in ES cell programming and differentiation, which could be used to distinguish ES cells of different pluripotent states. These findings indicate that proline metabolism is an important factor in mitochondrial metabolic regulation, which has been previously demonstrated in ES cell programming. The investigation of ROS production has revealed that mitochondrial metabolism can be used to profile ES cells in different pluripotent states. Even though no firm conclusion can be made on the role of proline metabolism and Prodh in ES cell differentiation, the findings of this study indicate that other proline acceptor sites in the cellular environment should be considered for future investigation of proline-induced changes in ES cells. It is

suggested that a model of *Prodh* knock-out ES cell line can be useful to study the role of Prodh and proline metabolism in ES cell differentiation.

List of Abbreviations

AAR	Amino acid response
ATP	Adenosine triphosphate
DHP	3,4-dehydro-L-proline
DMSO	Dimethyl sulfoxide
DNMT3B	DNA methyltransferase 3B
EpiSC	Epiblast stem cell
EPL	Early primitive ectoderm-like
ERK1/2	Extracellular signal-regulated kinase-1 and 2
ES	Embryonic stem
FAD	Flavin adenine dinucleotide
GSA	Gama-glutamate semialdehyde
GSH	Glutathione
GSK3	Glycogen synthase kinase 3
hESC	Human embryonic stem cell
HIF-1α	hypoxic inducible factor 1 alpha
ICM	Inner cell mass
iPSC	Induced pluripotent stem cells
Leu	Leucine
LIF	Leukemia inhibitory factor
MEK	Mitogen-activated protein kinase kinase (A member of MAPK)
Met	Methionine
MMP	Mitochondrial membrane potential
mTOR	Mammalian (or mechanistic) target of rapamycin
mTORC1	Mammalian (or mechanistic) target of rapamycin complex 1
NAC	N-acetyl-L-cysteine
NAD	Nicotinamide adenine dinucleotide
OAT	Ornithine aminotransferase
Orn	Ornithine
OXPHOS	Oxidative phosphorylation
p38-MAPK	p38 mitogen-activated protein kinases
P4H	Prolyl 4-hydroxylases
P5C	Δ-pyrroline-5-carboxylate
P5CDH	P5C dehydrogenase
P5CR	P5C reductase
P5CS	P5C synthase
PCA	Principle component analysis
PHD	Hypoxia-inducible factor prolyl 4-hydroxylases
Pro	Proline
PRODH	Proline dehydrogenase
PSC	Pluripotent stem cell
ROS	Reactive oxygen species
SAH	S-adenosyl-homocysteine

SAM	S-adenosylmethionine
SLC	Solute carrier family
Snat2	Sodium-dependent neutral amino acid transporter-2
SOD	Superoxide dismutase
Src	Proto-oncogene tyrosine-protein kinase Src
STAT3	Signal transducer and activator of transcription 3
TCA	Tricarboxylic acid
THFA	L-tetrahydro-2-furoic acid
Thr	Threonine
Vit C	Vitamin C

Table of Contents

Appendix

List of Tables and Figures

Chapter 1 Introduction

1.1. Metabolism and the role in cell programming

1.1.1. Overview of cellular metabolism

Cell metabolism can be described as a chain of chemical reactions and transformations that occur within a cell and that are required for the maintenance of life. In higher eukaryote cells like mammals, metabolic pathways form a complex network to provide energy and building blocks that are needed for cell growth and development; moreover, recent discoveries have shown that metabolism is involved in most cellular processes, which covers almost every cell compartment and plays an important role in regulating cell behaviours (DeBerardinis and Thompson, 2012, Snaebjornsson and Schulze, 2018). There are a number of regulatory mechanisms that have been proposed to describe the crosstalk between metabolic activities and cell programming, which do suggest that metabolism plays a critical role in cell fate definition (DeBerardinis and Thompson, 2012). Research also proposes that the controlling of cell functions can occur at any stage along the metabolic pathway. In some circumstances, metabolic regulation is reported to take place when cells sense the presence of particular metabolites (Yuan et al., 2013) and a number of nutrient sensing mechanisms have also been identified, such as the AMPK (energy sensing), GLUT2 (glucose sensing) and mTOR (glucose and amino acid sensing) pathways (Efeyan et al., 2015). This indicates that metabolism is an effective way for cells to respond to environmental resources. Indeed, metabolism coordinates the cells and the exogenous environment, which supports the cells to cope with the changes in physiological conditions and nutrition availability (Metallo and Vander Heiden, 2013), and thus, cell programming and metabolic programming should be considered at the same time in biological investigation. The question of how different types of metabolism control cell fate has been well-established and there is a growing number of studies that are looking to better understand the metabolic control over cell programming, which has made metabolism an emerging topic of medical research in recent years.

1.1.2. Metabolism and cell programming

Metabolic regulation and cell programming are affected by changes in the microenvironment, the response to the new conditions can lead to metabolic modifications to prepare the cells for growth and function (Metallo and Vander Heiden, 2013). However, it is still undetermined as to which factors are first initiated in the relationship between

metabolic regulation and cell programming. In other words, the question of whether the cell modifications result in metabolic programming or metabolic programming precedes cell regulation is critical to determine what is actually being manipulated to alter the cell fate. This research will provide useful information for future attempts to control cell behaviours.

1.1.2.1. Non-canonical subcellular translocation of metabolic enzymes reveals non-metabolic functions

Metabolic enzymes are the key players in many cellular reactions. Spatial cellular arrangement of metabolic enzymes and metabolites in the cells have an important function in balancing the cell physiology and has been shown to be involved in the direct regulation of cell fate (van der Knaap and Verrijzer, 2016, Li et al., 2018). Apart from metabolic functions, metabolic enzymes are found to play an additional role in the regulation of different types of biological activity, which is their non-canonical function (Snaebjornsson and Schulze, 2018). In general, metabolic enzymes are required to localise into specific cell compartments to perform particular chemical reactions. For example, glycolytic enzymes are mostly located in the cytosol and TCA cycle enzymes are found in the mitochondria. When performing non-canonical functions, metabolic enzymes are known to reside into different cell compartments including the nuclei. The translocation into subcellular compartments allows metabolic enzymes to regulate cell cycle, apoptosis, epigenetic modifications, and gene expression, which results in alterations to cell growth, proliferation, and pathological progression (Huangyang and Simon, 2018). For instance, glycolytic enzyme phosphofructokinase (PFK) has been shown to localise into the nuclei and interact with transcriptional activators YAP/TAZ (Enzo et al., 2015). The protein glyceraldehyde 3-phosphate dehydrogenase (GAPDH) is reported to activate nuclear protein PARP1 (Nakajima et al., 2015). Cytosolic enzyme fumarase, which is known to translocate itself into the nuclei to perform DNA repair in cancer cells, is actually a metabolic enzyme of the TCA cycle and is responsible for the reversible catalysis of fumarate to malate (Jiang et al., 2015). The enzyme pyruvate kinase isozyme type 2 (PKM2), which is involved in glycolytic reactions, is known to interact with the transcription factor OCT-4 (also called POU5), being a key regulator of pluripotency, in the nuclei (Lee et al., 2008). Evidence shows that intracellular migration of cell compartments also plays a role in controlling cell growth and behaviours. For example, mitochondria have been shown to migrate to different sites within pluripotent stem cells during differentiation (Lees et al., 2017). Accordingly, this process is associated with mitochondrial rejuvenation and maturation

and is required for cellular homeostasis (Lees et al., 2017), thus, it is important to consider translocation and distribution of the metabolic enzymes in relation to the metabolic regulation of cell behaviours.

1.1.2.2. Nutrient sensing pathway and cell programming

The sensing of nutrient availability, both endogeneously and exogenously, is an example of metabolic regulation and has been described as a conservational mechanism throughout evolution (Chantranupong et al., 2015). There are specific metabolites, which activate cell programming by triggering the acceptor and transducer proteins. Furthermore, depending on the type of nutrients, nutrient sensors can be located either on the cell membrane or inside the cytosol. For example, in glucose sensing, the glucose transporter 2 (GLUT2) is located on the cell membrane to detect glucose availability in the microenvironment while the enzyme glucokinase (GCK) alternatively senses intracellular glucose levels (Thorens, 2015, Matschinsky, 1990). As these glucose sensors are contributative to the development of diseases such as diabetes, they have been put forward as potential targets for diabetic treatment (Matschinsky, 2002). Sensing amino acid availability can be performed by the activation of the proteins general control nonderepressible 2 (GCN2) kinase and mammalian (or mechanistic) target of rapamycin complex 1 (mTORC1) (Yuan et al., 2013). GCN2 senses amino acid availability during protein synthesis inside the cells. Any reduction in amino acid pool can lead to uncharged tRNAs and activate GCN2 to prevent initiation of the protein translation process and activate protein degradation to refill amino acid content (Efeyan et al., 2015).

mTOR is a pivotal pathway of nutrient sensing, which responds to both intracellular and exogenous amino acids, glucose and energy. mTOR is known to play an important role in cell growth and proliferation (Jewell and Guan, 2013), however, mTOR is not equally controlled by all amino acid availability. Amino acids such as leucine and arginine are shown to activate mTOR more vigorously than other amino acids (Hara et al., 1998). Only recently, glutamine and glutamine metabolism were found to play a role in regulating mTOR (van der Vos and Coffer, 2012, Nicklin et al., 2009, Jewell et al., 2015). The mTOR complex 1 (mTORC1) is not itself an amino acid sensor. Intracellular amino acids activate mTOR via the induction of the transducer proteins Rag and Rheb GTPases (Kim et al., 2008, Parmar and Tamanoi, 2010). There is evidence that growth factors and amino acids are both required to activate mTOR.

Additionaly, mTOR regulation of cell programming may involve different pathways (Jewell and Guan, 2013). While the actual sensors of the mTOR pathway remain unclear, the activation sites include the lysosomal surface and possibly the Golgi apparatus (Jewell and Guan, 2013, Goberdhan et al., 2016). It was also suggested that amino acid transporters such as members of the solute carrier family (SLC): SLC38A9, SLC38A2, SLC1A5 and SLC3A2 could transduce signals to activate mTOR via the transport of specific amino acids (Nicklin et al., 2009, Pinilla et al., 2011, Rebsamen et al., 2015). Upstream regulation of mTOR includes the roles of AMPK (AMP-activated protein kinase) or PI3K (class I phosphoinositide 3-kinase) (Dibble and Cantley, 2015, Jewell and Guan, 2013). AMPK senses energy and glucose availability, which is activated by increased intracellular AMP and ADP levels (Jewell and Guan, 2013). Downstream regulation of mTOR includes changes occured in the translation of mRNA via the suppression of initiation factor 4E-BP1 (4E-binding protein 1), S6K (S6 kinase) and other metabolic and biosynthetic effects (Dibble and Manning, 2013). In fact, GCN2 has been shown to inhibit mTOR pathway and this inhibition may be mediated by the deprivation of amino acids such as leucine and arginine (Rebsamen et al., 2015), suggesting that mTOR and other nutrient sensors may be important to the regulation of cell programming. In conclusion, it appears that nutrient sensing is comprised of complex systems of metabolic regulation, this suggests that the metabolic regulation of the cell fate is monitored at different levels and can occur as early as when the cells first acquire metabolites. Understanding the involvement of nutrient sensing is critical in controlling cell behaviours and this will fulfil the mechanism of metabolic regulation of the cell fate.

1.1.2.3. Metabolic profiles and cell fate determination

The changes in metabolic profiles have been reported to be involved in disease progression (DeBerardinis and Thompson, 2012). A number of studies have shown that at critical points of the decision making process, metabolic profiles play an important role in defining cell fate and determining the outcomes of the cell functions (Pavlova and Thompson, 2016, Dang, 2012, Galgani et al., 2015). In metabolic diseases such as diabetes, metabolic profiles and mitochondrial functions have been extensively discussed for their roles in the development of these diseases (Wollheim and Maechler, 2002, Kaufman et al., 2015). In high glucose condition or hyperglycaemia, pancreatic insulin-secreting cells, also known as β-cells, showed significant changes in gene expression and metabolic pathways that favoured glucose metabolism and glycogen synthesis, which eventually results in glycogen accumulation and

cell death fundamental of type 2 diabetes (Brereton et al., 2016). The metabolic effects on cell functions can also be observed in age-related diseases such as Alzheimer's disease. The role of glucose uptake has been discussed in the development of cognitive impairment associated with aging (Yin et al., 2016), example, the increased activity of PI3K/Akt and mTOR has been suggested to be important in the homeostasis process of amyloid β (Aβ) and tau, the two major proteins that are linked to neurodegeneration in aged people (C, 2013). The evidence shows that metabolic profiles, which take part in defining the pool of metabolites, are critical in the development of disease initiation. As such, cell metabolism has become a potentially important area for research on the pathway to new therapeutic treatments.

The metabolic control of cell fate has been targeted to direct immune cell programming of the immune system. During T cell differentiation, naïve $CD4^+$ T cells give rise to cell subsets with a specific immune function. It was shown that daughter T cells with higher glycolytic profile and mTOR activity are more likely to become effector cells, which respond quickly to immune stimuli (Michalek et al., 2011). On the other hand, enhanced lipid oxidation promotes differentiated T cells into regulatory T cells, which function to suppress other cells of the immune system (Michalek et al., 2011). Similarly, asymmetric division of $CD8^+$ T cells results in different subsets of high and low mTORC1 activities that are correlated with different metabolic profiles in these cells (Pollizzi et al., 2016). Accordingly, $CD8^+$ T cells with lower mTORC1 activity possess higher mitochondrial mass and lipid metabolism and are associated with long-lived characteristics (Pollizzi et al., 2016). Indeed, the understanding of metabolic profiles in immune cells does suggest several applications in which, manipulating metabolism could enhance and direct functions of the immune cells to defend cancers and reduce autoimmunity effects (Galgani et al., 2015, Sukumar et al., 2017, Pearce et al., 2009).

Alternatively, different cell types may utilise their metabolism differently to support the cell functions. An efficient use of metabolic regulation requires cells to have appropriate metabolic programs in different cell states, for instance, in cancers, the changes in metabolic profiles are required for cancer cells to adapt to high proliferation characteristic, and in many cases, to support the cells to escape the immune system (Cascone et al., 2018, Kerkar and Restifo, 2012). Cancer cells are found to possess the ability to perform glycolysis in the presence of oxygen, which is called the Warburg effect (Warburg, 1956). The main purpose of the Warburg effect is to support cancer cell growth in low nutrient and unstable conditions

by generating energy in a shorter time period compared to oxidative phosphorylation (OXPHOS) (Epstein et al., 2017, Liberti and Locasale, 2016). Cancer cells also acquire multiple metabolic programs and mitochondrial metabolism to progress during their development (Pavlova and Thompson, 2016, Dang, 2012). For instance, cancer cells are shown to have higher fatty acid oxidation (FAO) and the inhibition of FAO can result in the cell apoptosis (Samudio et al., 2010). To support the growth of cancer cells, myeloid derived suppressor cells (MDSC) are able to escape the immune system by depleting cysteine and limiting cysteine availability, which is required for T cell activation (Srivastava et al., 2010). Other metabolic elements have also been identified to contribute to the progression of disease (Sica et al., 2017, Pavlova and Thompson, 2016, Galluzzi et al., 2013). Glutamine addiction is a feature of many types of cancers and glutamine metabolism has been proposed as a potential therapeutic target (Wang et al., 2018). In fact, many metabolic elements are currently under development including preclinical trials (Samudio et al., 2010, Galluzzi et al., 2013, Pavlova and Thompson, 2016). However, the potential for targeting metabolism in diseases remains challenging due to the limitations in understanding the global effect of metabolic regulation on cell functions and development. The understanding of how metabolism is contributing to the control of cell physiology will enhance the potential to be able to perform cell fate control and manipulation that can be applied to pathological diseases.

1.1.3. Metabolic programming and pluripotent stem cell development

PSCs are highly proliferative cells which possess the ability to manifest into numerous cell types. Dynamic changes of PSCs during differentiation demonstrate the modifications that occur in cell functions and activities. Hence, PSC differentiation presents as a robust model for the study of the metabolic regulation on cell fate determination. PSC reprogramming or differentiation are acquired not only by metabolic modification but are associated with mitochondrial rejuvenation and specification (Lees et al., 2017, Suhr et al., 2010). Given mitochondria are the major sites of metabolism and metabolic homeostasis, the changes in mitochondrial activities and metabolism have been shown to be important to support PSC fate (Lees et al., 2017). Together with mitochondrial changes, the rewiring of basic metabolism such as glycolysis, oxidative phosphorylation and amino acid metabolism have been identified to play a critical role in the PSC reprograming and differentiation process.

1.1.3.1. Glycolysis is the preferred metabolism in pluripotent stem cells

Glycolysis and low oxygen consumption are known to be the preferred metabolism in PSCs such as human ES cells (hESCs), murine ES cells and iPSCs (Moussaieff et al., 2015, Folmes et al., 2011). Mice ES cells derived from day 4.5 embryo displayed a high rate of glycolysis with a high expression of glycolytic enzymes and increased glycolytic flux (Kondoh et al., 2007). In hESCs, the expression of protein hexokinase II (HKII) was found to significantly elevate when compared to their differentiated counterparts (Varum et al., 2011). As HKII is a glycolytic enzyme catalysing the first reaction in glycolysis, it is suggested that PSCs require high glycolysis. In addition, by measuring the rate of oxygen consumption and the extracellular acidification rate from lactate production, it is reported that human pluripotent cells predominantly use glycolysis for ATP production (Zhang et al., 2011a). In fact, ES cells still rely on glycolysis for ATP generation even when they are exposed to a high oxygen environment (Kondoh et al., 2007, Chung et al., 2007). To further support the idea that glycolysis is more favoured than oxidative phosphorylation (OXPHOS) in these cells, pyruvate dehydrogenase (PDH), the enzyme that promotes the TCA (tricarboxylic acid) cycle from OXPHOS-derived pyruvate, has been reported to be inactivated in human PSCs (Varum et al., 2011, Zhang et al., 2011a). This suggests that the selection of glycolysis over OXPHOS in PSCs is correlated to the maintenance of pluripotency.

In pluripotent reprograming, the preference for glycolysis in pluripotent cells is demonstrated by a metabolic switch from OXPHOS in somatic cells to glycolysis in iPSCs (Folmes et al., 2011). A study in mice iPSCs has found that glycolytic profiles were highly expressed about one week before pluripotent genes could be detected in iPSCs and a reduction in glucose content in the environment is associated with the inhibitory effect on the formation of iPSCs (Folmes et al., 2011). Increased glycolytic genes was also found to be associated with cell fate reprogramming, which is modulated by the hypoxic inducible factor 1 alpha (HIF-1α) (Prigione et al., 2014). Given that iPSCs generation from somatic cells involves nuclear reprograming (Takahashi and Yamanaka, 2006), the metabolic switch from OXPHOS to glycolysis was found to have a role in increasing reprograming efficiency to drive the cells towards pluripotency (Folmes et al., 2011). Since ES cells and iPSCs possess high proliferation, glycolysis is a preferred metabolism in PSCs. This can be explained by the fact that glycolysis provides energy and building blocks rapidly, which supports biosynthesis for self-renewal and proliferation (Varum et al., 2011, Zhang et al., 2011a, Kondoh et al., 2007). Furthermore,

OXPHOS is prevented in these cells as it produces increased amounts of the by-product reactive oxygen species (ROS), causing damage to the PSC genetic integrity and also affecting the cell survival (Ito and Suda, 2014). It has been shown that the induction of hiPSCs is followed by a change in defences against ROS, similarly to what is observed in hESCs (Armstrong et al., 2010). A decrease in mitochondrial numbers and the increased expression of ROS defencive genes are associated with OXPHOS repression to provide the cells with protection from oxidative stress (Armstrong et al., 2010). More studies are required to fully understand the roles of the glycolytic switch and its metabolites in PSC differentiation and reprogramming.

Glycolysis preference in PSCs is supported by mitochondrial infrastructure, which reduces oxidative reactions by restricting the number of mitochondria (Varum et al., 2011, Zhang et al., 2011a, Armstrong et al., 2010). PSCs such as hESCs and murine ES cells possess a low number of spherical and immature mitochondria, which are arranged around the nuclei and are characterised with low membrane potential and undeveloped inner membrane cristae (Cho et al., 2006b, Chung et al., 2010). These features favour anaerobic glycolysis in ES cells by preventing other substrates that are metabolised by oxidation from entering the mitochondria, thus, the cells are protected from damaging oxidative stress (Zhang et al., 2011a, Chung et al., 2010, Cho et al., 2006b). In human PSCs, mitochondrial membrane potential is maintained through the hydrolytic process of glycolytic ATP, which is performed by the enzyme ATP hydrolase, to support the cell proliferation and viability (Zhang et al., 2011a). The changes in mitochondrial infrastructure are correlated with the entrance permission to particular substrates, which results in different mitochondrial metabolism that is correlated with different cell functions. Modifications in mitochondrial features and their location in the cells were reported to be important in cardiogenesis of ES cells (Chung et al., 2008). Perhaps, in PSC differentiation, mitochondrial features and functions appear to be correlated and more investigation is required to explore this aspect of PSC biology.

1.1.3.2. Amino acid metabolism in pluripotent stem cells

Amino acid metabolism has been shown to be an important aspect in PSC programming and functions and even though PSCs possess low amino acid metabolism, it in fact resembles pluripotent cells of the embryos (Beckman et al., 1990, Schultz et al., 1981, Meissen et al., 2012, Beckman et al., 1991). Oocytes and embryonic cells in the pre-

implantation period are adapted to the low nutrient availability of the embryonic environment and are shown to have limited amino acid metabolism compared to somatic cells (Schultz et al., 1981, Meissen et al., 2012). This characteristic is carried over into *in vitro* environment and somatic cells reduce amino acid metabolism when reprogramed to PSCs (Meissen et al., 2012). Studies on embryonic amino acid pools suggest that limited amino acid metabolism is responsible for the maintenance and development of the embryos and the transportation of amino acids may function as a regulator for successful implantation (Van Winkle and Dickinson, 1995), however, the mechanism of amino acid metabolism in embryonic development is still under investigation.

In *in vitro* studies, amino acid metabolism is responsible for PSC cell maintenance and differentiation, the mechanism of which highlighted the involvement of the generation of specific metabolites. For instance, threonine (Thr) metabolism has been shown to be important for ES cells to effectively regulate the proliferation and differentiation (Wang et al., 2009). Threonine is oxidised by the enzyme threonine dehydrogenase (TDH) in the mitochondria to produce two elements, glycine and acetyl-CoA (Wang et al., 2009). TDH expression in ES cells was found to be about 1000-fold higher than which that was observed in the differentiated cells and the deprivation of threonine in the medium inhibits ES cell growth (check context) (Wang et al., 2009). An analogue of threonine, 3-hydroxynorvaline, can give rise to glycine and propionyl-CoA similarly to threonine oxidation but it is insufficient to maintain ES cell growth (Wang et al., 2009). The supplement of glycine itself was inefficient in rescuing the cells. The findings showed that among the two elements of threonine metabolism, only TDH-mediated acetyl-CoA has a role in ES cell maintenance (Wang et al., 2009). This selective metabolite appears to be a common regulatory mechanism in ES cells and similar effect of threonine metabolism has also been observed *in vivo,* suggesting that threonine is a critical element for early embryonic development in mice (Wang et al., 2009).

Metabolic products from methionine (Met) metabolism are required to trigger differentiation of human PSCs (Shiraki et al., 2014). S-adenosylmethionine (SAM) is an important metabolite generated directly from methionine catabolism by the methionine adenosyltransferase (MAT). MAT converts methionine and ATP into SAM (Finkelstein, 1990). It is reported that undifferentiated cells show a higher Met metabolic rate than their differentiated counterparts and deprivation of Met results in rapid loss of intracellular SAM

and decreased methionine metabolism enzymes, including DNA methyltransferase 3B (DNMT3B) (Shiraki et al., 2014). Decreased SAM levels in methionine depletion can result in reduced proliferation, G0/G1 phase arrested in cell cycle and will eventually result in apoptosis if depletion prolongs (Shiraki et al., 2014). Treatment with SAM was shown to be effective to rescue Met deprivation, suggesting that SAM is an essential regulator of ES cell self-renewal and survival. In addition, SAM is also a product of threonine metabolism acting as a methyl donating molecule for transmethylation reaction (Shiraki et al., 2014). This process converts SAM to S-adenosyl-homocysteine (SAH) (Shyh-Chang et al., 2013), which is shown to inhibit the transmethylation reaction catalysed by methyltransferase enzymes such as DNA methyltransferases (DMNTs) (Shyh-Chang et al., 2013).

Another example of amino acid metabolism-induced differentiation is L-proline metabolism, which was shown to promote ES cell differentiation (Washington et al., 2010). In the addition of exogeneous L-proline, ES cells change morphology, gene expression, and the ability to form chimeras *in vivo* (Washington et al., 2010, Rathjen et al., 1999). Recently, a study has shown that L-proline addition leads to remodelling of ES cell transcriptome and epigenetic modification at H3K26me2 and K3K9me3, which marks a distinguished pluripotent state (Comes et al., 2013). Even though the precise mechanism of L-proline activity in ES cell differentiation has not been explored, it has been suggested to involve the process of metabolism and metabolic enzymes (Comes et al., 2013). Further investigation is ongoing to understand how L-proline metabolism influence the nuclei to perform ES cell programming.

1.1.4. The crosstalk between metabolism and nuclear programming in pluripotent stem cells

1.1.4.1. Metabolic products and epigenetic regulation in pluripotent stem cells

The generation of metabolites from PSC metabolism has been shown to be associated with the changes in the epigenetic landscape during the differentiation and reprogramming steps (Figure 1.1.4). For example, the synthesis of SAM from glycine and acetyle-CoA has been reported to create a link to epigenetic modifications in mice ES cells through the histone methylation process (Shyh-Chang et al., 2013). A reduction in threonine content in the culture medium resulted in an 80% reduction of glycine pool in the ES cell intracellular environment and caused a significant decrease in SAM/SAH ratio in the cells (Shyh-Chang et al., 2013). Consequently, a reduction in SAM/SAH ratio results in the loss of histone H3 lysine 4 tri-

(H3K4me3) and di-methylation (H3K4me2) (Shyh-Chang et al., 2013). Similar results were observed in methionine metabolism, which produces SAM/SAH for epigenetic modifications in hES cells and supports the cell maintenance (Shiraki et al., 2014). However, H3 methylation when induced by SAM/SAH has not been found on other lysine residues except for lysine 4 (K4), suggesting that SAM/SAH may have a specific site of reaction, in other words, histone methylation in ES cells may be controlled by a network of multiple epigenetic regulators.

In mammalian cells, epigenetics can be regulated by different metabolic elements and is specific to different types of metabolites. For instance, the enzyme lysine-specific demethylase 1 (LSD1 or KDM1a) was found to be specific for mono- and di-methylated H3K4 and H3K9 in demethylation. LSD1 protein contains a flavin-site, where it binds to flavin adenine dinucleotide (FAD) (Shi et al., 2004, Forneris et al., 2005). FAD is required for LSD1 to target methylated histone, the reaction of which, requires the reduction of FAD to FADH2 and then the reoxidisation of FADH2 to produce formaldehyde and hydrogen peroxide H_2O_2 (Forneris et al., 2005). During H3 histone demethylation, the regulation of trimethylation at K9, K27 and K36 is proven to be associated with the production of α-ketoglutarate (αKG), which is important to the maintenance of ES cell pluripotency (Carey et al., 2015). αKG is an intermediate product of glucose and glutamine metabolism in fuelling the TCA cycle. The depletion of glutamine results in reduced histone monomethylation and increased trimethylation on H3K9, H3K27, H3K36 and H4K20 in ES cells (Carey et al., 2015). The supplementation of αKG could only reverse H3K27me3 and H4K20me3, suggesting that only glutamine-dependent αKG is sufficient to promote these changes (Carey et al., 2015). Furthermore, αKG is directly fed to TCA cycle for energenesis. In the TCA cycle, the conversion of αKG to succinate has been shown to regulate αKG-dependent dioxygenase family to induce demethylation (Kaelin, 2011). As these enzymes comprise of the Jumonji C (JmjC) domain of histone demethylases and Tet DNA demethylases family, the demethylation activity of these enzymes is then correlated to αKG production (Tsukada et al., 2006, Yang et al., 2014). At least ten translocation DNA methylation sites are Tet dependent and are regulated by αKG/succinate ratio (Carey et al., 2015).

Similar to methylation, the acetylation process is subjected to metabolic regulation. Research has successfully indicated the links between acetylation and glucose metabolism in mice ES cells. Acetyl-CoA derived from citrate of glycolysis can serve as substrates for

acetylation of H3K4/K27, resulting in delayed early differentiation of ES cells (Moussaieff et al., 2015). This evidence suggests that glycolysis not only provides energy and building blocks for proliferation, it can also promote epigenetic modifications in differentiation. Histone deacetylation occurs when the acetyl group is removed from the histone residues by histone deacetylases (HDAC) and histone acetyltransferases (HAT) (Gong and Miller, 2013). Sirtuins (SIRTs) are a class of histone deacetylases that can convert the acetyl group and NAD+ to acetyl containing ribose during histone deacetylation (Ryall, 2012). As SIRTs require NAD+ and their activity affects the NAD+/NADH reduction/oxidation, SIRTs are often linked to redox sensing pathways (Canto et al., 2015). This relationship has been highlighted in a recent study that the reduction of NAD+ from increased glycolytic activity promotes SIRT1 mediated deacetylation on histone H4K16 (Ryall et al., 2015). Since PSCs possess high glycolytic profiles, there is possibly a link between glycolysis, the TCA cycle, redox status and SIRTs activity in the regulation of epigenetics. This reveals that changes in metabolite pools can lead to modifications in PSC gene regulation, indeed, selective metabolic components are associated with a typical cellular change via specific epigenetic modifications. This may suggest that the metabolic regulation network, while complexed, its specificity works toward increasing the efficiency in controlling PSC fate.

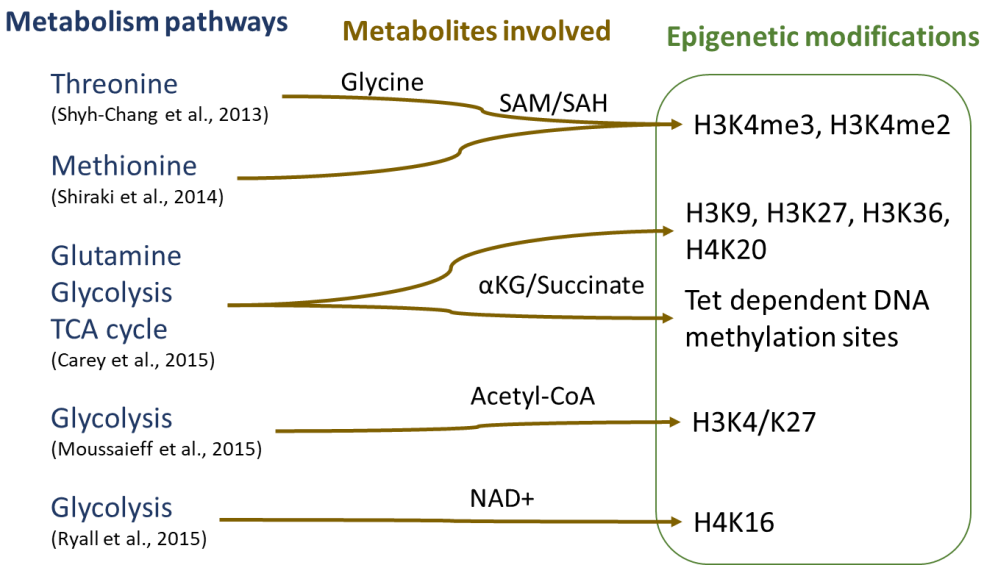

Figure 1.1.1. Metabolism and specificity in epigenetic modifications.

A number of metabolic pathways have been shown to generate specific metabolites that are involved in the regulation of epigenetic landscape in ES cells, which in turn, regulates the cell fate determination. SAM: S-adenosylmethionine, SAH: S-adenosyl-homocysteine, TCA: tricarboxylic acid, αKG: α-ketoglutarate, NAD: Nicotinamide adenine dinucleotide.

1.1.4.2. Metabolic regulation of redox homeostasis in pluripotent stem cells

Redox homeostasis plays an important role in maintaining cell growth and functions (Holmstrom and Finkel, 2014). Metabolism is the major source of redox molecules, which provides a variety of different redox potent substances such as nicotinamide adenine dinucleotide (NAD^+) coenzyme derivatives, reactive oxygen species (ROS), flavin adenine dinucleotide (FAD^+) cofactor family and multiple antioxidants (Forman et al., 2014). Redox molecules are mediated by specific regulatory enzymes and factors that involve NADPH oxidases (NOXs), forkhead box O (FoxO) proteins and hypoxic inducible factors (HIFs) (Yeo et al., 2013, Murray et al., 2013, Zou et al., 2007). The interaction between redox regulators and redox molecules forms a controlled network to guarantee the optimal cell function.

PSCs are characterised by the ability to infinitely self-renew and proliferate *in vitro*. Changes in redox status of the cells can induce the cells to leave the undifferentiated state to enter differentiation (Sart et al., 2015). ROS is the dominant redox molecule in PSC biology. ROS family includes superoxide anion (O_2^-), hydrogen peroxide (H_2O_2) and hydroxyl radical (HO^-) (Nordberg and Arner, 2001). The major intracellular sources of ROS are result from the mitochondrial respiration and metabolisms (Holmstrom and Finkel, 2014). Mitochondria are thought to produce the most amount of ROS among ROS sources, mainly from ATP production through the electron transport chain (Murphy, 2009). Superoxide anion O_2^- is formed by the addition of an electron to oxygen molecules, which often takes place in an electron rich aerobic environment such as the respiratory chain on the inner mitochondrial membrane, or through the oxidation process of the mitochondrial enzymes such as flavoenzymes and lipoxygenase (Nordberg and Arner, 2001). O_2^- anions are unable to cross lipid membranes and thus are compartmentalised to where it is produced (Nordberg and Arner, 2001). Superoxide O_2^- anions can also be produced by NADPH-dependent oxidase (NOXs), which consumes NADPH to generate O_2^-, and subsequently, H_2O_2, with the additional activity of superoxide dismutases (SODs) (Fridovich, 1997). Hydrogen peroxide H_2O_2 is not a free radical, however, its long half-life and the ability to penetrate lipid membrane make it the main ROS species in intracellular signalling (Holmstrom and Finkel, 2014). H_2O_2 can react with metal ions in protein complex to form hydroxyl radical HO^- and increase ROS levels inside the cells (Nordberg and Arner, 2001). In response to the increased levels of H_2O_2, which may cause damage to the DNA integrity, the cells upregulate the expression of antioxidant enzymes such as catalyse, glutathione (GSH) peroxidase and peroxiredoxins to inhibit H_2O_2 activities (Chae et al., 1999b,

Chae et al., 1999a). The differentiation of ES cells to vascular smooth muscle cells has been shown to be specifically mediated by H_2O_2 generated from NADPH oxidase 4 (Nox4) activity and it was suggested that different sources of ROS might correlate with a specific differentiation program (Xiao et al., 2009). Thus, ROS is an important metabolic player in the redox system of PSC biology. To compensate with the increase in oxidative stress that occurs during the differentiation process PSCs can regulate the mitochondria and the stress pathways to minimise the damage to the cells (Prigione et al., 2010). Reducing agents are involved in this fine modulation process of redox balance. Glutathione (GSH) and ascorbic acid are two strong reducing agents that have been shown to respond to differentiation (Yanes et al., 2010). GSSG is an oxidised form of GSH and a decrease in GSH/GSSG ratio has been shown to be associated with ES cell differentiation, which is accompanied by an increase in ascorbic acid levels (Yanes et al., 2010). This suggests that ES cells have a well-regulated redox system to safeguard them during the differentiation process.

The activities of redox enzymes and the transcription factors are reported to autoregulate homeostasis in stem cells as they adapt to oxidative stress, which indirectly regulates stem cell function. For example, the enzyme thioredoxin can dissociate and prevent the effect of Cys oxidation and restore the DNA binding activity of Oct4 to maintain ES cell self-renewal (Guo et al., 2004). In the case of the forkhead box O (FoxO) family, which is a transcription factor family, they can respond to oxidative stress as part of their functions (Brunet et al., 2004, Storz, 2011). FoxO targeted genes include those that are involved in ROS detoxification such as SOD2 and catalase, which act to neutralise intracellular ROS (Storz, 2011). In turn, FoxO proteins are triggered by the AMP kinase and suppressed by the PI3K signalling pathways, which are upstream of mTOR (Tothova and Gilliland, 2007). FoxO1 has a role in ES cell maintenance and self-renewal and when absent can result in the downregulation of Oct4, Nanog and Sox2, known as key factors of pluripotency (Zhang et al., 2011b). In addition, FoxO3 can coordinate the metabolism pathways of glutamine and glucose by directly activating the expression of metabolic enzymes to maintain the proliferation potential of neural stem cells (Yeo et al., 2013). This may be the mechanism that explains why FoxO3-/- neural stem cells have been reported to exhibit decreased self-renewal and the loss in the ability to differentiate to neural lineages (Renault et al., 2009).

Redox regulation can be extended to regulating the master transcription factors such as p53 and Nanog in ES cells (Han et al., 2008). Accordingly, the production of ROS activates p53 translocation into the mitochondria under the modulation of Sirt1. Based on this, the absence of Sirt1 led to ROS-induced p53 translocation into the nucleus to suppress the expression of *Nanog* (Han et al., 2008). As a result, ROS supports ES cell differentiation due to the reduction in *Nanog* expression, a key pluripotent gene in ES cell maintenance. Indeed, metabolic regulation of the PSC fate can imply multiple mechanisms that cover a wide network of signalling pathways. Regulation of ES cell proliferation has been shown to be controlled by PPARδ or peroxisome proliferator-activated receptor delta, a known nuclear receptor protein (Jeong et al., 2009). Particularly, PPARδ agonist increased the ROS production of ES cells, which led to the activation of p38-MAPK and possibly the canonical signal transduction Wnt/β-catenin pathway. It is shown that vitamin C and taurine, two ROS antioxidants, effectively reduce both Wnt protein levels and cell proliferation (Jeong et al., 2009). Redox regulation can be performed by a wide range of proteins. The protein Ape1, which is involved in regulating DNA binding of transcription factors such as p53 and HIF1a, has been shown to perform a regulatory function of the haematopoiesis from ES cells (Zou et al., 2007). The inhibition of Ape1 redox activity appears to prevent the development of haemangioblast from embryoid bodies (Zou et al., 2007). Thus, the evidence suggests that the autoregulating ROS levels via the redox sensors and metabolism are important in the maintainance oif stem cell activities and functions. Exploring different types of metabolism in relation to the function of cell programming will enhance and improve the currently limited ability of sceince in the application and management of PSCs. Understanding metabolism and its roles in PSCs will also develop different opportunities for using PSCs in regenerative medicine and can be applied in research related to metabolic driven pathology.

Table 1.1.1. Redox homeostasis and the effects in ES cell programming

Redox homeostasis	Redox species	Cell effects
NADPH oxidase 4 (Nox4)	H_2O_2	Vascular smooth muscle differentiation
GSH/GSSG balance, Ascorbic acid production (Yanes et al., 2010)	Possibly H_2O_2 and other ROS	Neuronal and cardiac differentiation
Thioredoxin (Guo et al., 2004)	Possibly ROS	Cysteine oxidation to restore DNA binding of Oct4 to maintain ES cell renewal
FoxO3 expression, GSH/GSSG balance (Yeo et al., 2013)	ROS	Neural stem cell self-renewal
Sirt1 expression (Han et al., 2008)	ROS	p53 translocation into the nucleus to suppress Nanog
PPARδ expression, Ascobic acid and Taurine production (Jeong et al., 2009)	ROS	p38-MAPK and possibly Wnt/β-catenin in cell proliferation

1.2. Embryonic stem cell differentiation and the involvement of L-proline metabolism

1.2.1. Early primitive ectoderm-like cell formation from embryonic stem cells reveals the involvement of L-proline metabolism in ES cell differentiation

1.2.1.1. Early primitive ectoderm-like cell (EPL) formation from embryonic stem cells cultured in conditioned media reveals the role of L-proline

Early primitive ectoderm-like cells (EPL) are characterised as a lineage of mice PSCs and are distinguished from ES cells (Rathjen et al., 1999). The formation of EPL cells are the result of ES cells responding to two bioactive factors present in the conditioned MEDII medium (Rathjen et al., 1999) and these two factors have been identified and consist of one as a larger molecular mass (>30kDa) and one smaller molecule mass (<3kDa) (Rathjen et al., 1999, Washington et al., 2010). The smaller molecule was further characterised and identified to be the amino acid L-proline (Rathjen et al., 1999, Washington et al., 2010, Rathjen et al., 2003). The addition of proline in ES cell culture was shown to be associated with the activation of the amino acid response via the mTOR signalling pathway (Washington et al., 2010). Other amino acids such as L-leucine and glycine are shown to activate mTOR, but they were not able to perform the L-proline activities in differentiating ES cells (Washington et al., 2010). This suggests that mTOR is not essential for ES cells differentiation and ES cell differentiation is only specific for L-proline content in MEDII. Even though the addition of L-proline on its own

is not sufficient enough to fully result in the EPL cell formation process, ES cells showed signs of differentiation towards EPL cell characteristics (Washington et al., 2010).

1.2.1.2. The characterisation of early primitive ectoderm-like cell (EPL) showed the transition of pluripotent lineages

Murine ES cells and EPL cells are distinct in morphology, gene expression and the ability to give rise of chimeric offspring (Rathjen et al., 1999). Morphologically, ES cell colonies are domed with defined edges and EPL cell colonies are monolayered colonies with irregular edges (Rathjen et al., 1999). It is known that EPL cells proliferate at a higher rate compared to ES cells (Rathjen et al., 1999). Both of the cell types show a high expression of three transcription factors *Oct4*, *Sox2* and *Nanog*, which are typical markers of pluripotent stem cells (Tang et al., 2010, Boroviak et al., 2014) and they are able to self-renew and differentiate infinitely *in vitro* (Evans and Kaufman, 1981, Rathjen et al., 1999, Washington et al., 2010). When ES cells are injected to a host blastocyst for embryonic development, they are able to give rise to all germ lines and somatic cells in chimeric offspring, which is not possible for EPL cells (Bradley et al., 1984, Rathjen et al., 1999). This should not be confused with the fact that EPL cells are pluripotent and they are able to differentiate to all cell types as a typical characteristic of PSCs. In the differentiation from embryoid bodies (EBs), the 3D aggregates of cell clusters, ES and EPL cell possess different abilities which give rise to the three germ layers (Lake et al., 2000). Particularly, EPL cell EBs are able to differentiate themselves into parietal endoderm but not visceral endoderm and they form mesoderm earlier and more intensive than ES cell EBs (Lake et al., 2000). EPL cells are marked with high gene expression of *Fgf5* (fibroblast growth factor 5), *Otx2* and *Espl1*, which are not seen in ES cells (Rathjen et al., 1999, Hughes et al., 2009, Lake et al., 2000, Pelton et al., 2002). The formation of EPL cells is associated with the decreased levels of *Rex1*, *Gbx2, Rmb27, Spp1* and *Nanog* genes, which are the markers of ES cells (Rathjen et al., 1999). EPL cells also show higher expression levels of the DNA methyltransferase gene *Dnmt3b* (Hughes et al., 2009, Washington et al., 2010), which is associated with DNA methylation. Mice ES cells have been shown to share most of the characteristics of the pre-implantation E4.5 ICM cells (Beddington and Robertson, 1989) and EPL cells are suggested to share characteristics of pluripotent primitive ectoderm cells or epiblast cells at E5.5-E6.0 (Rathjen et al., 1999). Phenotypic changes in EPL cell formation have suggested that the transition from ES cell to EPL cell may recapitulate the differentiation

process from ICM cells (about E4.5) to early primitive ectoderm cells (about E5.5) in the embryo (Lake et al., 2000, Rathjen and Rathjen, 2003).

1.2.1.3. Differentiation of ES cell in response to proline is specific to primed pluripotency.

The observations of current published data show evidence that perhaps only ES cells at a certain pluripotent state or lineages may differentiate in response to proline (Tan et al., 2016a). *In vitro,* ES cells can be maintained infinitely in two pluripotent states: naïve and primed. ES cells of these pluripotent stats are distinct in their characteristics and differentiation potential (Nichols and Smith, 2009). Differentiation potential of ES cells is initiated by the activation of glycogen synthase kinase 3 (GSK-3) and Fgf4 stimulation from extracellular signal-regulated kinase-1 and 2 (Erk1/2) pathways (Kunath et al., 2007, Sato et al., 2004). Inhibition of these pathways restricts the ES cell ability to differentiate, which helps to maintain ES cells in naïve state (Plusa and Hadjantonakis, 2014, Nichols and Smith, 2009, Kunath, 2011, Ying et al., 2008). Naïve state of ES cells *in vitro* can be reserved by the addition of Gsk-3 and Mek/Erk1/2 inhibitors (2i) and the relief of these inhibitors confers the ES cell primed state (Plusa and Hadjantonakis, 2014, Ying et al., 2008). A distinct characteristic of naïve ES cells is the capacity of extensive clonal propagation in 2i medium (Boroviak et al., 2014). Without the inhibition of Gsk-3 and Mer/Erk-1/2 (or the relief from 2i), ES cells are primed for differentiation (Plusa and Hadjantonakis, 2014, Nichols and Smith, 2009, Kunath, 2011, Ying et al., 2008). Primed ES cells show higher levels of DNA methylation (>70% methylcytosine or mC) compared to naïve ES cells (Smith et al., 2012, Meissner et al., 2008). 2i medium has been shown to sufficiently return ES cell genome to low levels of DNA methylation (30%mC) (Ficz et al., 2013, Habibi et al., 2013). The addition of L-proline and PD0325901, a Mek1 inhibitor, was insufficient to confer ES cell differentiation (Tan et al., 2016a), this suggests that there is no bypass process to proline-induced differentiation from naïve ES cells. Thus, L-proline-induced differentiation is only specific for primed ES cells. The changes from naïve- to primed- and then to proline-induced differentiated cells recapitulate a lineage development of PSCs (Figure 1.2-1). Understanding the role of proline and proline metabolism in the specification of pluripotency will enhance our knowledge of the functional role of amino acids and metabolism in embryonic development.

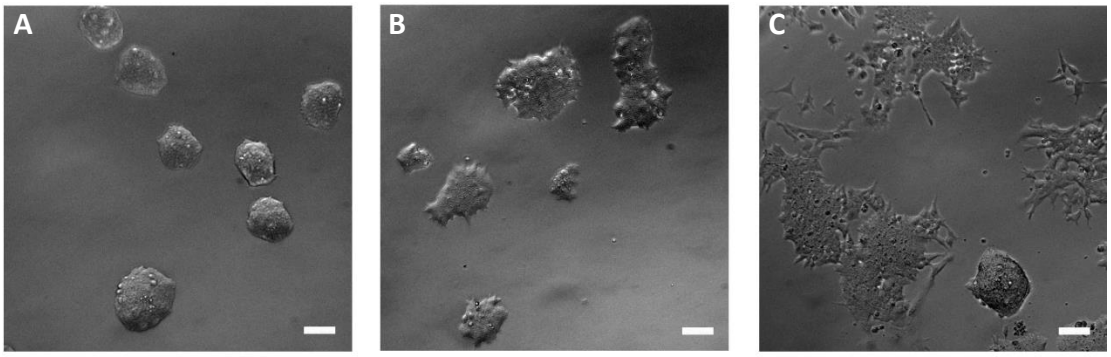

Figure 1.2.1. The lineage development of pluripotent stem cells.

A. Naïve ES cells are round and domed and appear to be regular and compact. The cells are maintained in the presence of 2i (GSK-3 and Mek/Erk1/2 inhibitors). **B.** Primed ES cells are less compact and domed when compared to naïve ES cells. The cells are conferred in the removal of 2i . **C.** Proline-induced differentiated cells are flat and irregular, formed from ES cells cultured with the addition of L-proline. Scale = 100 µm.

1.2.2. L-proline and proline metabolism in embryonic stem cells

1.2.2.1. L-proline-induced differentiation in ES cells involves L-proline amino acid sensing pathways

L-proline (here called proline if not specified) is a nonessential amino acid and proline metabolism is conserved from prokaryotes to eukaryote cells. Proline is among the amino acids that can be incorporated into proteins. Its conformation comprises of an amine group binding to both alkyl groups to form a pyrrolidine ring. Proline is also classified as an imino acid as it contains both an imine (R-C=NH) and a carboxyl groups (R-COOH). The L- form of proline is commonly seen in nature and is known for its biological functions (Kaul et al., 2008, Qamar et al., 2015, Zhu et al., 2002). These special characteristics classify proline as the only imino acid that is involved in biochemistry. This unique conformation also makes proline unable to be metabolised by classical metabolism such as aminotransferation, decarboxylation and racemisation (Adams and Frank, 1980). Proline metabolism is present in plants and mammals. In mammals, proline is metabolised by a single mitochondrial enzyme called proline dehydrogenase (PRODH) (Adams and Frank, 1980).

Proline activities in mice ES cells have been shown to involve two nutrient sensing pathways, mTOR and the nutrition stress pathway Gcn2-Atf4 (D'Aniello et al., 2015, Washington et al., 2010). In the proline-induced differentiation of ES cells, the activation of mTOR is required for the formation of EPL cells because the addition of mTOR inhibitor, rapamycin, significantly inhibits the activity of proline in differentiating the cells (Washington et al., 2010). The downstream mTOR pathway substrates were also shown to be reduced in ES cells that were treated with rapamycin (Washington et al., 2010). However, mTOR is not the main pathway that stimulates ES cell differentiation, suggesting that proline has other mechanisms which affect ES cell programming. In fact, proline was also shown to control ES cell identity through the stress pathway known as the amino acid starvation response (AAR) (D'Aniello et al., 2015). In ES cells, the addition of proline to the medium downregulated stress-activated transcription factor 4 (Atf4) in nonessential amino acid biosynthesis, which in turn, increased the synthesis of endogenous proline (D'Aniello et al., 2015). As a result, this relieved the cell dependence on exogenous proline and at the same time, increased proliferation (D'Aniello et al., 2015). As ES cells are starved for proline, they reduce the expression of genes necessary for proline synthesis and increase the requirement for proline uptake, which helps to maintain ES cell identity (D'Aniello et al., 2015). Thus, proline sensing is important in ES cell maintenance that includes the autoregulation of both proline biosynthesis enzymes and proline metabolism (D'Aniello et al., 2015), it suggests that amino acid sensing may not be the only mechanism at play in relation to the proline-induced regulation on ES cell fate.

1.2.2.2. Proline metabolism is involved in ES cell differentiation

The differentiation of ES cells requires the activity of exogenous proline at a concentration level of more than 40 µM (Rathjen et al., 2003, Washington et al., 2010). The uptake of proline to ES cells via the key transporter Snat2 was reported to play a part in mediating the differentiation process (Tan et al., 2011). Inhibition of proline transport through Snat2 was performed by using other amino acids such as L-alanine, glycine and L-glutamate, which are also transported by Snat2 into ES cells (Tan et al., 2011). It is known that ES cells cultured in the addition of excessive amino acids L-alanine, glycine, L-glutamate and other Snat2 substrates, have reduced differentiation compared to the addition of other amino acids, which are not Snat2 substrates (Tan et al., 2011). This suggests that proline uptake is

required for the differentiation and proline performed effect on ES cell programming internally.

The role of proline metabolic enzyme has been indicated to play a role in ES cell differentiation, demonstrating that the proline metabolism process is involved (Casalino et al., 2011). In mammalian cells, the first step of the proline breakdown process is proline oxidation, which is performed by the mitochondrial enzyme proline dehydrogenase (PRODH) (Adams and Frank, 1980). PRODH is the only enzyme that catabolises proline in mammalian cells (Pandhare et al., 2006, Ostrander et al., 2009). The use of proline analogue such as 3,4-dehydro-L-proline (DHP) can inhibit proline catabolism by competing for the binding sites of proline on Prodh (Smith et al., 1962). It has been shown that in the addition of DHP, changes of ES cells towards differentiated morphology in response to proline were prevented (Casalino et al., 2011). Differentiated gene expression such as *Otx2* and *Dnmt3b* was also reported to decrease in the addition of DHP (Tan et al., 2016a). This suggests that the process of L-proline metabolism by Prodh is important for ES cell differentiation.

1.2.3. Proline metabolism in mammals and embryonic stem cells

1.2.3.1. Transportation of proline in embryonic stem cells

Proline transportation is a sodium dependent transport system (Broer, 2014, Yao et al., 2000). Amino acid transport systems can be classified by their characteristics such as substrate affinity (eg. system Gly), sodium dependence (eg. System A and X_{AG}-/system ASC) and pH association (eg. System y+); or by their genetic families of the solute carriers (SLC) (Taylor, 2014, Kilberg et al., 1993, Dawson and Baltz, 1997). Depending on the tissues type, transportation of amino acid can be metabolic or non-metabolic (Taylor, 2014, Kilberg et al., 1993, Dawson and Baltz, 1997). The transportation of proline as osmolality regulation has been shown to be efficient in rescuing the early development of the 8-cell stage emryo to the blastocyst formation (Van Winkle, 2001), yet, little is known about the role of the metabolic transport of proline in early embryonic development. Two transporters of the system A transporters, SNAT1 and SNAT2 are known for their function in transporting L-proline intracellularly (Broer, 2014). SNAT1 (SLC38A1) and SNAT2 (SLC38A2) of system A transporters, which are characterised as sodium-amino acid cotransporters and highly pH sensitive, belong the SLC38 family and support the transport of small and neutral amino acids such as alanine, proline, glutamine and serine (Palacin et al., 1998, Broer, 2014). Different rates and

preferences of these amino acid transport processes support the specificity of SNAT1 and SNAT2 (Sugawara et al., 2000, Reimer et al., 2000, Yao et al., 2000, Hyde et al., 2007).

Among the two, SNAT2 is the main transporter of proline in the mice ES cells (Broer, 2014). Snat2 protein structure is comprised of eleven transmembrane domains with an intracellular N terminus and a highly conserved extracellular C-terminal histidine residue (Zhang et al., 2011c, Hyde et al., 2007). The N and C termini play a role in regulating amino acid transportation, particularly, C terminus is associated with pH sensitivity through the voltage independent process, whereas N terminus is critical to stabilise the expression of Snat2 on the cell membrane in response to environmental amino acid pool (Zhang et al., 2011c, Hyde et al., 2007). Snat2 but not Snat1 has been confirmed to be the major transporter of proline in mice ES cells and play a role in regulating the uptake of proline in differentiation (Tan et al., 2011). Snat2 is suggested to function as a transceptor, which is capable of detecting amino acid availability in both intra- and extracellular environment (Hyde et al., 2007). Snat2 transports proline via a sodium dependent manner and it is able to transport amino acids that are substrates for the System A transporters such as L-alanine, L-serine and glycine (Broer, 2014). Transportation of these amino acids through Snat2 effectively inhibits the uptake of proline into ES cells and consequently, prevents ES cell differentiation (Tan et al., 2011). However, the excessive amount of other amino acids that are not Snat2 substrates has been shown to be insufficient to prevent ES cell differentiation (Tan et al., 2011), suggesting that the differentition process is regulated by the uptake of L-proline by Snat2 and is specific for L-proline.

1.2.3.2. Proline dehydrogenase specifically metabolise proline in the mitochondria

Due to the special chemistry conformation, proline is only metabolised by the flavoprotein dependent enzyme proline dehydrogenase (PRODH) (or also called proline oxidase, POX) in the mitochondria. PRODH gene homologous to *Drosophila melanogaster sluggish A* (*slgA*) is present on the human and the mice chromosome 22q11 and is encoded by p53-induced gene 6 (PIG6) (Campbell et al., 1997, Donald et al., 2001). In mice, Prodh transcript has been identified with the length of 2.4-2.5 kb of various tissues including the brain (Gogos et al., 1999). Mutations of PRODH gene decrease catalysis efficiency and cause the accumulation of proline, which can lead to diseases in various organisms (Campbell et al., 1997, Luo et al., 2012, Gogos et al., 1999, Blake et al., 1976). Isolation of PRODH protein in

bacteria shows that the structure of PRODH undergoes conformational changes to perform proline catalysis (Ostrander et al., 2009, Zhang et al., 2004). It is suggested from the structural models that proline is buried inside the complex as the first step of proline oxidation occurs (Ostrander et al., 2009, Zhang et al., 2004, Luo et al., 2012). Oxidation of proline by PRODH to Δ-pyrroline-5-carboxylate (P5C) is coupled with the reduction of cofactor flavin adenine dinucleotide (FAD), which produces two electrons and feeds the electron transport chain for further ATP (adenine-5'-triphosphate) production (Tanner, 2008, Zhang et al., 2004). PRODH catalytic activity is controlled by the active gate formed from the ion pair associated with FAD chain on PRODH protein (Luo et al., 2012). These conformation changes of the active ion gate allow the access of electron acceptors to reduce FAD and at the same time, to facilitate the release of products (Luo et al., 2012).

The PRODH function for proline metabolism can be regulated by introducing inhibitors through the substrate recognition domains (Zhang et al., 2004, Adams and Frank, 1980). PRODH isolated from rat livers have been shown to be inhibited reversibly by L-lactate and pyruvate whereas D-lactate can inhibit PRODH in bacteria (Adams and Frank, 1980). Other substrate analogous to proline such as L-tetrahydro-2-furoic acid (THFA) and acetate are also reversible inhibitors of PRODH activity in proline metabolism (Zhu et al., 2002, Zhang et al., 2004), among them, 3,4-dehydroproline (DHP) is an antagonist of PRODH that can reversibly inhibit the proline catalysis process by competing for the binding sites on PRODH (Smith et al., 1962). Proline metabolism is activated by the recognition of three functional groups on the proline molecule, including carboxyl, amine and the methylene groups (C3-C5) of the ring (Zhang et al., 2004). Inhibitors of PRODH can compete with proline for the binding domains and the reduction by FAD on PRODH complex (Tanner, 2008). Irreversible inhibition of PRODH is introduced by N-propargylglycine through mechanism-based inactivation, in which, the oxidation of N-propargylglycine is concomitant to the reduction of FAD, being the first step of proline metabolism (White et al., 2008). PRODH has been shown to be involved in a number of cellular pathways that are associated with proline catabolism and the formation of products (Phang et al., 2008a, Phang et al., 2008b). For example, the production of ROS induced by PRODH activity in proline metabolism under the regulation of p53 has been shown to play a role in apoptosis (Rivera and Maxwell, 2005). The expression of PRODH has also been shown to increase in response to inflammatory and genotoxic stress, suggesting its critical role in various cellular effects (Pandhare et al., 2006, Hu et al., 2007). Inhibition of PRODH by

dehydroproline (DHP) has been shown to counteract proline activity to formation of EPL cells from ES cells, indicating that the activity of PRODH is required for this process (Casalino et al., 2011). However, the PRODH inhibitors can also interfere with other cellular activities. For example, the addition of DHP to human and mice fibroblasts in culture has been shown to affect the formation of collagen synthesis and propyl hydrolase activities (Kerwar and Felix, 1976), suggesting that the cellular outcomes may be generated from the effects of multiple inhibition, thus, specifying the important role of PRODH and PRODH activity in ES cells may require the understanding of the proline network and the characteristics of the proline metabolic pathway.

1.2.3.3. Proline metabolic reactions in mammalian cells

Proline catabolism: Proline is oxidised when two electrons are removed from its molecule by the cofactor FAD on PRODH which determines the formation of P5C. The electrons once removed from proline are stored in the reduced form of FAD, which will be subsequently transferred to the electron transport chain through ubiquinone proteins. The accumulation of these electrons is an essential source for the production of ROS. Production of ROS from proline metabolism has been shown to be involved in a number of biological pathways, which can regulate cellular activity (Donald et al., 2001, Liu et al., 2006). The next step in proline metabolism is the non-enzymatic hydrolysis of P5C that opens the ring structure in a process called tautomerisation to form the intermediate gama-glutamate semialdehyde (GSA), which will be further oxidised by P5C dehydrogenase (P5CDH) enzyme to form glutamate as the final product to contribute to the source of the TCA cycle. Both PRODH and P5CDH are conserved in eukaryote and prokaryote cells (Adams and Frank, 1980). Monofunctional P5CDH enzymes are typically 400-600 amino acids (reviewed in (Arentson et al., 2012)) and they are located in the mitochondria. P5CDH enzyme is one of the aldehyde dehydrogenase (ALDH) superfamily. Human and mice P5CDH genes belong to the ALDH family 4 and are referred to as ALDH4A1 (Sophos and Vasiliou, 2003). P5CDH uses the coenzyme NAD+ (nicotinamide adenine dinucleotide) as an electron acceptor to oxidise GSA, which is the real substrate for P5CDH rather than P5C (Adams and Frank, 1980), suggesting that proline metabolism involves a variety of intermediates that create a complexed and dynamic metabolic network (Figure 1.2.3).

Proline synthesis: Proline can be synthesised inside the cells from different sources such as glutamate, ornithine and P5C. The synthesis of proline from glutamate is initiated by mitochondrial P5C synthase (P5CS) enzymes through the functioning of two domains, gamma-glutamyl kinase (GK), and gamma-glutamyl phosphate reductase (GPR), which use ATP and NADPH (nicotinamide adenine dinucleotide phosphate) to produce GSA from glutamate (Adams and Frank, 1980). GSA circles its arms into a ring and become P5C. A complete structure of P5CS is not yet constructed, however, GK and GPR domains have been studied in bacteria (Marco-Marin et al., 2007, Perez-Arellano et al., 2006). In mammalian cells, P5CS proteins undergo splicing to form two isoforms, both differing with the addition of two amino acids at the N-terminal of the GK site (Hu et al., 1999). The short isoforms are present in gut cells and the long isoforms are present in all tissue (Hu et al., 1999). In human and mice, the P5C synthase gene is an 18A1 member of the ALDH family (known as *ALDH18A1*) (Hu et al., 1999, Liu et al., 1996). In mice, the activity of P5CS enzyme was first measured in Chinese hamster ovary cells through the formation of the intermediate P5C (Smith et al., 1980). P5C can act as an intermediate to synthesise both proline and ornithine from glutamate (Adams and Frank, 1980). The synthesis of ornithine from P5C requires the ornithine aminotransferase (OAT) enzyme, which reverses ornithine back to P5C (Adams and Frank, 1980). In mice, the OAT gene is located on chromosome 7q26 and some related sequences of the gene, which are found on X chromosome and chromosome 3, have been identified as pseudo genes (Ramesh et al., 1992). The final enzyme in the proline metabolic pathway is the enzyme catalysing the reduction of P5C to proline in the cytosol, P5C reductase (P5CR), the reaction of which requires the conversion of NADPH to $NADP^+$. P5CR proteins have two isozymes P5CR1 and P5CR2 encoded by *Pycr1* and *Pycr2* with a conserved N-terminal fold for NADPH binding (Arentson et al., 2012, Hu et al., 2008). Both of the isozymes are located within the cytoplasm causing P5C to leave the mitochondria to be converted back to proline (Arentson et al., 2012, Hu et al., 2008). As proline synthesis can use different sources of substrates to generate proline, it is necessary to understand how the cell environment regulate the L-proline pool and support the cell needs.

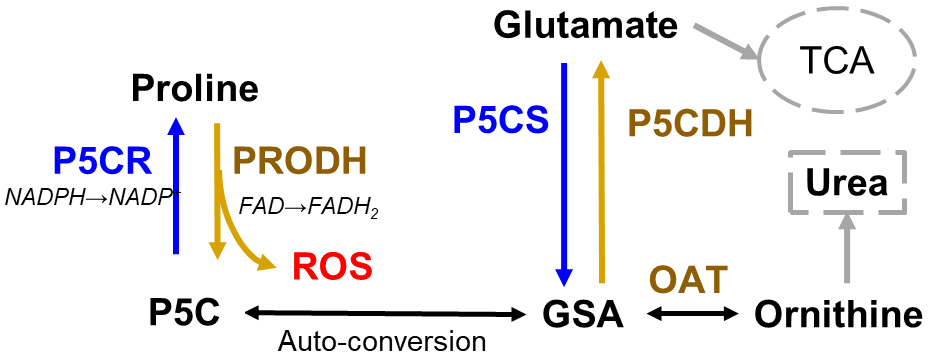

Figure 1.2.2.Proline metabolism and synthesis in ES cells.

PRODH (Prodh): proline dehydrogenase. **P5CR** (Pycr1): P5C reductase. **P5CDH** (Aldh4a1): P5C dehydrogenase. **OAT** (Oat): ornithine aminotransferase. **P5CS** (Aldh18a1): P5C synthase. **P4HA1**: Prolyl 4-hydroxghovbylase subunit alpha 1 (P4ha1) **P5C**: Δ-pyrroline-5-carboxylate. **ROS**: reactive oxygen species. **GSA**: glutamic-gamma-semialdehyde.

Yellow arrows: Proline catabolism: Proline enters ES cells primarily through the transporter SNAT2 and is oxidised by the enzyme PRODH in the mitochondria, which releases two products ROS and P5C. P5C is autoconverted into GSA, which can be used to synthesise glutamate via the enzyme P5CDH or orthine via the enzyme OAT. Glutamate can then enter other pahtways such as the TCA cycle and ornithine enters the urea cycle. Blue arrows: Proline biosynthesis: Proline can be synthesised from glutamate by the enzyme P5CS or from ornithine by the enzyme OAT, which form the intermediate product GSA/P5C. P5C is converted back to proline via the enzyme P5CR.

1.2.3.4. Biological roles of pyrroline-5-carboxylate and the involvement of pyrroline-5-carboxylate in early primitive ectoderm-like cell formation

P5C is a bioactive and labile intermediate substrate that can be directly involved in cell signalling (Nomura and Takagi, 2004, Farrant et al., 2001, Phang, 1985). In yeast, P5C has been found to be a direct inhibitor of mitochondria respiration, resulting in the generation of intracellular ROS (Nishimura et al., 2012). P5C has also been shown to be a vitamin B6 antagonist which effectively reacts with aldehydes and ketones to form adducts in type II hyperprolinemia disease (Farrant et al., 2001). The conversion of P5C to proline creates a proline-P5C cycle associating with the NADPH/NADP+ redox regulation inside the cell microenvironment (Adams and Frank, 1980). The proline-P5C cycle is important to maintain the level of NADP+ between the mitochondria and the cytosol for the pentose phosphate pathway (Hagedorn and Phang, 1983, Hagedorn and Phang, 1986). The end products of the pentose phosphate pathway are critical for the nucleotide synthesis process (Phang, 1985), which is suggested to influence the caspase activities resulting in cell death in some tumour cells and thus affecting cell growth (Maxwell and Davis, 2000). In the cellular microenvironment, P5C achieves an equilibrium with its tautomeric form, GSA, which makes P5C an intermediate agent for various important metabolic pathways (Pandhare et al., 2009, Arentson et al., 2012, Tanner, 2008, Adams and Frank, 1980).

The characterisation P5C and its biological studies have been performed in plants, yeasts and human plasma, which revealed aspects of their regulatory effect (Fleming et al., 1984, Nishimura et al., 2012, Qamar et al., 2015). However, the P5C biological role still remains to be further examined in mammalian cells. The reason for the limitation in studies around P5C might be due to its high bioactivity, which makes it difficult to measure and manipulate P5C production even though radioactive methods have been applied (Hu et al., 1999, Smith et al., 1980).

In ES cells, the attempt to increase L-proline synthesis and P5C production from ornithine has been carried out by using DMSO and shown to prevent ornithine from entering the polyamine synthesis processes, forcing ornithine to enter the proline synthesis pathway (Casalino et al., 2011). The result has suggested that P5C formation in this direction plays an important role in the morphological changes in ES cells (Casalino et al., 2011). However, given

that P5C is an intermediate for different metabolism pathways, the chance for P5C formation from ornithine to be returned to L-proline would be possible (Alonso and Rubio, 1989). Thus, further investigation is required to identify the role of P5C.

1.2.4. Pyrroline-5-carboxylate and reactive oxygen species are suggested to be involved in proline-induced ES cell differentiation

1.2.4.1. Biological roles of reactive oxygen species in embryonic stem cell differentiation

PSCs tend to utilise high levels of glycolysis and low levels of OXPHOS to secure their DNA integrity. It is also important for PSCs to maintain their redox homeostasis to self-renew and to differentiate (Folmes et al., 2012, Ito and Suda, 2014, Wang et al., 2013). It has been shown that when adult stem cells maintain quiescence in the hypoxic niche, the production of ROS in normoxia forces the cells into a more proliferative state (Tothova and Gilliland, 2007, Chen et al., 2008, Renault et al., 2009).

In the proline metabolic process, ROS is formed from the oxidation reaction of proline by PRODH to produce free electrons to feed the electron transport chain, which subsequently generate ROS (Murphy, 2009, Liu et al., 2009). It has been shown that inside the mitochondria, and in the presence of proline, PRODH is not the dominant source of ROS, particularly superoxide and H_2O_2 (Goncalves et al., 2014). Instead, PRODH is an important source for electrons that are directly fed to the electron transport chain through ubiquinone reduction, and indirectly through other sites from the downstream metabolism (Liu et al., 2009). The formation of ROS in proline metabolism involves different metabolic processes making it potential for a role in cellular activity. Current data propose that ROS production is a key factor in proline metabolic regulation of ES cell programming. The addition of the PRODH inhibitor, DHP, is effective to return ROS levels to the basal level (Tan et al., 2016a). Thus, ROS level changes in ES cells may be correlated with proline metabolism in ES cells. Antioxidants are known as ROS neutralisers and the addition of glutathione as an antioxidant to ES cell culture in the L-proline-containing medium has been shown to reduce ROS level (Tan et al., 2016a). In addition, the inhibition of L-proline metabolism-induced ROS by introducing antioxidants such as glutathione (GSH), N-acetyl-L-cysteine (NAC) and especially vitamin C, has been shown to effectively prevent the morphological and gene expression changes of ES cells towards differentiated cells (Casalino et al., 2011, Comes et al., 2013). However, the link connecting this evidence is still to be discovered. Research is still attempting to discover whether the

source of ROS is the result of proline oxidation or is it the result of proline-induced stress in the cells (Tan et al., 2016a), thus, proline may play a different role. It is also critical to understand if the enzyme Prodh and its catalytic activity are necessary to provide ROS for ES cell differentiation and just how specific this ROS is to the differentiation process, this given the fact that the presence of proline metabolic enzymes in ES cells are unknown and whether these different enzyme activities would have an effect on directing the proline metabolism in ES cells. Even though the changes in ES cell morphology were observed in Prodh and ROS inhibition, it still needs to be confirmed if these changes actually reflect the differentiation process rather than the stress responses (Casalino et al., 2011).

Two redox sensing molecules have been identified to be involved in ES cell differentiation, c-Src (proto-oncogene tyrosine-protein kinase Src) and p38-MAPK (p38-mitogen activated-protein kinase) (Tan et al., 2016a). In previous studies, c-Src are known to be directly involved in the differentiation process of ES cells to primitive ectoderm cells (Meyn and Smithgall, 2009, Meyn et al., 2005). In addition, p38-MAPK is important for ES cell regulation of the self-renewal and differentiation process (Ding et al., 2008). Studies indicate that with the addition of the inhibitor of Scr tyrosine phosphorylation into proline containing media can result in a reduction in proline-induced differentatiated cells (Tan et al., 2016a). However, the inhibitory effects are unable to fully prevent differentiation as the differentiated morphology and gene expression changes are not complete or maintained (Tan et al., 2016a). This suggests that Src protein kinases may play a role in maintening differentiated phenotype and ROS may be the regulatory factor as c-Src is a ROS sensing molecule. In addition, the lack of p38-MAPK, an isoform of p38-MAPK directly affects the formation of differentiated cells and ES cells fail to downregulate pluripotent gene expression in proline containing media (Tan et al., 2016a). Futhermore, p38-MAPK signalling has no role in maintenaning differentiated cells (Tan et al., 2016a). Both c-Src and p38-MAPK can be directly activated by ROS induced-oxidation (Giannoni et al., 2005, Ding et al., 2008), suggesting the role of ROS in these signalling pathways. However, the precise mechanism of this signalling pathway is not well-characterised. Filling in these gaps will greatly contribute to a more complete picture of the proline metabolism process and ES cell differentiation.

1.3. Objectives

Metabolism provides the foundation and the source of energy required for sustaining life. As the microstructure of life, cellular metabolism is gaining interest as research demonstrates that metabolism operates well beyond the simple function of life maintenance (Mason and Rathmell, 2011, Metallo and Vander Heiden, 2013). The involvement of metabolism in regulating cell programming has made metabolism an important factor in disease progression and opened up new avenues for the discovery of treatments (Dang, 2012, Cunnane et al., 2011). Understanding the different types of metabolism and how they impact upon and affect cell biology, and cell development, will enhance and increase our knowledge base and provide new approaches for future studies on the search toward providing improved treatment solutions for diseases.

L-proline metabolism is conserved in plants and eukaryote organisms and is an essential requirement for cell growth and development (Miller et al., 2009, Nishimura et al., 2012, Phang et al., 2015). Proline metabolism plays a pivotal role in the regulation of cancer cell progression and is nominated as a potential area for study in therapeutic development (Elia et al., 2017, Phang et al., 2012). Proline metabolism was first known to be involved with eukaryote cell programming (Donald et al., 2001, Phang et al., 2008a), however, the precise mechanism have not yet been completely established. Proline is shown to activate ES cell differentiation, this provides an opportunity and a system for investigation into the central role of proline metabolism and its functions in relation to cell programming. In conclusion, further examination into understanding how proline metabolism function in ES cells, and how each element of the proline metabolic system contributes specifically to ES cell differentiation is required.

1.4. Hypothesis and Aims:

The overarching hypothesis of the work in this thesis is that the L-proline metabolic product, ROS, is directly involved in the differentiation process of ES cells. To address this hypothesis the following aims will be explored:

1. To determine the proline metabolic system in ES cells via the expression and localisation of the proline metabolic enzyme family,

2. To quantify proline metabolism-induced ROS production in response to the addition of proline to ES cell culture,
3. To determine the roles of proline oxidation and ROS production in ES cell differentiation.

Chapter 2 Methodology

2.1. Tissue culture

2.1.1. Mouse ES cells:

D3 ES cell line (Doetschman et al., 1985) was generously given by Dr Lindsay Williams, Ludwig Institute, Melbourne. WA30 ES cell line were obtained by Dr. Marnie Blewitt, Walter and Eliza Hall, Australia and maintained in naïve state conditions as described below.

2.1.2. Culturing media:

Medium to maintain D3 ES cell line is described below[1], this medium will be referred as basal medium.

Components	Final concentration
FBS	10%
DMEM	90%
Pen-strept	100 units/mL (U/mL)
βME	0.1 mM
LIF	1 unit (U)

Medium to maintain WA30 ES cell line contained basal medium with the addition of PD0325901 and CHIR99021 following the concentration below:

PD0325901	1 µM
CHIR99021	3 µM

All cells were maintained on a 6mm tissue culture treated dishes in the incubator at 37°C and 5% CO_2 supply. All cells were passaged every 2-4 days and cells that reached passage 29 were discarded. To passage the cells, they were washed 2 times with PBS before being trypsinised by 500 µL of trypsin for 2 minutes (Life technology, 12563011). Then 1 mL of

[1] All reagents are to be referred to the list of reagents (Table 2.1)

medium was added to the dish to deactivate and wash the cells off the surface. The mixture was then transferred into a fresh 15mL falcon tube. Trypsin-medium mixture was removed by centrifugation and the cells were resuspended in 1 ml of new media. $5x10^5$ – $1x10^6$ cells were seeded in a new dish for maintenance.

Table 2.1.1. List of reagents

Abbrev.	Name	Company	Reference
DHP	3,4-Dehydroproline	Sigma Aldrich	D4893
DMEM	Dulbecco's Modified Eagle Medium	Life Technologies	11965-084
DMSO	Dimethyl sulfoxide	Sigma Aldrich	472301
DTT	Bolt Reducing Agent	Life Technology	B0009
DTT	DL-Dithiothreitol	Sigma Aldrich	D9163
EDTA	Ethylenediaminetetraacetic acid disodium salt dihydrate	Sigma Aldrich	E5134
EGTA	Ethylene glycol-bis(2-aminoethylether)-N,N,N',N'-tetraacetic acid	Sigma Aldrich	E3889
FBS	Heat inactivated Foetal Bovine Serum	Life Technologies	10082-139
GSH	Glutathione		
LIF	Leukaemia Inhibitory Factor	Produced in house (Smith, 1991)	-
NAC	N-acetyl-cysteine	Sigma Aldrich	A9165
Pen-strep	Penicillin (10 000 units/mL) - Streptomycin (10 000 µg/mL)	Life Technologies	15140-122
SDS	Sodium dodecyl sulfate	Sigma Aldrich	L3771
THFA	L-Tetrahydro-2-furoic acid	Sigma Aldrich	341517
Tris	Trizma-base	Sigma Aldrich	T1503
Vit C	Vitamin C	Sigma Aldrich	A4403
βME	Beta-mercaptoethanol	Sigma Aldrich	M3148
	Acetic acid, glacial	Sigma Aldrich	ARK2183
	CHIR 99021	Stem cell technologies	252917-06-9
	Chloroform	Sigma Aldrich	C2432
	Gelatine	Sigma Aldrich	G1890
	Glycerol	Sigma Aldrich	G5150
	Glycine	Sigma Aldrich	G8898-1KG
	GoTag Green	Promega	M712C
	HEPES	Sigma Aldrich	H3375
	IGEPAL CA-630	Sigma Aldrich	I8896-100ML
	L-Ornithine monohydro-chloride	Sigma Aldrich	O6503-25G
	L-Proline	Sigma Aldrich	P6607-25G
	PD 0325901	Stem cell technologies	391210-10-9
	Potassium chloride	Sigma Aldrich	P9541
	Sodium chloride	Sigma Aldrich	S3014-1KG

	Triton X-100	Sigma Aldrich	T8787-50ML
	Trizol	Life Technologies	15596026
	Tween-20	Sigma Aldrich	P9416
	Ultrapure Water	Invitrogen	10977-015
	Acetic acid, glacial	From general laboratory resources	
	Ethanol		
	HCl		
	Methanol		
PCA	Perchloric acid		
	Potassium hydroxide		

2.2. Gene expression analysis via PCR

2.2.1. RNA extraction

RNA was extracted from cell pellet with 200 µL Trizol/sample. Samples were incubated on ice for 20-30 minutes before Trizol reagent was separated by adding 1:5 (40 µL) chloroform. Mixture of Trizol : Chloroform was inverted for 2 minutes and returned on ice. After Trizol : Chloroform mixture settle in the tube, RNA in each sample was separated from the trizol : chloroform mixture using centrifugation at the highest speed for 10 minutes. Aqueous layer of RNA in each sample was transferred and mixed with isopropanol in a new tube. RNA precipitation was set overnight at -20^{o}C. Precipitated RNA was collected by centrifugation at the 10,000g speed for 10 minutes at 4^{o}C. RNA samples were washed with ice cold ethanol 70%. RNA pellets were resuspended in 20 µL ultra-pure (nuclease free) water and stored at -80^{o}C.

2.2.2. DNase treatment for RNA samples

Ten (10) µL of each RNA sample (or at least 1.5 µg of RNA) were DNase treated to remove DNA contamination. DNase treatment kit (DNA-free™ DNA Removal Kit) was purchased from Life-technology (Ref: AM1906) and DNA treatment was performed following the manufacture instruction. Particularly, 1 µL (or 1/10 RNA volume) of 10x DNase I buffer was added to each RNA sample, followed by 1 µL of rDNase I. The combination was gently mixed and then incubated on a heat block at 37^{o}C for 20-30 minutes. This was followed by adding 2 uL DNase Inactivation Reagent. The final combination was incubated and mixed occasionally for two minutes at room temperature. The precipitated reagents were removed by centrifugation at 10,000 g speed for 1.5 minutes. Treated RNA in the aqueous layer was transferred to a clean tube and stored at -80^{o}C.

2.2.3. cDNA synthesis by reverse transcription

Treated RNAs were quantitated on the Nano drop machine (Spectrometer ND1000) using ND-1000 program (version V3.3.1). 1 µg of RNA from each sample was used for cDNA synthesis by reverse transcription. cDNA synthesis was performed following the provided protocol (GoScript™ Reverse Transcriptase, Promega, Ref: A5001). Accordingly, 0.5 µL (or 1 µg) of Oligo-dT was added to each RNA sample and water to make 10 µL of template mix. This was then incubated at 70^{o}C for 5 minutes, following by chilling on ice for 5 minutes. Reaction master mixture was prepared as the following:

Components	**Concentration**
5x GoTaq Reaction Buffer	1x
MgCl2	1.5 mM
PCR Nucleotide Mix	0.5mM
RNasin® Ribonuclease Inhibitor	20 U
GoScript™ Reverse Transcriptase	1 µl
Water	
Total	**10 µl**

Then, 10 µl of reaction master mixture was added to the ice-cold template and gently mixed to form 20 µl/reaction. The final reaction mixture was sit for 5 minutes at room temperature and then incubated on a heatblock for 90-120 minutes at 42^{o}C and 15 minutes at 70^{o}C. The cDNA products were diluted 1 in 2.5 by the addition of 30µL of ultra-pure water before use. Negative controls with two sample of i/a none-GoScript™ Reverse Transcriptase sample and ii/a none-RNA sample were included for every cDNA synthesis procedure.

2.2.4. Real time PCR (PCR)

Each PCR reaction mix contained 1 µL of cDNA (from cDNA synthesis), 1x GoTag Green (Promega, M7122), 0.5 µM forward and reverse primers. PCR condition for each reaction is listed in Table 2.2.1.

PCR products were loaded on 2% Agarose gel (Promega, Ref: V3121) containing 1 µL SYBR Safe DNA dye (Invitrogen, Ref: S33102). Separation of PCR was performed in TAE buffer (recipe below) and observed under UV in the Bio-rad Chemidox XRS Imager.

Table 2.2.1: General conditions for real time PCR examination

Denaturation	95°C for 1 mins
Cycling X25 cycles	95°C for 30 seconds 55°C for 30 seconds 74°C for 30 seconds
Melting	95°C for 1 minute 50°C for 1 minute 95°C continuous
Cooling	40°C for 2 minutes

TAE buffer:

Components	**Concentration**
Tris-Base	40mM
Acetic acid	20 mM
EDTA	1 mM

2.2.5. Quantitative real time PCR (qPCR)

qPCR for each sample was run in triplicates (3 reactions/sample/gene) in a Roche Light Cycler 480 II. Data were collected by LightCycler 480 program version 1.5.1.62.SP3. For each reaction, 1 µL of cDNA from each sample (from cDNA synthesis) was mixed with 0.5 µM forward and reverse primers in 12.5 µL GoTaq® qPCR Master Mix (Promega #A6001). PCR conditions were optimised for different genes and will be described where applicable. General condition is described in table 2.2.1.

Table 2.2.2: General conditions for qPCR examination

Denaturation	95°C for 15mins
Cycling x40 cycles	95°C for 15 seconds 55°C for 20 seconds** 72°C for 20 seconds
Melting	95°C for 1 minute 50°C for 1 minute 95°C continuous
Cooling	40°C for 2 minutes

** for pluripotent marker genes, this was set at 40 seconds

2.2.6. Statistical analysis of qPCR data

Ct values were collected as raw data. Raw data were then cleaned to exclude outliner and curated. Ct values were collected from each gene were normalised to the house keeping gene Beta-actin using qGene method (Simon, 2003). Mean normalised expression values were used for statistical analysis. Statistical analysis was done in Graphpad Prism program version 6.05. Mean normalised expression (MNE) values were used as the inputs to perform t-test to compare the gene expression in different treatment or pluripotent states to primed (Serum + LIF) ES cells. The values were set up for paired-ratio 2-tailed t-tests (test the fold change of each treatment to the control primed ES cells). Extended analysis included paired 2-tailed t-tests, which looked at the absolute difference in gene expression. Ratio- and difference statistical analyses of qPCR data provide different aspects to view the data. Graphs were generated based on the mean of MNE values for each gene in each cultivation condition. Error bars were generated from standard error of the mean (SEM) of all replicates of the same condition.

2.3. Flow cytometry

2.3.1. Reactive oxygen species (ROS) measurement

D3 ES cells were maintained in either 2i+LIF or Serum + LIF conditions before being seeded on a gelatine coated 24-well plates at the density of 3.2-4x10^5 cells/well in 500 µL of similar media. The cells were incubated at 37^{o}C, 5% CO_2 for 24 hours before ROS measurement occurred. 30 minutes before ROS measurement, cells were checked for the confluence of 80-100%, if media turned yellow, cells were disqualified for further procedure. Qualified cells were incubated with 7.5 µM of MitoSOX Red dye (Life technologies, M36008) for 30 minutes. After this incubation, cells were washed 2 times in warm PBS and detached with 100 µL trypsin for 2 minutes. Trypsin was gently removed to prevent cell loss and 500µL of imaging buffer containing 10% FBS and 0.1 mM βME in DMEM, no phenol red (Life technologies, 21063029) was added to suspend single cells. All cells were transferred into FACS tubes and ready to be analysed by flow cytometry. Beckman Coulter CyAn ADP flow cytometry machine was used at single tube sample mode to analyse cell samples. Data were collected by Summit program version 4.3. The protocol of detection input was set for Threshold of 13% and Gain of 1.0. Forward scatter (FS) was acquiring peak and area with no voltage specificity. Side scatter (SS) was acquiring Peak and Area at the voltage of 450.

Channel FL-3 was set for MitoSOX Red to acquire Peak, Area and Log at the voltage of 595 and FL-6 was set for DAPI at the voltage of 490. All samples were analysed by the machine and sample flow was set at medium speed. The maximum of 125000 cells (or also called events) were detected and features were recorded for final analysis.

For time point measurement of ROS production in response to proline, D3 ES cells were grown for 24 hours. Proline was added to the cells at 24, 12, 6, 3, 1 and 0.5 hours before staining with 7.5 µM MitoSOX Red dyes. Three technical replicates were used for each time points. At least three independent experiments at different cell passages were done for each time point. Technical control included samples with no staining and single colour staining. Untreated ES cells were used as biological controls.

N-acetyl-cysteine (NAC), glutathione (GSH) and vitamin C (Vit C) were used as antioxidants. These antioxidants were added to the cells 4 hours before ROS measurement. 3, 4-Dehydroproline (DHP) and L-Tetrahydro-2-furoic acid (THFA) were used as Prodh inhibitors. These inhibitors were added to the cells at the same time with proline. The concentration of use for each chemical is summarised in Table 2.3.1.

Table 2.3.1: The concentration of different treatments to ES cells

	Concentration
NAC	50 µM
GSH	1 mM
Vit C	500 µM
DHP	200 µM
THFA	200 µM

2.3.2. Mitochondrial membrane potential (MMP) measurement

Mitotracker Green was used to measure MMP in ES cells at the same time with ROS measurement. At the same time with Mitosox Red addition, 3 mM Mitotracker Green (M7514) was added to a random technical repeat of each treatment. The cells were then analysed by flow cytometry machine. Mitrotracker Green was detected in FL-1 channel at the voltage of 500 to acquire the Peak, Area and Log of each event. Four independent experiments were repeated for statistical analysis. Single colour samples were included for technical control and compensation.

2.3.3. Analysing Flow cytometry data

Data acquired by Summit program was analysed in Kaluza Analysis program version 1.5a. Gating from side scatter (SS) and forward scatter (FS) parameters allowed the selection of cells acquisitions (or also called "Events"). Events of the same size and granular complexity represented "ES cells" population. "ES cells" were further selected for "Singlets" based on their area as larger area were associated with doublets or cell clumps. "Singlets" cells were gated for "DAPI negative" population to select live cells. Live cells (DAPI negative) were analysed in a histogram graph that was set for count of cells and MitoSOX Red parameter. Two population of ROS was gated in the histogram to analyse cells with high (ROS^{hi}) and low (ROS^{lo}) ROS level. An example of gating strategy is demonstrated in Figure 2.3.1. If cells were double stained with MitoSOX Red and Mitotracker Green, further gating was required (Figure 2.3.2). ROS^{hi} and ROS^{lo} cells were analysed in a new histogram under the green parameter for statistical numbers (Figure 2.3.3).

From the histograms, information about the number of cells based and their fluorescent intensity were accessed. Based on the data provided by Summit, Kaluza program provided statistic values that could be used to identify the characteristics of MitoSOX Red (or ROS production) from each sample. Among these values, percentages of gated populations, geometric mean fluorescent intensity, mode (largest population among the events) and the minimum and maximum values of all gated events were accessed for further analysis and comparisons in statistical analysis. Definitions of statistical values are to be referred to "Instructions for Use" from Kaluza Flow cytometry analysis software (ref. "*Instructions for Use - Kaluza Flow Cytometry Analysis Software",* A75667AC, September 2011, Manufactured by Beckman Coulter, Inc. 250 S. Kraemer Blvd. Brea, CA 92821). The manual can be accessed from on the manufacturer website.

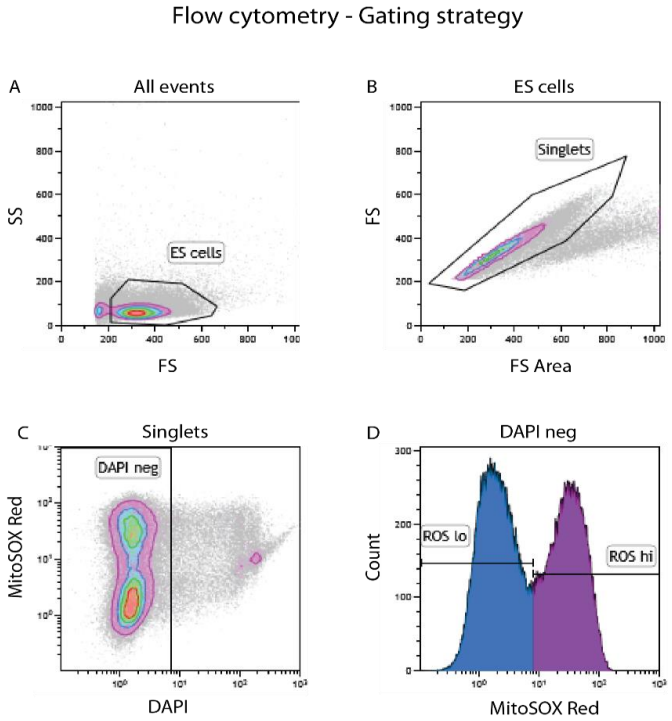

Figure 2.3.1. Flow cytometry plots and gating strategy for analysis and statistics.

A. Gating all events for ES cell population. **B.** ES cells gated for singlet cells. **C.** Gating from singlets to DAPI negative or live cells (DAPI neg). **D.** ROS production from live cell was visualised and quantitated for MitoSOX Red parameter.

2.3.4. Flow cytometry compensation

Compensation was performed to prevent the spill over of fluorescence from one channel to another, which may cause auto-fluorescence in a channel without actual staining. Red single colour control was first adjusted for the spill over to green channel. This adjustment was applied to Green single colour control, where further adjustment was applied on the top of the previous one to prevent the spill over from green to red channel. These adjustments were then applied to all samples. Figure 2.3.2 showed the differences of single- and double colour staining before and after compensation. Table 2.3.1 showed the compensation matrix generated from Figure 2.3.2. Compensation was repeated for each biological replicate or each independent experiments.

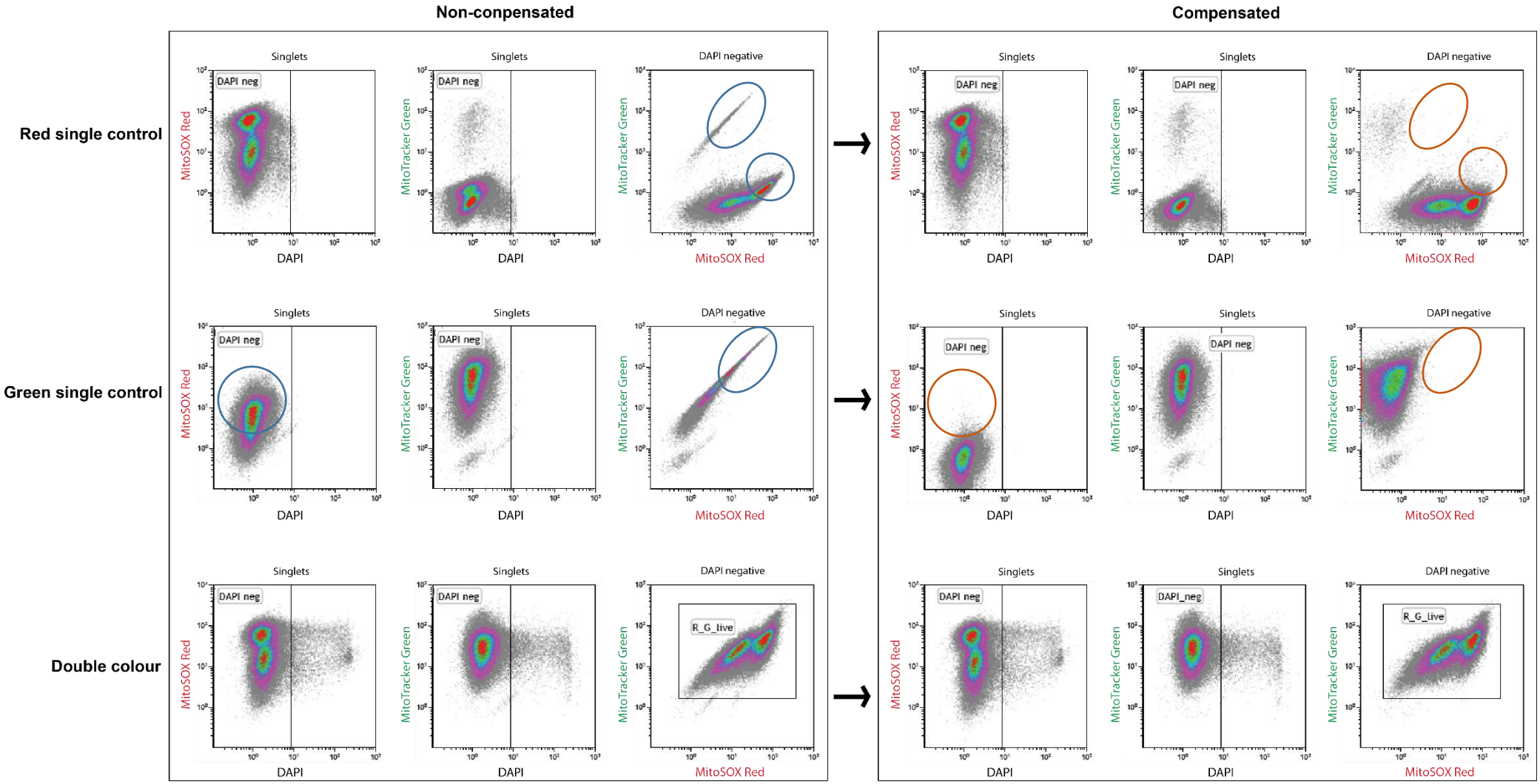

Figure 2.3.2: Flow cytometry compensation.

Primary gating was performed similarly to Figure 2.3.1. Red single colour was compensated for the spill-over of fluorescence to the green channel. This compensation was applied to Green single colour control for further adjustment. Blue circles showed where spill-over appeared, red circles showed spill-over was corrected. All adjustments were combined in a matrix to apply to double colour staining.

Table 2.3.2. Compensation matrix applied to all samples in one experiment.

Auto fluorescent (%)	FL1	FL3	FL6	FL8
FL1	100	1.1	0	0
FL3	11.89	100	0	0
FL6	0	0	100	0
FL8	0	0	0	100

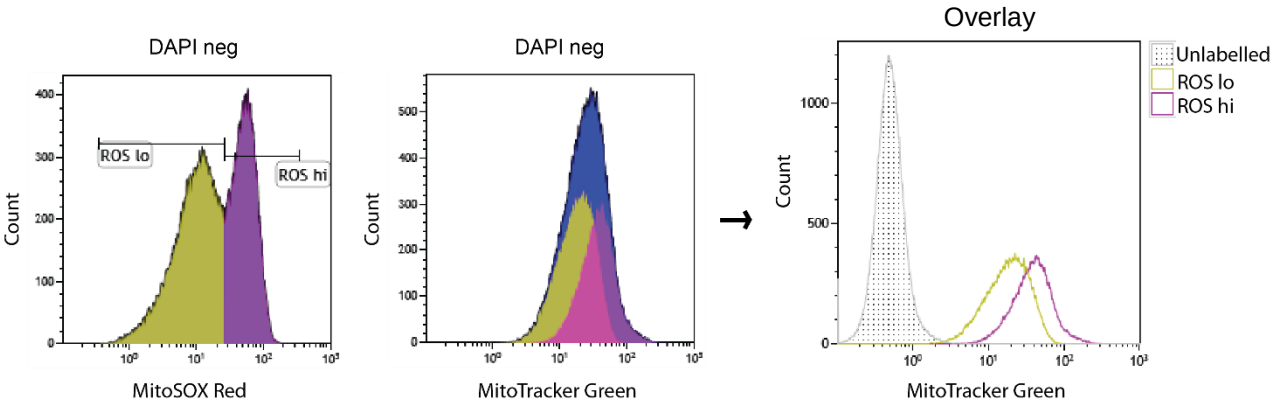

Figure 2.3.3. Mitochondrial membrane potential of ROS^{lo} and ROS^{hi} populations

Gated ROS^{lo} and ROS^{hi} populations were overlayed under Mitotracker Green parameter. Overlay histogram was used to generate statistical numbers for Green fluorescence.

2.3.5. Statistical analysis of flow cytometry data

GraphPad Prism version 6.05 were used for statistical analysis. The comparison between two conditions was performed in paired 2-tailed t-tests. Paired-difference and paired-ratio were acquired to examine the different and fold change difference in each treatment when compared to controls. Graphs were generated from the mean values from all replicates. SEM (standard error of the mean) was used to generate error bars.

2.4. Western Blot

2.4.1. Buffer preparation

i. Hypotonic buffer

Components	**Concentration**
HEPES	10 mM
KCl	10 mM
EDTA	0.1 mM
EGTA	0.1 mM
Protease inhibitor cocktails	1U (freshly added before use)
DTT	1 mM

ii. 4x Laemlli buffer

Components	**Concentration**
Tris HCl pH 6.8	50mM
SDS	2%
Glycerol	10%

iii. SDS-PAGE running buffer – Freshly made and cooled before use

Components	**Concentration**
Glycine	25 mM
Tris base	192 mM
SDS	0.1%

iv. Transferring buffer

Components	**Concentration**
Glycine	25 mM
Tris base	192 mM
Methanol	20%

v. Washing (TBST) buffer

Components	Concentration
Tris pH 7.4	50 mM
NaCl	150 mM
Tween 20	0.5%

vi. Blocking buffer

5% skim milk in PBST

2.4.2. Protein extraction

Cells were collected into Eppendorf tubes and washed with PBS. Cell pellets were snap frozen in liquid nitrogen and stored at -80^{o}C. Cells were lysed in ice cold hypotonic buffer lysis buffer. After 15 minutes incubation on ice, 1/10 volume of 10% IGEPAL CA-630 (Sigma, I8896) was added to the lysed cell, vortexed for 10 seconds and returned on ice. To ensure full protein extraction, lysed cells were sonicated for the total time of 30 seconds (3x 10 second intervals). Cell lysates were inverted for another 30 minutes on a rotator in the 4^{o}C cold room. Cell lysates were then centrifuged at 15000 rcf at 4^{o}C to remove cell debris. The supernatants containing soluble proteins were transferred into new labelled Eppendorf tubes. After the quantification step of protein concentration, cell lysate was diluted to the concentration of 2mg/mL in Laemlli buffer and aliquots were immediately stored at -20^{o}C for short term use and at -80^{o}C for long-termed use.

2.4.3. Protein quantitation

Protein quantitation was performed using a Pierce BCA protein assay kit (Thermo Scienctific, Ref: 23227) following the protocol provided by the manufacturer. Accordingly, 5 µL of each lysate was diluted into 20 µL of PBS (1:5 dilution). Then, 8 µL of each dilution was measured in duplicates in a 96-well clear plate at the same time with standard protein samples. Each well were mixed with 64 µL of 50:1 mixture of Reagent A – Reagent B. The plates were then incubated at 37^{o}C for 5 minutes before detection for quantitation. Colours of protein-reagent mixture were absorbed at 550 nm in the Spark 20M Tecan plate reader.

2.4.4. SDS-PAGE (sodium dodecyl sulfate polyacrylamide gel electrophoresis)

Before loading on the gel, fresh 10mM DTT and 5% βME were added to the protein lysate and boiled for 10 minutes at 90^{o}C. Cooled 20 µg protein lysate from each sample was loaded on 12% acrylamide gel (Bio-rad, Ref: 546-1045) at the same time with pre-stained protein ladder (Thermo

Fisher, Ref: 26619). The. SDS-PAGE was performed in cold running buffer using Bio-rad electrophoresis equipments at room temperature at 160 V for 50 minutes. Protein from the gel was then transferred onto a nitrocellulose membrane (Thermo Fisher, Ref: 88018) using a transferring cassete from Bio-rad. The cassete was then merged into cold transferring buffer. Transfering was performed using Bio-rad transferring tank in a cold room at 4^{o}C at 110 V for 65 minutes. After transferring, the membrane was washed twice (5 minutes/each) in TBST buffer and then incubated in blocking buffer for an hour at room temperature on a orbital shaker at low speed.

2.4.5. Blotting the proteins and visualisation

The membrane was incubated with primary antibodies (listed in Table 2.4) in 1:5 dilution of blocking buffer overnight at 4^{o}C with regular mixing. The membrane was then washed 3-4 times in TBTS (5 minutes/each) and incubated again in HRP conjugated secondary antibodies (listed in Table 2.4) for an hour at room temperature with regular mixing. Finally, the membrane was washed 3-4 times in TBST (5 minutes/each) and incubated with ECL mixture (Amersham ECL Western Blotting Analysis sytem, Ref: RPN2109) for 3 minutes. The membrane was visualised under chemluminescent exposure in the AI600 Amersham imager.

Table 2.4.1. List of antibodies

	Antibodies	Company	Cat#	Lot#	Dilution		
					WB	IF	Flow cytometry
Primary Ab	Rabbit polyclonal - Anti-Mouse Oat	Abcam	Ab137679	GR145275-29	1:1000	1:500/ 1:750	
	Rabbit polyclonal - Anti-Mouse Prodh	Abcam	Ab93210	GR293737-1	1:100/ 1:200	1:100/ 1:200	
	Mouse monoclonal - Anti-COX IV	Abcam	Ab33985	-	1:500	1:500	
Secondary Ab	HRP-conjugated Goat polyclonal - Anti-Rabbit	DAKO	P0448	000072118	1:5000		
	Alexa Fluor 488-Goat Anti-Rabbit IgG	Invitrogen	A11034	760000		1:1000	
	Alexa Fluor 594 Goat Anti-Mouse IgG	Invitrogen	A11032	621333		1:1000	
Dyes	DAPI (4’,6-Diamidine-2’-phenylindole dihydrochloride)	Sigma Aldrich	32670	-		1 µg/ml	1 µg/ml
	MitoSOX Red	Life Technologies	M36008				5 mM
	MitoTracker Green	Life Technologies	M7514				3 mM
	Hoechst	Life Technologies	H3570			1 µg/ml	

2.4.6. Western Blot quantitation

Data collected from Amersham Imager AI600 were analysed either from provided program conjugated with the Imager program or by a separated program, ImageQuantTL 1D v8.1. Protein lanes were manually aligned and bands was manually or automatically detected. Normalisation were performed by to GAPDH bands. Normalised values or Normalised volume values were collected for statistical analysis.

2.5. Immunocytochemistry

2.5.1. Immunocytofluorescence

Cells were seeded either on a 0.1% gelatine coated black 96-well plate (BD Falcon, Ref: 353219) or an 8-well imaging chamber (Sigma Aldrich, Ref: C7182-1PAK) and incubated for growth in up to 12 hours (if in imaging chamber) and 24 hours (if 96-well plate). Cells were collected and washed three times in cold PBS and then fixed with 100% methanol for 10-20 minutes at -20^{o}C. After three washes (5 minutes/wash) in cold PBST on a shaker at a medium speed, PBST containing 10% serum was added to the cells to perform antigen blocking. In this blocking step, cells were incubated for 1 hour on a shaker at a medium speed. After blocking buffer is removed, cells were immediately incubated in primary antibody on a shaker in a 4^{o}C room overnight. All antibodies were prepared in PBST and 1% serum and the working concentrations are stated in Table 2.2. The next day, cells were washed three-to-five times and incubated with secondary antibodies and DAPI for an hour on a shaker at room temperature and are covered by a dark chamber. Finally, cells were washed three-to-five times with cold PBST. Cells were kept in PBST and protected from light at 4^{o}C for microscopic examination. If cells were grown in imaging chamber, after incubation with secondary antibodies and DAPI and washing, the chamber wells were detached. Excessive water was tap dried on a paper towel and cells were covered with a thin layer of 20-50 µL of Fluoroshield (Sigma, F6182) followed by a glass coverslip.

2.5.2. Live cell imaging

All live cell imaging was performed under the inverted Leica DMIRB microscope. For examination of ROS visualisation in live cells, cells were plated at the rate of 2 x 10^5 cells in 100 µL medium in each well of an optical 96-well plate (BD Falcon #353219), coated with 0.1% gelatine. Similar treatments and ROS dyes were applied similarly to flow cytometry method. After that, media were removed, and the cells were gently washed twice with PBS and then covered in imaging buffer

(See section 2.3.1). Hoechst (Life Technologies, H3570) was used as per manufacturer's procedure in imaging buffer. Imaging was performed under the inverted Leica DMIRB microscope. Images were taken by NIS v.6.4 program.

2.6. ATP assay

2.6.1. Enzyme and substrate preparation

Enzyme luciferase solution

Components	Concentration
Firefly luciferase	10 µg/ml
DL-dithiothreitol (DTT)	75 µM
Magnesium chloride (MgCl2)	6.25 mM
EDTA	625 µM
Bovine serum albumin (BSA)	1 mg/ml in 25 mM 4-(2-hydroxyethyl)piperazine-1-ethanesulfonic acid (HEPES) buffer, pH 7.25

Substrate luciferin solution

Components	Concentration
D-luciferin	600 µM
DTT	75 µM
$MgCl_2$	6.25 mM
EDTA	625 µM
BSA	1 mg/ml in 25 mM HEPES buffer, pH 7.25

Enzyme-substrate solution:

Enzyme and substrate solution was mixed at 1:1 ratio and incubated at room temperature for 10 minutes before use.

Lysis buffer

Components	Concentration
EDTA	4 mM
Triton X-100	0.2 %

2.6.2. ATP detection and quantitation

Cells were seeded in a 96-well plate at $1x10^4$ cells/well in 100 µl growth medium. After 24-hour incubation under standard conditions, cells were washed three times in 100 µl PBS and then lysed in 100 µl lysis solution for 5 minutes at room temperature (RT) on an orbital shaker at medium speed. After that, 10 µl of cell lysate was prepared in triplicates in a white opaque U-bottom 96-well

plate with standard ATP samples (for standard curves). Immediately before measurement, 90 µl of 1:1 enzyme-substrate solution was added on to each well. Luminescence produced from the ATP-dependent oxidation of luciferin by luciferase enzyme was in the Spark 20M Tecan plate reader. An ATP standard curve was generated to quantitate the level of ATP (µM) produced by each sample. This measurement was then normalised to the total protein (see section 2.5.3) of each sample to allow comparation between different treatments and cell types.

2.7. NADP/NADPH assay

Cells were seeded in duplicates in 24-well plates at $4x10^5$ cells/well and incubated in standard conditions. After 24 hours, cells were washed 2 times in PBS and lysed in 200 µl lysis buffer (recipe in section 2.7.1). Lysing process was performed quickly at room temperature by vigorously pipetting the cells in cold lysis buffer. Then 100 µl of lysate was transferred into a fresh tube containing 22 µl cold perchloric acid 2M (PCA) for deproteinisation. The mixture was vortexed for 5 second at full speed and incubated on ice for 5 minutes. The mixture was then spun at 4^{o}C at 13000 rcf for 2 minutes to separate precipitated protein. Then, 100 µl of the aqueous solution was transferred into a fresh tube containing 25 µl KOH 2M and 3 µl KOH 0.1M and shortly vortexed for neutralisation of PCA. No incubation was required for this step. The solution was then spun at 4^{o}C for 15 minutes at 1300 rcf for the removal of precipitated PCA. After that, 100 µl of the final solution was transferred into a fresh tube. From this tube, 30 µl of solution was added in duplicates onto a black-wall, clear and flat bottom 96-well plate (BD Falcon, Ref 353219). Each well was then added with 30 µl of mixture of enzyme-substrate solution (Abcam, Ref: ab186033) prepared as suggested by the manufacturer. The plate was incubated at room temperature for 10 minutes on an orbital shaker at medium speed. Colours from the reaction of NAPD with the enzyme-substrate solution were measured at the absorbance wavelength of 460 nm every 5 minutes for 8 consecutive times in the Spark 20M Tecan plate reader.

2.8. Cell proliferation assay

Cells were seeded in triplicates in four 24-well plates at $1x10^4$ cells/well in 500 µl growth medium. After 24 hours (day 1), plate 1 was collected to set up basal number. Cells were washed twice and then trypsinised into 500 µl PBS. Cells were counted on a counting chamber and set up as a baseline. On day 2, plate 2 were collected similarly to plate 1 and cells in plate 3 and 4 were fed with fresh media. Similar processes were continued on day 3 and 4 until all plates were collected.

Collective cell counts were used to generate the proliferation curves for different cell types and treatments. Proliferation rate was calculated as previously described (Sherley et al., 1995).

Chapter 3 Proline metabolic enzyme family is differentially expressed in different pluripotent states of ES cells

3.1. Introduction

In mammalian cells, proline metabolism is a key node in the metabolic network that links mitochondrial activities to cytosolic redox reactions and is involved in cell programming and decision making (Washington et al., 2010, Casalino et al., 2011, Elia et al., 2017, Liu et al., 2015, Liu et al., 2012). Studies of proline metabolism suggest that proline metabolism is variable in different cell types and the proline metabolic switch is required as the cells reach a particular state (Adams and Frank, 1980, Elia et al., 2017, Liu et al., 2015, Phang et al., 2012). However, the purposes of this variation in relation to cell growth and functioning are not well characterised. In cancers, metastatic cells favoured the consumption of exogenous proline when compared to attached cells (Elia et al., 2017). It is important for tumour cell growth and T lymphocyte activation to switch from free proline catabolism to proline biosynthesis using glutamine and ornithine resources (Wang et al., 2011, Liu et al., 2015). These studies raise the possibility that different proline metabolic processes are important to cell fate determination and can be regulated in different states of the cell development. However, the regulation of proline metabolic switches remains under-investigated and the precise mechanism of their regulatory effects go unresolved.

Embryonic stem (ES) cell differentiation is a cell development system in which proline metabolism plays a regulatory role (Comes et al., 2013, Washington et al., 2010, Casalino et al., 2011, Tan et al., 2016a, Tan et al., 2011). Studies have shown that the differentiation of primed ES cells in response to proline is specific to L-proline (Washington et al., 2010, Tan et al., 2011). The regulation of the proline primary transporter, Snat2, was found to be higher in primed- compared to naïve ES cells and proline uptake was required for ES cell differentiation (Tan et al., 2011). The involvement of the proline oxidation enzyme, Prodh, was suggested (Casalino et al., 2011, Tan et al., 2016a), however, it is not known whether the regulation of Snat2 is correlated to Prodh activity in proline-induced ES cell differentiation. The expression of Snat2 is varied in different cell types and may be dependent on the condition of the environment (Velazquez-Villegas et al., 2014, Jones et al., 2006). In human trophoblast cells,

the expression of SNAT2 is regulated via the active STAT3 signalling pathway, which is triggered by the cytokine IL-6 (Jones et al., 2009). The reduction of SNAT2 expression was observed in *STAT3* knockdown cells, suggesting that STAT3 is directly upstream of SNAT2 (Jones et al., 2009, Borg et al., 2015). The decreased level of phosphorylated STAT3 and SNAT2 expression was correlated with lower SNAT2-specific amino acid levels that were transported into the cells (Jones et al., 2009), which illustrates the relationship between STAT3 activation and SNAT2 function in cellular amino acid transport. In human ES cells, the phosphorylation activation of STAT3 is mediated by the LIF receptor signal via the binding to exogenous LIF (Daheron et al., 2004). The presence of LIF in ES cell culture is important to the cell self-renewal, and LIF is associated with STAT3 activation in maintaining ES cells (Daheron et al., 2004, Morgani and Brickman, 2015, Onishi and Zandstra, 2015). However, the role of LIF in ES cell culture and the contribution to SNAT2 expression has not been addressed.

Carbognin et al suggested that the proliferation of ES cells, which are cultured in 2i conditions and LIF, required Stat3 activation that led to increased mitochondrial respiration (Carbognin et al., 2016), and may be a “spare capacity” in addition to the basal glycolysis energy supply under LIF/Stat3 signalling (Carbognin et al., 2016). It is questionable if LIF/Stat3 signalling and Snat2 are correlated to enhance mitochondrial respiration by increasing the amino acid uptake into the cells. In fact, the LIF/Stat3 pathway is important for ES cells in the reprograming to naïve pluripotency (van Oosten et al., 2012, Tang et al., 2012). Snat2 expression was found to be low in naïve ES cells and upregulated in the primed state (Tan et al., 2016b). The observation of human embryos transcriptome revealed that SNAT2 expression was lower in cells in the morulae state than cells in the blastocysts (Vassena et al., 2011). In mice preimplantation embryos, Snat2 expression was lower in cells at early embryonic day 3.5 (E3.5i) compared to those at the later time E3.5 (E3.5ii) (Tan et al., 2016b). It is possible that the regulation of the proline uptake is important for pluripotent cells during development. Questions then arise as to whether the variation of Snat2 expression is correlated with the activities of proline metabolism in the cells, given that Snat2 is required for proline uptake in ES cells (Tan et al., 2011). That leads to the hypothesis that proline metabolic enzymes are also regulated in different pluripotent states of ES cells: naïve, primed and primed + proline. In this study, we defined primed state ES cells as the cells that were derived from the inner cell mass of the embryo and were released from 2i containing media.

This primed state must be distinguished from the primed state that is normally assigned to epiblast-derived stem cells (EpiSCs) or epiblast-like cells (EpiLCs), which are at the later state along the pluripotent lineage specification.

The proline metabolic enzyme family has been nominated as a new target for the treatment of cancers and other pathological diseases such as stroke, neurodegeneration, and diabetes, due to the fact proline metabolic reprograming is known as a requirement for the cell changes in the adaptation to new functions and to support the cell growth in tumorigenesis (Elia et al., 2017, Liu and Phang, 2012, Liu et al., 2012, Liu et al., 2015, Wu et al., 2011). Understanding the regulation of proline metabolism via its enzyme family in a normal cell development system such as ES cells could advance future research efforts in cancer treatments. To examine the regulation of proline metabolic process in ES cells, this chapter will determine the expression of the proline enzyme family involved in proline transport, catabolism and biosynthesis. This will assist our understanding of the proline metabolic processes that are associated with ES cell pluripotency. Genes that are involved in these processes, including *Slc38a2, Prodh, Pycr1, Pycr2, Pycrl, Oat, Aldh4a1, Aldh18a1* and *P4ha1* (Figure 3.1.1) will be investigated for their expression in ES cells of different pluripotent states.

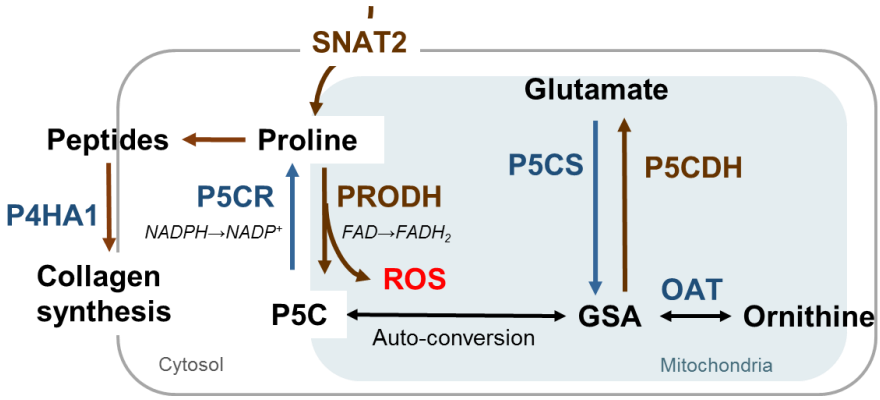

Figure 3.1.1. Proline metabolic pathway in mouse ES cells.

SNAT2 (Slc38a2): transporter sodium-dependent neutral amino acid transporter-2. **PRODH** (Prodh): proline dehydrogenase. **P5CR** (Pycr1): P5C reductase. **P5CDH** (Aldh4a1): P5C dehydrogenase. **OAT** (Oat): ornithine aminotransferase. **P5CS** (Aldh18a1): P5C synthase. **P4HA1**: Prolyl 4-hydroxghovbylase subunit alpha 1 (P4ha1) **P5C**: Δ-pyrroline-5-carboxylate. **ROS**: reactive oxygen species. **GSA**: glutamic-gamma-semialdehyde.

3.2. Results

3.2.1. Morphological investigation of ES cells in different pluripotent states and culture conditions

After 4 days in culture, the morphology of D3 and WA30 cells in different pluripotent states were observed under the microscope. Morphological heterogeneity was observed in all conditions and from both cell lines. However, each pluripotent state displayed distinct characteristics related to the major populations of those cell states (Figure 3.2.1.A and B). ES cell colonies growing in 2i+LIF conditions reflected the naïve pluripotent state, which were round, compacted and domed with defined edges. ES cells in Serum+LIF conditions were partially flattened and the edge of each colony became irregular in shape. With the addition of proline, ES cells were more flattened and showed irregular colonies. The morphology of ES cells in each condition were matched to the descriptions in the literature, thus confirming that ES cells were at the right pluripotent state (Ying et al., 2008, Washington et al., 2010). ES cells in 2i conditions exhibited similar patterns of morphology between LIF and non LIF conditions. However, non LIF conditions appeared to supress ES cell growth in 2i. Increased cell death and cell float were observed in both D3 and WA30 cell lines cultured in 2i–LIF conditions (Figure 3.2.1.C and D), suggesting that ES cells require LIF for their maintenance and self-renewal. The release from 2i appeared to be stressful to WA30 ES cells, which resulted in increased cell death after 4 days (Figure 3.2.1.D). The addition of proline to these cells further stressed the cells and inflated cell death rate.

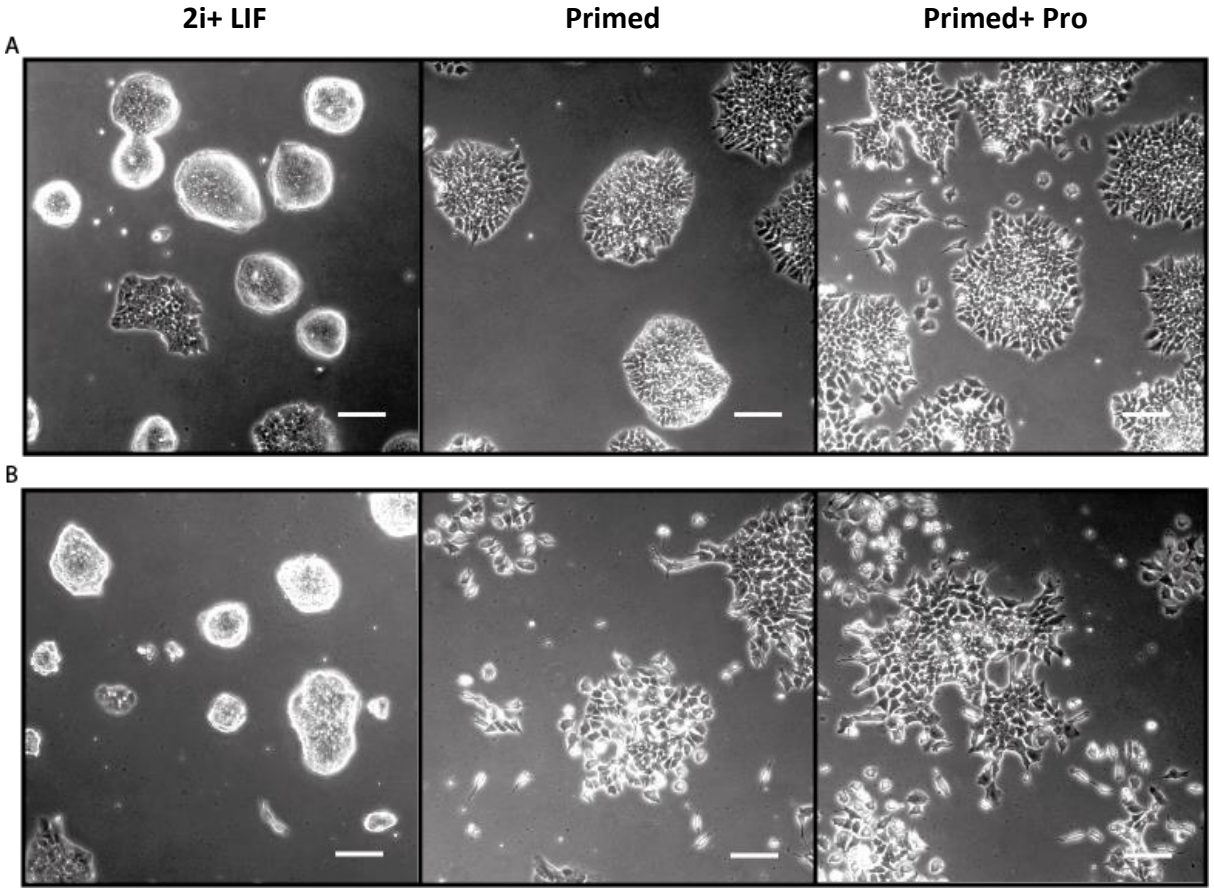
2i+ LIF
Primed
Primed+ Pro
A
B

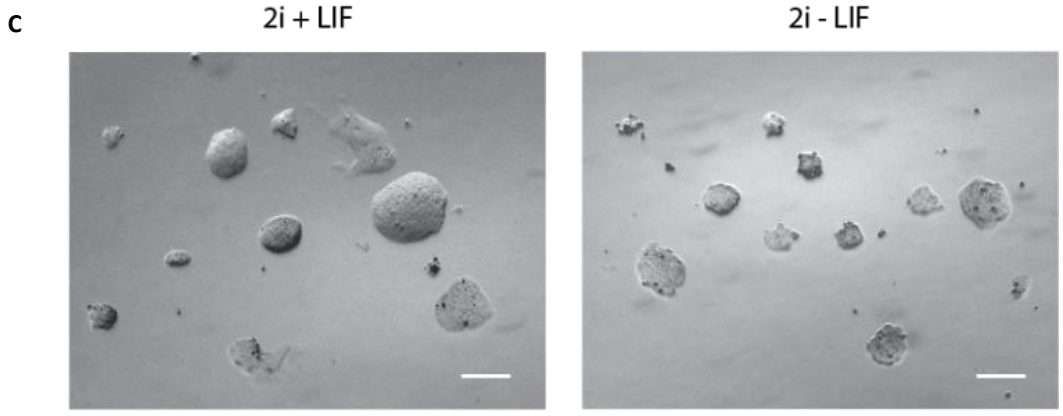
c
2i + LIF
2i - LIF

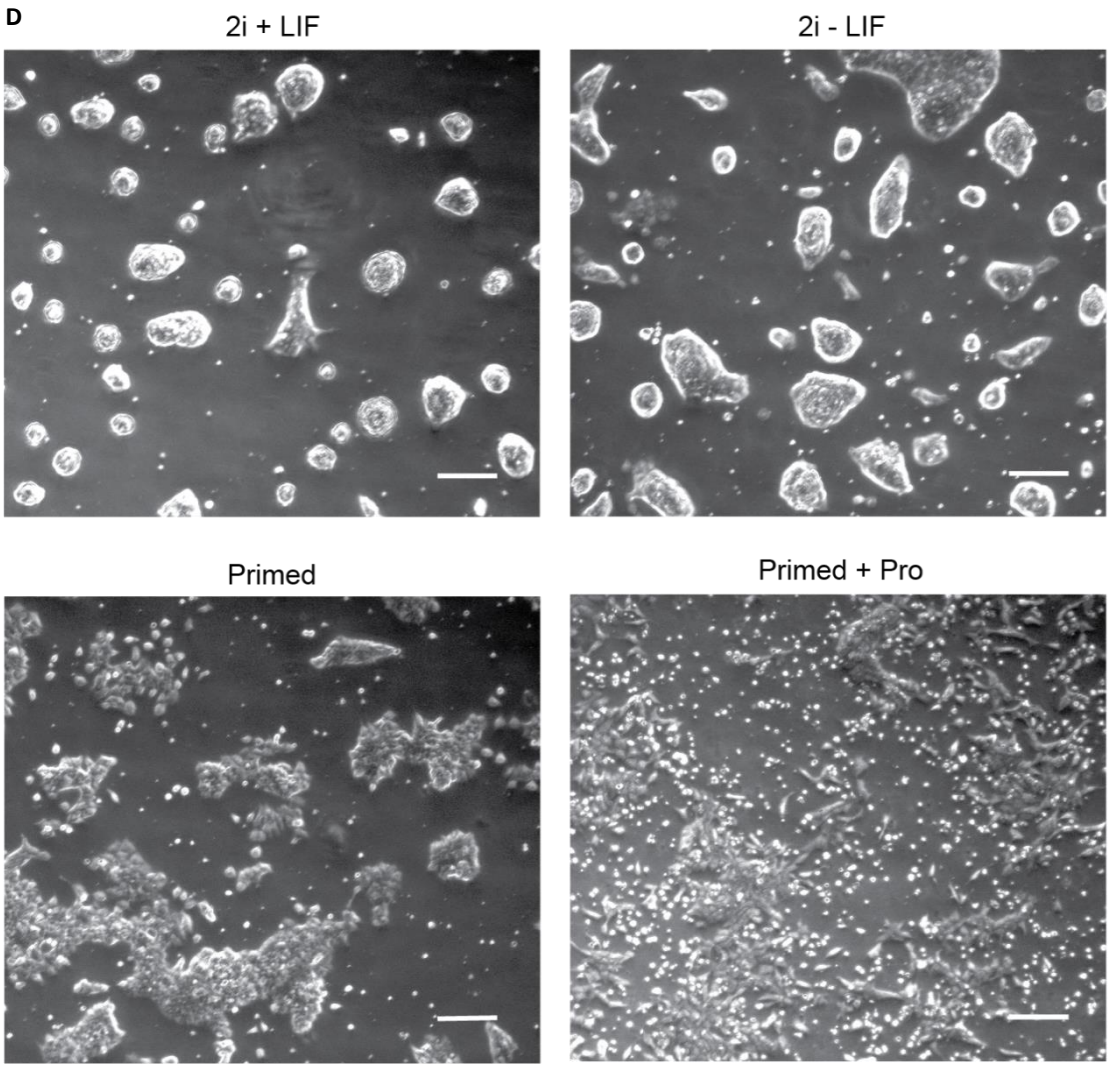

Figure 3.2.1. Morphology of ES cells in different culture conditions

Cell morphology was observed after 4 days in culture**. A.** D3 and **B.** WA30 ES cell lines in 3 conditions: 2i+LIF, Serum+LIF and Serum+LIF+Pro. **C.** D3 ES cells in 2i+/-LIF. **D.** Overlooking WA30 ES cells in 4 conditions showing white dead cells detached from the adhered colonies. In **A** and **B**, scale = 100 µm. In **C** and **D**, scale = 200 µm.

3.2.2. The expression of proline metabolic enzymes in ES cells was subject to regulation in different pluripotent states and different culture conditions

To investigate proline metabolism in ES cells, the key enzymes of the proline metabolic reaction chain were separated into three different processes: biosynthesis, transportation, and catabolism. The primary proline transporter expression, *Slc38a2*, was examined in different ES cell states and conditions in both D3 and WA30 cell lines. Given that *Slc38a2* gene expression is correlated with the expression of Stat3 protein (Jones et al., 2009) and Stat3 is affected by the presence of LIF (Liu et al., 2013, Onishi et al., 2014), it was questioned if the presence of LIF could affect *Slc38a2* gene expression. However, only naïve ES cells could be maintained without the addition of LIF and therefore, to examine the effects of LIF in ES cell culture, only naïve ES cells were cultured with or without LIF in 2i. Examination of *Slc38a2* expression was performed in 2i+/-LIF conditions in both D3 and WA30 cell lines. In the D3 ES cell line, there was a small but significant increase in *Slc38a2* expression in the 2i+LIF condition when compared to the 2i-LIF condition (Figure 3.2.2.A). However, the ratio of *Slc38a2* expression between the two conditions was not significantly different, suggesting that the addition of LIF only added a shift to *Slc38a2* expression in 2i medium but did not create a major effect upon the expression of the gene. WA30 cells did not exhibit any changes in *Slc38a2* expression in 2i+/-LIF conditions. When examined in different pluripotent states, *Slc38a2* was expressed higher in primed, but not in the naïve state of ES cells in both D3 and WA30 lines (Figure 3.2.2.B). This result is consistent with previous findings in the literature (Tan et al., 2016b). In D3 ES cells, the addition of proline reduced *Slc38a2* expression after 4 days of culture (Figure 3.2.2.B). However, there was no significant changes in *Slc38a2* expression observed in WA30 ES cells with the addition of proline.

The expression of the proline catabolic enzymes was investigated in different pluripotent states to confirm whether proline metabolism is similar in the cells of all pluripotent states. The proline catabolic process includes the oxidation of proline to P5C by Prodh. And P5C is further converted into glutamate by the enzyme P5C dehydrogenase (P5Cdh or Aldh4a1). After all, proline from the original source is expected to be converted to different metabolites and synced to other sites of cell activities. The enzyme Oat is bidirectional and can convert P5C into ornithine to remove proline out of the proline cycle. The direction of Oat catalytic activity is largely dependent on the environment; however, it

was suggested that Oat may have more potential in breaking down ornithine to form P5C (Ginguay et al., 2017). Therefore, in this study, Oat is classified as a proline biosynthetic enzyme for further examination. Alternatively, the incorporation of proline into peptides and then proline hydroxylation by prolyl-hydroxylase (P4ha1) enzyme also removed free proline from the reaction chain. These key enzymes: Prodh, P5Cdh and P4ha1 were examined for their gene expression. Both D3 and WA30 cell lines showed a higher expression of *Prodh* in the primed than naïve ES cells (around 2- to 3 folds) (Figure 3.2.2.C). There is no difference in the expression of *Aldh4a1* in all pluripotent states. *P4ha1* was highly expressed in the naïve state of D3 but not WA30 ES cells. No literature has suggested similar findings.

Proline biosynthesis from ornithine and glutamate can be performed by 3 different reactions, including the conversion of ornithine, and glutamate to P5C/GSA, which is then reduced to synthesise proline. P5C/GSA can be utilised either from ornithine by the enzyme Oat and from glutamate by the enzyme P5C synthase (P5Cs or Aldh18a1). P5C, but not its interconversion form, GSA, is reduced by the P5C reductase family (P5Cr or Pycr) to form proline. The examination of these genes showed that naïve ES cells significantly expressed higher *Oat* (~3 folds) than primed ES cells (Figure 3.3.2.D). No difference in the expression of three isoforms of the Pycr enzymes, *Pycr1*, *Pycr2* and *Pycrl* was observed in D3 ES cells, however, *Pycr2* was reduced in primed WA30 ES cells. While the addition of proline into primed ES cells significantly decreased the expression of *Aldh18a1* in D3 cells, only a minor reduction was observed in WA30 cells (Figure 3.2.2.D). This result has not been shown elsewhere in the literature.

In summary, key proteins and enzymes of the proline metabolic reaction chain were found to be differentially expressed in different pluripotent states of ES cells. This was replicable in both D3 and WA30 cell lines. LIF only had a minor effect on the expression of *Snat2* in 2i medium in D3 ES cells and did not have any effects on any other genes examined in this experiment. Except for *Prodh* and *Oat*, the expression of other proline metabolic enzyme genes might have been subjected to the long-term maintenance of the cells and they were more sensitive to the variation in culture in the WA30 cell line when compared to D3 ES cells. Due to the robust differential expression in naïve and primed ES cells, *Prodh* and *Oat* were selected for protein expression validation. These findings are novel and may need further validation with different cell lines and culture conditions.

A

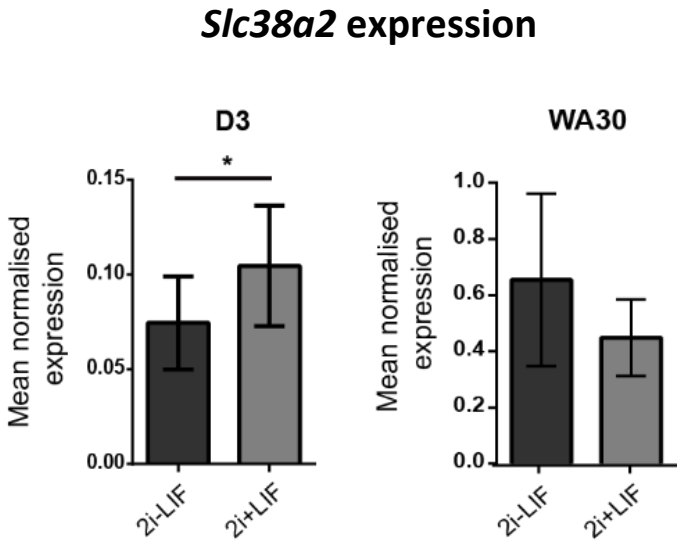
Slc38a2 expression
D3
WA30
Mean normalised expression
0.15
0.10
0.05
0.00
1.0
0.8
0.6
0.4
0.2
0.0
*
2i-LIF
2i+LIF

B

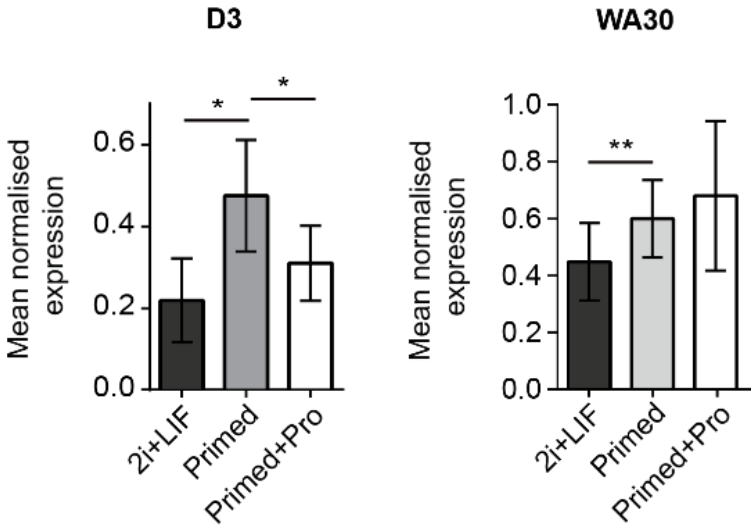
Slc38a2 expression
D3
WA30
Mean normalised expression
0.6
0.4
0.2
0.0
1.0
0.8
*
**
2i+LIF
Primed
Primed+Pro

C

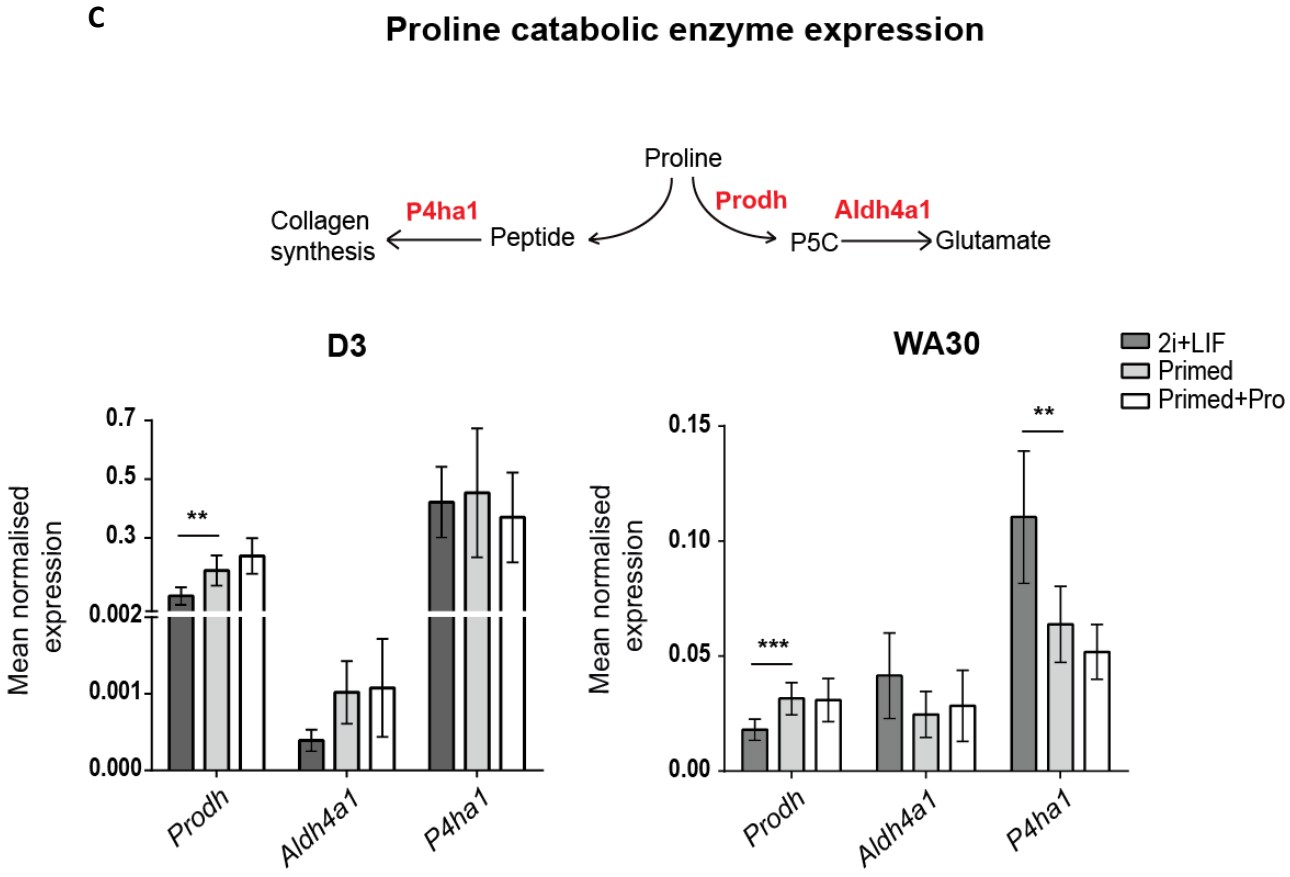
Proline catabolic enzyme expression
Proline
Collagen synthesis
P4ha1
Peptide
Prodh
Aldh4a1
P5C
Glutamate
D3
WA30
2i+LIF
Primed
Primed+Pro
Mean normalised expression
0.7
0.5
0.3
0.002
0.001
0.000
0.15
0.10
0.05
0.00
**
***
Prodh
Aldh4a1
P4ha1

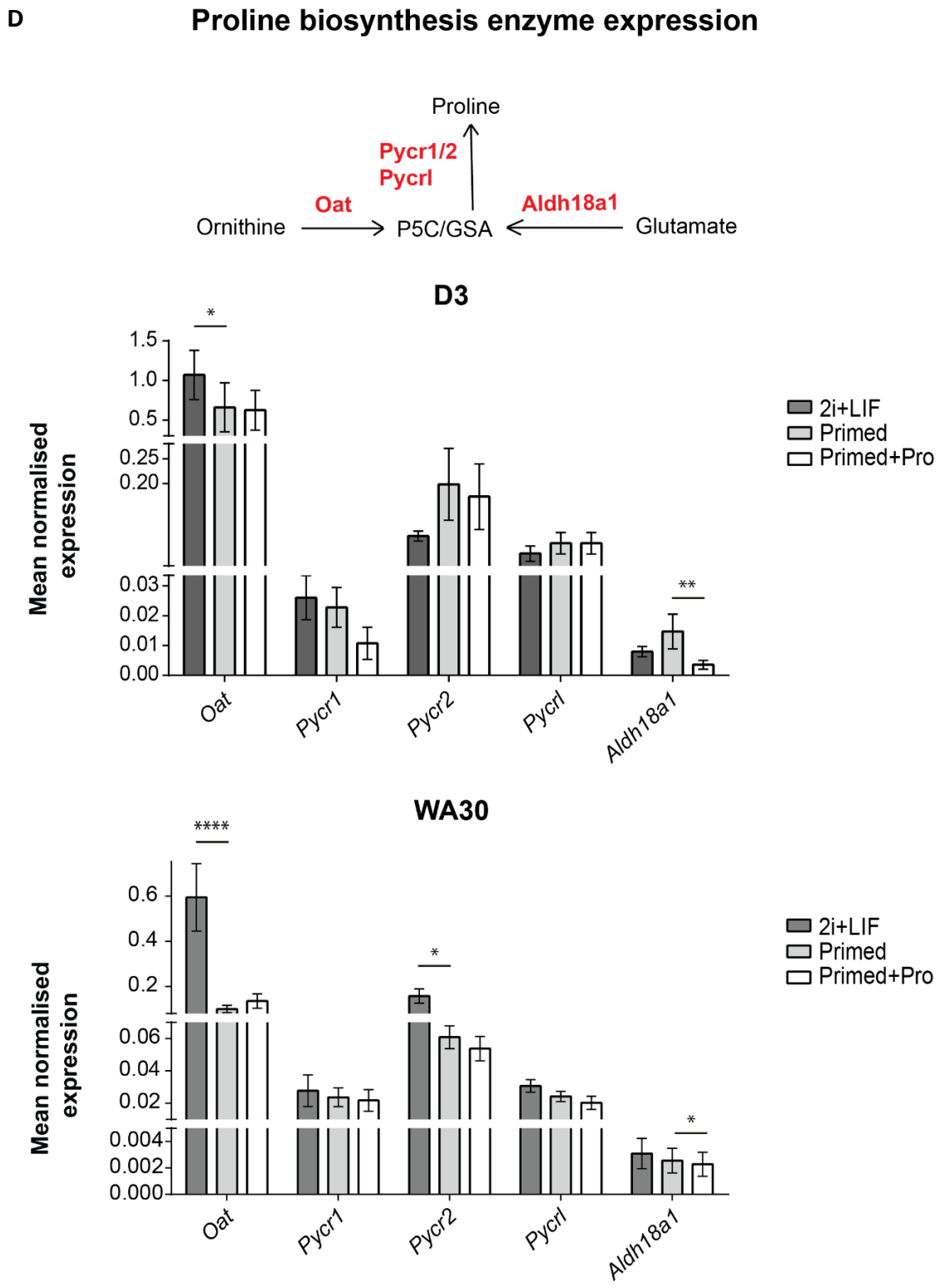

Figure 3.2.2. Gene expression of the proline metabolic enzymes.

A. Proline transporter**,** *Slc38a2* expression in 2i+/-LIF conditions in D3 and WA30 cell lines. **B.** *Slc38a2* expression in different pluripotent states of ES cells. **C.** Proline catabolic enzyme expression. **D.** Proline biosynthesis enzyme expression. **p≤0.05, **p≤0.01, ***p≤0.001, ****p≤0.0001, n=4-6. Error bar = SEM*.

3.2.3. Protein expression of Prodh and Oat confirmed their gene expression in different pluripotent states of ES cells

To confirm the gene expression results, Prodh and Oat proteins were examined by Western blot and immunofluorescence. In these experiments, only D3 ES cells were used. Western blot results illustrated that both Prodh and Oat proteins appeared with two isoforms in ES cells. These isoforms are here called large and small isoforms as based on their sizes. Only the functional isoforms of each protein (Prodh ~ 68 KDa and Oat ~ 49 KDa) provided by Uniprot database and also appeared in the liver and kidney samples, were used to compare for the differential expression of each protein. The other isoforms were unidentified by the Uniprot database and were not obvious in both mice liver and kidney samples (Data not shown). The protein expression of functional Prodh (68 KDa) was significantly higher (~ 9 folds) in primed ES cells when compared to their naïve counterparts (Figure 3.3.3.A). There was no significant difference in the large Prodh isoform (93 KDa) within the pluripotent states (Data not shown). The functional Oat enzyme (49 KDa) was expressed at around 37-fold higher in naïve- than primed ES cells, either with or without proline addition (Figure 3.3.3.B). No significant difference was observed in any comparison with large isoform of Oat (59 KDa). No follow up experiment was performed to identify the isoforms of Prodh and Oat. Possibly, they could be the result of unspecific staining of the antibodies in ES cells. The microscopic examination of Prodh and Oat protein was performed to identify the subcellular location of the proteins. Patchy and punctate staining was observed in both Prodh and Oat immunocytochemistry of naïve and primed ES cells. Prodh staining did not show any difference in the intensity between naïve and primed ES cells (Figure 3.3.4.A). The colocalisation of Prodh with Cox IV, a mitochondrial membrane protein, showed that Prodh was present within the mitochondria (Figure 3.3.4.A).

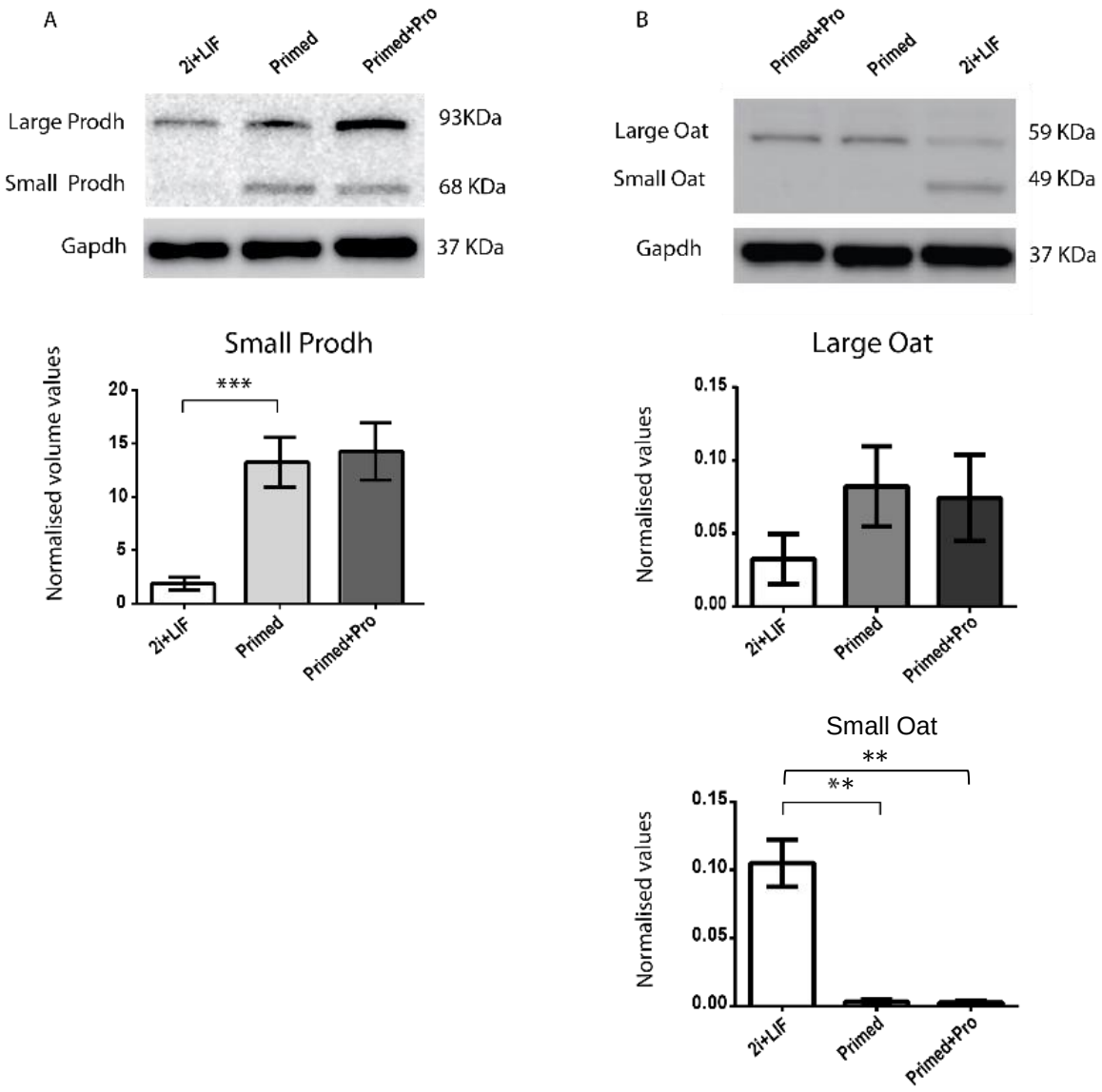

Figure 3.2.3. Protein expression of Prodh and Oat enzymes in D3 ES cells.

A. Prodh. **Column B.** Oat. ***p≤0.01, ***p≤0.001, n=3-6. Error bar = SEM.*

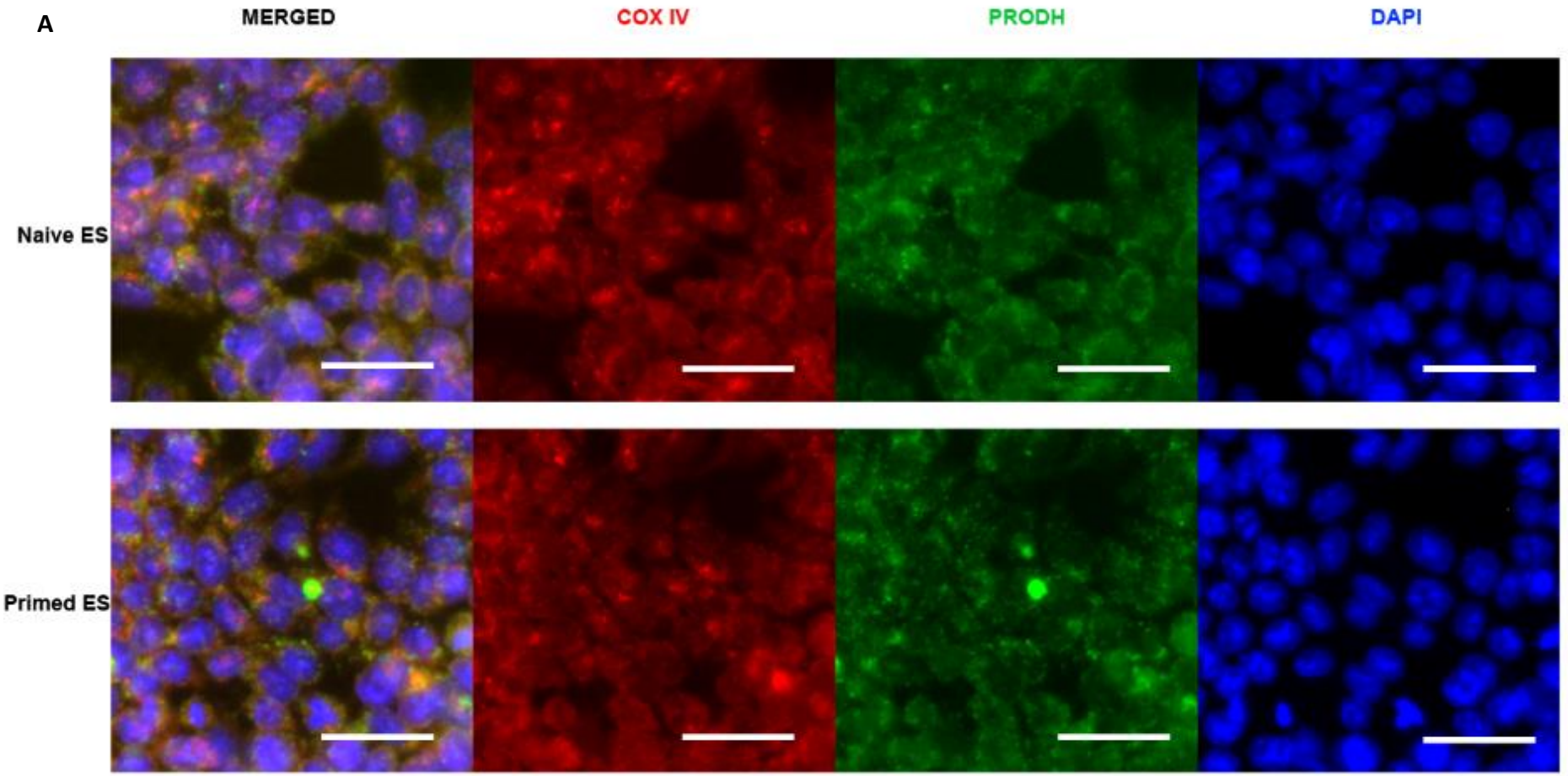
A
MERGED
COX IV
PRODH
DAPI
Naive ES
Primed ES

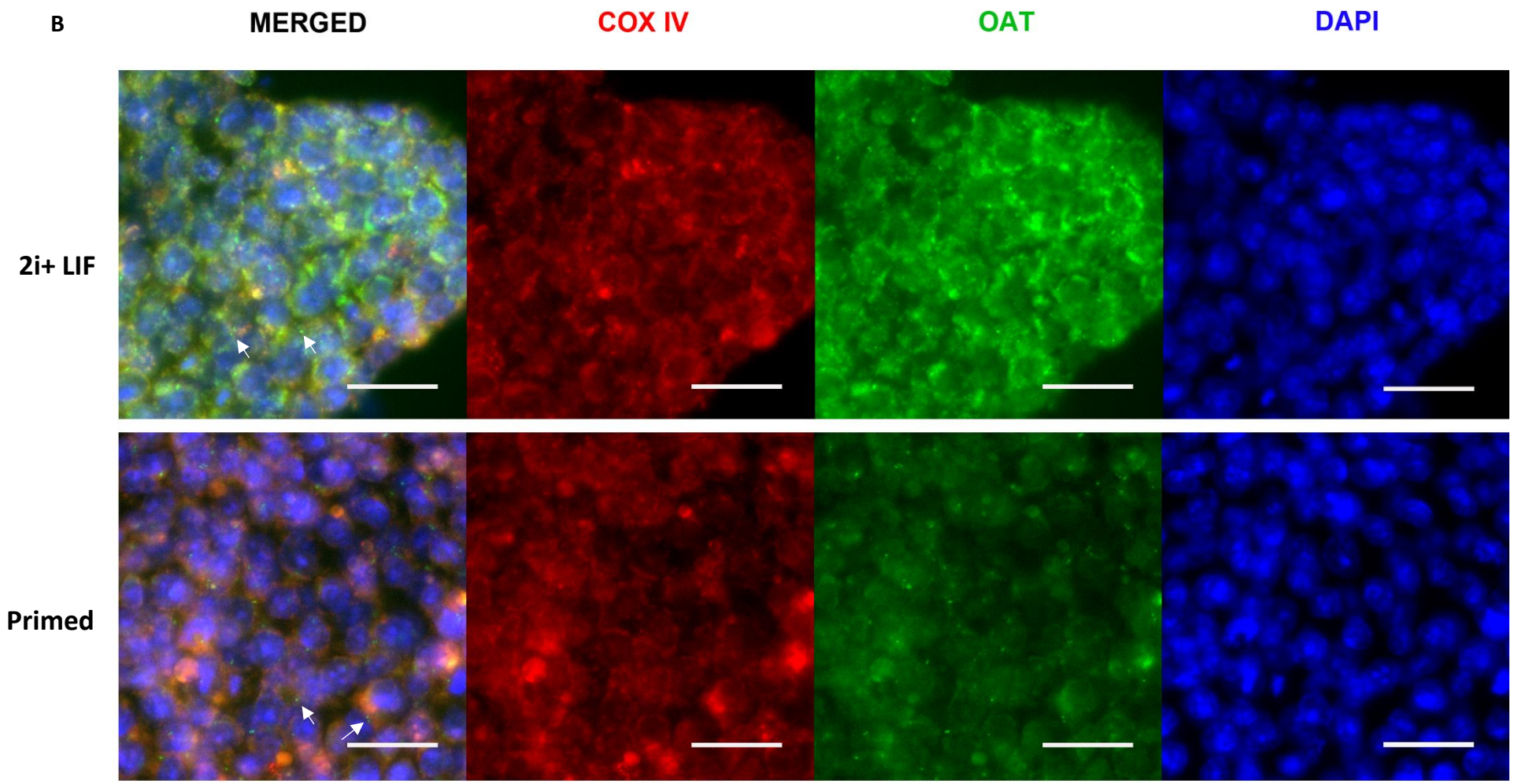

Figure 3.2.4. Immunofluorescent images of Prodh and Oat enzymes in D3 ES cells in two pluripotent state: Naïve (2i+LIF) and Primed.

A. Prodh. **B.** Oat. Arrows: pointing at protein accumulation in the perinuclear/cytosolic regions of the cells. All scales = 50 µm.

3.2.4. Pilot study: Image analysis of Prodh staining

Objectives

The immunofluorescent examination of Prodh protein in naïve and primed ES cells demonstrates signs of distinguished distribution across the cell areas. As Prodh is a mitochondrial enzyme and localised into the mitochondria (Figure 3.3.4.A), the differences in Prodh distribution are potentially associated with the mitochondrial distribution in ES cells. Mitochondria are dynamic organelles and play an important role in regulating cellular homeostasis of PSCs (Lees et al., 2017). The changes in the mitochondrial functions and distribution are known to be involved in PSC reprogramming and differentiation (Prowse et al., 2012, Suhr et al., 2010). The pluripotent lineage specification describes the natural changes of dynamic pluripotency towards the more committed cell states and differentiation (Savatier et al., 2017). Accordingly, there are states that are referred to as "no-returning points", occuring when the cells are committed to a certain pluripotency and a distinct differentiation potential. Both naïve and primed ES cells have a full potential for differentiation and while primed ES cells are more active to respond to differentiation factors, naïve ES cells are distinguished with infinite self-renewal capability in culture (Ying et al., 2008, Nichols and Smith, 2012). Previous evidence has shown that ES cells of different pluripotent states such as naïve and primed ES cells have distinct metabolic states and mitochondrial profiles (Kolodziejczyk et al., 2015). Alterations in metabolic preferences in naïve and primed ES cells are required to maintain cell growth and stabilisation (Sperber et al., 2015, Wu and Izpisua Belmonte, 2015) and changes in metabolism accommodate ES cells to step into the definitive commitment state such as differentiation (Sauer et al., 2000, Schmelter et al., 2006, Kilberg et al., 2016). In a lesser definitive ES cell fate transition such as the exit from naïve to primed pluripotent states, no changes have been suggested for mitochondrial phenotypes. It is questionable whether a transition in mitochondrial phenotype between naïve ES and differentiated cells could be detected. As primed ES cells are ready for differentiation, the transition from naïve to enter the primed pluripotency illustrates a dynamic change in ES cells that could include some of the mitochondrial infrastructure modifications. In fact, perinuclear mitochondrial organisation has been reported in undifferentiated ES cells with the dispersion of mitochondria being associated with mitochondrial maturation a characteristic of differentiated cells (Prowse et al., 2012, Lees et al., 2017), but when this event is first observed during the pluripotent lineage specification and differentiation process is not known. Detecting the transition in mitochondrial properties in different pluripotent states of ES cells will reveal presently unknown information about the mitochondrial maturation process in pluripotent lineage specification and differentiation. In this pilot study, it is hypothesised that, naïve and primed ES cells

have different distribution of the mitochondria enzyme, Prodh. This work aims to quantitate Prodh staining and determine the differences in the immunofluorescence of Prodh, in two pluripotent states, naïve and primed ES cells. This pilot work has not followed a commonly designated study, and the analysis is based on Prodh staining in the naïve and primed ES cells that had already been generated, thus, the purpose of this study is to describe the features of Prodh staining in ES cells.

Materials and Methods

Experimental design

The immunofluorescence of Prodh was performed in naïve and primed ES cells after the cells were seeded on a gelatine coated imaging plate for 12 hours. The staining technique was similar to the protocol provided in Chapter 2, section 2.6 of this thesis. Two sets of experiments were performed at the same time using naïve and primed ES cells. In sample set 1 (to generate Dataset 1), naïve and primed ES cells were stained with 1:200 concentration of Prodh (here called Ab^{lo}). In sample set 2 (to generate dataset 2), naïve and primed ES cells were stained with 1:100 concentration of Prodh (Ab^{hi}). The experiment was performed once only (biological replicates, n=1). In each well of naïve and primed ES cells on the imaging plate, three separated areas were imaged (technical replicates m=3) at the 60x magnification of the Leica DMRBI microscope. The examples of images used for this pilot study are shown in Figure 3.2.5

Methods

Images of DAPI and Prodh staining in naïve and primed ES cells were analysed in Cellprofiler (version 2.2.0) using the provided pipelines and modules (Supp.Fig 1) as previously described (Gustafsdottir et al., 2013). After correcting the background, the program set up an algorithm to identify each cell by their positive DAPI staining (or nuclear DNA), which will be overlayed with Prodh staining to define the cell area. This algorithm will subtract Prodh area to DAPI area to give rise to the cell cytoplasm area. For each of these identified objects: cell (combined DAPI and Prodh), nuclear DNA (or DAPI) and cytoplasm (Prodh (or GFP)), different features of the staining such as intensity, shape, area, intensity location and distribution were quantitated. A list of features is summarised in Supp.Table 1. All data processing and analysis were performed in R studio (version 1.1.456) and packages are available from R (version 3.5.1) using the codes that is publicly available online and can be found from the following site:

https://github.com/cytomining/cytominer/blob/master/vignettes/cytominer-pipeline.Rmd.

A principle component analysis (or PCA) was performed to reveal if the distribution (shapes and area) of Prodh was mostly contributing to the separation between naïve and primed cells. Each step of the analysis process and codes are summarised in Supp.Fig 3 and Supp.Text 1. Two studies were performed, in which, Study 1 analysed dataset 1 (samples were stained with 1:200 Prodh) and 2 (samples were stained with 1:100 Prodh) in parallel, and Study 2 performed similar analysis to study 1 but to the combined dataset 1 and 2. Study design and the analytic workflow are summarised in Figure 3.2.6.

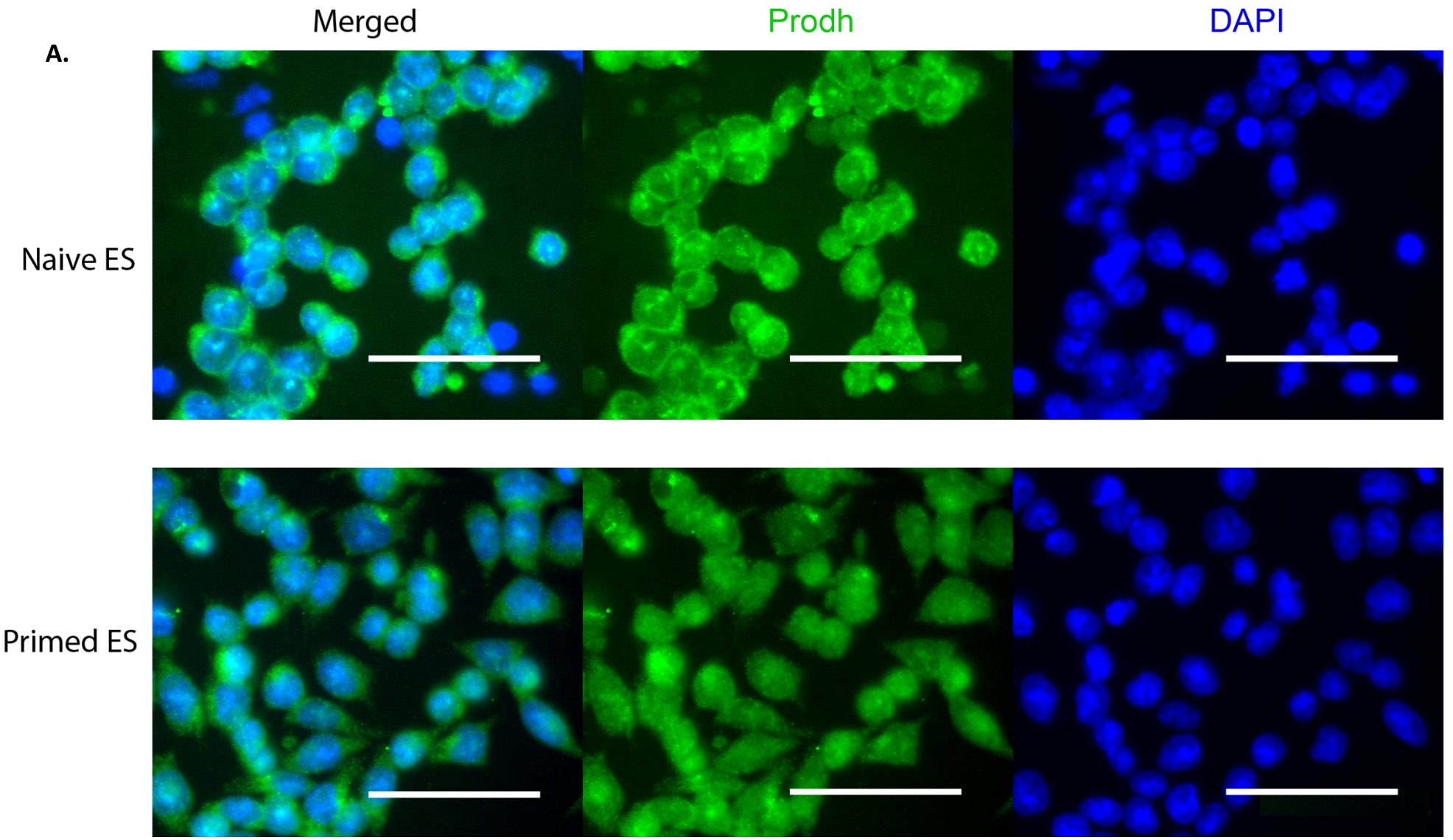
A.
Merged
Prodh
DAPI
Naive ES
Primed ES

B.

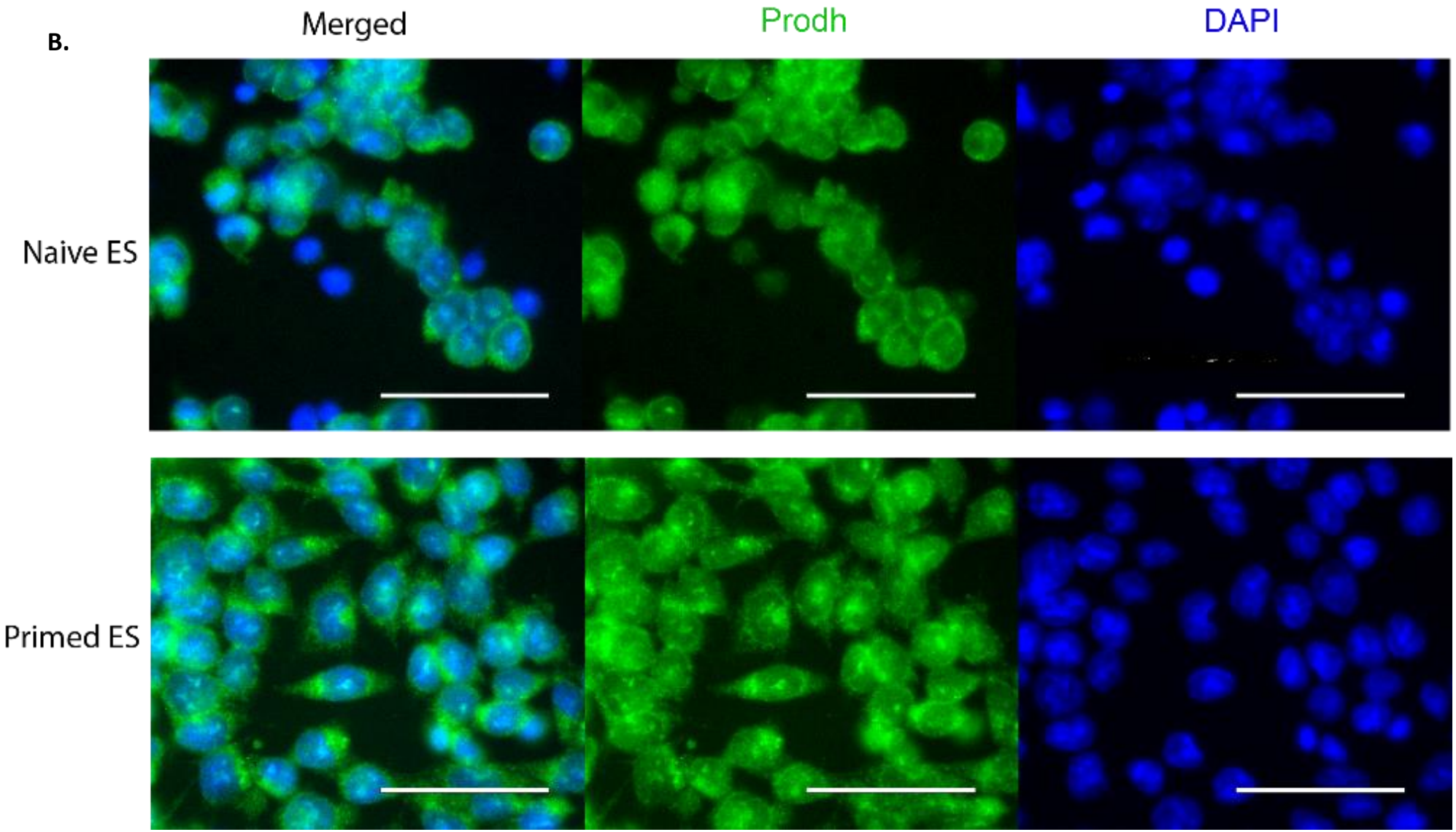

Figure 3.2.5: Immunofluorescent images of Prodh in naïve and primed ES cells

In 2 experiments using A. Low and B. High Prodh antibody concentrations [Ab]. Dataset 1 was generated from images with low [Ab] and dataset 2 was generated from images with high [Ab]. Scale = 50 µm.

A.

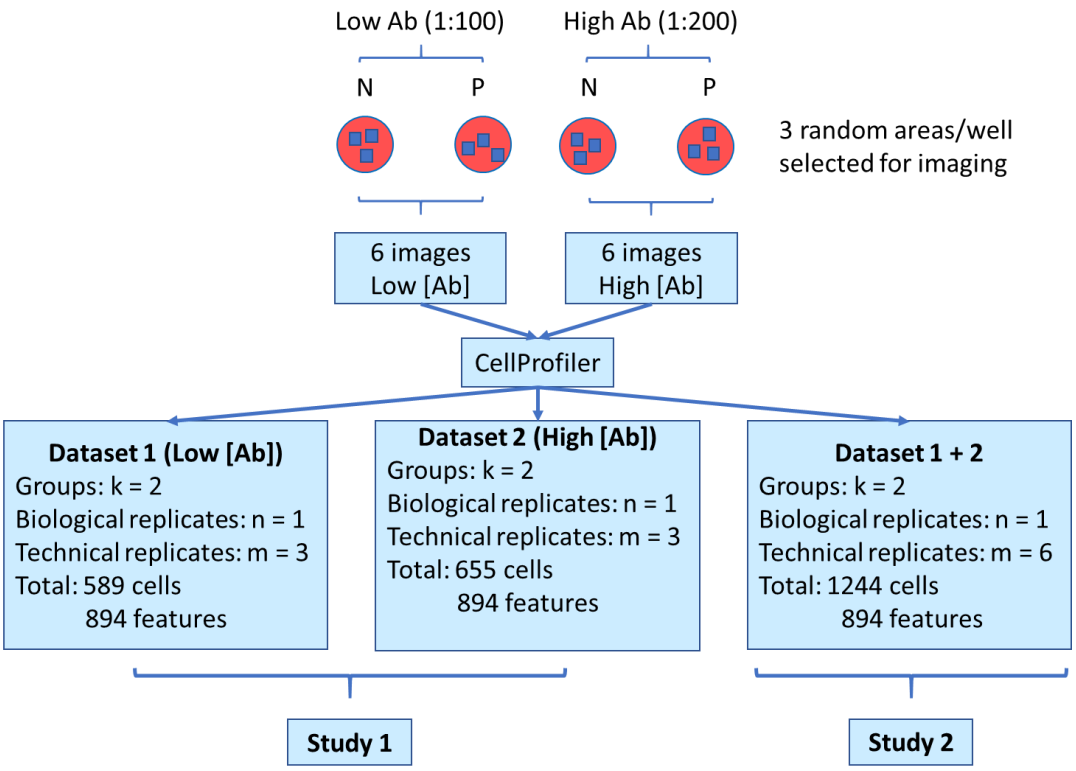
Low Ab (1:100)
High Ab (1:200)
N
P
N
P
3 random areas/well selected for imaging
6 images Low [Ab]
6 images High [Ab]
CellProfiler
Dataset 1 (Low [Ab])
Groups: k = 2
Biological replicates: n = 1
Technical replicates: m = 3
Total: 589 cells
894 features
Dataset 2 (High [Ab])
Groups: k = 2
Biological replicates: n = 1
Technical replicates: m = 3
Total: 655 cells
894 features
Dataset 1 + 2
Groups: k = 2
Biological replicates: n = 1
Technical replicates: m = 6
Total: 1244 cells
894 features
Study 1
Study 2

B.

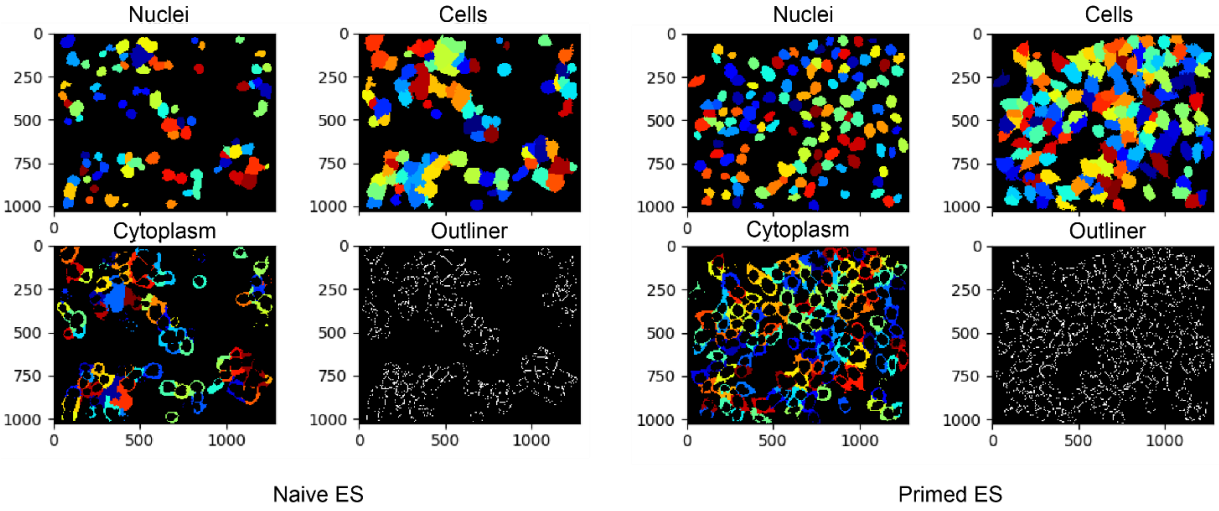
Nuclei
Cells
Cytoplasm
Outliner
Nuclei
Cells
Cytoplasm
Outliner
Naive ES
Primed ES

C.

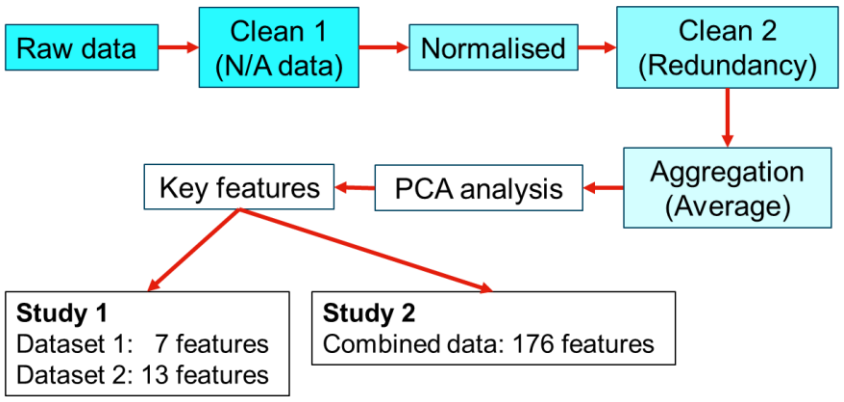
Raw data
Clean 1 (N/A data)
Normalised
Clean 2 (Redundancy)
Aggregation (Average)
PCA analysis
Key features
Study 1
Dataset 1: 7 features
Dataset 2: 13 features
Study 2
Combined data: 176 features

Figure 3.2.6: Image analysis – Study design and analysis workflow

A. Structure of the pilot study. Naïve and primed ES cells were seeded for more than 6 hours before collecting for immunofluorescent experiment. Two experiments were performed on the same plate using high (1:100) and low (1:200) concentrations of Prodh antibodies. For each well of naïve and primed ES cells, 3 random central areas were imaged under the microscope. The total of 6 images from each experiment were used for analysis by CellProfiler to generate dataset 1 and 2. Study 1 performed analysis for dataset 1 and 2 in parallel. Study 2 analysed the combined data of dataset 1 and 2. **B.** An example of how algorithms in CellProfiler detected single objects (or single cells). The subtraction of cells to nuclei gave rise to cytoplasm. Outliners of each object were drawn by the programmed. All features calculated for each object were exported to dataset 1 and 2. **C.** Workflow of data analysis for study 1 and 2 in R. Data analyses revealed key features of variation in each dataset and in the combined data.

Results

The PCA analyses of study 1 and 2 showed a high variation among all samples, and naïve and primed ES cells were not separated on the first two dimensions (Figure 3.2.7), which could be due to the low replicate number. In study 1, six components for each dataset were generated. Component 1 and 2 contributed respectively to ~40% and ~30% of the variation in all samples (Figure 3.2.7). Twelve components were generated in study 2, in which, component 1 and 2 contributed to ~20% and ~17% of the variation, respectively. From these PCA analyses, the contribution of each feature to the total variation of all samples was calculated. In study 1, the analysis of dataset 1 highlighted a trend of differences in the cytoplasmic and nuclear shape (total ~30%) and the texture (total ~25%) of each cell as these features contributed mostly to the first component (Table 3.2.1). Specifically, cytoplasmic shape Zernike 4.2 (or astigmatism shape) contributed mostly to the differences in the samples of dataset 1, followed by the nuclear shape Zernike 7.5. The explanation of Zernike moments is shown in Figure 3.2.8. Cell and nuclear texture contributed to the total of ~38% of the variation in the second components (Table 3.2.1.A). Samples in dataset 2 were mostly separated by the nuclear (Zernike 5.5) and cytoplasmic (Zernike 6.0 or spherical) shapes. These features contributed to the total of ~50% of the first component of the variation in all samples (Table 3.2.1.B). The second component show that distances exist between cells, and the cell texture is different in dataset 2 (Table 3.2.1.B). Based on the CellProfiler's manual about the measurements that are performed by the program, these features might describe the heterogeneity in each sample. In study 2, with the combined data of dataset 1 and 2, ten features of each component were examined. The first component displayed cell and cytoplasmic shapes (total ~6.2%), nuclear texture (~6.1%), cell correlated DNA (~4.5%) and heterogeneity (~4.3%). The second component mostly illustrated the variations in cell and cytoplasm shape (~11.9%), nuclear texture (~6.5%) and heterogeneity (~4.5%) (Table 3.2.1.C).

In conclusion, study 1 showed that trends in sample variation are represented by the astigmatism and spherical shapes of the cells and cytoplasm. Nuclear shapes, nuclear texture, cell texture and heterogeneity also contributed to the differences of all samples, however, there is no significant difference in the measurements of these features between naïve and primed ES cells (data not shown). Study 2 showed similar results to study 1, that cell and nuclear shapes of the cells are more variable than other features. However, these features were slightly different from those in study 1. In addition, the correlation between cells and DNA are the features of variation in all samples in study 2 and no significant difference between naïve and primed ES cells were detected in these features (data not shown)

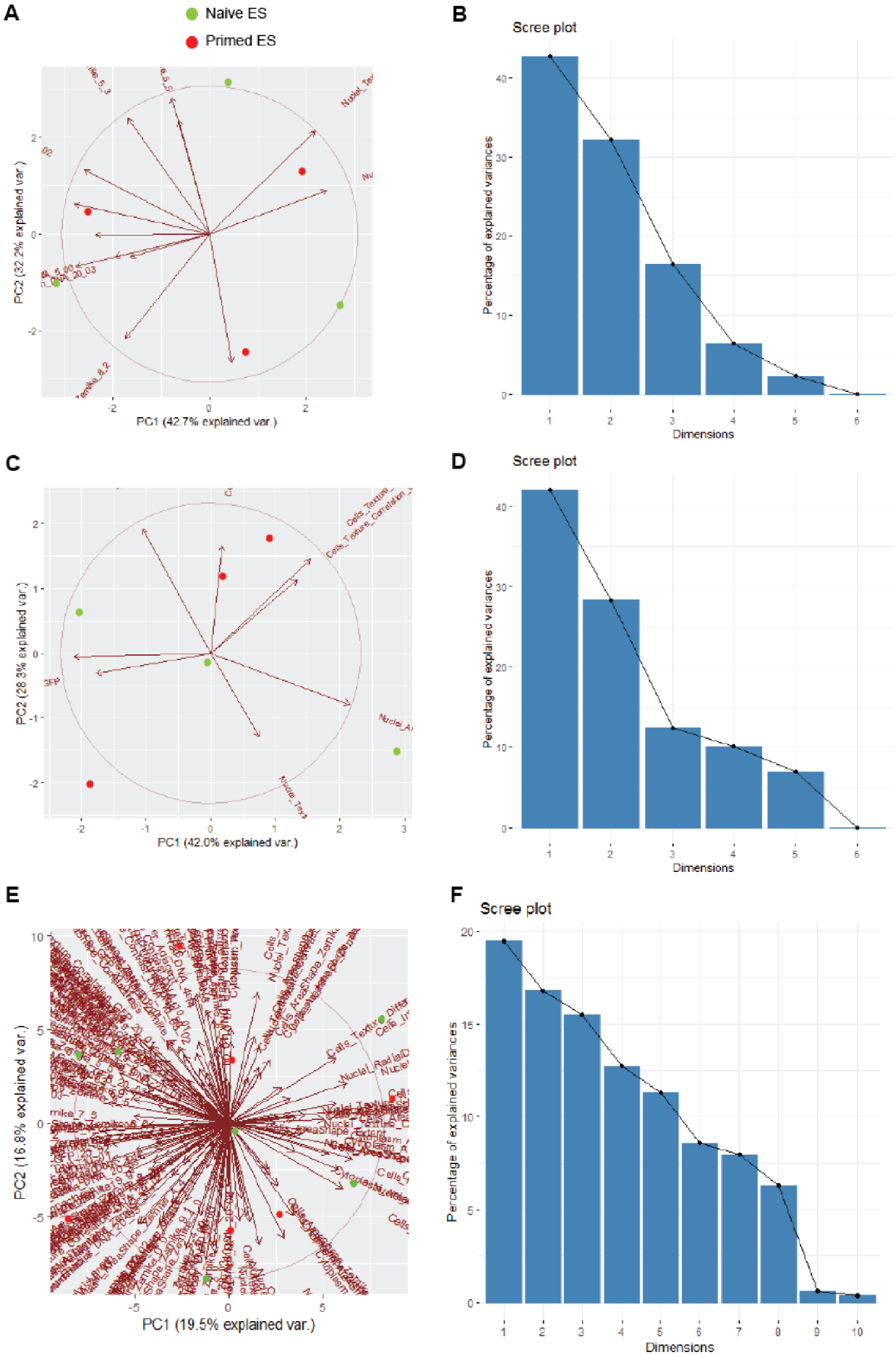
A
Naive ES
Primed ES
PC2 (32.2% explained var.)
PC1 (42.7% explained var.)
B
Scree plot
Percentage of explained variances
Dimensions
C
PC2 (28.9% explained var.)
PC1 (42.0% explained var.)
D
Scree plot
Percentage of explained variances
Dimensions
E
PC2 (16.8% explained var.)
PC1 (19.5% explained var.)
F
Scree plot
Percentage of explained variances
Dimensions

Figure 3.2.7 Clustering of samples in relation to each feature and the contribution of each cluster to the variation of all samples.

Principle component analysis showed the clustering of **A.** Dataset 1, **C.** Dataset 2 and **E.** Combined dataset of dataset 1 and 2. Contribution of each cluster (or dimension) to the variation of the samples in each dataset were shown in Scree plots **B**, **D** and **F**, respectively.

Table 3.2.1. Statistic contribution of all features to the variation of each dimension in Study 1 and 2

A. The contribution of each feature to the variation of different dimensions (or components) in dataset 1. All features contribute to the total of 100% variation of each dimension. The highest contributions from each dimension are highlighted.

	Dim.1	Dim.2	Dim.3	Dim.4	Dim.5	Dim.6
Cytoplasm_AreaShape_Zernike_4_2	**15.09**	0.97	4.52	1.52	4.30	29.56
Nuclei_AreaShape_Zernike_7_5	**14.71**	1.13	2.91	8.36	1.52	10.57
Cells_Texture_InfoMeas2_DNA_5_02	**12.89**	4.48	1.41	7.20	2.24	12.02
Nuclei_Texture_Correlation_DNA_10_00	**11.24**	2.06	3.02	23.26	10.74	2.06
Cells_Neighbors_SecondClosestObjectNumber_Adjacent	10.67	0.00	18.65	0.81	1.05	0.83
Nuclei_Texture_Correlation_DNA_5_00	9.12	11.53	0.01	1.27	0.02	1.49
Cells_Texture_DifferenceEntropy_DNA_5_00	7.38	0.55	21.21	5.69	23.05	11.47
Nuclei_AreaShape_Zernike_8_2	5.83	11.93	8.12	0.18	0.52	16.63
Nuclei_AreaShape_Zernike_5_3	5.53	**14.54**	1.96	3.37	4.67	8.22
Cells_Texture_Correlation_DNA_20_03	5.16	0.58	25.68	3.65	37.99	2.40
Cells_Texture_Correlation_DNA_5_00	1.20	**20.22**	2.28	0.98	10.04	2.22
Nuclei_AreaShape_Zernike_5_5	0.78	**14.00**	0.05	43.72	1.53	2.28
Nuclei_Texture_InfoMeas1_DNA_5_03	0.40	**17.99**	10.18	0.00	2.34	0.25

B. The contribution of each feature to the variation of different dimensions (or components) in dataset 2.

	Dim.1	Dim.2	Dim.3	Dim.4	Dim.5	Dim.6
Nuclei_AreaShape_Zernike_5_5	**25.65**	5.19	1.40	0.75	0.02	42.58
Cytoplasm_AreaShape_Zernike_6_0	**24.65**	0.02	1.93	12.88	8.39	0.11
Cells_Intensity_MassDisplacement_GFP	**17.27**	0.80	28.32	0.06	21.10	21.25
Cells_Texture_InverseDifferenceMoment_GFP_20_00	**13.08**	**17.22**	0.04	17.27	5.19	8.60
Cells_Texture_Correlation_DNA_20_03	9.92	10.49	20.21	16.07	17.22	15.01
Cells_Neighbors_FirstClosestDistance_Adjacent	6.14	**30.20**	1.23	0.00	17.14	5.91
Nuclei_Texture_DifferenceVariance_GFP_20_01	3.12	13.54	41.10	0.64	30.82	6.13
Cells_Texture_AngularSecondMoment_GFP_20_02	0.17	**22.53**	5.77	52.34	0.12	0.42

C. The top 10 features (out of 176 features) contributing most to the first three dimensions (or components) to the combined dataset 1 and 2.

	Dim.1
Cells_AreaShape_Zernike_9_5	2.49
Cells_RadialDistribution_FracAtD_GFP_1of4	2.49
Nuclei_Texture_Correlation_DNA_5_02	2.39
Cells_Texture_Correlation_DNA_5_03	2.38
Cells_Texture_Correlation_DNA_10_00	2.08
Cytoplasm_AreaShape_Zernike_4_2	1.99
Nuclei_Texture_Correlation_DNA_5_01	1.91
Cytoplasm_Intensity_MassDisplacement_GFP	1.86
Cytoplasm_AreaShape_Zernike_5_3	1.83
Nuclei_Texture_Correlation_DNA_5_03	1.79

	Dim.2
Cells_AreaShape_Zernike_7_3	2.63
Cells_AreaShape_Orientation	2.43
Cytoplasm_AreaShape_Orientation	2.41
Nuclei_Neighbors_SecondClosestDistance_Adjacent	2.40
Cells_Neighbors_SecondClosestDistance_Adjacent	2.35
Nuclei_Texture_DifferenceEntropy_DNA_20_03	2.25
Cytoplasm_AreaShape_Zernike_8_6	2.23
Cytoplasm_AreaShape_Area	2.23
Nuclei_Texture_SumEntropy_DNA_20_01	2.16
Nuclei_Texture_DifferenceEntropy_DNA_20_01	2.14

	Dim.3
Cells_Texture_SumVariance_DNA_20_02	2.90
Cells_AreaShape_Zernike_6_0	2.75
Nuclei_AreaShape_Solidity	2.49
Nuclei_AreaShape_FormFactor	2.44
Nuclei_Texture_Contrast_DNA_20_03	2.29
Nuclei_Texture_Contrast_DNA_10_02	2.25
Nuclei_Texture_Correlation_DNA_20_01	2.23
Cells_Texture_SumEntropy_DNA_20_01	2.18
Nuclei_Texture_Correlation_DNA_10_01	2.13
Cells_Texture_DifferenceEntropy_DNA_20_01	2.09
Cells_Texture_SumEntropy_DNA_20_03	2.06

A

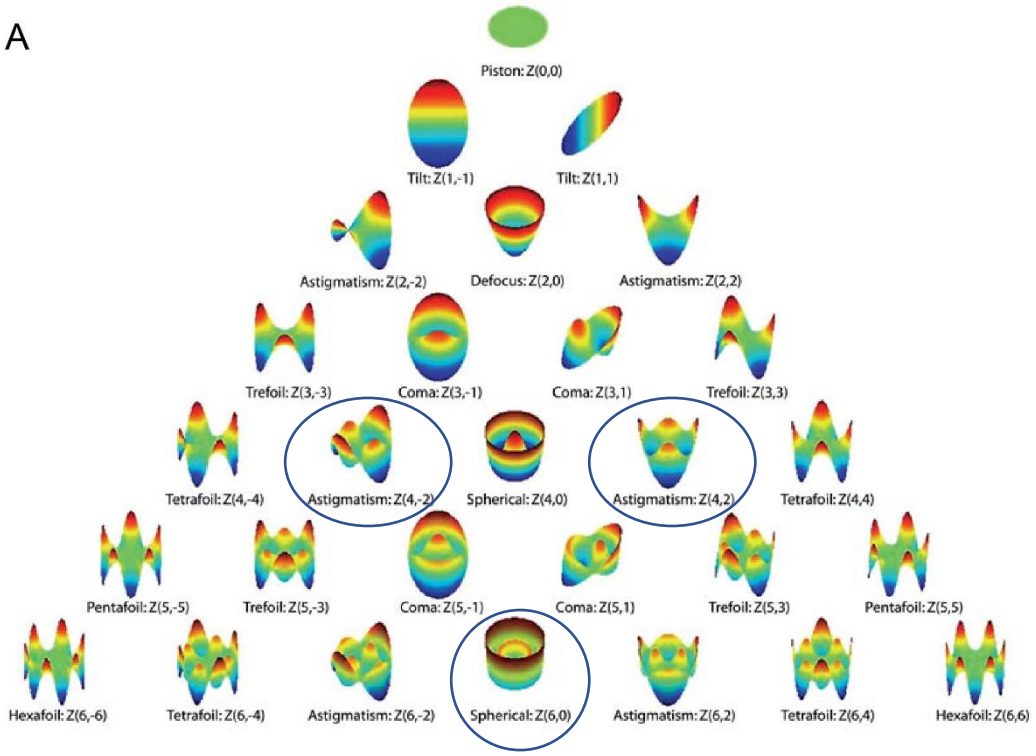
Piston: Z(0,0)
Tilt: Z(1,-1)
Tilt: Z(1,1)
Astigmatism: Z(2,-2)
Defocus: Z(2,0)
Astigmatism: Z(2,2)
Trefoil: Z(3,-3)
Coma: Z(3,-1)
Coma: Z(3,1)
Trefoil: Z(3,3)
Tetrafoil: Z(4,-4)
Astigmatism: Z(4,-2)
Spherical: Z(4,0)
Astigmatism: Z(4,2)
Tetrafoil: Z(4,4)
Pentafoil: Z(5,-5)
Trefoil: Z(5,-3)
Coma: Z(5,-1)
Coma: Z(5,1)
Trefoil: Z(5,3)
Pentafoil: Z(5,5)
Hexafoil: Z(6,-6)
Tetrafoil: Z(6,-4)
Astigmatism: Z(6,-2)
Spherical: Z(6,0)
Astigmatism: Z(6,2)
Tetrafoil: Z(6,4)
Hexafoil: Z(6,6)

B

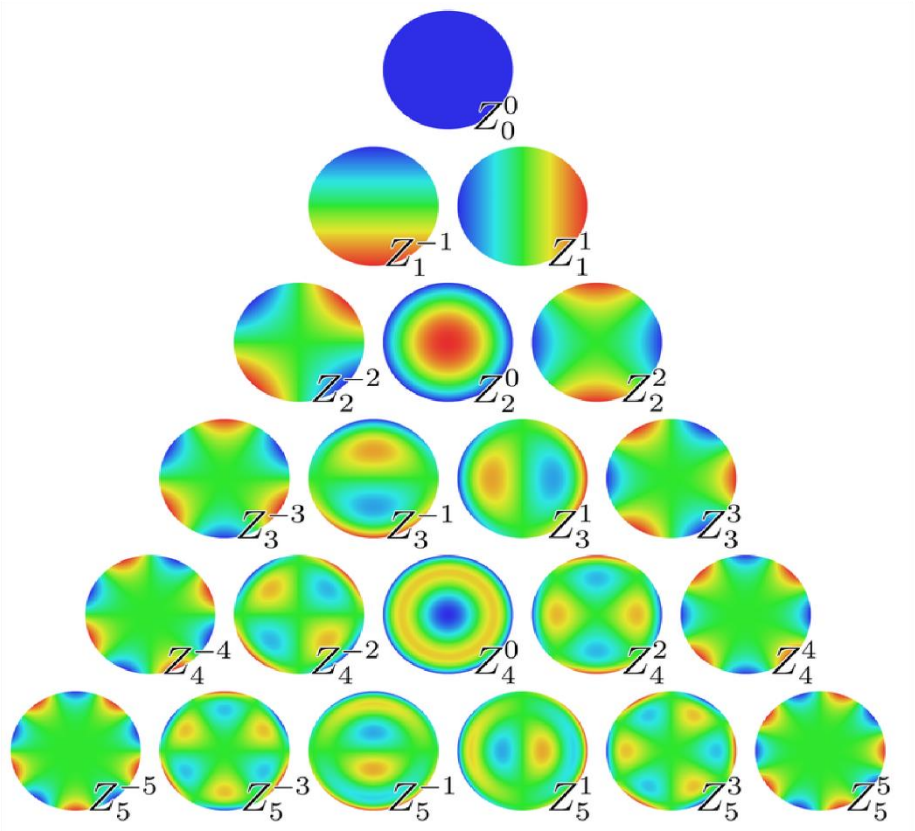
Z_0^0
Z_1^{-1}
Z_1^1
Z_2^{-2}
Z_2^0
Z_2^2
Z_3^{-3}
Z_3^{-1}
Z_3^1
Z_3^3
Z_4^{-4}
Z_4^{-2}
Z_4^0
Z_4^2
Z_4^4
Z_5^{-5}
Z_5^{-3}
Z_5^{-1}
Z_5^1
Z_5^3
Z_5^5

Figure 3.2.8: Zernike polynomials

The fundamentals of Zernike wavefronts (**A**) were used to define 2D Zernike shapes and distribution (**B**) of the staining in CellProfiler. Zernike moments are vertically arranged in radial order and horizontally arranged in angular meridional frequency. In this pilot study, polar distribution Zernike (4,2) (astigmatism shape) and Zernike (6,0) (spherical) (in blue circles) were specifically highlighted as contributing the most to the variation of objects in all samples. The above images can be accessed via the links: http://bme240.eng.uci.edu/students/08s/ticenogl/Wavefront-Guided%20LASIK/Wavefront.html (A) and https://en.wikipedia.org/wiki/Zernike_polynomials (B).

Conclusion

Image-based profiling of cell phenotypes have been previously described (Boutros et al., 2015, Caicedo et al., 2017). Image analysis of Prodh reveals that there is a trend of variation in Prodh staining in the cells of all samples. Particularly, astigmatism and spherical shapes of the cells and cytoplasm, which were marked by Prodh staining, contributing mostly to the variation in all samples. Due to the small sample size, the data were inconclusive as to what shape of Prodh distribution was correlated with the naïve or primed ES cells. Prodh was localised into the mitochondrial in chapter 3 of this thesis, the suggestion of different Prodh distribution may also reflect the distribution of mitochondria in ES cells. How this is related to the cell functions and physiology will need further validation, but perhaps, the changes in mitochondrial distribution may be initiated during the early pluripotent transition of ES cells. Whether these cells were a part of the differentiated population of ES cells and how far they are in the differentiation process will warrant future examination which will clarify how early on in the pluripotent lineage specification process that mitochondrial dispersion occurs for the first time.

Prodh has been shown to be differentially expressed in naïve and primed ES cells, however, the intensity of Prodh was not suggested to be a factor of variation in different samples based on data resulting from this work. If Prodh is correlated with mitochondria, the question remains that, whether the distribution of mitochondria is the cause behind the differential transcription of Prodh. Naïve ES cells are known to have homogenous mitochondria of round shape, that are immature and arranged perinuclearly, while primed ES cells possess heterogeneous mitochondria of both round and elongated shapes (Mandal et al., 2011, Mathieu and Ruohola-Baker, 2017). It would be interesting to discover if the difference in mitochondrial numbers or morphology are correlated with Prodh expression in naïve and primed ES cells and if that is a sign for differentiation initiation. In fact, mitochondrial DNA (mtDNA) copy numbers were reported to increase during ES cell differentiation, however, mitochondrial replication was not observed in D3 ES cells in the transition to neuronal differentiation (Facucho-Oliveira et al., 2007). Accordingly, the increase in mtDNA copy number was only observed in D3 ES cells at day 6 post-differentiation and the change in mtDNA copy numbers was associated with cell expansion (Facucho-Oliveira et al.,

2007). Therefore, it is likely that the modification of Prodh distribution suggested in this pilot study could have reflected a small population of the differentiated cells.

Nuclear shape and texture were mentioned as the contributing factors to the variation of all samples in both study 1 and 2, suggesting that ES cells could have different nuclear contents such as DNA, nucleoli and bar bodies (Coronado et al., 2013, Takahashi et al., 2018). These differences could potentially originate from the different cell cycles and cell states, which could contribute to the variation in DNA condensation and nuclear contents. A measurement of proliferation between naïve and primed ES cells showed that the average division rates of naïve and primed ES cells are 18 and 21.5 hours respectively (Figure 3.2.9), suggesting that the ES cells of different pluripotent states have different division rates and different cells may stay in different phases of the cell cycle. Furthermore, the results revealed that cells in different samples have different textures, which reflected the heterogeneity of the cell populations. This is consistent with previous reports that ES cells are heterogeneous, and cells of a particular pluripotent states may have different subpopulations due to spontaneous differentiation (Kolodziejczyk et al., 2015, Hayashi et al., 2008, Tanaka, 2009). In addition, the results in study 2 showed that cell and DNA are correlated in ES cells. The definition of this feature in the Cellprofiler's manual describes the relationship between Prodh and DNA staining, which could reflect the differences of the intensity of Prodh and DNA staining across samples or even the colocalisation of these staining. This may be caused by different antibody concentrations that were applied and the heterogeneous characteristics of ES cells because heterogeneity could potentially introduce bias effects on the profiling of ES cells of different states (Hayashi et al., 2008, Osorno and Chambers, 2011, Godwin et al., 2017, Neupane et al., 2015, Tanaka, 2009). Further replications could support and confirm these findings. In studies using small sample sizes, as with this particular pilot study, using each cell in the population as a replicate, which is also called single cell profiling, could help to reduce the bias artefact and would provide useful information on the cell subpopulations. In fact, single cell analysis has also been suggested in image-based cell profiling for heterogeneous populations (Caicedo et al., 2017). Finally, to correlate the staining of Prodh with mitochondria, co-staining of Prodh with mitochondrial marker would give a more definitive conclusion on the mitochondrial distribution in ES cells. At the same time, a more consistent standard of Prodh staining in a less crowded population will be useful to provide

images of a better resolution and therefore, will create a more precise quantitation of the data. Overall, the use of image analysis will be useful for adding information into the research database of ES cell biology. The integration of cell imaging data and other -omics data will provide a more precise picture on cell phenotyping and will enhance the ability to profile different cell types.

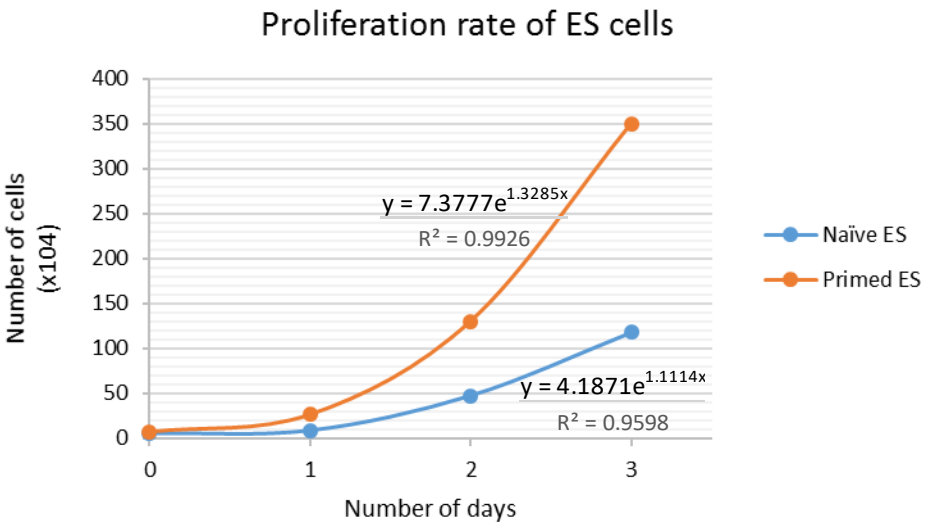

	days/division	hours/division
naïve	0.90	21.54
Primed	0.75	18.07

Figure 3.2.11: Proliferation rate of naïve and primed ES cells.

Naïve and primed ES cells were seeded at the same rate. The cells were counted on a counting chamber every 24 hours for 4 days. The first count for each cell type was used as day 0 reference. An exponential equation: $y = N^{tx}$ was generated based on the count data, where y is the total number of cells on day x. Division rate r (days/division) was calculated based on previously published method (Sherley et al., 1995) and is equal 1/t. Division rate in hours h is calculated as h = r*24 (hours/division).

3.3. Discussion

3.3.1. The gene expression of the proline metabolic enzymes is differentially regulated in different pluripotent states and is affected by long term culture conditions

In mammalian cells, the expression of the proline metabolic enzyme family, including *Prodh*, *Aldh18a1*, *Aldh4a1*, *Pycr1*, and *Oat*, is regulated by the master transcription regulators p53 and Myc (Rivera and Maxwell, 2005, Donald et al., 2001, Wang et al., 2011, Liu et al., 2012). It is suggested that within cancer cells, P53 is responsible for activating the expression of *PRODH* and leads to the increase in proline metabolism (Rivera and Maxwell, 2005, Donald et al., 2001). Furthermore, MYC might act as a suppressor for *PRODH* expression via *miR-23b* (Liu et al., 2012). However, in T cells, the reduction of MYC is correlated with the decreased expression of *PRODH*, *OAT* and *ALDH18A1* (Wang et al., 2011). It is possible that P53 and MYC may exert a reversed regulation on the proline metabolic enzyme family and P53 could repress the regulatory effect of MYC (Puzio-Kuter, 2011, Liang et al., 2013). Recent data have found that P53 and MYC also control the expression of other proline metabolic enzymes (Wang et al., 2011, Liu et al., 2012, Yoon et al., 2004). Particularly, P53 activates the expression of P5CDH gene (*ALDH4A1*) and *MYC* is reported to regulate the expression of P5C synthase (*ALDH18A1*), P5C reductase (*PYCRs*) and *OAT* genes(Yoon et al., 2004, Wang et al., 2011, Liu et al., 2012), thus, it is possible for MYC and P53 to coordinate the expression of the proline metabolic enzyme family depending on the physiological conditions, which generate metabolic switches between proline catabolism and biosynthesis in mammalian cells.

Here it is shown that proline metabolic switches also occurred during the pluripotent lineage specification of ES cell growth, particularly, the gene of proline metabolic enzyme family is regulated and differentially expressed in different pluripotent states. Similar results are observed in both ES cell lines, D3 and WA30, indicating that this is a robust metabolic change during the pluripotent lineage specification. The increase in *Prodh* when ES cells are released from 2i into the primed state occurred at the same time with the increase in the proline primary transporter *Slc38a2* (encoding Snat2 protein) in the cells. This result is consistent with previous data in the literature (Tan et al., 2016b). Moreover, this is not limited to ES cell culture. It has been reported that the regulation of *Slc38a2* recapitulates the *in vivo* development of the pluripotent cells in mice embryo (Tan et al., 2016b). The observation of

the human embryonic data also showed evidence that blastocyst cells show higher expression of *Slc38a2* when compared to the morula cells, the earlier state of blastocyst cells (Vassena et al., 2011). Therefore, the increase of *Slc38a2* is a requirement for pluripotent cells at the primed state, but not the naïve state. The inhibition of Erk1/2 pathway in T cells is known to affect the expression of MYC, a regulator of Prodh (Wang et al., 2011), thus, the inhibition of Erk1/2 in naïve ES cells may produce an effect on the expression of *Prodh* via suppressing MYC. The combination of increased expression of the transporter, *Slc38a2,* and the key enzyme, *Prodh*, suggested that when moving from naïve to primed state, ES cells switch on proline uptake and proline catabolism. It is hypothesised that this switch may be needed for ES cells in this transition to prepare ES cells to utilise proline metabolism for differentiation into the later pluripotent states, thus more investigation is required to confirm this possibility.

In contrast, primed ES cells expressed lower levels of *Oat* compared to naïve ES cells. As Oat plays a role in proline biosynthesis, a decrease in Oat expression predicts a reduction in P5C synthesis, while the increased levels of *Prodh* expression is expected to increase P5C levels from proline. It is possible that the reduction in *Oat* may act to compensate the increase of *Prodh* in primed ES cells by stopping P5C synthesis from ornithine as high levels of P5C has been shown to inhibit cell respiration in yeast (Nishimura et al., 2012). However, as Oat is a bidirectional enzyme, it is uncertain if any direction was favoured in ES cells and if it is subject to the changes in ES cell programming. It is also possible that the reduction of Oat may retain P5C in the proline cycle to support ES cell maintenance by preventing P5C escaping via Oat catalytic activity. This hypothesis will require investigation of the P5C levels within the cells. The robust changes in gene expression of *Slc38a2*, *Prodh* and *Oat* shows that the proline metabolic shift is more likely to correlate with the release of ES cells from 2i to serum because other modifications of the culture conditions did not provide additional effects to this shift. This is the first data that highlights the shift in proline metabolism in naïve and primed ES cells, which could potentially be used to perform the discrimination of these ES cells. The examination of various naïve and primed ES cell expression data will be useful for further validation of this finding.

It was noted that the proline-induced differentiated ES cells showed a reduction of the P5C synthase (*Aldh18a1*) expression in both ES cell lines, but this effect was clearer in D3 cells when compared to WA30 cells. This is in agreement with the recent study that *Aldh18a1* is

reduced early after the addition of L-proline into ES cells (D'Aniello et al., 2015), however, it disagrees with the earlier report that *Aldh18a1* was not changed with proline treatment (Comes et al., 2013). This suggests that *Aldh18a1* gene may be subject to variation in different ES cell lines and different culture conditions, similarly to the variation of other proline metabolic genes that were examined in cancers (Phang et al., 2008a, Phang et al., 2012, Phang et al., 2015, Phang et al., 2008b, Elia et al., 2017). The expression of Snat2 gene, *Slc38a2*, also decreased in D3, but not in WA30 ES cells in the addition of proline. This result is in contrast with the previous findings whereby *Slc38a2* was not affected by the differentiation process (Comes et al., 2013). The reduction of Snat2 and P5C synthase is expected to decrease the proline uptake and thus preventing its precursor from glutamate to be fed back to the catabolic process. This regulation may provide protection to the cells by limiting proline availability for oxidation given proline oxidation could lead to ROS production (Donald et al., 2001) and ROS-induced apoptosis in cancer cells (Rivera and Maxwell, 2005). The data suggests that D3 ES cells were more responsive to the proline addition than WA30 ES cells in regulating key genes of the proline metabolic enzyme family. In contrast, the variation observed with *Pycr2* and *P4ha1* genes between the naïve and primed pluripotent states was only found in WA30, but not in D3 ES cells (Figure 3.3.2.C and D), suggesting that WA30 may be more sensitive to the pluripotent lineage specification than D3 ES cells, which led to increased variation in the gene expression. This result could be correlated with the differences in the long term cultivation of these cell lines because the long term suppression of Mek1/2 in 2i medium was reported to impact upon ES cell development and differentiation (Choi et al., 2017), thus, WA30 ES cells may be more sensitive to the developmental changes induced by proline, which resulted in the increased cell death in proline addition.

In conclusion, the data suggested that the proline metabolic enzyme expression in ES cells was subjected to regulation by changes to different pluripotent states, but possibly not by the variation in the culture conditions. WA30 ES cells were more responsive to the release from 2i than D3 ES cells and that led to increased WA30 cell death in serum. It is suspected that the long-term cultivation of different ES cell lines contributes to the enhanced effects upon proline metabolic enzymes. In other words, as the WA30 cell line is maintained in 2i and D3 cells are maintained in serum, their original media could lead to different responses to the same culture conditions. In fact, naïve and primed state ES cells have distinguished metabolic

processes that serve their stability in defined conditions (Sperber et al., 2015, Wu and Izpisua Belmonte, 2015). The pluripotency of different ES cell lines are unstable in different conditions and can be affected by the extrinsic factors within the environment, this allowing the interconversion of naïve and primed ES cells (Hanna et al., 2010). Moreover, the difference in pluripotent cell states could result in different responses to amino acid availability in the environment (Kilberg et al., 2016, Shan et al., 2013). Therefore, the different cultivation conditions in different ES cell lines could result in the unstable achievement of naïve and primed states and the oscillation of gene expression signatures (Guo et al., 2009), which could include proline metabolism. More studies are required to fully describe the precise mechanisms of the changes in proline metabolic enzyme expression.

3.3.2. Differential expression of the proline enzyme genes is correlated with the functional proteins

Validation of the gene expression data in D3 ES cells proposed two isoforms of Prodh and Oat, one of which was not seen in the literature and were not obvious within the liver and kidney controls. Even though the result was consistent across all independent experiments and with different lytic techniques, however, it did not exclude the possibility of unspecific binding of the antibodies in D3 ES cell line and the chance that these unspecific proteins are more abundant in ES cells than in livers and kidneys. The quantitation of protein expression of the functional Prodh and Oat enzymes confirms the gene expression data in naïve and primed ES cells but at a much higher magnitude of differences. This result confirms the proline metabolic switch in naïve and primed ES cells, which could be used to perform as a metabolic discrimination between the two pluripotent states. Naïve and primed ES cells are generally distinguished by their metabolic profiles (Sperber et al., 2015) and naïve ES cells showed an increase in metabolic activity with a higher respiration rate and lower glycolysis when compared to its primed counterparts (Kilens et al., 2018, Takashima et al., 2014, Gu et al., 2016). The differences in amino acid and fatty acid metabolism have been demonstrated by the metabolomic data of naïve and primed ES cells (Sperber et al., 2015), evidence that methionine and nicotinamide levels were downregulated in naïve ES cells and S-adenosyl methionine (SAM) levels were increased in primed ES cells (Sperber et al., 2015). The examination of single-cell RNA sequencing found that basic metabolism such as glycolysis and glutathione metabolism are key differences separating between the two pluripotent states

(Kolodziejczyk et al., 2015). Therefore, with this finding of the proline metabolic switch in naïve and primed ES cells, proline metabolism is a potential metabolic marker to distinguish these pluripotent states. A precise mechanism of proline metabolic regulation, thus warrants further investigation to unravel the correlation between ES cell development and proline metabolic needs.

Prodh and Oat are mitochondrial enzymes and are functional within the mitochondria (Adams and Frank, 1980, Hancock et al., 2016, Ginguay et al., 2017). The correlation between Prodh enzyme and mitochondrial activities has been reported (Hancock et al., 2016, Liu et al., 2009), confirming Prodh activities within the mitochondria. Localisation examination of Prodh in D3 ES cells illustrated that the protein is located within the mitochondria while it is circulating the nuclei. This is further supported by the previous findings that ES cells and other highly proliferative cells have punctate and perinuclear mitochondria (Kuroda et al., 2006, Prowse et al., 2012, Cho et al., 2006a), which may be important for cell proliferation and self-renewal (Lees et al., 2017).

Oat enzymes in naïve and primed ES cells appeared to be distinguished in their expression levels. The accumulation of Oat protein was observed in both naïve and primed ES cells, and when compared to naïve ES cells, Oat accumulated at a higher level in primed cells. Additionally, Oat accumulation appeared to mismatch the expression of Cox IV protein, a mitochondrial membrane protein, indicating that Oat may have a different cell location other than the mitochondrial matrix. Previous studies suggest that OAT can interact with ATF2 protein in human skin cells and could be located in the mitochondrial outer membrane (Lau et al., 2012) and precursors of Oat were found to be bound to the mitochondrial membrane before they were translocated into the mitochondria (Ono and Tuboi, 1986). However, Oat protein was also suggested to localise into the nuclei with an unknown function (Ginguay et al., 2017). In ES cells, the proline transporters Snat1 and Snat2 were found to accumulate in the perinuclear area, which is potentially used to back up the cells in nutrition restricted conditions (Tan et al., 2016b), and possibly the accumulation of Oat in order to support cells in devastating conditions. The examination of Oat proteins in relation to other cell compartments under a high-performance microscope will help to determine and confirm Oat accumulation and further study is required to understand the other biological functions of the Oat enzymes and the role of Oat accumulation in ES cells.

In conclusion, the protein expression and localisation of Prodh and Oat confirm their differential gene expression in the naïve and primed ES cells, which is correlated with their functional isoforms and their sites of activities. Therefore, Prodh and Oat are expected to perform their catalytic functions in ES cells. The increase of Prodh in primed, but not naïve ES cells suggest that proline catabolism is higher in these cells. Given that primed ES cells can differentiate in the presence of proline, the question remains as to whether the upregulation of Prodh in primed ES cells is required for the initiation of the differentiation process, thus it is possible that the proline metabolic switch is required for ES cells in different pluripotent states, not only to support the cell needs, but also to prepare the cells for a cell response to differentiation cues. More research into this hypothesis is required in order to establish the role of the proline metabolic switch in ES cell programming.

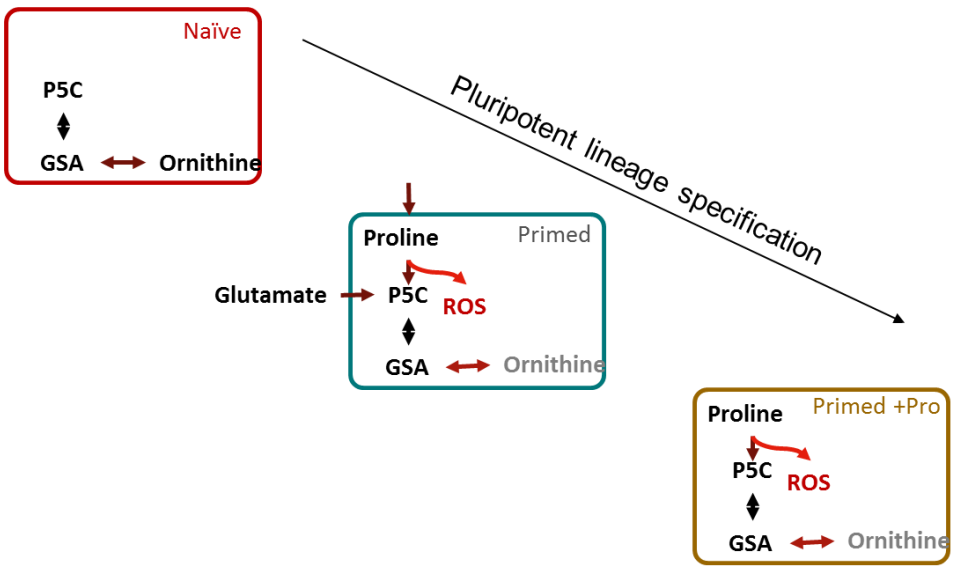

Figure 3.3.1. Proline metabolic models in different pluripotent states of ES cells based on the expression of proline metabolic enzyme family.

Figure 3.3.2. Proline metabolic models in different pluripotent states of ES cells based on the expression of proline metabolic enzyme family.

Naïve state of ES cells expressed low levels of Snat2 and Prodh, and high levels of Oat, which reduces the intake and breakdown of proline and increases the breakdown of ornithine to form P5C. In primed ES cells, Snat2 and Prodh expression is increased and the cells were more

active in proline uptake and transport. Primed ES cells also express the gene that potentially increased the synthesis of proline from glutamate. However, Oat is reduced in primed ES cells, which would potentially sync proline out of the cycle. Thus, this would keep the proline cycle high in primed state. In the addition of proline, Snat2 is reduced and P5Cs reduced to prevent the uptake and the synthesis of proline. Therefore, the central reactions of the proline cycle are maintained.

Chapter 4 The production of reactive oxygen species (ROS) in ES cells in response to proline is regulated in different pluripotent states of ES cells and is correlated with differentiation

4.1. Introduction

Reactive oxygen species (ROS) have long been considered as a sign of cellular stress and damages that are associated with pathological conditions and aging. In recent years, ROS has been raised as an interest in research for its biological role in cell signalling and programming (Covarrubias et al., 2008, Murphy et al., 2011), indicating the important involvement of ROS in development. Mitochondria is the major sites of ROS production (Murphy, 2009). The generation of ROS is often correlated with the mitochondrial membrane potential (MMP) and mitochondrial functions (Balaban et al., 2005). ROS is mainly produced from mitochondrial activities, which comprise a complex network of metabolism and redox balancing systems (Murphy, 2009, Balaban et al., 2005). In the field of stem cell research, mitochondrial functions including metabolic activities and ROS production were found to play an important role in regulating PCS growth and differentiation, which contribute to the control of cell fates (Bukowiecki et al., 2014, Suhr et al., 2010, Jeong et al., 2009, Schmelter et al., 2006, Ji et al., 2010, Ronn et al., 2017, Song et al., 2014, Birket et al., 2013, Crespo et al., 2010, Zhou et al., 2016, Schieke et al., 2008, Birket et al., 2011, Chung et al., 2007, Mandal et al., 2011).

Metabolic regulation of ROS signalling has been shown in stem cell growth and differentiation (Kubli and Sussman, 2017, Ryu et al., 2015). The regulation of ROS production involves multiple mitochondrial activities, in which, metabolism is an important factor (Lushchak, 2014, Murphy, 2009). An example of metabolic regulation of ROS in PSC function is indicated by Crespo and colleagues (2010), who investigated the correlation between high glucose content in the culture media and the increase in ROS production and suggesting that this correlation was required for cardiomyocyte differentiation from ES cells (Crespo et al., 2010). Glutamine metabolism mediated ROS production was also found to have a role in PSC differentiation, where ROS-regulated redox homeostasis in human ES cells was associated with the oxidation of the transcription factor OCT4 to mediate the cell changes (Marsboom et al., 2016). However, the link between mitochondrial metabolic regulation of ROS and PSC

decision making is not well characterised. The correlation of metabolic ROS regulation in different pluripotent states of the cells is also poorly understood. Sperber et al., 2015 found that naïve and primed ES cells are distinct in their metabolic profiles and suggested that mitochondrial respiration was higher in naïve, compared to primed, ES cells (Sperber et al., 2015). Naïve ES cells were previously shown to have high metabolic rate (Kilens et al., 2018, Taleahmad et al., 2015); however, comparing to primed ES cells, naïve ES cells were suggested to have lower glycolytic activities and higher oxidative phosphorylation (Gu et al., 2016), predicting that naïve ES cells may produce higher mitochondrial ROS than primed ES cells. No study has investigated the production of ROS in ES cells in different pluripotent states, making it challenging to address the origin of ROS and its involvement in cellular signalling. Understanding the basal production of ROS will provide information for studying ES cell metabolism in the correlation to pluripotent states, culture conditions and their differentiation potential.

There is increasing evidence for a role of proline metabolism and mitochondrial ROS production in ES cell differentiation (Tan et al., 2016a, Casalino et al., 2011, Tan et al., 2016b, Tan et al., 2011). Findings in chapter 3 of this thesis revealed that the expression of proline metabolic enzymes was regulated in different pluripotent states of ES cells in the way that favoured proline metabolism (or proline breakdown) in primed, but not naïve, state of pluripotency. Increased ROS production by proline metabolic enzyme, Prodh, and proline availability has been shown to regulate mitochondrial respiration (Hancock et al., 2016). As mitochondrial regulation of ROS is a determining factor of cell fates and plays a role in cellular redox signalling (Prigione and Adjaye, 2010, Chen et al., 2008, Varum et al., 2009, Crespo et al., 2010), proline metabolic regulation of ROS may suggest a role in ES cell development via redox homeostasis. Even though it was recently argued that redox homeostasis might not be the primary effect of proline induced differentiation in ES cells (D'Aniello et al., 2017), the involvement of ROS signalling pathways was suggested (Tan et al., 2016a). Given the results in chapter 3 that naïve ES cells have lower Prodh expression compared to primed counterparts, it is hypothesised that they will respond differently to exogenous proline to produce different levels of ROS. Specifically, it is hypothesised that ROS production will be higher in primed ES cells compared naïve ES cells with proline addition.

To address this hypothesis, mitochondrial ROS was examined in ES cells in a controlled (non-treated) condition to define the standard ROS levels in different pluripotent states: naïve and primed ES cells. The detection of ROS was validated by the antioxidant, ascorbic acid or vitamin C was used to neutralise ROS generation. The production of ROS in response to proline was also investigated in these states to examine the involvement of ROS upon differentiation. Understanding ROS production in ES cells at different pluripotent states would enhance the current knowledge of metabolic regulation of ROS and support the discrimination of ES cell fates.

4.2. Results

4.2.1. ES cells have distinct subpopulations of proline-induced ROS

To investigate the role of proline induced ROS production in ES cell differentiation, ROS was measured in D3 ES cells by flow cytometry using a mitochondrial superoxide dye, MitoSOX Red, 24 hours after the cells were seeded into new plates. ES cells formed two distinct populations with different ROS profiles, here called low and high ROS populations: ROS^{lo} and ROS^{hi} (Figure 4.3.1.A). Analysis of the data have revealed that low-ROS producing cells accounted for ~65% of the total ES cell population. To further understand if the production of ROS in response to proline was correlated with mitochondrial activities and respiration, mitochondria membrane potential (MMP) was measure for each population of ROS in D3 ES cells in a randomly selected untreated sample of five different replicates. It was found that ES cells were homogenous for MMP, but ROS^{lo} and ROS^{hi} populations were associated with low and high MMP respectively (Figure 4.3.1.B and C), which reflects different mitochondrial activities in these populations.

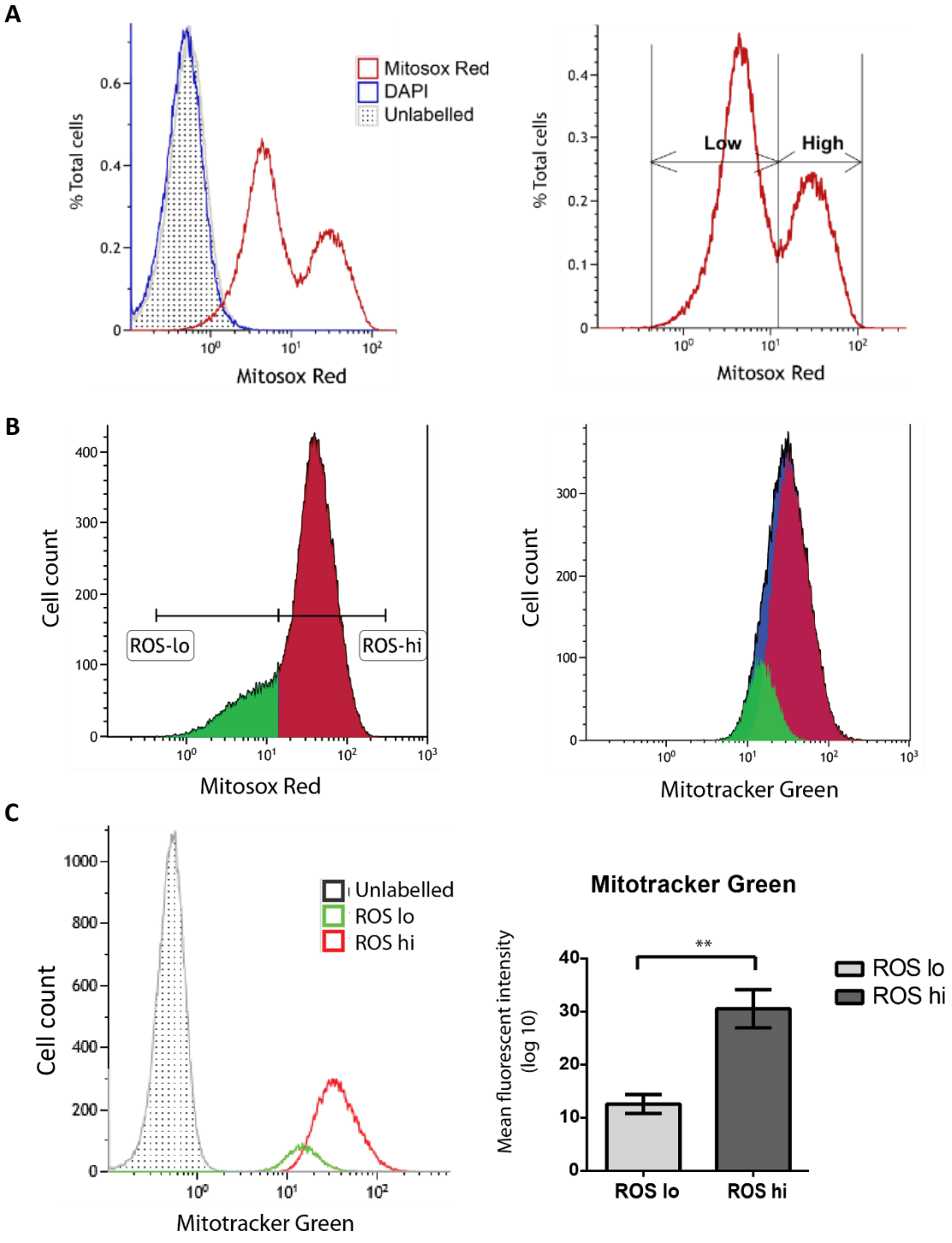

Figure 4.2.2. ROS measurement by flow cytometry in ES cells in a control (untreated or Serum + LIF) condition.

D3 ES cells were grown on a gelatine coated 24-well plate for 24 hours before collection. Cells were measure with **A.** MitoSOX Red, **B.** MitoSOX Red and Mitotracker Green. **C.** ROS^{lo} and ROS^{hi} populations were gated as in (B) to examine the levels of Mitotracker Green fluorescence. *n=5, **p≤0.01*

4.2.2. Dynamics of ROS production in the addition of proline in primed ES cells

It was previously reported that ROS production, both total hydrogen peroxide and mitochondrial superoxide, increased in primed ES cells in the addition of proline (Tan et al., 2016a). However, how quickly ES cells respond to proline to produce ROS was not investigated. To examine the dynamics of ROS production and subpopulations of ROS producing cells in response to proline, ROS was measured at different time points: 0.5, 1, 3, 6, 12 and 24 hours after proline addition. It appears that total ROS levels increased significantly at 1, 6, 12 and 24 hours after 200 μM proline was added to the medium (Figure 4.3.2). It was observed that the peak of ROS production, which identify the point where most of ES cells produced the same level of ROS, significantly increased at 1 hour in both high and low ROS populations and at 6 hours in ROS^{lo} population, which then returned to the original levels (Figure 4.3.3.A). This demonstrates that most of ES cells have a stable point of ROS production in response to proline. Aside the significant spike of ROS immediately after proline addition at 0.5 hours, which was the maximal level of ROS production at this time, no other significant changes in the lowest and highest ROS production points were detected for 24 hours responding to proline (Figure 4.3.3.B), suggesting that ES cells have a defined range of ROS production.

When looking at ROS levels in ROS^{lo} and ROS^{hi} populations, ROS production increased at 1 hour in ROS^{hi} population and at 6 hours in ROS^{lo} population, which returned to the control level after 24 hours (Figure 4.3.3.D). This is explained by the fact that in the long term responding to proline, low-ROS producing cells significantly shifted to producing high ROS at 1, 12 and 24 hours (Figure 4.3.3.C). Live imaging of ROS (Figure 4.3.4) confirmed this result at 24 hours after proline addition. This suggests that ES cells have a controlled production of ROS in response to proline and the increased in ROS production occurred by shifting ROS production within a defined range of ROS in individual cells. No changes in nuclear staining by DAPI, an indication of cell death, was obtained in this experiment. These data showed that the addition of proline to ES cells activated ROS production while maintaining the physiological level of ROS, and ROS production was not a response to cell stress or a sign of apoptosis.

The antioxidant, ascorbic acid (or vitamin C), was used to reduce ROS level. ROS production increased in response to proline (Figure 4.3.4), and vitamin C reduced ROS in ES

cells to the same level either with or without proline addition (Figure 4.3.5), which is consistent with previous findings (Tan et al., 2016a). The reduced ROS level in the present of vitamin C was significantly lower than the basal ROS level in the untreated ES cells. Compared to other treatments, ROS level detected in ES cells treated with vitamin C has appeared to be the lowest level that could be detected. Microscopic examination showed that ES cells had no signs of stress or apoptosis in the addition of vitamin C or both proline and vitamin C, suggesting that the decreased or increased ROS production was not a response to environmental stress.

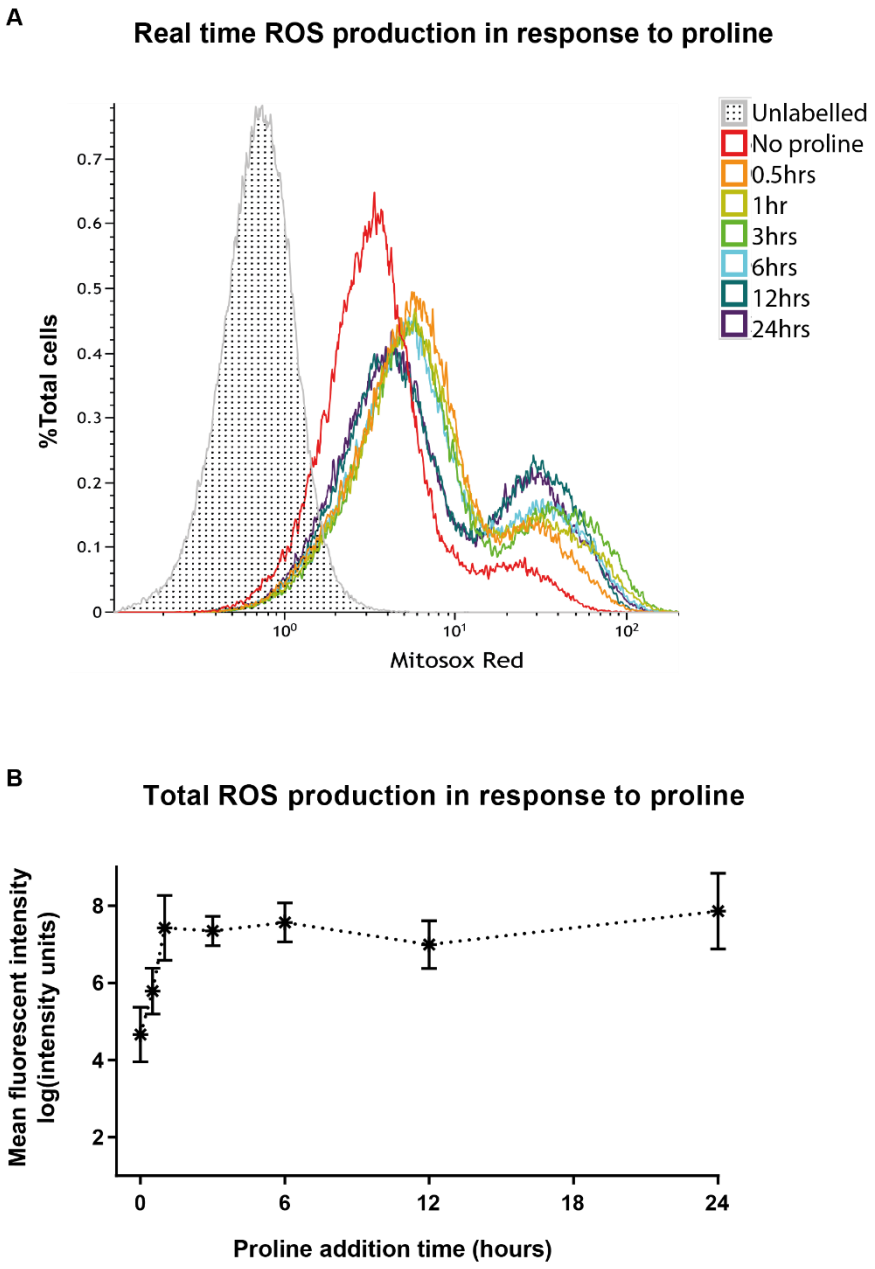

Figure 4.2.5. Real time ROS production measured by flow cytometry in ES cells in response to proline at different time points.

A. Histogram of MitoSOX Red intensity (ROS production). **B.** Total ROS production in ES cells in response to proline at different time points. *n=3-6,* **p*≤0.05.

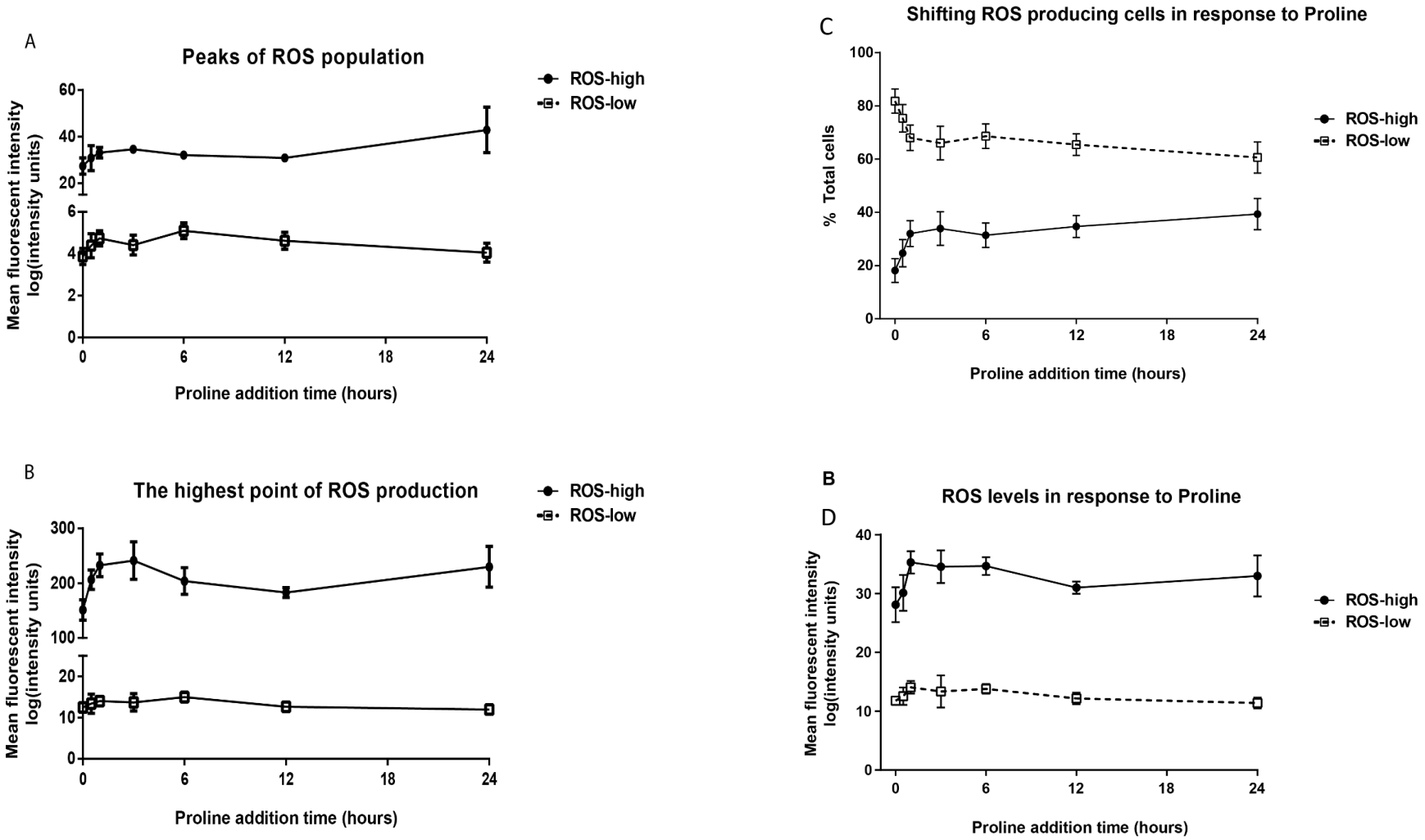

Figure 4.2.8. ROS production of heterogeneous populations of ES cells in response to proline at different time points.

ROS production in ROS-high and ROS-low population of ES cells was accessed for **A.** The point of where most of the cells produced the same level of ROS. **B.** The highest points of ROS levels produced. **C.** Percentages of cell counts. **D.** Total ROS levels in each population. *n=5,* ***p*≤0.05.

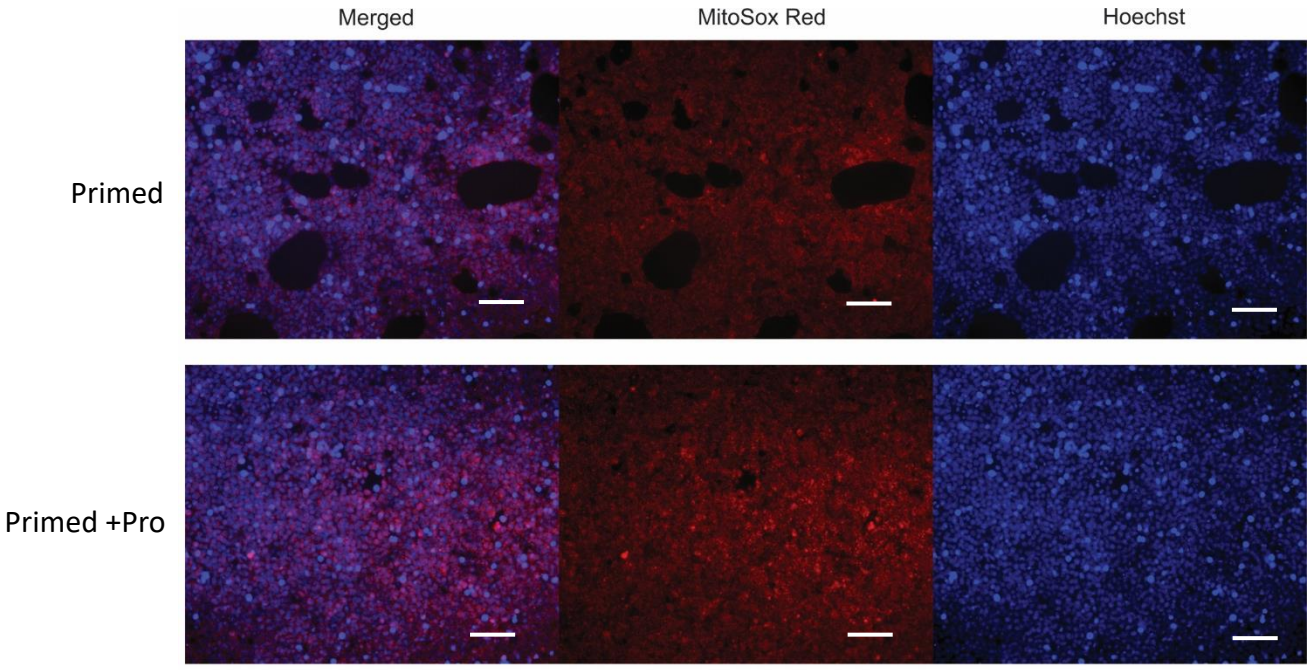

Figure 4.2.11. Live cell ROS imaging in D3 ES cells.

ES cells were grown on gelatine coated 96-well plates and treated with 200 µM proline for 24 hours and vitamin C for 4 hours. 30 minutes imaging, cells were stained with 7.5 µM MitoSOX Red dyes for 30 minutes at 37°C. Cells were in imaging buffer during the imaging process. Scale = 50 µm.

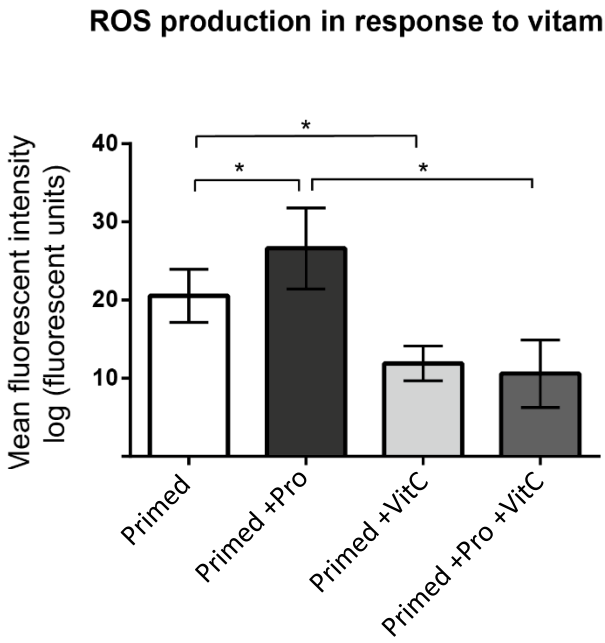

Figure 4.2.14. ROS production in ES cells in response to ascorbic acid (or vitamin

ROS production in ES cells was validated with the addition of Vitamin C by **A.** Immunofluorescence and **B.** Flow cytometry. *n=3,* ***p*≤0.05.

4.2.3. ROS production in response to proline is regulated in naïve and primed ES cells

Given that ROS production is a direct product of proline oxidation by the enzyme Prodh and naïve and primed ES cells have differential expression of this enzyme, it was hypothesised that this could lead to different proline metabolism in different ES cell states and only primed ES cells with high level of Prodh will increase ROS in the addition of proline. Therefore, ROS production in the mitochondria was measured by flow cytometry in naïve and primed D3 ES cells in response to proline. First, the level of ROS production in naïve ES cells was compared to that of primed ES cells. It was found that the total ROS production was similar in naïve and primed ES cells. However, in naïve ES cells, ROS^{lo} population produced significantly lower ROS than those of primed counterparts (Figure 4.3.6.B), most probably because naïve-ROS^{lo} cells sit in a lower range of ROS compared to primed ES cells (Figure 4.3.6.A). Different constitution of ROS^{lo} and ROS^{hi} populations was also observed in naïve and primed ES cells. Particularly, there was a tendency that naïve state of ES cells had higher percentages of ROS^{hi} and lower percentages of ROS^{lo} cells compared to primed state (in all 5 replicates with $p = 0.053$), suggesting that ES cells of different pluripotent states may have distinguished ROS profiles. As ROS profiles were different in different pluripotent states: naïve, primed and primed + proline ES cells, it was hypothesised that this ROS was correlated with the production of ATP in these cells and that cells with higher ROS production generate higher ATP levels. ATP assay was performed in these cells to examine this question. Interestingly, naïve ES cells produced significantly higher ATP than primed ES cells (Figure 4.3.7). Primed ES cells treated with proline showed a trend of increased ATP synthesis (in 4 out of 5 experiments) compared to control cells (Figure 4.3.7). This has not been shown before in the literature even though it was shown that ATP level is higher in naïve ES cells cultured in 2i+LIF compared to EpiSC cells cultured on KOSR and MEF (Zhou et al., 2012).

Based on the ROS profiles, naïve and primed ES cells were then examined for their ROS production in response to proline. After 3 hours of proline addition to the culture media (at the concentration of 200µM), only primed but not naïve ES cells, significantly increased the production of ROS (Figure 4.3.8). Morphological investigation of naïve ES cells in response to proline informed that naïve ES cells were not able to obtain differentiated morphology in proline addition (Figure 4.3.9), confirming that proline-induced differentiation only occurs in primed ES cells and is correlated with the ROS production. Due to time restrain, WA30 ES cells were not investigated f or ROS production.

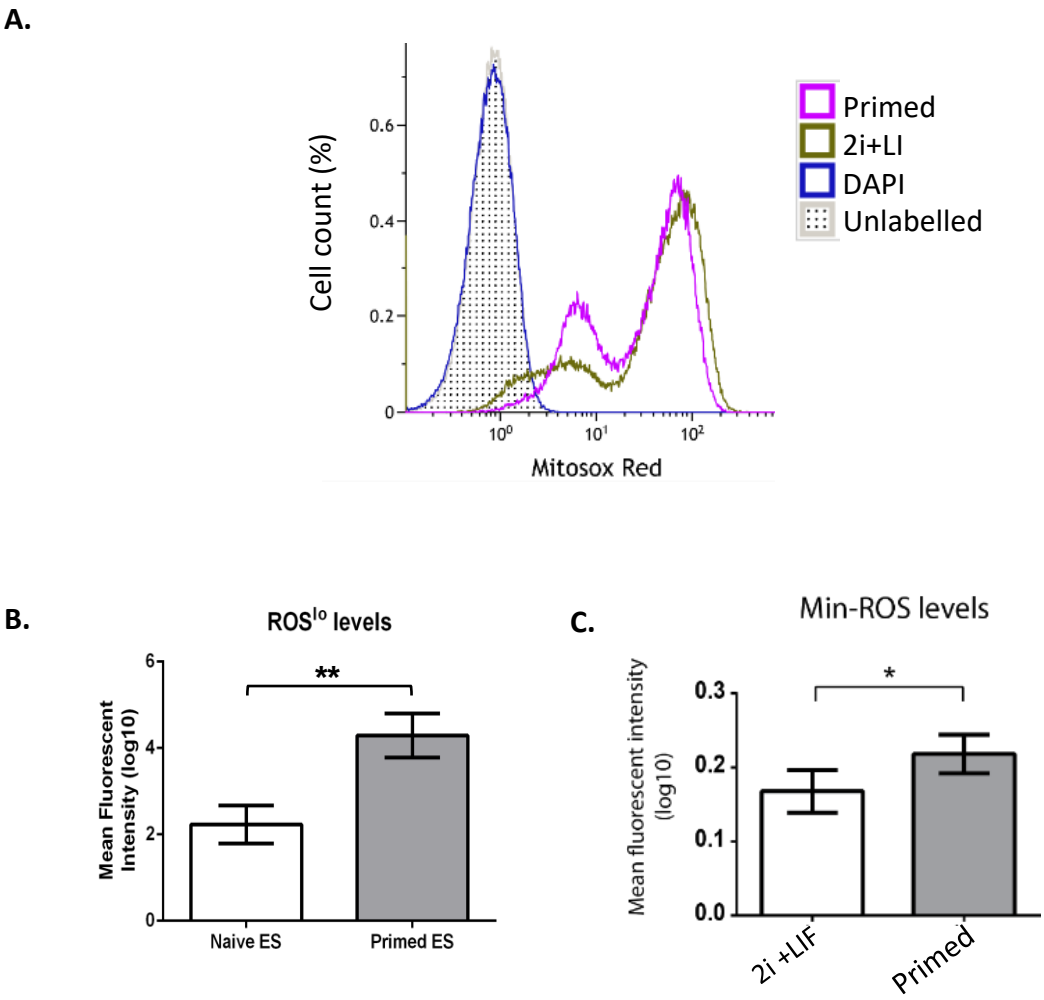

Figure 4.2.17. ROS production in naïve (2i+LIF) compared to primed (Serum+LIF) D3 ES

D3 ES cells grown in 2i+LIF and Serum+LIF conditions for at least 2 passages were used for ROS measurement by flow cytometry. **A.** Flow cytometry histogram of MitoSOX Red intensity (ROS production) in naïve and primed ES cells. **B.** Comparison of ROS^{lo} production and the lowest or minimal (Min) levels of ROS detected in naïve and primed ES cells. *n=5*, ***p*≤0.05, ****p*≤0.01.

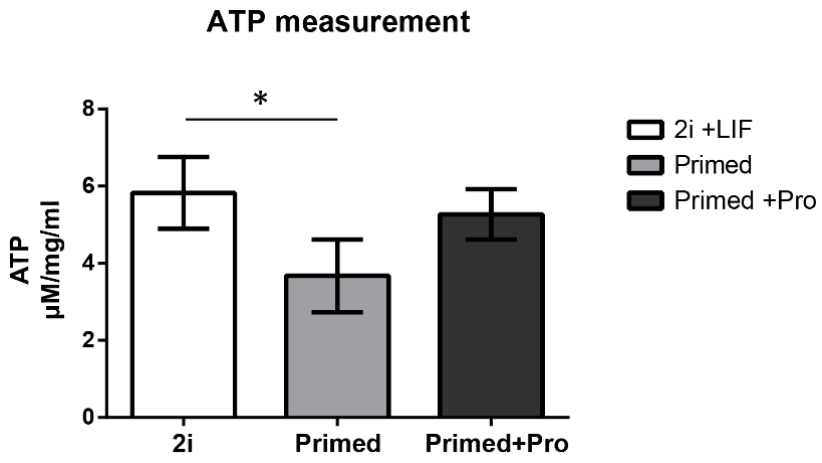

Figure 4.2.20. ATP measurement in ES cells in different pluripotent states.

Cells were grown in coat-free 96-well plate 24 hours before harvest. ATP measurement (µM) were normalised to the protein content (mg/mL) of the cells.

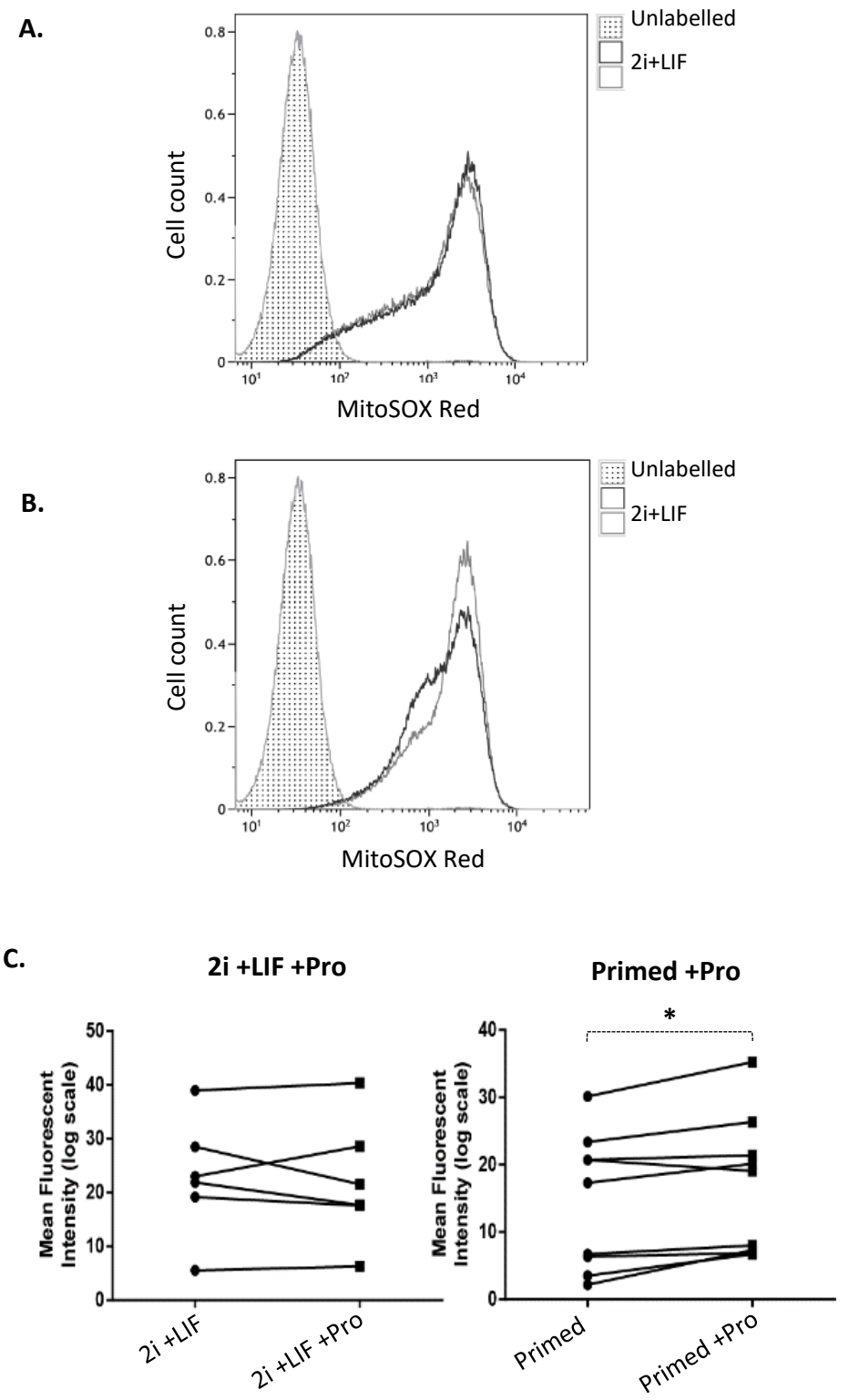

Figure 4.2.23. Reactive oxygen species production in D3 ES cells in response to 200µM ..

Histogram of MitoSOX Red intensity (ROS production) of naïve (2i+LIF) (**A**) and primed (Serum+LIF) (**B**) D3 ES cells. **C.** ROS production in response to 3 hr proline addition (200 µM) in naïve and primed D3 ES cells. The cells were grown for 24 hours before collection for analysis. 30 minutes before collection, MitoSOX Red dye was added to detect ROS production in the cells. ***p*≤0.05, *n=6-9.*

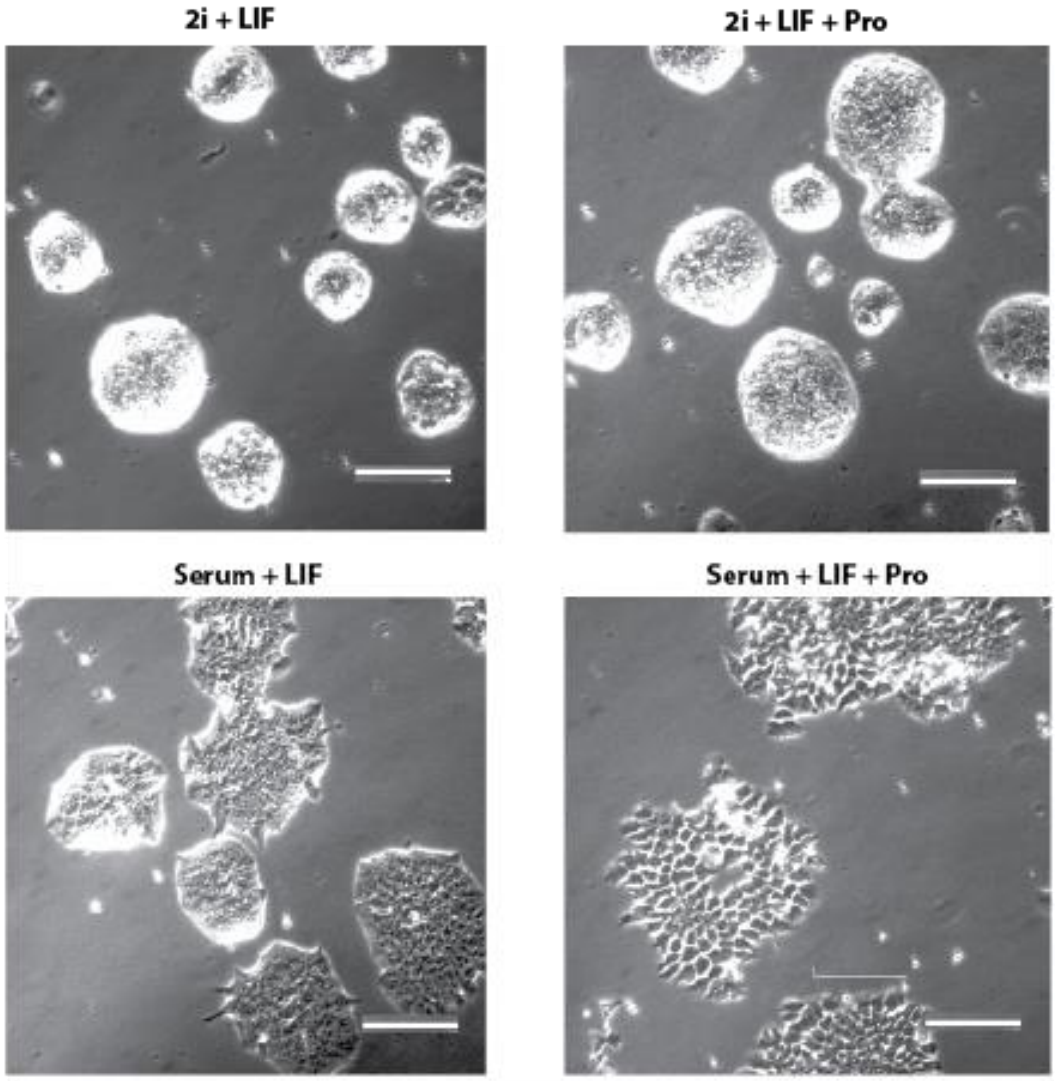

Figure 4.2.26. Morphological investigation of naïve (2i+LIF) and primed (Serum+LIF) D3 ES cells in response to proline for 4 days.

Scale = 50 µm.

4.3. Discussions

4.3.1. ROS production revealed ES cell heterogeneity

ES cell heterogeneity has been studied from different molecular aspects including epigenetics, DNA property, and transcriptomic and metabolomic diversity, which demonstrated the common presence of different ES cell subpopulations in culture (Hayashi et al., 2008, Wang et al., 2017, Turco et al., 2012, Singer et al., 2014, Tanaka, 2009, Herberg et al., 2016). In this chapter, the data show that D3 ES cell subpopulations could be defined by mitochondrial ROS production, adding a new parameter to determining ES cell heterogeneity. Many studies have investigated ROS production in ES cells using MitoSOX Red, which measure mitochondrial superoxide levels as the major source of ROS in the cell microenvironment (Prowse et al., 2012, Heo et al., 2016, Varum et al., 2009). None of these studies have mentioned the heterogeneous profile of ROS in their ES cell lines, even though the signs of ROS heterogeneity could be observed in the data of some experiments (Prowse et al., 2012, Heo et al., 2016, Marsboom et al., 2016). As a major product from mitochondrial activities, it is questionable whether the separation of ROS populations could link ES cell heterogeneity to their mitochondrial function.

Spontaneous reversible differentiation occurring during cell growth appears to promote heterogeneity in ES cell *in vitro* (Nair et al., 2015, MacArthur et al., 2012). The transcription regulation network including Nanog, Oct4, Sox2 and Zfp42 forms a pluripotent circuity to govern ES cell fates (Masui et al., 2007, Mitsui et al., 2003). The changes in mitochondrial function were known to be associated with the changes in the pluripotent circuit that defines embryonic development (Harvey et al., 2011), somatic cell reprograming (Suhr et al., 2010) and ES cell differentiation (Cho et al., 2006a, Chung et al., 2007). Understanding the origin of ROS heterogeneity would be useful to confirm the role of mitochondrial activities in ES cell growth and help to predict potential ES cell fate.

Physiological regulation of ROS is required to maintain genomic integrity in ES cells as the excessive ROS production of ROS could lead to oxidative damage to DNA content (Li and Marban, 2010, Saretzki et al., 2008) and the extreme suppression of ROS could affect the efficiency of DNA repair (Li and Marban, 2010). In the conversion of mice embryonic fibroblasts (MEFs) to mice induced pluripotent stem cells (iPSCs), physiological level of ROS was reported to be required for efficient nuclear reprograming, in which, both the decreased

and increased levels of ROS in MEFs resulted in the low iPSC yield (Zhou et al., 2016). In contrast, other data have documented that the use of antioxidants was efficient to reduce DNA damage in iPSC reprograming and support cell survival during the reprogramming process (Ji et al., 2014, Esteban et al., 2010). Indeed, ROS signalling has a range for optimal effects in ES cell growth. The data show that ROS production range is stable around the lowest points but not the highest points and vitamin C reduced ROS production by shifting the total population towards ROS^{lo} position. It is suggestive that ES cell may have a minimal maintenance of ROS production and this may reflect the basic activities of the mitochondria to sustain the cell function.

The need of minimal ROS production has been described in a model that was used for examinating mitochondrial uncoupling protein (UCPs) functions and was reviewed by Echtay and Brand (Echtay and Brand, 2007), but no study has examined the roles of minimal ROS requirement in PSCs. In fact, as ROS populations were associated with different MMP, it is possible that ROS heterogeneity could originate from cells with different mitochondrial properties. Ascorbic acid, which is commonly called vitamin C, is a strong antioxidant and is effective in reducing mitochondrial ROS by interacting with other mitochondrial enzyme activities (Valdecantos et al., 2010). It is questionable if low ROS level in vitamin C treatment is correlated with minimal MMP of the cells, and how vitamin C neutralise mitochondrial superoxide from the cells, or how cothe remaining ROS was still detectable. Further validation is needed to identify the relationship between ROS production and MMP as Mitotracker Green was observed to be affected by the presence of ROS or may be insensitive of MMP (Pendergrass et al., 2004, Xiao et al., 2016). At the same time, Mitotracker Green may also stain other organelles at high concentration as stated by the producers. The use of other MMP dyes may be informative and perhaps, the detection of mitochondrial features using electron microscope may be useful to understand mitochondrial profile of ES cell subpopulations during differentiation.

In this experiment, no correlation was made for ROS production, MMP and ATP production in naïve and primed ES cells, however, as naïve ES cells appear to have a higher percentage of ROS^{hi} cells, they also produce significant higher levels of ATP when compared to primed ES cells. This, perhaps, is in the agreement with the previous finding that ES cells leaving naïve pluripotency show a reduction in glycolysis and OXPHOS (Kalkan et al., 2017),

and that ATP generation in naïve ES cells is higher than primed and differentiated ES cells (Zhou et al., 2012). This is also supported by the data in the literature, which suggests that naïve ES cells as grown in 2i, possess higher mitochondrial respiration and oxygen consumption rate compaired to primed ES cells, which are grown in MEF feeder and knock-out serum (Guo et al., 2016, Zhou et al., 2012, Takashima et al., 2014). With the acknowledgement that media contents can contribute bias to the metabolic changes of ES cells (Rathjen et al., 2014, Zhang et al., 2016), the results in the literature are still consistent with the data in this thesis, where the culture media contents are more comparable, in that naïve ES cells are more active in energy generation compared to primed ES cells. In conclusion, the evidence suggests that high energy requirement is likely to be the characteristic of naïve ES cells cultured in 2i.

The results also show a sign of increased ATP requirement in the transition of primed ES cells toward proline-induced differentiated cells. This is contrast with the data in human PSCs, which indicate that undifferentiated cells rely on glycolysis for energy production and produce more ATP than the differentiated counterparts, which are less dependent on glycolysis (Zhang et al., 2011a, Birket et al., 2011). However, compared to the differentiated cells from other types of differentiation, proline-induced differentiation generates pluripotent stem cells at a different commitment state of cell fate determination, and thus, more examination is required to confirm the increase in ATP level in proline-induce differentiated ES cells.

4.3.2. Proline-induced ROS production is regulated in different pluripotent states

Given that proline metabolic enzymes, including Prodh and Oat, were differentially expressed in naïve and primed ES cells, these cells may perform different mechanisms to respond to proline and thus, the dynamics of proline metabolism could be regulated in different pluripotent states. As ROS is a product from proline metabolism catalysed by Prodh (Donald et al., 2001), ROS could be controlled in different pluripotent states in ES cells by different response to proline. Recent studies have shown that metabolic profiles of naïve and primed ES cells are distinguished by different glycolytic gene expression (Kolodziejczyk et al., 2015), lipid oxidation and amino acid metabolism (Sperber et al., 2015). These differences were correlated with the inhibition of GSK3 and MEK/ERK pathways (Kolodziejczyk et al., 2015, Sperber et al., 2015), however, proline metabolism is not mediated by this inhibition,

but instead, by the expression of p53 and Myc (Donald et al., 2001, Yoon et al., 2004, Rivera and Maxwell, 2005, Liu et al., 2012). Myc plays a role in the proliferation and biogenesis of naïve ES cells cultured in 2i conditions (Scognamiglio et al., 2016) and proline metabolism was not mentioned to be involved in the biogenesis process of these cells. No changes in ROS production or morphology of naïve ES cells in response to proline were detected, suggesting that naïve ES cells did not have similar mechanism to produce ROS and to differentiate when being compared to primed ES cells. Previous data have shown that the inhibition of MEK by PD0325901 did not affect ES cell differentiation in MEDII media (Tan et al., 2016a). Perhaps, forcing the conversion of primed ES cells back to naïve state by 2i could be correlated with the inhibition of proline-induced ROS production and the differentiation potential in these cells. In other words, releasing inhibition of GSK3 and MEK/ERK pathways may activate proline response via proline metabolism and Prodh induced ROS production to prime ES cells for differentiation. More investigations into this hypothesis is required to understand the correlation of proline metabolism and ROS production in ES cell differentiation.

Previous studies have reported that mitochondrial activities are regulated during the differentiation process, which results in the increased expression of the metabolic genes associated with oxidative metabolism and the decreased expression of stress defences (Saretzki et al., 2008, Chung et al., 2007). The question remains as of whether the changes in mitochondrial activities, including proline metabolism, could provide a signal for differentiation or are a consequence of differentiation initiation. Perhaps the production of ROS is likely to be an effect of differentiation process as the cells increase mitochondrial biogenesis upon differentiation initiation (Saretzki et al., 2008), but is not the requirement for differentiation. More investigations are required to clarify this posibility. However, the increased ROS production is observed in primed, but not naïve ES cells, and occurs early after proline addition and prolongs until 24 hours afterwards. In a time manner, the effect of ROS on nuclear reprograming occurred at the early state of reprograming and the later stage inhibition of ROS was found to have no effects on inhibiting MEFs reprograming (Zhou et al., 2016). As pluripotent stem cells rely on glycolysis (Folmes et al., 2011, Prigione et al., 2010), which produces less ROS than OXPHOS to protect their DNA content (Li and Marban, 2010), a robust increase in ROS production in ES cells at the early stage of proline addition indicates that ROS production could be a requirement for the differentiation process of ES cells. Considering increased ROS production as a response of proline metabolism (Donald et al.,

2001), and that ROS could be involved in ES cell differentiation via proline metabolism (Tan et al., 2016b, Tan et al., 2016a), the data in this chapter suggest that mitochondrial ROS could be induced by proline metabolism and provide signals to initiate the differentiation process.

Chapter 5 The involvement of Prodh activities and proline-induced reactive oxygen species in ES cell differentiation

5.1. Introduction

Mitochondrial metabolism provides a source of active biochemicals that are involved in the regulation of pluripotent stem cells (PSCs), (Prigione and Adjaye, 2010, Lisowski et al., 2018). The mitochondrial reshaping is achieved as the cells escape or enter pluripotency (Suhr et al., 2010, Bukowiecki et al., 2014) along with the cell metabolic programming, which can be observed in glycolysis, OXPHOS, and amino acid metabolism (Panopoulos et al., 2012). For programming, the cells need to adjust the mitochondrial activities and control the expression of the key metabolic enzymes, such as the oxidant and antioxidant factors (Saretzki et al., 2008, Armstrong et al., 2010), which promotes the balance in the cell redox homeostasis and supports cell maintenance (Lisowski et al., 2018). As a result, modifications occur to the cell pluripotent circuit transcription and the epigenetics (Tatapudy et al., 2017). Given that the mitochondrial metabolism is critical to the cell response to the environment and is contributing to the determination of PSC fate, little is known about the links between the mitochondrial metabolic factors and their mechanisms of action on PSC programming. It remains unclear as to how the metabolism and metabolites interact with PSC developmental cues.

Proline metabolism is known to play an important role in redox homeostasis of the mammalian cells to protect the cells from oxidative stress (Krishnan et al., 2008, Liu and Phang, 2012). The proline cycle, including proline catabolism and proline biosynthesis, was found to be required in the regulation of proline mediated tumour cell growth (Liu et al., 2015). Not only are the products of proline catabolism important for cell programming, but the synchronised effects of generating and feeding P5C, a proline precursor, back to the cycle are also required for the cell proliferation (Liu et al., 2015). The proline cycle includes multiple reactions that create a pool of metabolites and redox molecules such as $NAD(P)^+$ and NAD(P)H, which are linked to glutamine metabolism and aerobic glycolysis (Hagedorn and Phang, 1986, Liu et al., 2015). Moreover, proline metabolism is positioned in the middle of the mitochondrial activities and its metabolites could be fed to the tricarboxylic (TCA) thus,

proline metabolism is proposed as a key node in the regulation of cell function via the interaction with other metabolisms and mitochondrial activities.

The proline oxidation enzyme, Prodh, is a p53-dependent protein that is required for the proline-driven ROS production to initiate apoptosis in a variety of cancer cells (Donald et al., 2001, Rivera and Maxwell, 2005). Prodh is also found to play a protective role against hydrogen peroxide induced cell death in melanoma and prostate carcinoma cells (Natarajan et al., 2012). Depending on environmental factors, Prodh may play a different role in mediating cell responses via ROS production, which includes the interaction with other metabolic pathways to maintain redox homeostasis in cancer cells (Phang et al., 2012). Multiple downstream regulators have been investigated in relation to Prodh and proline, reporting their functions in activating key proteins via phosphorylation such as Akt, p38-MAPK and Src (Natarajan et al., 2012, Tan et al., 2016a). In contrast, the increased expression of Prodh without additional exogenous proline results in the reduced phosphorylation of MAPK and MEK/ERK (Liu et al., 2006). It is questionable whether proline is involved in other redox regulatory roles rather than its own metabolism. The production of mitochondrial ROS has been documented to cause the phosphorylative and oxidative activation of proteins (Ito et al., 2006, Ding et al., 2008). However, there is a missing connection that links Prodh activity and proline metabolism to the generation of ROS and redox signalling. In proline-induced ES cell differentiation, exogenous proline is known to generate ROS production, and the use of Prodh inhibitors prevents both ROS and the differentiation process (Tan et al., 2016a). The use of antioxidants inhibited the morphological differentiation of ES cells with the addition of proline (Casalino et al., 2011) and the activation of ROS signalling pathways was suggested (Tan et al., 2016a). However, the link from proline catabolism to ROS activation during the differentiation process has not been discovered. In this thesis, the regulation of proline metabolic enzyme expression and the dynamic ROS production following proline addition have been examined, and the correlation of ROS production with the differentiation of ES cells has been suggested. The mechanism of proline-induced ROS production in ES cell differentiation remains unknown. It is hypothesised that the proline oxidation reaction catalysed by Prodh is correlated with ROS production and this ROS is required for ES cell differentiation.

To address this hypothesis, ROS production was measured in D3 ES cells with the addition of Prodh inhibitors in the presence of proline. This would create a correlation of ROS production with the proline oxidation. ES cells in this treatment were also examined for the differentiated phenotype and pluripotent gene expression to confirm if the inhibition of Prodh and proline catabolism is associated with the differentiation process. To access the role of ROS in differentiation, multiple antioxidants were used to keep ROS at low levels, where after, the phenotypic and transcriptional investigation of ES cells was performed to validate whether ROS was required for differentiation. In addition, $NADP^+$/NADPH ratio was quantified to demonstrate the changes to the redox status within the cells following the proline treatment and to confirm the role of ROS via redox homeostasis. The results would establish the link between Prodh activity and ROS production to the differentiation of ES cells.

5.2. Results

5.2.1. Proline-induced ROS production is dose dependent and is correlated with ES cell differentiation

The data in the previous chapter showed that ROS production increased in response to 200 µM proline, which was efficient enough to induce ES cell differentiation. However, at a lower concentration, 40 µM proline has been shown to be ineffective to induce ES cell differentiation (Washington et al., 2010). The question remains as to whether ES cells increase ROS production as a response to proline at this low concentration. Therefore, ROS was measured in ES cells 24 hours after 40 µM proline was added, which showed no significant increase in ROS production in ES cells, and ROS production was significantly lower in ES cells that were treated with 200 µM proline (Figure 5.2.1.B), suggesting that ROS production is dependent on the concentration of proline and is correlated with ES cell differentiation.

Proline metabolism involves the conversion of ornithine to proline via the activity of Oat enzyme (Adams and Frank, 1980). In this conversion, the production of the intermediate, P5C, was suggested to be involved in the differentiation process (Casalino et al., 2011). It is unknown whether the conversion of ornithine to proline by Oat enzyme can raise the cellular concentrations of proline, which increases proline oxidation by Prodh to produce ROS in ES cells as a consequence. Previous observations suggested that ornithine did not lead to ES cell differentiation (data not shown). It raises the hypothesis that the addition of ornithine does not lead to the production of ROS and therefore does not lead to ES cell differentiation. To test this hypothesis, ROS was measured in response to 200 µM ornithine and ES cell differentiation was examined via the morphological changes and gene expression. At the same concentration to proline, 200 µM ornithine was not sufficient to increase ROS production and induce ES cell differentiation (Figure 5.2.1 and 5.2.4.D.). This was ten-fold lower than the concentration that was used successfully in the literature to induce differentiation (Casalino et al., 2011), but reflected the physiological range of ornithine amino acid in mammals (Kwon et al., 2003, Wu et al., 2008, Ginguay et al., 2017). Thus, the biosynthesis of proline from ornithine was not sufficient to replace proline in inducing ROS production and in driving ES cell differentiation, at least with the addition of ornithine at the physiological level.

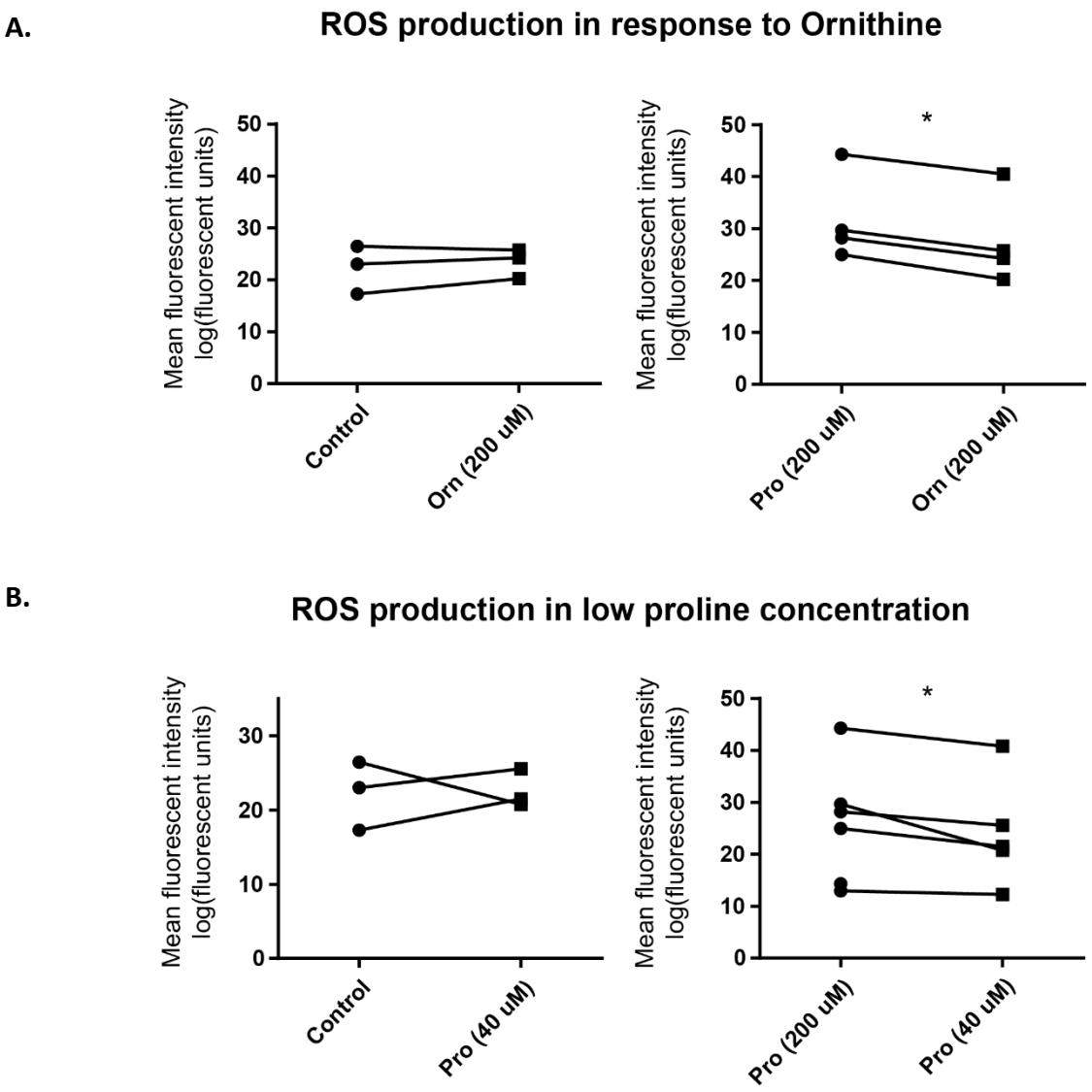

Figure 5.2.1. ROS production in ES cells in response to A. Ornithine (200 µM) and B. Low proline concentration (40 µM).

ES cells were treated with 200 µM ornithine and 40 µM proline concentration for 24 hours before collection. 30 minutes before collection, cells were stained with 7.5 µM MitoSox Red in complete media in the incubator. Cells were then visualised by flow cytometry. Non-treated ES cells and ES cells treated with 200 µM proline were included for controls. *$*p \leq 0.05$*, *n=3-5*.

5.2.2. Prodh inhibitors were not sufficient to prevent proline-induced ROS production and differentiation

To evaluate whether proline oxidation is correlated with ROS production and differentiation, the Prodh inhibitors, 3, 4- Dehydroproline (DHP) and L- tetrahydro-2-furoic acid (THFA) were used to compete with proline for the binding on Prodh as previously described (Smith et al., 1962, Natarajan et al., 2012). After 24-hours of treatment with 200 µM DHP and THFA, none of the inhibitors were effective to prevent ROS production in ES cells in response to proline (Figure 5.2.2.B). Furthermore, the addition of DHP increased ROS production significantly when compared with both proline treated and untreated control ES cells (Figure 5.2.2.B), and this is the highest ROS level that could be detected in ES cells during this study. However, when DHP was added to ES cells treated with proline, ROS production was returned to the same level as proline treatment alone (Figure 5.2.2.B), suggesting that proline inhibited the effect of DHP in inducing extreme ROS production. At the same time, the morphological examination of Prodh inhibitors showed that DHP led to growth arrested in ES cells, which was rescued by the addition of proline (Figure 5.2.3.C). The addition of proline not only restored the growth arrested condition, but also induced ES cell differentiation, suggesting that DHP was not efficient enough to inhibit the proline effect on ES cell differentiation (Figure 5.2.3.C). This contrasts with the previous findings that DHP can inhibit proline-induced differentiation and ROS production (Tan et al., 2016a, Casalino et al., 2011), possibly due to different types of measurements and different use of the proline/DHP ratios. However, even when the similar proline/DHP ratios were applied, ROS production did not alter (data not shown). When compared to control ES cells, the addition of DHP alone to ES cells significantly reduced the expression of *Dnmt3b* while *Otx2* expression increased (Figure 5.2.4.B), which is significantly different from both the controlled and proline-induced differentiated ES cells, suggesting that DHP produced different effects to ES cells and is not related to proline. Similarly, even though TFHA did not create any alterations to ES cell pluripotency and ROS production, it was not efficient to reduce proline-induced ROS after 24 hours and was not effective in preventing proline-induced ES cell differentiation after 4 days (Figure 5.2.2.B and 5.2.4.B).

A.

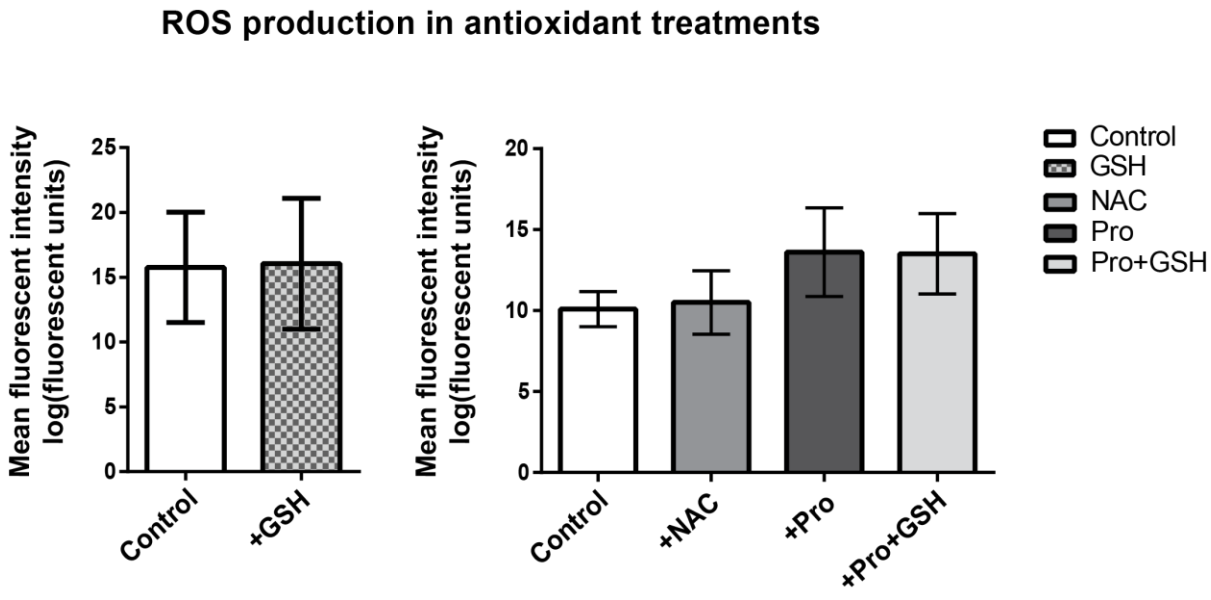

B.

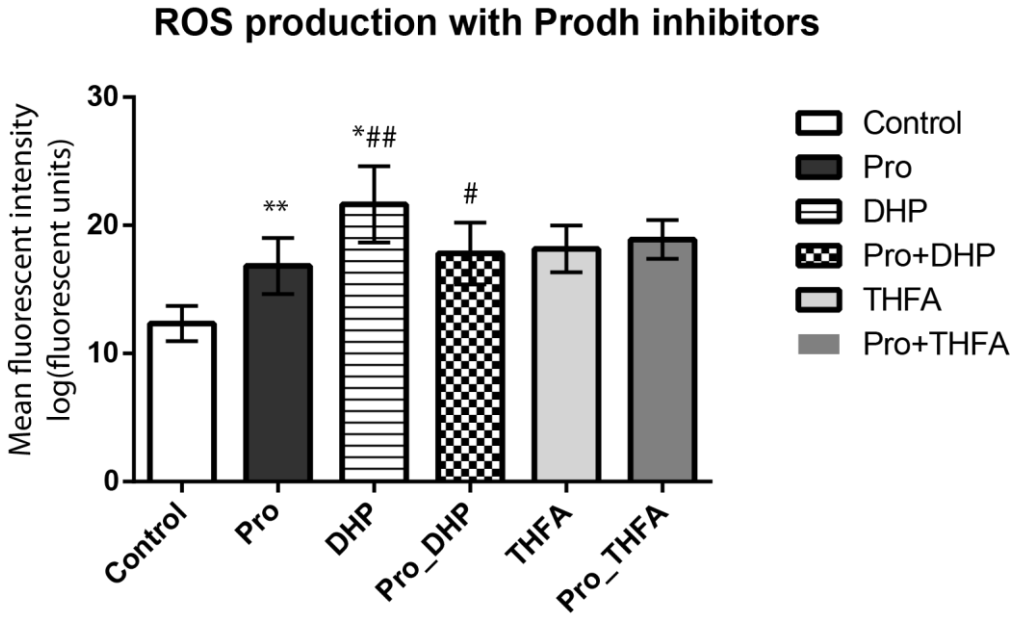

Figure 5.2.2. ROS production in ES cells with the addition of antioxidants and Prodh inhibitors.

A. Antioxidants. B. Prodh inhibitors. GSH (1mM), NAC (50 µM), DHP (200 µM) and THFA (200 µM). *n*=3, * or # $p \leq 0.05$, ** or ## $p \leq 0.01$ *compared to ES control, # compared to ES+ 200 µM Pro. Bar: SEM

5.2.3. The coeffect of ROS production and mTOR activation did not lead to ES cell differentiation

Given that mTOR is activated by a number of amino acids such as proline, leucine and glycine (Washington et al., 2010), the question remains whether ROS production and mTOR activation are both required in order to initiate ES cell differentiation. Since DHP could increase ROS production, but not necessarily activate mTOR, leucine was also used to contribute the additional mTOR signal (Washington et al., 2010) thus, DHP and leucine (1mM) were added to ES cells to examine if this combination would be sufficient enough to activate the differentiation process. DHP (200 μM) and leucine (1mM) were added to ES cells for 24 hours, which showed that the co-activation of ROS production and mTOR was insufficient to cause ES cell morphology toward proline-induced differentiation (Figure 5.2.2.B and 5.2.4.B). In addition, DHP still caused arrested cell growth and leucine could not restore this effect (Figure 5.2.3.C). It then raised the question, of whether the pluripotency of ES cells was changed by the addition of DHP, and thus, led to the arrested growth observed in the experiment. To confirm this possibility, the gene expression of *Oct4* (or *Pou5*) and *Nanog* was examined in DHP treated ES cells. The resulting data showed that *Oct4* and *Nanog* expression in ES cells was not altered in DHP treatment (Figure 5.2.4.C). Similar results were observed in ES cells treated with both DHP and leucine (Figure 5.2.4.C), confirming that leucine was insufficient to overcome the effects of DHP.

A.

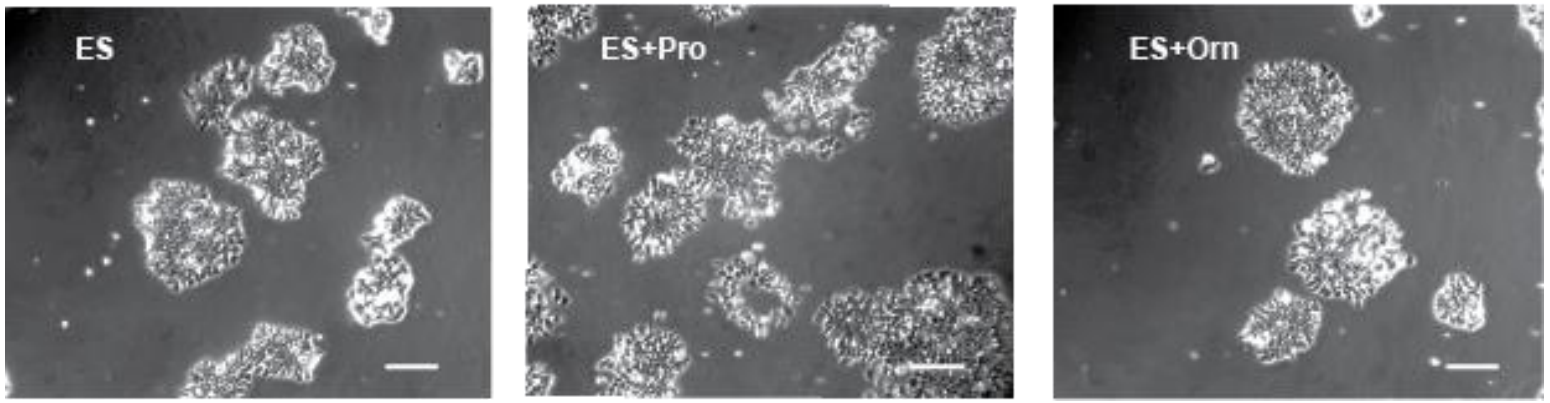
ES
ES+Pro
ES+Orn

B.

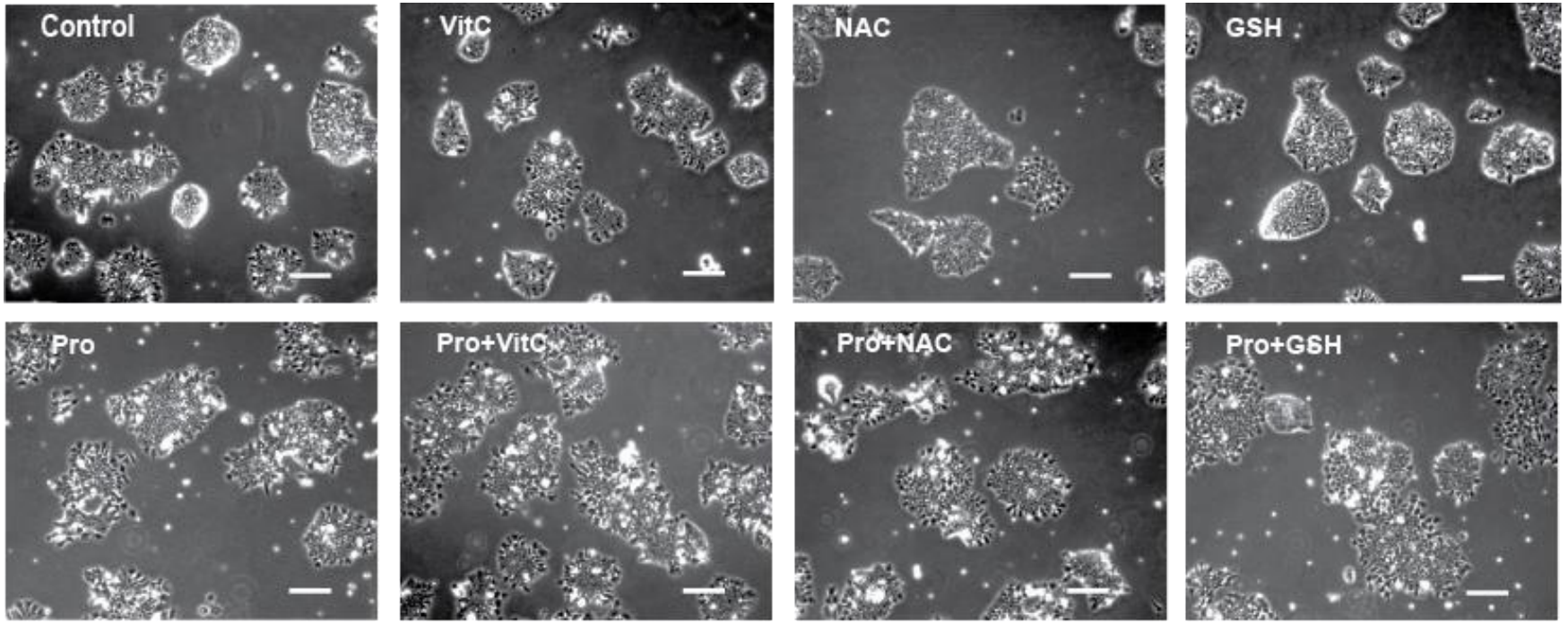
Control
VitC
NAC
GSH
Pro
Pro+VitC
Pro+NAC
Pro+GSH

C.

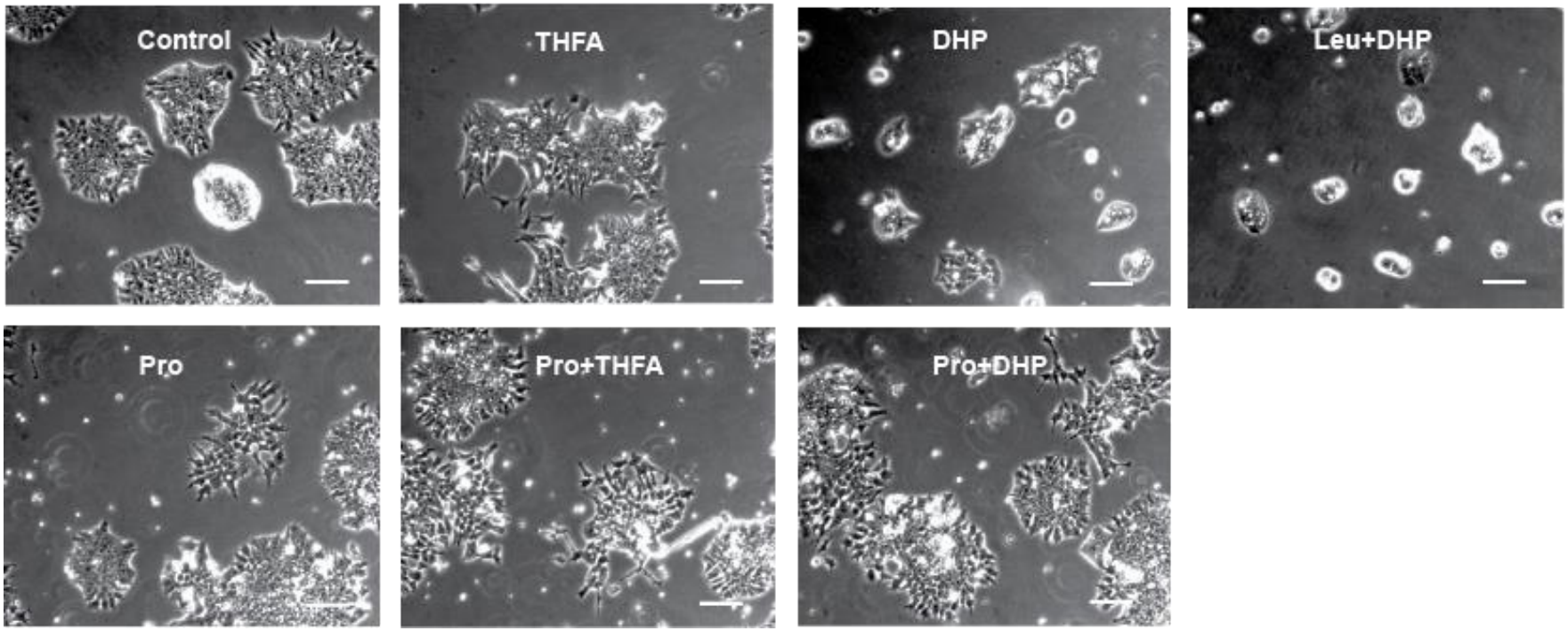

Figure 5.2.5. Morphology examination of ES cells

ES cells were treated with Ornithine (**panel A**), Antioxidants (**panel B**), and Prodh inhibitors (**panel C**). D3 ES cells were treated with different components at fixed concentrations: 200 µM proline, 200 µM ornithine, 50 µM Vitamin C, 500 µM NAC, 1 mM GSH, 200 µM THFA, 200 µM DHP and 1 mM Leucine. The cells were grown for 4 days with new media replaced every 24 hours. Images were taken at the end of day 4. All scales = 100 µm.

5.2.4. Antioxidants were insufficient to reduce proline-induced ROS production and ES cell differentiation

When addressing whether ROS production in ES cells in response to proline is required for ES cell differentiation, popular antioxidants including N-acetyl-cysteine (NAC) and glutathione (GSH) were used to prevent the production of ROS in ES cells. The cells were then collected to investigate the effects of the antioxidants on the differentiation of ES cells via the morphological changes and the pluripotent marker gene expression. There was no significant reduction of ROS in the treatment with either NAC or GSH (Figure 5.2.2.A). The less popular antioxidants such as vitamin E and Trolox were also tested but none of them were effective in reducing ROS production in ES cells in response to proline (data not shown). None of the antioxidants were effective in preventing the morphological differentiation of ES cells in response to proline (Figure 5.2.3.B). The examination of the pluripotent marker expression indicated that Vitamin C had a mild effect on preventing ES cell differentiation (Figure 5.2.4.A). However, none of other antioxidants were effective in inhibiting the activity of proline (Figure 5.2.4.A), suggesting that the use of antioxidants, apart from Vitamin C, was not sufficient enough to reduce ROS and prevent the differentiation of ES cells. Vitamin C, even though exerting a strong effect on reducing ROS production in ES cells, was not able to fully reduce the effects of proline on ES cell differentiation. This confirms that ES cell differentiation was not solely driven by ROS but also by other factors from the addition of proline. It should be noted, that the cells were collected for the gene expression examination at the 96-hour time point and 24 hours after fresh antioxidants were replaced. As the measurement of ROS was only taken at the 24-hour time intervals, and 4 hours after the antioxidants were added to the cells, it remains unclear as to whether the half-life of each antioxidant in the cell environment was sufficient to overcome the effects of proline.

A.

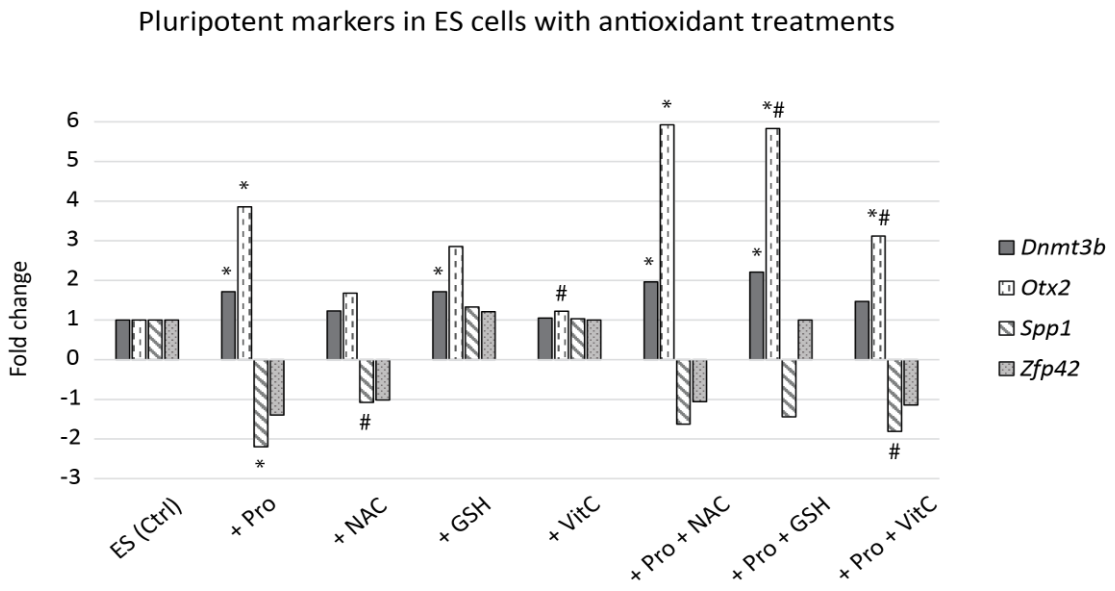
Pluripotent markers in ES cells with antioxidant treatments
Fold change
6
5
4
3
2
1
0
-1
-2
-3
ES (Ctrl)
+ Pro
+ NAC
+ GSH
+ VitC
+ Pro + NAC
+ Pro + GSH
+ Pro + VitC
Dnmt3b
Otx2
Spp1
Zfp42

B.

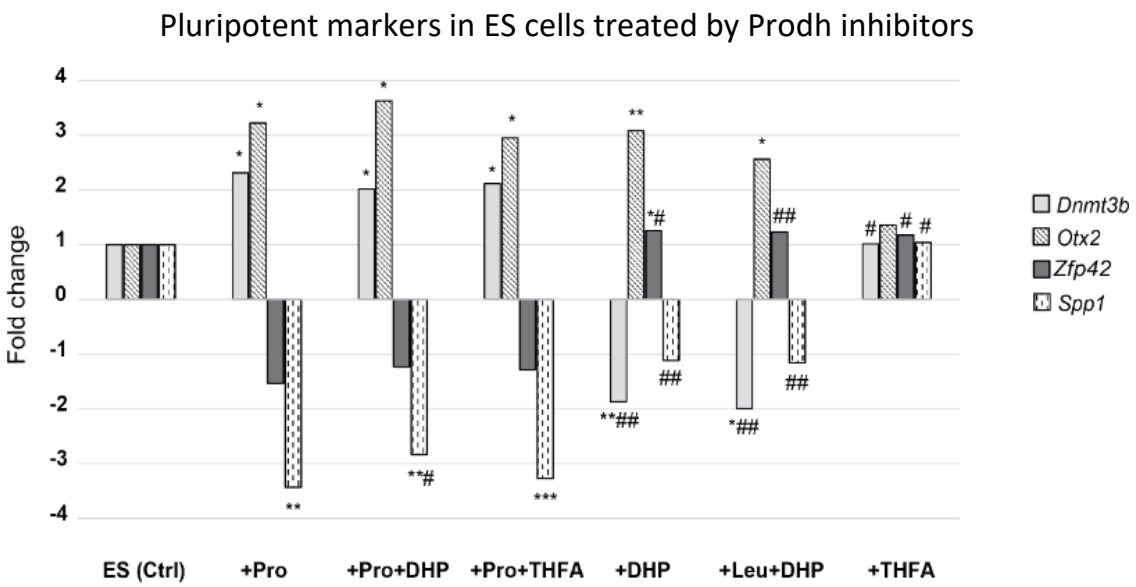
Pluripotent markers in ES cells treated by Prodh inhibitors
Fold change
4
3
2
1
0
-1
-2
-3
-4
ES (Ctrl)
+Pro
+Pro+DHP
+Pro+THFA
+DHP
+Leu+DHP
+THFA
Dnmt3b
Otx2
Zfp42
Spp1

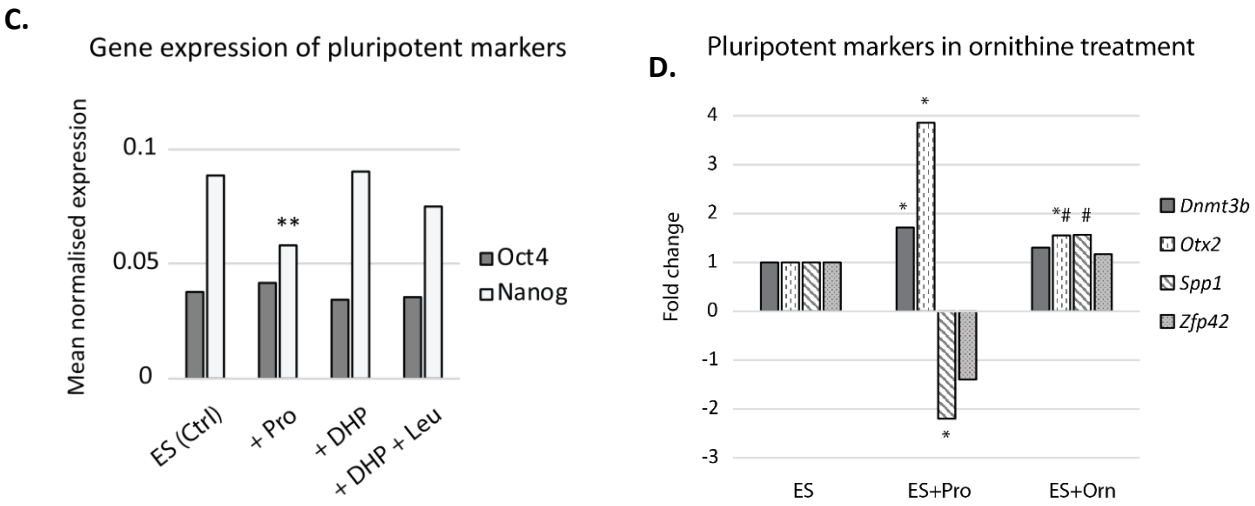

Figure 5.2.8. Gene expression of key pluripotent markers from D3 ES cells

ES cells treated with Antioxidants (A) and Prodh inhibitors (B, C) and Ornithine (D). D3 ES cells were treated with different components as stated in Figure 5.2.3. The expression fold change was calculated by dividing the normalised expression values from each treatment by ES cell control's (or **ES (Ctrl)** as marked). Paired t test based on the ratio of expression to ES cells (*p* values in *) or to ES + Pro cells (**+Pro** as marked, *p* values in #) were performed. The presence of a ***** shows that the expression of the gene was significantly different from ES cells, or more similar to EPL cells. The presence of a **#** shows that the expression was significantly different from EPL cells, or more similar to ES cells. The presence of both a ***** and a **#** shows that the expression of the gene was significantly different from both ES and EPL cells. n=3, * or #$p \leq 0.05$, ** or ## $p \leq 0.01$, *** or ### $p \leq 0.001$.

5.2.5. The increase in ROS production was not associated with the changes in NADP/NADPH ratio

Given the robust increase in ROS production in ES cells in response to proline, it was hypothesised that these changes in ROS levels were associated with the changes in the redox status of the cells. To address this question, nicotinamide adenine dinucleotide phosphate ($NADP^+$) and its reduced form, NADPH, was measured in ES cells in response to the addition of proline. The conversion of NADP/NADPH was also suggested to illustrate the proline biosynthesis process by P5C reductase as shown in intact mitochondria (Hagedorn and Phang, 1986) thus, the increase in NADP/NADPH levels could indicate that proline completes a catalytic cycle and P5C is reversed back to proline. This conversion may play a role in proline-induced differentiation given that P5C is suggested to be involved (Casalino et al., 2011). The measurement of the total cell lysates showed no significant difference in the NADP/NADPH ratios in ES cells between the untreated controls and proline treated cells (Figure 5.2.5), suggesting that ROS was not involved in the redox balance of the total NADP/NADPH levels. However, in this experiment, NADP/NADPH ratio was measured at the cellular, but not, the mitochondrial levels and the dynamics of proline catalysis within the mitochondria, and thus inconclusive.

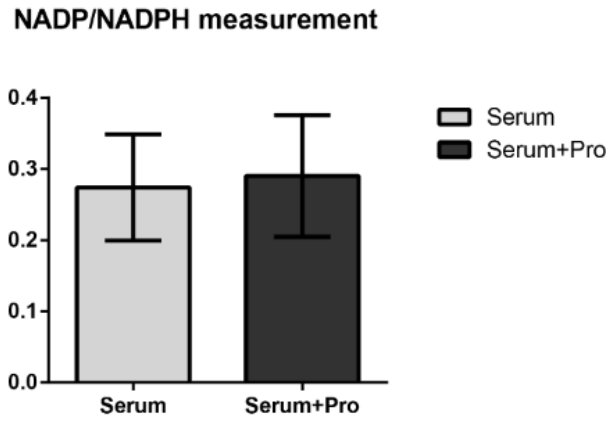

Figure 5.2.10. NADP/NADPH measurement in D3 ES cells in response to proline.

ES cells were grown in non-coated 24-well plate at the density of $4x10^5$ cells/well/500 µL media for 24 hours in Serum+LIF or Serum+LIF+Proline media before they were collected for NADP/NADPH assay. The absorbance at 460 nm wavelength reflected the concentration of NADPH concentration inside the cells. The concentration of NADPH (µM) was then normalised to the total protein concentration (mg/ml). Bar: SEM.

5.3. Discussion

5.3.1. Proline oxidation is not primarily required for proline-induced ROS production and ES cell differentiation

Proline oxidation that is catalysed by Prodh was suggested as a source of mitochondrial superoxide and hydrogen peroxide production in insects and human cell lines (Goncalves et al., 2014). Without the presence of the enzyme Prodh, proline itself is insufficient to increase ROS production in cancer cells (Donald et al., 2001), indicating that proline-induced ROS production is associated with proline oxidation catalysed by Prodh. In this study, the use of Prodh inhibitors, DHP and L-THFA showed no effects in reducing proline-induced ROS production in ES cells or preventing ES cell differentiation, suggesting two possibilities: a/ the mitochondrial ROS production that was measured in ES cells, was not a product from proline metabolism but was a result of other effects of proline-induced differentiation in ES cells and/or b/ DHP and L-THFA were not sufficient, at least at the 1:1 ratio to proline, in inhibiting Prodh and proline oxidation.

Proline metabolism can be linked to multiple cell metabolic processes such as the TCA and urea cycles (Liu and Phang, 2012). The presence of Prodh and Prodh activity are known to increase the levels of α-ketoglutarate (α-KG) and decrease the levels of succinate, fumarate and lactate (Liu et al., 2009). In addition, proline was found to increase the levels of NAD(P)H reduction in the presence of rotenone (Goncalves et al., 2014). This evidence suggests that proline and proline metabolism both play a multiple role in regulating mitochondrial functions. It is possible that the detection of mitochondrial superoxide with the addition of proline in ES cells came from the summary effect of this regulation. The sources of proline-induced ROS production were investigated in mammalian cells (Hancock et al., 2016, Goncalves et al., 2014). Prodh is known to provide electrons to the electron transport chain (ETC) and is an indirect source of superoxide and H_2O_2 production in intact mitochondria (Goncalves et al., 2014). Prodh was also shown to transfer electrons directly to the Coenzyme Q1 and the expression of Prodh directly down-regulated proteins of the ETC, leading to a decreased respiratory rate (Hancock et al., 2016). The data raise the possibility that the production of ROS in response to proline could be generated from different sites of the mitochondria. In addition, the use of the Prodh inhibitor, DHP, alone could inhibit the suppression effect of Prodh on ETC proteins which results in an increase in mitochondrial

respiration (Hancock et al., 2016). It is thus suspected that the use of DHP may not be effective in preventing mitochondrial ROS production but may provide an effect upon ETC proteins and mitochondrial respiration. As L-THFA should inhibit Prodh oxidation similarly to DHP, the use of L-THFA is expected to increase mitochondrial respiration. However, this was not supported by the ROS measurement data, which showed that L-THFA itself did not change ROS production in ES cells. It is also noticed that ES cells or PSCs do not have mature mitochondrial features and low mitochondrial functions (Suhr et al., 2010, Bukowiecki et al., 2014). This makes it challenging to study the efficiency of the mitochondrial transport. The understanding of immature mitochondria and their roles in ES cells is poorly understood, thus the effect of DHP and L-THFA as an inhibitor of Prodh in ES cells may be inconclusive based on ROS production. It was found that DHP inhibited the formation of hydrogen peroxide H_2O_2 in ES cells with the addition of proline (Tan et al., 2016a). DHP and L-THFA may provide different outcomes in ES cells and none of those outcomes directly affect the proline-induced mitochondrial superoxide production. ROS production could be the total sum effect of cell responses to proline rather than an effect of proline metabolism, and therefore, the conversion of proline to P5C may be more useful to study DHP and L-THFA in Prodh inhibition (Hagedorn and Phang, 1986, Nishimura et al., 2012, Hancock et al., 2016).

DHP has been previously used for preventing proline-induced differentiated morphology in ES cells at the three to one ratio with proline (150 µM DHP and 50 µM proline) (Casalino et al., 2011). The addition of DHP was reported to prevent the differentiation of ES cells by decreasing the expression of *Dnmt3b* and *Otx2*, key markers of proline-induced differentiated cells (Tan et al., 2016a). However, the morphology of ES cells in response to DHP reflected the growth arrested condition at the concentration of 200 µM, in which, the cell colonies appeared in a similar shape to the undifferentiated populations. The addition of proline restored this effect, and at the same time, induced differentiation. The restoration of the DHP-induced growth arrested morphology in ES cells was only specific to proline and was independent from mTOR activation due to the use of leucine which was ineffective. Together, these data suggest that the combination of mTOR activation and ROS production were not involved in ES cell differentiation and that the differentiation process was only specific to proline, confirming the previous finding on proline-induce differentiation (Washington et al., 2010). While DHP has shown adverse effects on cell growth, the addition of DHP on its own did not affect ES cell key pluripotent markers *Oct4* and *Nanog*. However, DHP reduced the

DNA methylation enzyme *Dnmt3b* expression and increased the differentiation marker *Otx2*. Previous studies have reported that Dnmt3b plays a role in DNA methylation and the reduced expression of *Dnmt3b* can result in the decrease of global DNA methylation in ES cells (Liao et al., 2015, Chen et al., 2003). Otx2 is known to play a role in the transition of ES cells to EpiSCs and in the maintenance of EpiSCs (Acampora et al., 2013). Therefore, DHP may serve a function in regulating ES cell methylation via the downregulation of *Dnmt3b* without affecting the cell pluripotency (Liao et al., 2015), while at the same time, inducing ES cell transition to the later primed state of pluripotency. To understand the role of DHP in ES cell programming and the regulation upon the pluripotent circuit, more investigation of DHP in ES cell function and pluripotency are required. However, given the extreme increase of ROS production in the addition of DHP, DHP effects may be more associated to the decrease in cell maintenance by increasing apoptosis in ES cells. This is supported by previous studies that DHP could inhibit collagen synthesis and the use of DHP was found to be toxic to bacterial cells (Kerwar, 1979, Smith et al., 1962). As the use of L-THFA did not affect ES cell growth, L-THFA may be safer than DHP in inhibiting the function of Prodh. Given that these inhibitors were not effective in reducing proline-induced ROS production and ES cell differentiation, the evidence proposes that ROS production in response to proline was not generated from the oxidation of proline and proline metabolism was not involved in the differentiation of ES cells. To confirm this finding, a cell system to track Prodh activity, and or, to effectively inhibit Prodh, may include the regulation of Prodh gene expression in ES cells, which may provide more opportunities to study the role of Prodh and proline metabolism in ES cell differentiation.

5.3.2. ROS production in ES cells is correlated with proline responses but is not primarily required for ES cell differentiation

Given that low concentrations of proline is ineffective in driving ES cell differentiation (Washington et al., 2010), and did not induce the production of ROS, it appears that the proline response is a dose dependent effect and proline may have a concentration threshold to generate ROS and regulate differentiation. At the same time, the biosynthesis of proline from ornithine did not produce ROS and did not lead to differentiation, demonstrating that there may be a correlation between proline-induced ROS production and ES cell differentiation. In fact, as primed ES cells did not express high levels of Oat, it was uncertain if the conversion of ornithine to proline was effective in primed ES cells or a high

concentration of ornithine may be required to initiate similar effects to proline (Casalino et al., 2011), which may fall out of the cell physiological range and may not recapitulate the natural pool of amino acids in mammals. It is known that the concentration of ornithine during the embryonic development does not exceed 600 µM, moreover, in adult humans a plasma concentration of 400 µM is considered to be toxic and damaging (Tanzer et al., 2011, Kwon et al., 2003, Ginguay et al., 2017). It is important to understand the transport and uptake of ornithine in ES cells in order to evaluate the role of ornithine in relation to the proline metabolic role in ES cell differentiation.

As none of the antioxidants used were effective in reducing ROS production or ES cell differentiation, except for vitamin C, it suggests that ROS production in response to proline and the differentiation process may be correlated. The addition of vitamin C reduced ROS to the lowest levels that could be detected in ES cells but only generated a minor effect in preventing ES cell differentiation, suggesting that ROS may be involved but is not a primary requirement for the differentiation process. In fact, proline was reported to play a role in the methylation of ES cell DNA that resulted in ES cells being primed towards epiblast stem cells (EpiSCs) and vitamin C reversed this effect and converted ES cells back to the naïve state of pluripotency (D'Aniello et al., 2017). ROS could be a response of the proline-induced differentiation, which provides the possibility that it is correlated with the differentiation initiation process rather than being a driven factor. Depending on the environmental factors and cell states, the expression of Prodh may support the withdrawal of proline from other sites that are contributing to the cell redox status. Specifically, proline and vitamin C are involved in the catalytic activities of the enzyme family prolyl-4-hydroxylase (P4H), which can function in collagen synthesis and the regulation of the hypoxia-inducible transcription factor HIF (Gorres and Raines, 2010, Myllyharju, 2013). P4H enzyme reaction requires 2-oxoglutarate (2-OG), which is also known as α-ketoglutarate (or α-KG), and ascorbate to bind to the catalytic site (Myllyharju, 2013). Furthermore, α-KG is a product of the TCA cycle that has been reported to correlate with the expression of Prodh to regulate the HIF-1α pathway (Liu et al., 2009). Even though it remains unclear as to the role of proline and vitamin C in the regulation of HIF-1α pathway of ES cells, the expression of HIF-1α downstream elements has been observed (D'Aniello et al., 2017), given that HIF-1α itself plays a role in regulating PSC metabolism and differentiation (Prigione et al., 2014, Zhou et al., 2012). More investigation

into this hypothesis is required in order to establish the mechanisms of proline-induced differentiation.

It should be noted that the measurement of ROS was limited to mitochondrial superoxide, which cannot be presented as the total ROS of the cells. Therefore, the use of antioxidants, GSH and NAC may be more effective in reducing hydrogen peroxide (H_2O_2) and hydroxyl radical (OH^-) levels rather than superoxide (Murphy et al., 2011). In addition, questions remain about the cell transport of these antioxidants into the mitochondria to suppress the production of ROS, as well as the half-life of each antioxidant, including vitamin C. For example, in this study the effects of vitamin C in reducing ROS was measured at a 4 hour interval and after being added to the cells, but the effect upon differentiation was examined at day 4 of the proline addition with media to be replaced every 24 hours. Thus, it may be inconclusive that these antioxidants were effective in preventing mitochondrial ROS production and proline-induced differentiation. In other words, proline may have exerted a longer half-life than vitamin C and regained its control after the antioxidant effects had ceased. It is possible that as vitamin C was sufficient to reduce mitochondrial superoxide and prevent differentiation to a small extent, it is possible that the differentiation may be partially dependent upon proline-induced mitochondrial superoxide. Furthermore, the conversion of superoxide into other types of ROS such as hydrogen peroxide can be performed by the mitochondrial enzyme manganese-dependent SOD (MnSOD) (Brand, 2016). The examination of different types of antioxidants such as MnSOD and different types of ROS could elucidate the active involvement of ROS in ES cell programming.

The redox pair NADPH/$NADP^+$ is an important metabolic factor of the mitochondrial homeostatic regulation system (Agledal et al., 2010, Xiao et al., 2018). The amount of oxidised NADPH was reported in the catalytic activity of proline metabolism by using the mitochondrial protein pool (Hagedorn and Phang, 1986). The conversion of $NADP^+$ and NADPH is also known to link proline to glucose metabolism via the pentose phosphate pathway (PPP) (Phang et al., 2012) however, it is unknown if the changes in $NADP^+$/NADPH ratios in the intact mitochondria can be generated into the changes within the whole cells. Given that no changes in the $NADP^+$/NADPH levels were observed after the 24 hour addition of proline to ES cells, it suggests that the redox balance could have been achieved at this time point, thus, this result may not be used to conclude the redox status of the cells, and it is suspected that the

measurement of other redox couples may provide similar outcomes as the redox balance is an immediate response. In fact, the global cell redox couple GSH/GSSG ratios was shown to remain unchanged in ES cells in response to proline (D'Aniello et al., 2017). Given that redox homeostasis in the cells is interchangeable, various time points and multiple redox targets should be considered for future investigation. Indeed, the downstream targets of these redox changes of ES cells would be useful to highlight the role of ROS in cell signalling, for example, protein oxidation may be more stable for quantitation and would provide a more reliable indicator for understanding the mechanism of ROS signalling in response to proline. This can be achieved by investigating different types of ROS-induced protein modifications such as thiol oxidation, disulfides and s-glutathionylation (Cai and Yan, 2013, Grimsrud et al., 2008). To finalise the role of proline metabolism and ROS production in the proline-induced differentiation of ES cells, effective neutralisation of ROS must be considered. Previously, superoxide dismutase (SOD) was used to effectively target mitochondrial ROS (Murphy et al., 2011, Fridovich, 1997) and thus, SOD can be used alternatively to reduce ROS production in ES cells. The effective inhibition of ROS production would be useful to investigate the role of ROS in ES cell programming, however, it should be considered that low ROS levels may potentially affect cell stability (Li and Marban, 2010). Therefore, the efficient manipulation of the Prodh-induced ROS production system may be more effective in addressing these issues, which again, highlights the need for a regulatory system of the Prodh expression in ES cells.

Chapter 6 Discussion and Future work

6.1. Overview of findings

Proline metabolism is conserved in multiple species including plants and mammals. Proline metabolism and its metabolites have been investigated in several cell models to elucidate their roles in cell programming. However, none of these studies have successfully identified those mechanisms which produce proline metabolically induced cell changes. As proline metabolism is a complex network which involves multi-reactions in the cell the environment, it is critical to understand the cross-talk between proline metabolism and cell modifications. This thesis is the first to study the relationship between the expression of the proline metabolic enzyme family and the production of proline-induced ROS in ES cell differentiation, which has been discussed in chapter 3 and 4. This is also the first study looking at ROS levels in different pluripotent states of ES cells, which confirms the distinguished proline metabolic dynamics in naïve and primed ES cells and suggests the roles of proline induced ROS in differentiation. The data in chapter 5 of this thesis have shown that proline metabolism may not be the source of ROS production and ROS may not be the key active component in proline-induced differentiation. However, the evidence could not completely exclude the involvement of Prodh and ROS in ES cell differentiation as their activities were inconclusive. Different approaches into the functions of Prodh and ROS should be considered for future investigation. For example, using *Prodh*$^{-/-}$ cell lines or the controlled knockdown of Prodh translation could potentially suggest if the change in Prodh expression influence changes in the spectrum of ES cell differentiation. The detection of other ROS types could possibly offer an opportunity to examine the overall pool of ROS within ES cells and its potentially significant role in the cell programming. Future work also warrants the involvement of P5C and the further investigation of other possible sites of proline acceptors within the cells.

6.2. The novel role of the proline metabolic switch in pluripotent lineage specification

Proline metabolic switches have been investigated in a number of cancer cells and were suggested to be involved in cancer development (Elia et al., 2017, Liu et al., 2012). The increase in proline biosynthesis from glutamine is required to support prostate cancer cell

growth and proliferation (Liu et al., 2012). However, in lung cancer cells, the gain of metastatic characteristics was associated with increased proline oxidation (Elia et al., 2017). The inhibition of Prodh, known as the key enzyme responsible for proline oxidation, was effective to prevent the growth and metastasis of cancer cells both *in vitro* and *in vivo* (Elia et al., 2017). Perhaps the proline metabolic switch is important for cell programming in high proliferative cells as it is also found in ES cells.

There have been debates in the literature about how ES cells of different pluripotent states can be best profiled. The data in chapter 3 of this thesis propose that proline metabolism may be an important indicator of the moving from naïve to primed pluripotency, although the possibility of using proline metabolism to identify ES cells of different pluripotent states will require further validation. A systematic review of the data of expression arrays in the literature may be useful for future investigation, thus, it is important to develop an algorithmic pipeline that can analyse expression data across multiple platforms. The integration of the gene expression and metabolomic data may potentially unravel and reveal new characteristics and cell pathways to better define the pluripotent lineages of ES cells based on their metabolism.

6.3. Mitochondrial superoxide production and mitochondrial activities

Mitochondrial superoxide production reflects mitochondrial activities, and this study is the first to suggest that ES cell heterogeneity can be detected by the measurement of mitochondrial ROS production in live ES cells. The origins of the heterogeneous populations are not known, and ES cell heterogeneity, in which, key pluripotent transcription factors fluctuate in spontaneous differentiation (Graf and Stadtfeld, 2008), still remain an unresolved question in stem cell biology. What cellular factors contribute to the phenomenon and how they cross-talk to cell changes are largely unknown. Therefore, it requires further examination to determine whether the heterogeneous ROS population are in correlation with the oscillatory expression of the pluripotent circuit and different metabolic signatures in ES cells. The increased mitochondrial superoxide production in primed ES cells soon after the addition of proline indicates that proline is an active supplement that can quickly accelerate ES cell response. It would be interesting to examine if the addition of other amino acids that are transported by Snat2 would give rise to similar responses in ES cells. Snat2 and mTOR have been shown to provide signals to mammalian cells in response to exogenous nutrients (Hyde

et al., 2007, Sahu et al., 2016). Examination of whether Snat2 or mTOR may be responsible for the increased mitochondrial ROS production in response to proline or other amino acids would clarify the role of nutrients in the culture of ES cells and how they cross-talk to the changes in the cell mitochondrial activities.

When considering ES cells with heterogenous ROS populations, questions are raised around what intrinsically defines these ROS levels and if the mitochondrial membrane potential is associated with ROS production, and as to whether these ROS populations have different metabolic properties or are in distinguished pluripotency or cell states. This knowledge may be beneficial in therapeutical application, given pluripotent stem cells are the key element necessary for regenerative medicine. The understanding that ES cells have different metabolic states and ROS production will also aid in the decision as to whether the use of low or high metabolic cells would be more beneficial in different types of treatments. With the understanding that the origins of different ROS profiles need validation and investigation, it is hypothesised that the use of a single population of ROS profile will be more stable and more predictable in justifying the outcomes of applying PSCs as a treatment. Perhaps the increase in ROS production in ES cells treated with proline is a direct result of the differentiation process as being suggested in chapter 5. It has been shown that the level of ROS production in ES cells and differentiated cells can be dependent on the cell size (Lyublinskaya et al., 2017). The question remains, as to whether this is correlated with mitochondrial function and will require further research.

6.4. The role of vitamin C and proline in ROS production in ES cells

Findings of the ROS measurement indicated that only vitamin C was efficient enough to reduce mitochondrial superoxide in both control and proline treated conditions. The role of vitamin C in mammalian cells and in ES cells specifically remains questionable, however, vitamin C and proline were reported to perform opposite effects on ES cell programming and plasticity as vitamin C reprogramed ES cells back towards the naïve state of pluripotency, while proline primed ES cells towards the epiblast stem cell state (D'Aniello et al., 2017). There possibly is a threshold for vitamin C activities as high Vitamin C/proline ratio which was effective in preventing ES cell differentiation (D'Aniello et al., 2017). Understanding the spectrum of Vitamin C and the proline effects in ES cells will contribute to our understanding of the role of these metabolites in cell programming.

6.5. Other preliminary findings that still require validation

6.5.1. Protein expression of Prodh and Oat and their cellular translocation

Different Prodh and Oat isoforms were detected in ES cells using the Western Blot technique. Even though it has been concluded that these isoforms could be a result of unspecific binding of the polyclonal antibodies, there is a possibility that these proteins could be isoforms of Prodh and Oat that are specific in ES cells. Different protein isoforms and protein splicing were shown to be involved in ES cell programming and differentiation (Buszczak et al., 2014, Gabut et al., 2011). The presence of the larger Oat isoform displayed a sign of differential expression in different pluripotent states, particularly, this was higher in primed and lower in naïve ES cells. It is suspected that this isoform may be regulated in different pluripotent states and may reflect the aggregation of the protein observed in the immunofluorescent experiment in chapter 3 as there is more Oat accumulation in the primed cells than there is in the naïve ES cells.

In image analysis pilot study with Prodh staining, the results suggested that there is a correlation between Prodh and DNA staining in all samples of the naïve and primed ES cells. The possible explanation for this result is the translocation of Prodh into the nuclei. The nuclear translocation of several metabolic enzymes has been reported in the literature (Snaebjornsson and Schulze, 2018, Boukouris et al., 2016). A study of the crystal structure of the PutA699 protein in *Escherichia coli*, which is the first structure of Prodh, shows evidence that Prodh is a multifunctional enzyme, which possesses a DNA-binding domain and is capable of performing transcription regulation (Lee et al., 2003). However, this has never been found in mammals. A question then arises as to whether this function has been lost during evolution or has evolved into different regulatory processes. Further investigation into this question would involve the isolation of the mitochondrial and nuclear proteins in ES cells, which would help to confirm if Prodh is present in the nuclei and mitochondria. Additionally, the painting of the cells with different organelle markers would possibly reveal the presence and location of Prodh and Oat in the cells.

6.5.2. Possible sites of proline-induced ES cell differentiation

Proline metabolism has been proposed as a potential mechanism for ES cell differentiation and has been studied in different mammalian cell models, which suggested a regulatory role in controlling cell fates. The involvement of proline metabolism in cell

programming and development is yet to be established. This thesis suggests that other sites of proline acceptors within the cells should also be considered in future investigation, specifically, prolyl hydroxylases, including P4Hs and prolyl hydroxylase domains (PHD), which hydroxylate proline residues in collagen synthesis and for the regulation of HIF-1α respectively. It is shown that proline and proline peptides are specific for the activation of ES cell differentiation (Washington et al., 2010). Free amino acid proline is not hydroxylated by P4Hs or PHDs, but they can interfere with the enzyme activity and the uncoupled 2-OG decarboxylation reactions (Gorres and Raines, 2010, Myllyharju, 2013). Any disruption of these enzymes could lead to the stabilisation of HIF-1α (Myllyharju, 2008, Myllyharju, 2013), which has been shown to play a role in ES cell differentiation (Bino et al., 2016). It is shown in this thesis that *P4ha*1, which encodes a subunit of P4Hs, are expressed in ES cells, suggesting that the system is present in these cells (as shown in chapter 3). The examination of PHDs in ES cells would potentially confirm whether these enzymes and the system play a role in the differentiation process. In fact, the Prodh inhibitor, DHP, is known to disrupt normal reactions catalysed by P4Hs and is a potential substrate for PHDs when replacing proline residues on HIF peptides (Kerwar and Felix, 1976, Li et al., 2004), moreover, DHP increases the rate of 2-OG decarboxylation reactions. Ascorbate, a derivative of vitamin C, is required for the uncoupled 2-OG decarboxylation reaction, which is catalysed by both P4Hs and PHDs. Given that both DHP and proline generate high ROS production and only Vitamin C reduces ROS in the proline treated ES cells, it is suggested that ROS production and these metabolites might be correlated with the uncoupled decarboxylation of 2-OG, and this effect may be separated from ES differentiation (as described in chapter 5). It is possible that these metabolites have different spectrums to contribute to ES cell programming and pluripotency as previously described (D'Aniello et al., 2017). This does not exclude the role of Prodh and proline metabolism in ES cell differentiation, and a *Prodh* knock-out cell line would be useful to confirm these conclusions.

6.6. Conclusion

This thesis is the first to produce data related to the proline metabolic enzyme family and the immediate cellular responses to proline that has been determined within ES cells, which revealed that proline metabolism and proline induced-ROS production are regulated in different pluripotent states. This thesis has further confirmed the critical role of proline and

proline metabolism in regulating ES cell fate at the early states of pluripotency. Even though the precise mechanisms of how proline induces the differentiation in ES cells still requires future research, the data in this thesis has largely proven that the proline metabolic switch is important in ES cells during the pluripotent lineage specification process, following which, ES cells responded differently to the addition of the exogeneous proline which produced different levels of ROS. How this metabolic switch supports ES cells in the different pluripotent states, and how it supports different metabolic outcomes requires further research and validation. This data suggests that the proline-induced differnetiation of ES cells may not originate from the proline metabolism process, and to confirm this possibility, the knock-out of *Prodh* is essential. Through the data it is proposed that the other proline receptor sites should be further examined in future research to fully clarify the specific role of proline in ES cell programing.

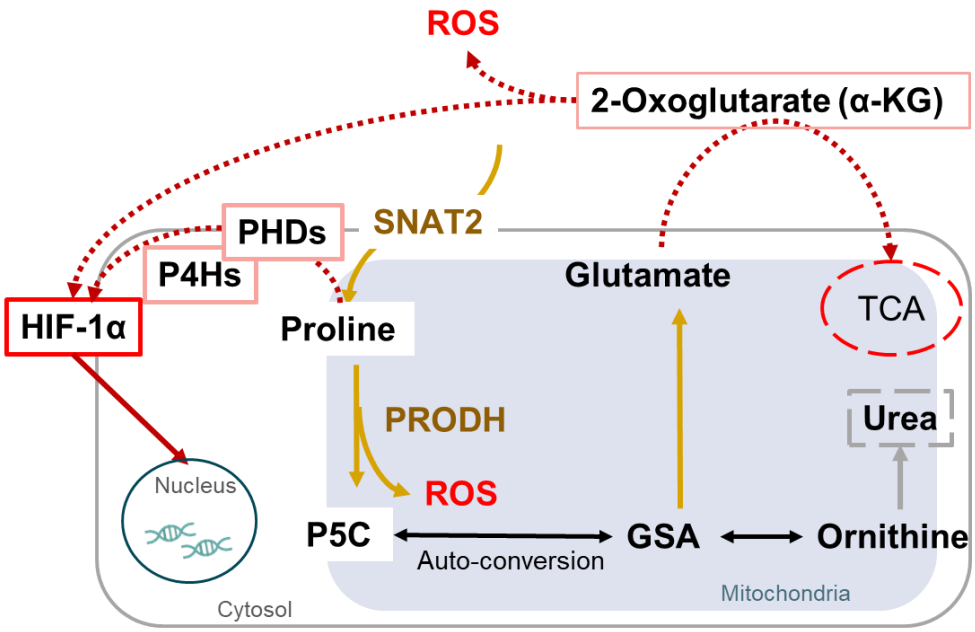

Figure 6.6.1: Possible sites of future investigation for the proline-induced differentiation in ES cells

Future work into proline-induced differentiation in ES cells would include the manipulation of Prodh gene expression, the conversion of proline into ornithine and glutamate, and the involvement of P4Hs and PHDs as well as α-KG and HIF-1α.

Appendix 1. Cell profiler module setup.

Supp. Fig 2: Summary of 13 modules in CellProfiler that were used for image analysis.

Module 1: Identify Primary Objects

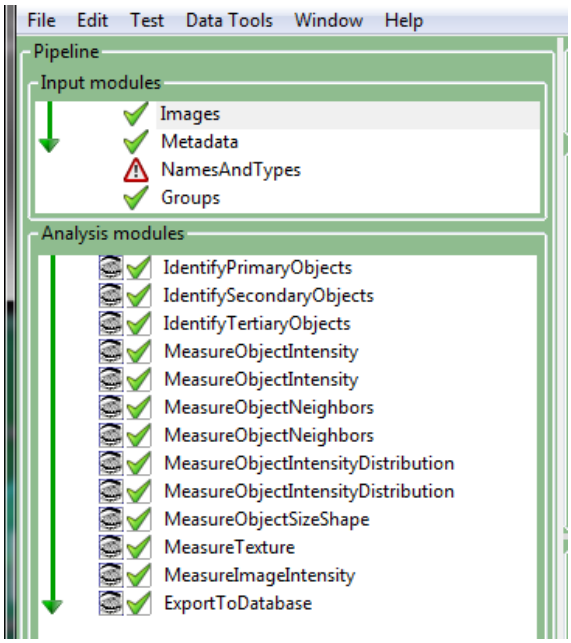

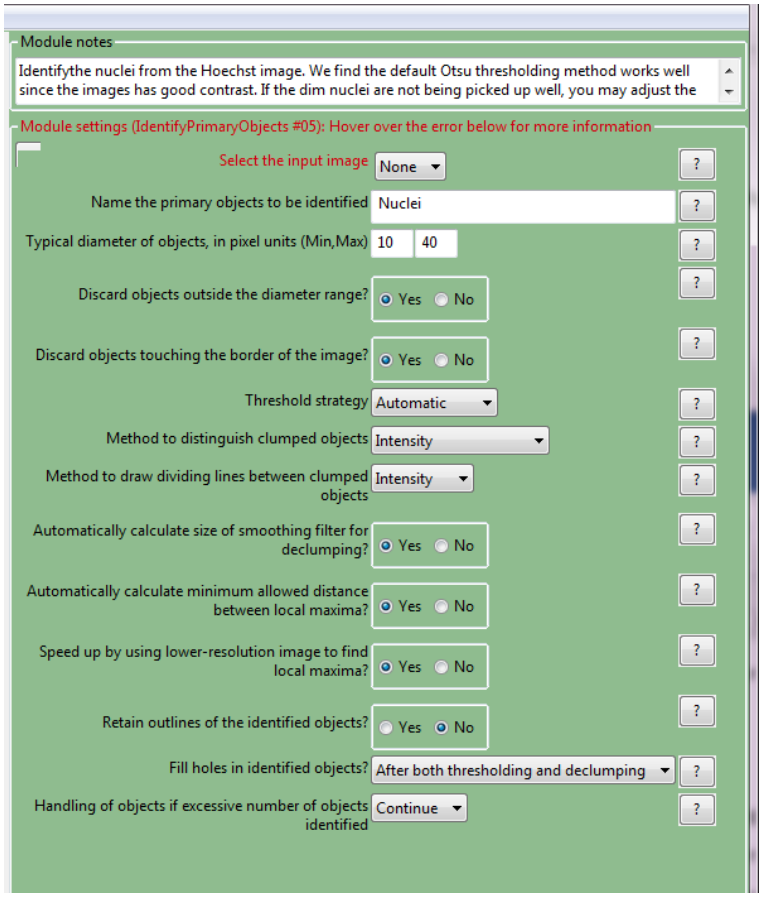

Module 2: Identify Secondary Objects

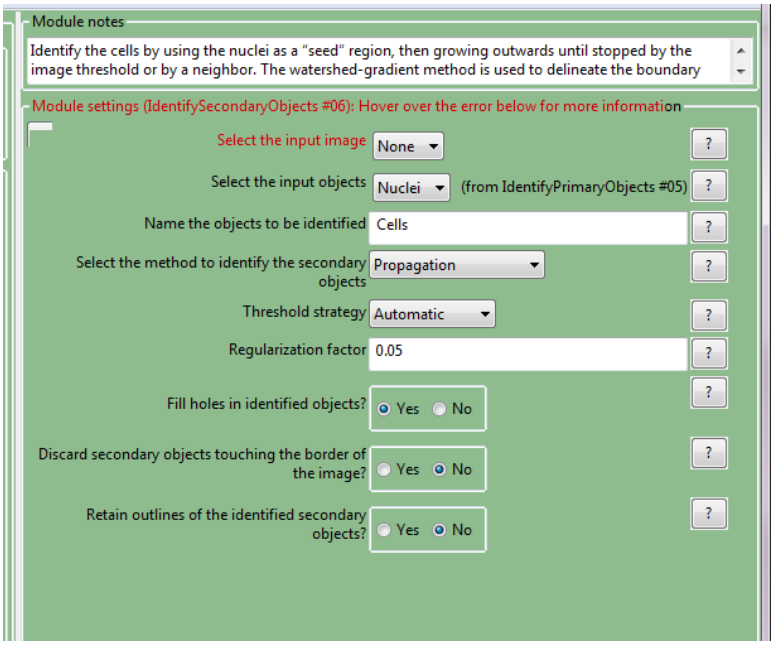

Module 3: Identify Teritiary Objects

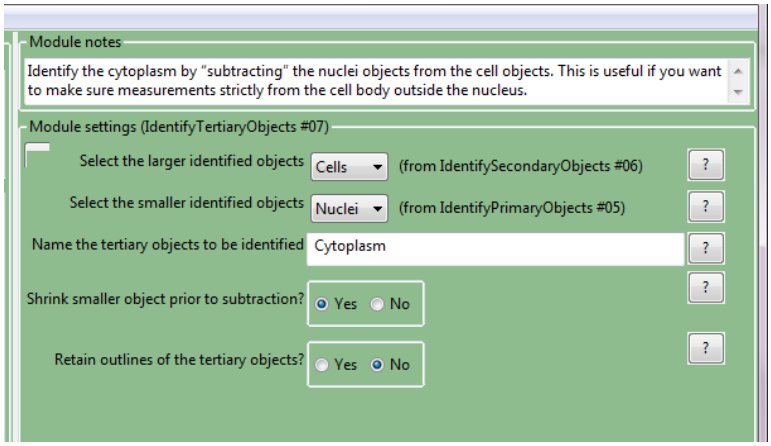

Module 4: Measure Object Intensity

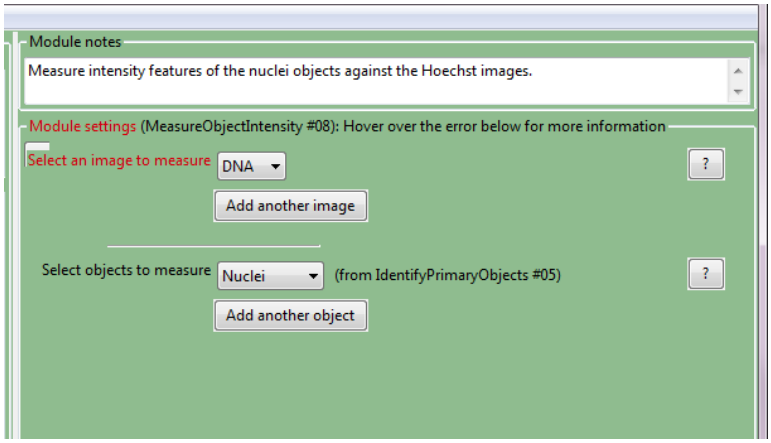

Module 5: Measure Object Intensity

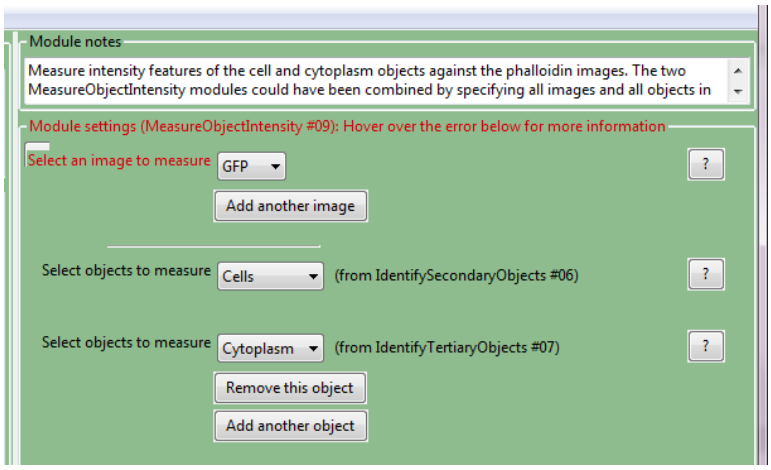

Module 6: Measure Object Neighbors

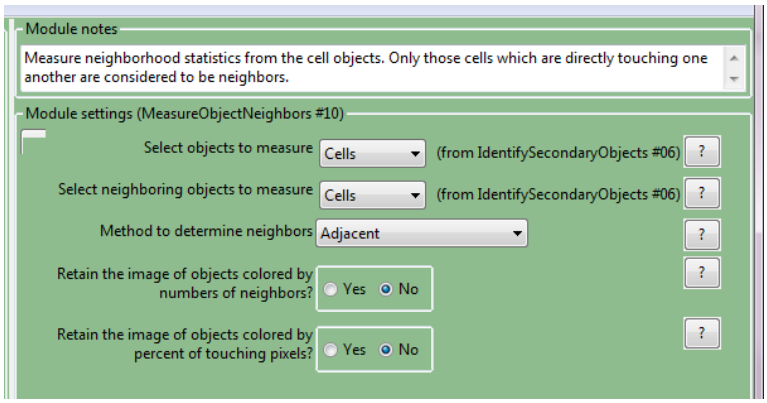

Module 7: Measure Object Neighbors

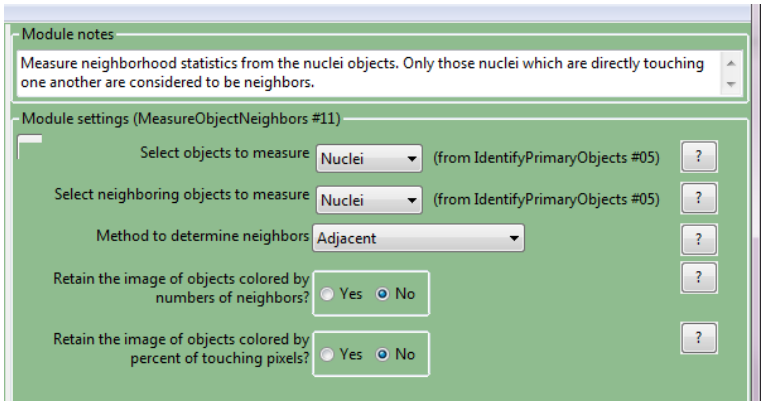

Module 8: Measure Object Intensity Distribution

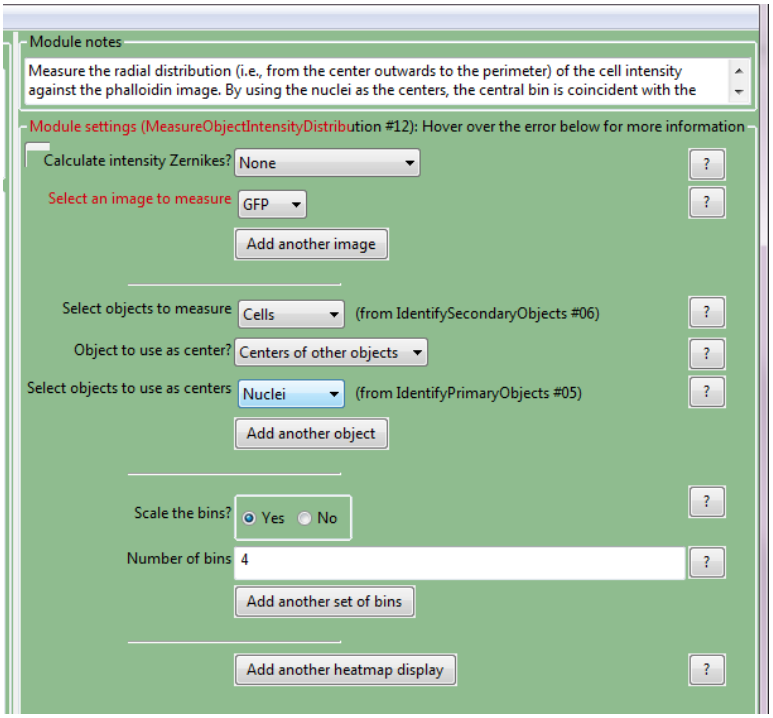

Module 9: Measure Object Intensity Distribution

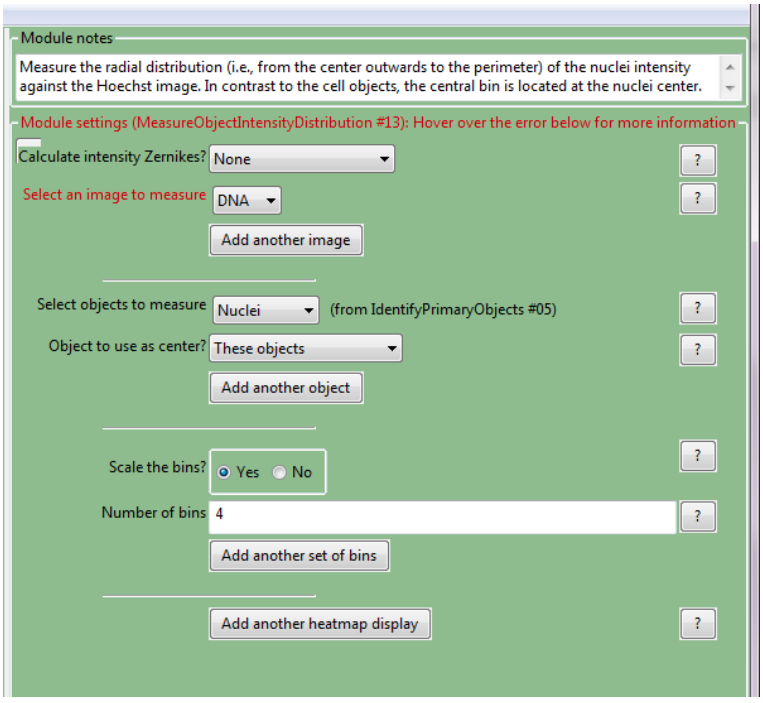

Module 10: Measure Object Size Shape

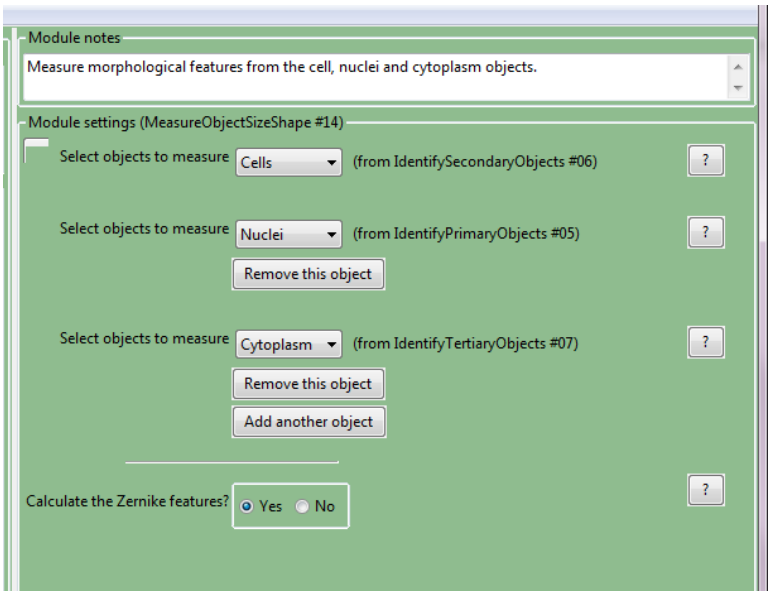

Module 11: Measure Texture

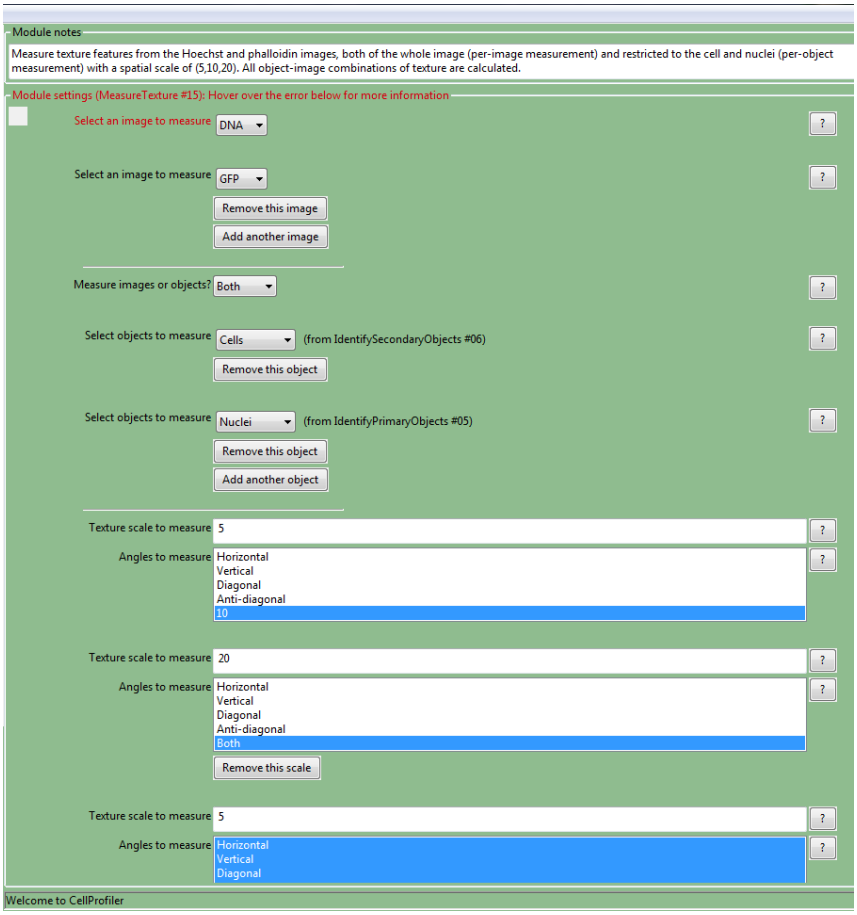

Module 12: Measure Image Intensity

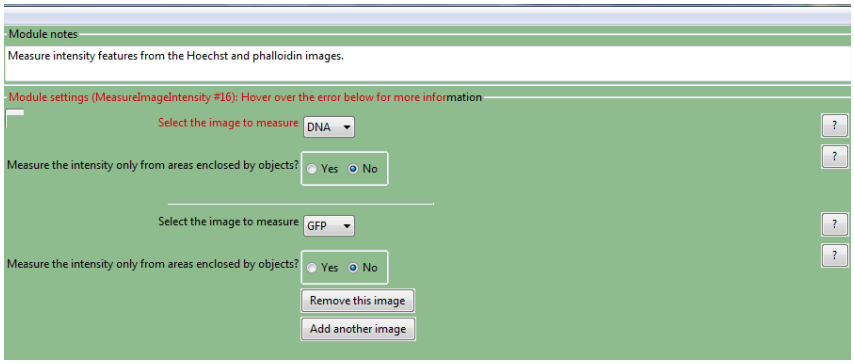

Module 13: Export To Database

Supp.Table 1: List of features remained after data clean up and processing.

Cells_AreaShape_Area	Cells_Intensity_LowerQuartileIntensity_GFP
Cells_AreaShape_Center_X	Cells_Intensity_MADIntensity_GFP
Cells_AreaShape_Center_Y	Cells_Intensity_MassDisplacement_GFP
Cells_AreaShape_Compactness	Cells_Intensity_MaxIntensityEdge_GFP
Cells_AreaShape_Eccentricity	Cells_Intensity_MaxIntensity_GFP
Cells_AreaShape_EulerNumber	Cells_Intensity_MeanIntensityEdge_GFP
Cells_AreaShape_Extent	Cells_Intensity_MeanIntensity_GFP
Cells_AreaShape_FormFactor	Cells_Intensity_MedianIntensity_GFP
Cells_AreaShape_MajorAxisLength	Cells_Intensity_MinIntensityEdge_GFP
Cells_AreaShape_MaxFeretDiameter	Cells_Intensity_MinIntensity_GFP
Cells_AreaShape_MaximumRadius	Cells_Intensity_StdIntensityEdge_GFP
Cells_AreaShape_MeanRadius	Cells_Intensity_StdIntensity_GFP
Cells_AreaShape_MedianRadius	Cells_Intensity_UpperQuartileIntensity_GFP
Cells_AreaShape_MinFeretDiameter	Cells_Location_CenterMassIntensity_X_GFP
Cells_AreaShape_MinorAxisLength	Cells_Location_CenterMassIntensity_Y_GFP
Cells_AreaShape_Orientation	Cells_Location_Center_X
Cells_AreaShape_Perimeter	Cells_Location_Center_Y
Cells_AreaShape_Solidity	Cells_Location_MaxIntensity_X_GFP
Cells_AreaShape_Zernike_0_0	Cells_Location_MaxIntensity_Y_GFP
Cells_AreaShape_Zernike_1_1	Cells_Neighbors_AngleBetweenNeighbors_Adjacent
Cells_AreaShape_Zernike_2_0	Cells_Neighbors_FirstClosestDistance_Adjacent
Cells_AreaShape_Zernike_2_2	Cells_Neighbors_FirstClosestObjectNumber_Adjacent
Cells_AreaShape_Zernike_3_1	Cells_Neighbors_NumberOfNeighbors_Adjacent
Cells_AreaShape_Zernike_3_3	Cells_Neighbors_PercentTouching_Adjacent
Cells_AreaShape_Zernike_4_0	Cells_Neighbors_SecondClosestDistance_Adjacent
Cells_AreaShape_Zernike_4_2	Cells_Neighbors_SecondClosestObjectNumber_Adjacent
Cells_AreaShape_Zernike_4_4	Cells_Parent_Nuclei
Cells_AreaShape_Zernike_5_1	Cells_RadialDistribution_FracAtD_GFP_1of4
Cells_AreaShape_Zernike_5_3	Cells_RadialDistribution_FracAtD_GFP_2of4
Cells_AreaShape_Zernike_5_5	Cells_RadialDistribution_FracAtD_GFP_3of4
Cells_AreaShape_Zernike_6_0	Cells_RadialDistribution_FracAtD_GFP_4of4
Cells_AreaShape_Zernike_6_2	Cells_RadialDistribution_MeanFrac_GFP_1of4
Cells_AreaShape_Zernike_6_4	Cells_RadialDistribution_MeanFrac_GFP_2of4
Cells_AreaShape_Zernike_6_6	Cells_RadialDistribution_MeanFrac_GFP_3of4
Cells_AreaShape_Zernike_7_1	Cells_RadialDistribution_MeanFrac_GFP_4of4
Cells_AreaShape_Zernike_7_3	Cells_RadialDistribution_RadialCV_GFP_1of4
Cells_AreaShape_Zernike_7_5	Cells_RadialDistribution_RadialCV_GFP_2of4
Cells_AreaShape_Zernike_7_7	Cells_RadialDistribution_RadialCV_GFP_3of4
Cells_AreaShape_Zernike_8_0	Cells_RadialDistribution_RadialCV_GFP_4of4
Cells_AreaShape_Zernike_8_2	Cells_Texture_AngularSecondMoment_DNA_10_00
Cells_AreaShape_Zernike_8_4	Cells_Texture_AngularSecondMoment_DNA_10_01
Cells_AreaShape_Zernike_8_6	Cells_Texture_AngularSecondMoment_DNA_10_02
Cells_AreaShape_Zernike_8_8	Cells_Texture_AngularSecondMoment_DNA_10_03
Cells_AreaShape_Zernike_9_1	Cells_Texture_AngularSecondMoment_DNA_20_00

Cells_AreaShape_Zernike_9_3
Cells_AreaShape_Zernike_9_5
Cells_AreaShape_Zernike_9_7
Cells_AreaShape_Zernike_9_9
Cells_Intensity_IntegratedIntensityEdge_GFP
Cells_Intensity_IntegratedIntensity_GFP
Cells_Texture_AngularSecondMoment_DNA_5_03
Cells_Texture_AngularSecondMoment_GFP_10_00
Cells_Texture_AngularSecondMoment_GFP_10_01
Cells_Texture_AngularSecondMoment_GFP_10_02
Cells_Texture_AngularSecondMoment_GFP_10_03
Cells_Texture_AngularSecondMoment_GFP_20_00
Cells_Texture_AngularSecondMoment_GFP_20_01
Cells_Texture_AngularSecondMoment_GFP_20_02
Cells_Texture_AngularSecondMoment_GFP_20_03
Cells_Texture_AngularSecondMoment_GFP_5_00
Cells_Texture_AngularSecondMoment_GFP_5_01
Cells_Texture_AngularSecondMoment_GFP_5_02
Cells_Texture_AngularSecondMoment_GFP_5_03
Cells_Texture_Contrast_DNA_10_00
Cells_Texture_Contrast_DNA_10_01
Cells_Texture_Contrast_DNA_10_02
Cells_Texture_Contrast_DNA_10_03
Cells_Texture_Contrast_DNA_20_00
Cells_Texture_Contrast_DNA_20_01
Cells_Texture_Contrast_DNA_20_02
Cells_Texture_Contrast_DNA_20_03
Cells_Texture_Contrast_DNA_5_00
Cells_Texture_Contrast_DNA_5_01
Cells_Texture_Contrast_DNA_5_02
Cells_Texture_Contrast_DNA_5_03
Cells_Texture_Contrast_GFP_10_00
Cells_Texture_Contrast_GFP_10_01
Cells_Texture_Contrast_GFP_10_02
Cells_Texture_Contrast_GFP_10_03
Cells_Texture_Contrast_GFP_20_00
Cells_Texture_Contrast_GFP_20_01
Cells_Texture_Contrast_GFP_20_02
Cells_Texture_Contrast_GFP_20_03
Cells_Texture_Contrast_GFP_5_00
Cells_Texture_Contrast_GFP_5_01
Cells_Texture_Contrast_GFP_5_02
Cells_Texture_Contrast_GFP_5_03
Cells_Texture_Correlation_DNA_10_00
Cells_Texture_Correlation_DNA_10_01
Cells_Texture_Correlation_DNA_10_02
Cells_Texture_Correlation_DNA_10_03
Cells_Texture_Correlation_DNA_20_00
Cells_Texture_AngularSecondMoment_DNA_20_01
Cells_Texture_AngularSecondMoment_DNA_20_02
Cells_Texture_AngularSecondMoment_DNA_20_03
Cells_Texture_AngularSecondMoment_DNA_5_00
Cells_Texture_AngularSecondMoment_DNA_5_01
Cells_Texture_AngularSecondMoment_DNA_5_02
Cells_Texture_Correlation_GFP_10_01
Cells_Texture_Correlation_GFP_10_02
Cells_Texture_Correlation_GFP_10_03
Cells_Texture_Correlation_GFP_20_00
Cells_Texture_Correlation_GFP_20_01
Cells_Texture_Correlation_GFP_20_02
Cells_Texture_Correlation_GFP_20_03
Cells_Texture_Correlation_GFP_5_00
Cells_Texture_Correlation_GFP_5_01
Cells_Texture_Correlation_GFP_5_02
Cells_Texture_Correlation_GFP_5_03
Cells_Texture_DifferenceEntropy_DNA_10_00
Cells_Texture_DifferenceEntropy_DNA_10_01
Cells_Texture_DifferenceEntropy_DNA_10_02
Cells_Texture_DifferenceEntropy_DNA_10_03
Cells_Texture_DifferenceEntropy_DNA_20_00
Cells_Texture_DifferenceEntropy_DNA_20_01
Cells_Texture_DifferenceEntropy_DNA_20_02
Cells_Texture_DifferenceEntropy_DNA_20_03
Cells_Texture_DifferenceEntropy_DNA_5_00
Cells_Texture_DifferenceEntropy_DNA_5_01
Cells_Texture_DifferenceEntropy_DNA_5_02
Cells_Texture_DifferenceEntropy_DNA_5_03
Cells_Texture_DifferenceEntropy_GFP_10_00
Cells_Texture_DifferenceEntropy_GFP_10_01
Cells_Texture_DifferenceEntropy_GFP_10_02
Cells_Texture_DifferenceEntropy_GFP_10_03
Cells_Texture_DifferenceEntropy_GFP_20_00
Cells_Texture_DifferenceEntropy_GFP_20_01
Cells_Texture_DifferenceEntropy_GFP_20_02
Cells_Texture_DifferenceEntropy_GFP_20_03
Cells_Texture_DifferenceEntropy_GFP_5_00
Cells_Texture_DifferenceEntropy_GFP_5_01
Cells_Texture_DifferenceEntropy_GFP_5_02
Cells_Texture_DifferenceEntropy_GFP_5_03
Cells_Texture_DifferenceVariance_DNA_10_00
Cells_Texture_DifferenceVariance_DNA_10_01
Cells_Texture_DifferenceVariance_DNA_10_02
Cells_Texture_DifferenceVariance_DNA_10_03
Cells_Texture_DifferenceVariance_DNA_20_00
Cells_Texture_DifferenceVariance_DNA_20_01
Cells_Texture_DifferenceVariance_DNA_20_02

Cells_Texture_Correlation_DNA_20_01
Cells_Texture_Correlation_DNA_20_02
Cells_Texture_Correlation_DNA_20_03
Cells_Texture_Correlation_DNA_5_00
Cells_Texture_Correlation_DNA_5_01
Cells_Texture_Correlation_DNA_5_02
Cells_Texture_Correlation_DNA_5_03
Cells_Texture_Correlation_GFP_10_00
Cells_Texture_DifferenceVariance_GFP_10_03
Cells_Texture_DifferenceVariance_GFP_20_00
Cells_Texture_DifferenceVariance_GFP_20_01
Cells_Texture_DifferenceVariance_GFP_20_02
Cells_Texture_DifferenceVariance_GFP_20_03
Cells_Texture_DifferenceVariance_GFP_5_00
Cells_Texture_DifferenceVariance_GFP_5_01
Cells_Texture_DifferenceVariance_GFP_5_02
Cells_Texture_DifferenceVariance_GFP_5_03
Cells_Texture_Entropy_DNA_10_00
Cells_Texture_Entropy_DNA_10_01
Cells_Texture_Entropy_DNA_10_02
Cells_Texture_Entropy_DNA_10_03
Cells_Texture_Entropy_DNA_20_00
Cells_Texture_Entropy_DNA_20_01
Cells_Texture_Entropy_DNA_20_02
Cells_Texture_Entropy_DNA_20_03
Cells_Texture_Entropy_DNA_5_00
Cells_Texture_Entropy_DNA_5_01
Cells_Texture_Entropy_DNA_5_02
Cells_Texture_Entropy_DNA_5_03
Cells_Texture_Entropy_GFP_10_00
Cells_Texture_Entropy_GFP_10_01
Cells_Texture_Entropy_GFP_10_02
Cells_Texture_Entropy_GFP_10_03
Cells_Texture_Entropy_GFP_20_00
Cells_Texture_Entropy_GFP_20_01
Cells_Texture_Entropy_GFP_20_02
Cells_Texture_Entropy_GFP_20_03
Cells_Texture_Entropy_GFP_5_00
Cells_Texture_Entropy_GFP_5_01
Cells_Texture_Entropy_GFP_5_02
Cells_Texture_Entropy_GFP_5_03
Cells_Texture_InfoMeas1_DNA_10_00
Cells_Texture_InfoMeas1_DNA_10_01
Cells_Texture_InfoMeas1_DNA_10_02
Cells_Texture_InfoMeas1_DNA_10_03
Cells_Texture_InfoMeas1_DNA_20_00
Cells_Texture_InfoMeas1_DNA_20_01
Cells_Texture_InfoMeas1_DNA_20_02
Cells_Texture_DifferenceVariance_DNA_20_03
Cells_Texture_DifferenceVariance_DNA_5_00
Cells_Texture_DifferenceVariance_DNA_5_01
Cells_Texture_DifferenceVariance_DNA_5_02
Cells_Texture_DifferenceVariance_DNA_5_03
Cells_Texture_DifferenceVariance_GFP_10_00
Cells_Texture_DifferenceVariance_GFP_10_01
Cells_Texture_DifferenceVariance_GFP_10_02
Cells_Texture_InfoMeas1_GFP_20_01
Cells_Texture_InfoMeas1_GFP_20_02
Cells_Texture_InfoMeas1_GFP_20_03
Cells_Texture_InfoMeas1_GFP_5_00
Cells_Texture_InfoMeas1_GFP_5_01
Cells_Texture_InfoMeas1_GFP_5_02
Cells_Texture_InfoMeas1_GFP_5_03
Cells_Texture_InfoMeas2_DNA_10_00
Cells_Texture_InfoMeas2_DNA_10_01
Cells_Texture_InfoMeas2_DNA_10_02
Cells_Texture_InfoMeas2_DNA_10_03
Cells_Texture_InfoMeas2_DNA_20_00
Cells_Texture_InfoMeas2_DNA_20_01
Cells_Texture_InfoMeas2_DNA_20_02
Cells_Texture_InfoMeas2_DNA_20_03
Cells_Texture_InfoMeas2_DNA_5_00
Cells_Texture_InfoMeas2_DNA_5_01
Cells_Texture_InfoMeas2_DNA_5_02
Cells_Texture_InfoMeas2_DNA_5_03
Cells_Texture_InfoMeas2_GFP_10_00
Cells_Texture_InfoMeas2_GFP_10_01
Cells_Texture_InfoMeas2_GFP_10_02
Cells_Texture_InfoMeas2_GFP_10_03
Cells_Texture_InfoMeas2_GFP_20_00
Cells_Texture_InfoMeas2_GFP_20_01
Cells_Texture_InfoMeas2_GFP_20_02
Cells_Texture_InfoMeas2_GFP_20_03
Cells_Texture_InfoMeas2_GFP_5_00
Cells_Texture_InfoMeas2_GFP_5_01
Cells_Texture_InfoMeas2_GFP_5_02
Cells_Texture_InfoMeas2_GFP_5_03
Cells_Texture_InverseDifferenceMoment_DNA_10_00
Cells_Texture_InverseDifferenceMoment_DNA_10_01
Cells_Texture_InverseDifferenceMoment_DNA_10_02
Cells_Texture_InverseDifferenceMoment_DNA_10_03
Cells_Texture_InverseDifferenceMoment_DNA_20_00
Cells_Texture_InverseDifferenceMoment_DNA_20_01
Cells_Texture_InverseDifferenceMoment_DNA_20_02
Cells_Texture_InverseDifferenceMoment_DNA_20_03
Cells_Texture_InverseDifferenceMoment_DNA_5_00

Cells_Texture_InfoMeas1_DNA_20_03
Cells_Texture_InfoMeas1_DNA_5_00
Cells_Texture_InfoMeas1_DNA_5_01
Cells_Texture_InfoMeas1_DNA_5_02
Cells_Texture_InfoMeas1_DNA_5_03
Cells_Texture_InfoMeas1_GFP_10_00
Cells_Texture_InfoMeas1_GFP_10_01
Cells_Texture_InfoMeas1_GFP_10_02
Cells_Texture_InfoMeas1_GFP_10_03
Cells_Texture_InfoMeas1_GFP_20_00
Cells_Texture_InverseDifferenceMoment_GFP_20_03
Cells_Texture_InverseDifferenceMoment_GFP_5_00
Cells_Texture_InverseDifferenceMoment_GFP_5_01
Cells_Texture_InverseDifferenceMoment_GFP_5_02
Cells_Texture_InverseDifferenceMoment_GFP_5_03
Cells_Texture_SumAverage_DNA_10_00
Cells_Texture_SumAverage_DNA_10_01
Cells_Texture_SumAverage_DNA_10_02
Cells_Texture_SumAverage_DNA_10_03
Cells_Texture_SumAverage_DNA_20_00
Cells_Texture_SumAverage_DNA_20_01
Cells_Texture_SumAverage_DNA_20_02
Cells_Texture_SumAverage_DNA_20_03
Cells_Texture_SumAverage_DNA_5_00
Cells_Texture_SumAverage_DNA_5_01
Cells_Texture_SumAverage_DNA_5_02
Cells_Texture_SumAverage_DNA_5_03
Cells_Texture_SumAverage_GFP_10_00
Cells_Texture_SumAverage_GFP_10_01
Cells_Texture_SumAverage_GFP_10_02
Cells_Texture_SumAverage_GFP_10_03
Cells_Texture_SumAverage_GFP_20_00
Cells_Texture_SumAverage_GFP_20_01
Cells_Texture_SumAverage_GFP_20_02
Cells_Texture_SumAverage_GFP_20_03
Cells_Texture_SumAverage_GFP_5_00
Cells_Texture_SumAverage_GFP_5_01
Cells_Texture_SumAverage_GFP_5_02
Cells_Texture_SumAverage_GFP_5_03
Cells_Texture_SumEntropy_DNA_10_00
Cells_Texture_SumEntropy_DNA_10_01
Cells_Texture_SumEntropy_DNA_10_02
Cells_Texture_SumEntropy_DNA_10_03
Cells_Texture_SumEntropy_DNA_20_00
Cells_Texture_SumEntropy_DNA_20_01
Cells_Texture_SumEntropy_DNA_20_02
Cells_Texture_SumEntropy_DNA_20_03
Cells_Texture_SumEntropy_DNA_5_00
Cells_Texture_InverseDifferenceMoment_DNA_5_01
Cells_Texture_InverseDifferenceMoment_DNA_5_02
Cells_Texture_InverseDifferenceMoment_DNA_5_03
Cells_Texture_InverseDifferenceMoment_GFP_10_00
Cells_Texture_InverseDifferenceMoment_GFP_10_01
Cells_Texture_InverseDifferenceMoment_GFP_10_02
Cells_Texture_InverseDifferenceMoment_GFP_10_03
Cells_Texture_InverseDifferenceMoment_GFP_20_00
Cells_Texture_InverseDifferenceMoment_GFP_20_01
Cells_Texture_InverseDifferenceMoment_GFP_20_02
Cells_Texture_SumEntropy_GFP_5_01
Cells_Texture_SumEntropy_GFP_5_02
Cells_Texture_SumEntropy_GFP_5_03
Cells_Texture_SumVariance_DNA_10_00
Cells_Texture_SumVariance_DNA_10_01
Cells_Texture_SumVariance_DNA_10_02
Cells_Texture_SumVariance_DNA_10_03
Cells_Texture_SumVariance_DNA_20_00
Cells_Texture_SumVariance_DNA_20_01
Cells_Texture_SumVariance_DNA_20_02
Cells_Texture_SumVariance_DNA_20_03
Cells_Texture_SumVariance_DNA_5_00
Cells_Texture_SumVariance_DNA_5_01
Cells_Texture_SumVariance_DNA_5_02
Cells_Texture_SumVariance_DNA_5_03
Cells_Texture_SumVariance_GFP_10_00
Cells_Texture_SumVariance_GFP_10_01
Cells_Texture_SumVariance_GFP_10_02
Cells_Texture_SumVariance_GFP_10_03
Cells_Texture_SumVariance_GFP_20_00
Cells_Texture_SumVariance_GFP_20_01
Cells_Texture_SumVariance_GFP_20_02
Cells_Texture_SumVariance_GFP_20_03
Cells_Texture_SumVariance_GFP_5_00
Cells_Texture_SumVariance_GFP_5_01
Cells_Texture_SumVariance_GFP_5_02
Cells_Texture_SumVariance_GFP_5_03
Cells_Texture_Variance_DNA_10_00
Cells_Texture_Variance_DNA_10_01
Cells_Texture_Variance_DNA_10_02
Cells_Texture_Variance_DNA_10_03
Cells_Texture_Variance_DNA_20_00
Cells_Texture_Variance_DNA_20_01
Cells_Texture_Variance_DNA_20_02
Cells_Texture_Variance_DNA_20_03
Cells_Texture_Variance_DNA_5_00
Cells_Texture_Variance_DNA_5_01
Cells_Texture_Variance_DNA_5_02

Cells_Texture_SumEntropy_DNA_5_01
Cells_Texture_SumEntropy_DNA_5_02
Cells_Texture_SumEntropy_DNA_5_03
Cells_Texture_SumEntropy_GFP_10_00
Cells_Texture_SumEntropy_GFP_10_01
Cells_Texture_SumEntropy_GFP_10_02
Cells_Texture_SumEntropy_GFP_10_03
Cells_Texture_SumEntropy_GFP_20_00
Cells_Texture_SumEntropy_GFP_20_01
Cells_Texture_SumEntropy_GFP_20_02
Cells_Texture_SumEntropy_GFP_20_03
Cells_Texture_SumEntropy_GFP_5_00
Cells_Texture_Variance_GFP_5_03
Cytoplasm_AreaShape_Area
Cytoplasm_AreaShape_Center_X
Cytoplasm_AreaShape_Center_Y
Cytoplasm_AreaShape_Compactness
Cytoplasm_AreaShape_Eccentricity
Cytoplasm_AreaShape_EulerNumber
Cytoplasm_AreaShape_Extent
Cytoplasm_AreaShape_FormFactor
Cytoplasm_AreaShape_MajorAxisLength
Cytoplasm_AreaShape_MaxFeretDiameter
Cytoplasm_AreaShape_MaximumRadius
Cytoplasm_AreaShape_MeanRadius
Cytoplasm_AreaShape_MedianRadius
Cytoplasm_AreaShape_MinFeretDiameter
Cytoplasm_AreaShape_MinorAxisLength
Cytoplasm_AreaShape_Orientation
Cytoplasm_AreaShape_Perimeter
Cytoplasm_AreaShape_Solidity
Cytoplasm_AreaShape_Zernike_0_0
Cytoplasm_AreaShape_Zernike_1_1
Cytoplasm_AreaShape_Zernike_2_0
Cytoplasm_AreaShape_Zernike_2_2
Cytoplasm_AreaShape_Zernike_3_1
Cytoplasm_AreaShape_Zernike_3_3
Cytoplasm_AreaShape_Zernike_4_0
Cytoplasm_AreaShape_Zernike_4_2
Cytoplasm_AreaShape_Zernike_4_4
Cytoplasm_AreaShape_Zernike_5_1
Cytoplasm_AreaShape_Zernike_5_3
Cytoplasm_AreaShape_Zernike_5_5
Cytoplasm_AreaShape_Zernike_6_0
Cytoplasm_AreaShape_Zernike_6_2
Cytoplasm_AreaShape_Zernike_6_4
Cytoplasm_AreaShape_Zernike_6_6
Cytoplasm_AreaShape_Zernike_7_1
Cells_Texture_Variance_DNA_5_03
Cells_Texture_Variance_GFP_10_00
Cells_Texture_Variance_GFP_10_01
Cells_Texture_Variance_GFP_10_02
Cells_Texture_Variance_GFP_10_03
Cells_Texture_Variance_GFP_20_00
Cells_Texture_Variance_GFP_20_01
Cells_Texture_Variance_GFP_20_02
Cells_Texture_Variance_GFP_20_03
Cells_Texture_Variance_GFP_5_00
Cells_Texture_Variance_GFP_5_01
Cells_Texture_Variance_GFP_5_02
Cytoplasm_Intensity_IntegratedIntensity_GFP
Cytoplasm_Intensity_LowerQuartileIntensity_GFP
Cytoplasm_Intensity_MADIntensity_GFP
Cytoplasm_Intensity_MassDisplacement_GFP
Cytoplasm_Intensity_MaxIntensityEdge_GFP
Cytoplasm_Intensity_MaxIntensity_GFP
Cytoplasm_Intensity_MeanIntensityEdge_GFP
Cytoplasm_Intensity_MeanIntensity_GFP
Cytoplasm_Intensity_MedianIntensity_GFP
Cytoplasm_Intensity_MinIntensityEdge_GFP
Cytoplasm_Intensity_MinIntensity_GFP
Cytoplasm_Intensity_StdIntensityEdge_GFP
Cytoplasm_Intensity_StdIntensity_GFP
Cytoplasm_Intensity_UpperQuartileIntensity_GFP
Cytoplasm_Location_CenterMassIntensity_X_GFP
Cytoplasm_Location_CenterMassIntensity_Y_GFP
Cytoplasm_Location_Center_X
Cytoplasm_Location_Center_Y
Cytoplasm_Location_MaxIntensity_X_GFP
Cytoplasm_Location_MaxIntensity_Y_GFP
Cytoplasm_Parent_Cells
Cytoplasm_Parent_Nuclei
Nuclei_AreaShape_Area
Nuclei_AreaShape_Center_X
Nuclei_AreaShape_Center_Y
Nuclei_AreaShape_Compactness
Nuclei_AreaShape_Eccentricity
Nuclei_AreaShape_Extent
Nuclei_AreaShape_FormFactor
Nuclei_AreaShape_MajorAxisLength
Nuclei_AreaShape_MaxFeretDiameter
Nuclei_AreaShape_MaximumRadius
Nuclei_AreaShape_MeanRadius
Nuclei_AreaShape_MedianRadius
Nuclei_AreaShape_MinFeretDiameter
Nuclei_AreaShape_MinorAxisLength

Cytoplasm_AreaShape_Zernike_7_3	Nuclei_AreaShape_Orientation
Cytoplasm_AreaShape_Zernike_7_5	Nuclei_AreaShape_Perimeter
Cytoplasm_AreaShape_Zernike_7_7	Nuclei_AreaShape_Solidity
Cytoplasm_AreaShape_Zernike_8_0	Nuclei_AreaShape_Zernike_0_0
Cytoplasm_AreaShape_Zernike_8_2	Nuclei_AreaShape_Zernike_1_1
Cytoplasm_AreaShape_Zernike_8_4	Nuclei_AreaShape_Zernike_2_0
Cytoplasm_AreaShape_Zernike_8_6	Nuclei_AreaShape_Zernike_2_2
Cytoplasm_AreaShape_Zernike_8_8	Nuclei_AreaShape_Zernike_3_1
Cytoplasm_AreaShape_Zernike_9_1	Nuclei_AreaShape_Zernike_3_3
Cytoplasm_AreaShape_Zernike_9_3	Nuclei_AreaShape_Zernike_4_0
Cytoplasm_AreaShape_Zernike_9_5	Nuclei_AreaShape_Zernike_4_2
Cytoplasm_AreaShape_Zernike_9_7	Nuclei_AreaShape_Zernike_4_4
Cytoplasm_AreaShape_Zernike_9_9	Nuclei_AreaShape_Zernike_5_1
Cytoplasm_Intensity_IntegratedIntensityEdge_GFP	Nuclei_AreaShape_Zernike_5_3
Nuclei_AreaShape_Zernike_5_5	Nuclei_RadialDistribution_FracAtD_DNA_4of4
Nuclei_AreaShape_Zernike_6_0	Nuclei_RadialDistribution_MeanFrac_DNA_1of4
Nuclei_AreaShape_Zernike_6_2	Nuclei_RadialDistribution_MeanFrac_DNA_2of4
Nuclei_AreaShape_Zernike_6_4	Nuclei_RadialDistribution_MeanFrac_DNA_3of4
Nuclei_AreaShape_Zernike_6_6	Nuclei_RadialDistribution_MeanFrac_DNA_4of4
Nuclei_AreaShape_Zernike_7_1	Nuclei_RadialDistribution_RadialCV_DNA_1of4
Nuclei_AreaShape_Zernike_7_3	Nuclei_RadialDistribution_RadialCV_DNA_2of4
Nuclei_AreaShape_Zernike_7_5	Nuclei_RadialDistribution_RadialCV_DNA_3of4
Nuclei_AreaShape_Zernike_7_7	Nuclei_RadialDistribution_RadialCV_DNA_4of4
Nuclei_AreaShape_Zernike_8_0	Nuclei_Texture_AngularSecondMoment_DNA_10_00
Nuclei_AreaShape_Zernike_8_2	Nuclei_Texture_AngularSecondMoment_DNA_10_01
Nuclei_AreaShape_Zernike_8_4	Nuclei_Texture_AngularSecondMoment_DNA_10_02
Nuclei_AreaShape_Zernike_8_6	Nuclei_Texture_AngularSecondMoment_DNA_10_03
Nuclei_AreaShape_Zernike_8_8	Nuclei_Texture_AngularSecondMoment_DNA_20_00
Nuclei_AreaShape_Zernike_9_1	Nuclei_Texture_AngularSecondMoment_DNA_20_01
Nuclei_AreaShape_Zernike_9_3	Nuclei_Texture_AngularSecondMoment_DNA_20_02
Nuclei_AreaShape_Zernike_9_5	Nuclei_Texture_AngularSecondMoment_DNA_20_03
Nuclei_AreaShape_Zernike_9_7	Nuclei_Texture_AngularSecondMoment_DNA_5_00
Nuclei_AreaShape_Zernike_9_9	Nuclei_Texture_AngularSecondMoment_DNA_5_01
Nuclei_Intensity_IntegratedIntensityEdge_DNA	Nuclei_Texture_AngularSecondMoment_DNA_5_02
Nuclei_Intensity_IntegratedIntensity_DNA	Nuclei_Texture_AngularSecondMoment_DNA_5_03
Nuclei_Intensity_LowerQuartileIntensity_DNA	Nuclei_Texture_AngularSecondMoment_GFP_10_00
Nuclei_Intensity_MADIntensity_DNA	Nuclei_Texture_AngularSecondMoment_GFP_10_01
Nuclei_Intensity_MassDisplacement_DNA	Nuclei_Texture_AngularSecondMoment_GFP_10_02
Nuclei_Intensity_MaxIntensityEdge_DNA	Nuclei_Texture_AngularSecondMoment_GFP_10_03
Nuclei_Intensity_MaxIntensity_DNA	Nuclei_Texture_AngularSecondMoment_GFP_20_00
Nuclei_Intensity_MeanIntensityEdge_DNA	Nuclei_Texture_AngularSecondMoment_GFP_20_01
Nuclei_Intensity_MeanIntensity_DNA	Nuclei_Texture_AngularSecondMoment_GFP_20_02
Nuclei_Intensity_MedianIntensity_DNA	Nuclei_Texture_AngularSecondMoment_GFP_20_03
Nuclei_Intensity_MinIntensityEdge_DNA	Nuclei_Texture_AngularSecondMoment_GFP_5_00
Nuclei_Intensity_MinIntensity_DNA	Nuclei_Texture_AngularSecondMoment_GFP_5_01
Nuclei_Intensity_StdIntensityEdge_DNA	Nuclei_Texture_AngularSecondMoment_GFP_5_02
Nuclei_Intensity_StdIntensity_DNA	Nuclei_Texture_AngularSecondMoment_GFP_5_03
Nuclei_Intensity_UpperQuartileIntensity_DNA	Nuclei_Texture_Contrast_DNA_10_00

Nuclei_Location_CenterMassIntensity_X_DNA	Nuclei_Texture_Contrast_DNA_10_01
Nuclei_Location_CenterMassIntensity_Y_DNA	Nuclei_Texture_Contrast_DNA_10_02
Nuclei_Location_Center_X	Nuclei_Texture_Contrast_DNA_10_03
Nuclei_Location_Center_Y	Nuclei_Texture_Contrast_DNA_20_00
Nuclei_Location_MaxIntensity_X_DNA	Nuclei_Texture_Contrast_DNA_20_01
Nuclei_Location_MaxIntensity_Y_DNA	Nuclei_Texture_Contrast_DNA_20_02
Nuclei_Neighbors_AngleBetweenNeighbors_Adjacent	Nuclei_Texture_Contrast_DNA_20_03
Nuclei_Neighbors_FirstClosestDistance_Adjacent	Nuclei_Texture_Contrast_DNA_5_00
Nuclei_Neighbors_FirstClosestObjectNumber_Adjacent	Nuclei_Texture_Contrast_DNA_5_01
Nuclei_Neighbors_NumberOfNeighbors_Adjacent	Nuclei_Texture_Contrast_DNA_5_02
Nuclei_Neighbors_PercentTouching_Adjacent	Nuclei_Texture_Contrast_DNA_5_03
Nuclei_Neighbors_SecondClosestDistance_Adjacent	Nuclei_Texture_Contrast_GFP_10_00
Nuclei_Neighbors_SecondClosestObjectNumber_Adjacent	Nuclei_Texture_Contrast_GFP_10_01
Nuclei_RadialDistribution_FracAtD_DNA_1of4	Nuclei_Texture_Contrast_GFP_10_02
Nuclei_RadialDistribution_FracAtD_DNA_2of4	Nuclei_Texture_Contrast_GFP_10_03
Nuclei_RadialDistribution_FracAtD_DNA_3of4	Nuclei_Texture_Contrast_GFP_20_00
Nuclei_Texture_Contrast_GFP_20_01	Nuclei_Texture_DifferenceEntropy_GFP_20_03
Nuclei_Texture_Contrast_GFP_20_02	Nuclei_Texture_DifferenceEntropy_GFP_5_00
Nuclei_Texture_Contrast_GFP_20_03	Nuclei_Texture_DifferenceEntropy_GFP_5_01
Nuclei_Texture_Contrast_GFP_5_00	Nuclei_Texture_DifferenceEntropy_GFP_5_02
Nuclei_Texture_Contrast_GFP_5_01	Nuclei_Texture_DifferenceEntropy_GFP_5_03
Nuclei_Texture_Contrast_GFP_5_02	Nuclei_Texture_DifferenceVariance_DNA_10_00
Nuclei_Texture_Contrast_GFP_5_03	Nuclei_Texture_DifferenceVariance_DNA_10_01
Nuclei_Texture_Correlation_DNA_10_00	Nuclei_Texture_DifferenceVariance_DNA_10_02
Nuclei_Texture_Correlation_DNA_10_01	Nuclei_Texture_DifferenceVariance_DNA_10_03
Nuclei_Texture_Correlation_DNA_10_02	Nuclei_Texture_DifferenceVariance_DNA_20_00
Nuclei_Texture_Correlation_DNA_10_03	Nuclei_Texture_DifferenceVariance_DNA_20_01
Nuclei_Texture_Correlation_DNA_20_00	Nuclei_Texture_DifferenceVariance_DNA_20_02
Nuclei_Texture_Correlation_DNA_20_01	Nuclei_Texture_DifferenceVariance_DNA_20_03
Nuclei_Texture_Correlation_DNA_20_02	Nuclei_Texture_DifferenceVariance_DNA_5_00
Nuclei_Texture_Correlation_DNA_20_03	Nuclei_Texture_DifferenceVariance_DNA_5_01
Nuclei_Texture_Correlation_DNA_5_00	Nuclei_Texture_DifferenceVariance_DNA_5_02
Nuclei_Texture_Correlation_DNA_5_01	Nuclei_Texture_DifferenceVariance_DNA_5_03
Nuclei_Texture_Correlation_DNA_5_02	Nuclei_Texture_DifferenceVariance_GFP_10_00
Nuclei_Texture_Correlation_DNA_5_03	Nuclei_Texture_DifferenceVariance_GFP_10_01
Nuclei_Texture_Correlation_GFP_10_00	Nuclei_Texture_DifferenceVariance_GFP_10_02
Nuclei_Texture_Correlation_GFP_10_01	Nuclei_Texture_DifferenceVariance_GFP_10_03
Nuclei_Texture_Correlation_GFP_10_02	Nuclei_Texture_DifferenceVariance_GFP_20_00
Nuclei_Texture_Correlation_GFP_10_03	Nuclei_Texture_DifferenceVariance_GFP_20_01
Nuclei_Texture_Correlation_GFP_20_00	Nuclei_Texture_DifferenceVariance_GFP_20_02
Nuclei_Texture_Correlation_GFP_20_01	Nuclei_Texture_DifferenceVariance_GFP_20_03
Nuclei_Texture_Correlation_GFP_20_02	Nuclei_Texture_DifferenceVariance_GFP_5_00
Nuclei_Texture_Correlation_GFP_20_03	Nuclei_Texture_DifferenceVariance_GFP_5_01
Nuclei_Texture_Correlation_GFP_5_00	Nuclei_Texture_DifferenceVariance_GFP_5_02
Nuclei_Texture_Correlation_GFP_5_01	Nuclei_Texture_DifferenceVariance_GFP_5_03
Nuclei_Texture_Correlation_GFP_5_02	Nuclei_Texture_Entropy_DNA_10_00
Nuclei_Texture_Correlation_GFP_5_03	Nuclei_Texture_Entropy_DNA_10_01
Nuclei_Texture_DifferenceEntropy_DNA_10_00	Nuclei_Texture_Entropy_DNA_10_02

Nuclei_Texture_DifferenceEntropy_DNA_10_01
Nuclei_Texture_DifferenceEntropy_DNA_10_02
Nuclei_Texture_DifferenceEntropy_DNA_10_03
Nuclei_Texture_DifferenceEntropy_DNA_20_00
Nuclei_Texture_DifferenceEntropy_DNA_20_01
Nuclei_Texture_DifferenceEntropy_DNA_20_02
Nuclei_Texture_DifferenceEntropy_DNA_20_03
Nuclei_Texture_DifferenceEntropy_DNA_5_00
Nuclei_Texture_DifferenceEntropy_DNA_5_01
Nuclei_Texture_DifferenceEntropy_DNA_5_02
Nuclei_Texture_DifferenceEntropy_DNA_5_03
Nuclei_Texture_DifferenceEntropy_GFP_10_00
Nuclei_Texture_DifferenceEntropy_GFP_10_01
Nuclei_Texture_DifferenceEntropy_GFP_10_02
Nuclei_Texture_DifferenceEntropy_GFP_10_03
Nuclei_Texture_DifferenceEntropy_GFP_20_00
Nuclei_Texture_DifferenceEntropy_GFP_20_01
Nuclei_Texture_DifferenceEntropy_GFP_20_02
Nuclei_Texture_Entropy_GFP_5_01
Nuclei_Texture_Entropy_GFP_5_02
Nuclei_Texture_Entropy_GFP_5_03
Nuclei_Texture_InfoMeas1_DNA_10_00
Nuclei_Texture_InfoMeas1_DNA_10_01
Nuclei_Texture_InfoMeas1_DNA_10_02
Nuclei_Texture_InfoMeas1_DNA_10_03
Nuclei_Texture_InfoMeas1_DNA_20_00
Nuclei_Texture_InfoMeas1_DNA_20_01
Nuclei_Texture_InfoMeas1_DNA_20_02
Nuclei_Texture_InfoMeas1_DNA_20_03
Nuclei_Texture_InfoMeas1_DNA_5_00
Nuclei_Texture_InfoMeas1_DNA_5_01
Nuclei_Texture_InfoMeas1_DNA_5_02
Nuclei_Texture_InfoMeas1_DNA_5_03
Nuclei_Texture_InfoMeas1_GFP_10_00
Nuclei_Texture_InfoMeas1_GFP_10_01
Nuclei_Texture_InfoMeas1_GFP_10_02
Nuclei_Texture_InfoMeas1_GFP_10_03
Nuclei_Texture_InfoMeas1_GFP_20_00
Nuclei_Texture_InfoMeas1_GFP_20_01
Nuclei_Texture_InfoMeas1_GFP_20_02
Nuclei_Texture_InfoMeas1_GFP_20_03
Nuclei_Texture_InfoMeas1_GFP_5_00
Nuclei_Texture_InfoMeas1_GFP_5_01
Nuclei_Texture_InfoMeas1_GFP_5_02
Nuclei_Texture_InfoMeas1_GFP_5_03
Nuclei_Texture_InfoMeas2_DNA_10_00
Nuclei_Texture_InfoMeas2_DNA_10_01
Nuclei_Texture_InfoMeas2_DNA_10_02
Nuclei_Texture_Entropy_DNA_10_03
Nuclei_Texture_Entropy_DNA_20_00
Nuclei_Texture_Entropy_DNA_20_01
Nuclei_Texture_Entropy_DNA_20_02
Nuclei_Texture_Entropy_DNA_20_03
Nuclei_Texture_Entropy_DNA_5_00
Nuclei_Texture_Entropy_DNA_5_01
Nuclei_Texture_Entropy_DNA_5_02
Nuclei_Texture_Entropy_DNA_5_03
Nuclei_Texture_Entropy_GFP_10_00
Nuclei_Texture_Entropy_GFP_10_01
Nuclei_Texture_Entropy_GFP_10_02
Nuclei_Texture_Entropy_GFP_10_03
Nuclei_Texture_Entropy_GFP_20_00
Nuclei_Texture_Entropy_GFP_20_01
Nuclei_Texture_Entropy_GFP_20_02
Nuclei_Texture_Entropy_GFP_20_03
Nuclei_Texture_Entropy_GFP_5_00
Nuclei_Texture_InfoMeas2_GFP_5_03
Nuclei_Texture_InverseDifferenceMoment_DNA_10_00
Nuclei_Texture_InverseDifferenceMoment_DNA_10_01
Nuclei_Texture_InverseDifferenceMoment_DNA_10_02
Nuclei_Texture_InverseDifferenceMoment_DNA_10_03
Nuclei_Texture_InverseDifferenceMoment_DNA_20_00
Nuclei_Texture_InverseDifferenceMoment_DNA_20_01
Nuclei_Texture_InverseDifferenceMoment_DNA_20_02
Nuclei_Texture_InverseDifferenceMoment_DNA_20_03
Nuclei_Texture_InverseDifferenceMoment_DNA_5_00
Nuclei_Texture_InverseDifferenceMoment_DNA_5_01
Nuclei_Texture_InverseDifferenceMoment_DNA_5_02
Nuclei_Texture_InverseDifferenceMoment_DNA_5_03
Nuclei_Texture_InverseDifferenceMoment_GFP_10_00
Nuclei_Texture_InverseDifferenceMoment_GFP_10_01
Nuclei_Texture_InverseDifferenceMoment_GFP_10_02
Nuclei_Texture_InverseDifferenceMoment_GFP_10_03
Nuclei_Texture_InverseDifferenceMoment_GFP_20_00
Nuclei_Texture_InverseDifferenceMoment_GFP_20_01
Nuclei_Texture_InverseDifferenceMoment_GFP_20_02
Nuclei_Texture_InverseDifferenceMoment_GFP_20_03
Nuclei_Texture_InverseDifferenceMoment_GFP_5_00
Nuclei_Texture_InverseDifferenceMoment_GFP_5_01
Nuclei_Texture_InverseDifferenceMoment_GFP_5_02
Nuclei_Texture_InverseDifferenceMoment_GFP_5_03
Nuclei_Texture_SumAverage_DNA_10_00
Nuclei_Texture_SumAverage_DNA_10_01
Nuclei_Texture_SumAverage_DNA_10_02
Nuclei_Texture_SumAverage_DNA_10_03
Nuclei_Texture_SumAverage_DNA_20_00

Nuclei_Texture_InfoMeas2_DNA_10_03
Nuclei_Texture_InfoMeas2_DNA_20_00
Nuclei_Texture_InfoMeas2_DNA_20_01
Nuclei_Texture_InfoMeas2_DNA_20_02
Nuclei_Texture_InfoMeas2_DNA_20_03
Nuclei_Texture_InfoMeas2_DNA_5_00
Nuclei_Texture_InfoMeas2_DNA_5_01
Nuclei_Texture_InfoMeas2_DNA_5_02
Nuclei_Texture_InfoMeas2_DNA_5_03
Nuclei_Texture_InfoMeas2_GFP_10_00
Nuclei_Texture_InfoMeas2_GFP_10_01
Nuclei_Texture_InfoMeas2_GFP_10_02
Nuclei_Texture_InfoMeas2_GFP_10_03
Nuclei_Texture_InfoMeas2_GFP_20_00
Nuclei_Texture_InfoMeas2_GFP_20_01
Nuclei_Texture_InfoMeas2_GFP_20_02
Nuclei_Texture_InfoMeas2_GFP_20_03
Nuclei_Texture_InfoMeas2_GFP_5_00
Nuclei_Texture_InfoMeas2_GFP_5_01
Nuclei_Texture_InfoMeas2_GFP_5_02
Nuclei_Texture_SumEntropy_DNA_10_01
Nuclei_Texture_SumEntropy_DNA_10_02
Nuclei_Texture_SumEntropy_DNA_10_03
Nuclei_Texture_SumEntropy_DNA_20_00
Nuclei_Texture_SumEntropy_DNA_20_01
Nuclei_Texture_SumEntropy_DNA_20_02
Nuclei_Texture_SumEntropy_DNA_20_03
Nuclei_Texture_SumEntropy_DNA_5_00
Nuclei_Texture_SumEntropy_DNA_5_01
Nuclei_Texture_SumEntropy_DNA_5_02
Nuclei_Texture_SumEntropy_DNA_5_03
Nuclei_Texture_SumEntropy_GFP_10_00
Nuclei_Texture_SumEntropy_GFP_10_01
Nuclei_Texture_SumEntropy_GFP_10_02
Nuclei_Texture_SumEntropy_GFP_10_03
Nuclei_Texture_SumEntropy_GFP_20_00
Nuclei_Texture_SumEntropy_GFP_20_01
Nuclei_Texture_SumEntropy_GFP_20_02
Nuclei_Texture_SumEntropy_GFP_20_03
Nuclei_Texture_SumEntropy_GFP_5_00
Nuclei_Texture_SumEntropy_GFP_5_01
Nuclei_Texture_SumEntropy_GFP_5_02
Nuclei_Texture_SumEntropy_GFP_5_03
Nuclei_Texture_SumVariance_DNA_10_00
Nuclei_Texture_SumVariance_DNA_10_01
Nuclei_Texture_SumVariance_DNA_10_02
Nuclei_Texture_SumVariance_DNA_10_03
Nuclei_Texture_SumVariance_DNA_20_00
Nuclei_Texture_SumAverage_DNA_20_01
Nuclei_Texture_SumAverage_DNA_20_02
Nuclei_Texture_SumAverage_DNA_20_03
Nuclei_Texture_SumAverage_DNA_5_00
Nuclei_Texture_SumAverage_DNA_5_01
Nuclei_Texture_SumAverage_DNA_5_02
Nuclei_Texture_SumAverage_DNA_5_03
Nuclei_Texture_SumAverage_GFP_10_00
Nuclei_Texture_SumAverage_GFP_10_01
Nuclei_Texture_SumAverage_GFP_10_02
Nuclei_Texture_SumAverage_GFP_10_03
Nuclei_Texture_SumAverage_GFP_20_00
Nuclei_Texture_SumAverage_GFP_20_01
Nuclei_Texture_SumAverage_GFP_20_02
Nuclei_Texture_SumAverage_GFP_20_03
Nuclei_Texture_SumAverage_GFP_5_00
Nuclei_Texture_SumAverage_GFP_5_01
Nuclei_Texture_SumAverage_GFP_5_02
Nuclei_Texture_SumAverage_GFP_5_03
Nuclei_Texture_SumEntropy_DNA_10_00
Nuclei_Texture_SumVariance_GFP_10_01
Nuclei_Texture_SumVariance_GFP_10_02
Nuclei_Texture_SumVariance_GFP_10_03
Nuclei_Texture_SumVariance_GFP_20_00
Nuclei_Texture_SumVariance_GFP_20_01
Nuclei_Texture_SumVariance_GFP_20_02
Nuclei_Texture_SumVariance_GFP_20_03
Nuclei_Texture_SumVariance_GFP_5_00
Nuclei_Texture_SumVariance_GFP_5_01
Nuclei_Texture_SumVariance_GFP_5_02
Nuclei_Texture_SumVariance_GFP_5_03
Nuclei_Texture_Variance_DNA_10_00
Nuclei_Texture_Variance_DNA_10_01
Nuclei_Texture_Variance_DNA_10_02
Nuclei_Texture_Variance_DNA_10_03
Nuclei_Texture_Variance_DNA_20_00
Nuclei_Texture_Variance_DNA_20_01
Nuclei_Texture_Variance_DNA_20_02
Nuclei_Texture_Variance_DNA_20_03
Nuclei_Texture_Variance_DNA_5_00
Nuclei_Texture_Variance_DNA_5_01
Nuclei_Texture_Variance_DNA_5_02
Nuclei_Texture_Variance_DNA_5_03
Nuclei_Texture_Variance_GFP_10_00
Nuclei_Texture_Variance_GFP_10_01
Nuclei_Texture_Variance_GFP_10_02
Nuclei_Texture_Variance_GFP_10_03
Nuclei_Texture_Variance_GFP_20_00

Nuclei_Texture_SumVariance_DNA_20_01	Nuclei_Texture_Variance_GFP_20_01
Nuclei_Texture_SumVariance_DNA_20_02	Nuclei_Texture_Variance_GFP_20_02
Nuclei_Texture_SumVariance_DNA_20_03	Nuclei_Texture_Variance_GFP_20_03
Nuclei_Texture_SumVariance_DNA_5_00	Nuclei_Texture_Variance_GFP_5_00
Nuclei_Texture_SumVariance_DNA_5_01	Nuclei_Texture_Variance_GFP_5_01
Nuclei_Texture_SumVariance_DNA_5_02	Nuclei_Texture_Variance_GFP_5_02
Nuclei_Texture_SumVariance_DNA_5_03	Nuclei_Texture_Variance_GFP_5_03
Nuclei_Texture_SumVariance_GFP_10_00	

Appendix 2: R codes for the analysis of Study 1 and 2

```
# Clean the data for each object using cytominer
# 1. clean the data
# 2. normalize the features so that they are comparable across experiments
# 3. transform the features so that their distributions are well-behaved (i.e.,
bring them in line with assumptions we want to make about their disributions)
# 4. select features based on their quality
# 5. aggregate the single-cell data, if needed
## The cytominer package makes these steps fast and easy.

## Load data

## read packages
library(dbplyr)
library(dplyr)
library(stringr)
library(magrittr)
library(cytominer)
library(lattice)
library(ggplot2)


# Read objective files and image files
do <-read.csv("Van_Per objectives.csv", header = TRUE, sep = ",")
df<- read.csv("Van_Per image.csv", header = TRUE, sep=",")hi_df<-
read.csv("hi_Per_image.csv", header = TRUE, sep=",")

df$Site<-substr(df$Image_FileName_DNA, 14,14)
df$Well<-substr(df$Image_FileName_DNA, 1,2)
df$Wellsite<-paste(df$Well,df$Site,sep = "_")
well<-levels(as.factor(df$Well))

image<-levels(as.factor(do$ImageNumber))
# add Well column to the table
dn<-factor(do$ImageNumber,labels = df$Wellsite)
do$Well<-substr(dn,1,regexpr("_",dn)-1)
do$Wellsite<-dn
do$row<-substr(dn,1,1)
##
do<-compute(do)

## For this example, lets filter the data down to a few wells.
measurements <-
  do %>%
  dplyr::filter(Well %in% well)

# How many rows does this table have?
measurements %>%
  dplyr::tally() %>%
  knitr::kable()

# Next, do some setup stuff that we will need later
qualities <- c("Cytoplasm_AreaShape_Area")
groupings <-
  c("ImageNumber", "ObjectNumber", "Cytoplasm_Number_Object_Number",
"Cells_Number_Object_Number", "Nuclei_Number_Object_Number",
"Well","Wellsite","row")

dn<-colnames(measurements)
b2<- which (dn %in% groupings)
variables <- dn[-b2]

measurements %<>%
  dplyr::select(dplyr::one_of(c(qualities,groupings, variables)))
```

```
## Clean

# Then, remove cells where all the measurements are NA's - this may happen
# if the identified cell mask was too small to measure any of the features.

debris_removed <- measurements %>% dplyr::filter(Cytoplasm_AreaShape_Area != 0)

na_rows_removed <-
  cytominer::drop_na_rows(
    population = debris_removed,
    variables = variables
  ) %>%
  dplyr::compute()

##Split data set 1 and 2 before normalisation
## Data set 1 includes images 1,2,3,7,8,9
## Data set 2 includes images 4,5,6,10,11,12

#Set up data set 1 object factors to include data from images (4,5,6,10,11,12)

datset1 <- na_rows_removed
datset1_list <- c (4,5,6,10,11,12)

#Remove these data to get data set 1
datset1 <- datset1[which(datset1$ImageNumber %in% datset1_list),]

#Set up data set 2 object factors to includle data from ImageNumber (1,2,3,7,8,9)

datset2 <- na_rows_removed
datset2_list <- c (1,2,3,7,8,9)

#Remove these data to get data set 2
datset2 <- datset2[which(datset2$ImageNumber %in% datset2_list),]


## Normalize the combined data so that features are on the same scale
normalized <-
  cytominer::normalize(
    population = na_rows_removed,
    variables = variables,
    strata = "Well",
    sample = na_rows_removed )

normalized %<>% dplyr::collect()

##Normalise dataset 1 and 2 so that the data and features are on the same scale

# For Dataset 1
dat1_norm <-
  cytominer::normalize(
    population = datset1,
    variables = variables,
    strata = "Well",
    sample = datset1 )

dat1_norm %<>% dplyr::collect()

# For Dataset 2

dat2_norm <-
  cytominer::normalize(
    population = datset2,
    variables = variables,
    strata = "Well",
    sample = datset2 )

dat2_norm %<>% dplyr::collect()
```

```
#In some cases, we may have features that have no variance at all (e.g. Euler
#number). If these features have not already been removed by this stage, the
#standardization step will result in all values for that feature being NA (
#because s.d. = 0). Lets remove them:

#First, count how many cells have NA values per feature:

#In combined data
na_frequency <-
  cytominer::count_na_rows(
    population = normalized,
    variables = variables)

na_frequency %>%
  tidyr::gather(feature, na_count) %>%
  knitr::kable()

#In dataset 1

dat1_na_frequency <-
  cytominer::count_na_rows(
    population = dat1_norm,
    variables = variables)

dat1_na_frequency %>%
  tidyr::gather(feature, na_count) %>%
  knitr::kable()

#In dataset 2

dat2_na_frequency <-
  cytominer::count_na_rows(
    population = dat2_norm,
    variables = variables)

dat2_na_frequency %>%
  tidyr::gather(feature, na_count) %>%
  knitr::kable()

##Next, let's run this cleaning operation

# For combined data
cleaned <-
  cytominer::variable_select(
    population = normalized,
    variables = variables,
    operation = "drop_na_columns"
  )

#For dataset 1

dat1_cleaned <-
  cytominer::variable_select(
    population = dat1_norm,
    variables = variables,
    operation = "drop_na_columns"
  )
# For dataset 2

dat2_cleaned <-
  cytominer::variable_select(
    population = dat2_norm,
    variables = variables,
    operation = "drop_na_columns"
  )

## Transform
```

```
#Tranform the data so that assumptions we may later make about the data
#distribution are satisfied (e.g. Gaussianity). The default here is
#`generalized_log`.

#For combined data

dn1<-colnames(cleaned)
excluded<-setdiff(dn,dn1)
ad<- which (variables %in% excluded)
na_removed_variables<- variables[-ad]

transformed <-
  cytominer::transform(
    population = cleaned,
    variables =na_removed_variables
  )

#For dataset 1

dat1<-colnames(dat1_cleaned)
excluded<-setdiff(dn,dat1)
ad<- which (variables %in% excluded)
dat1_removed_variables<- variables[-ad]

dat1_transformed <-
  cytominer::transform(
    population = dat1_cleaned,
    variables =dat1_removed_variables
  )

#For dataset 2

dat2<-colnames(dat2_cleaned)
excluded<-setdiff(dn,dat2)
ad<- which (variables %in% excluded)
dat2_removed_variables<- variables[-ad]

dat2_transformed <-
  cytominer::transform(
    population = dat2_cleaned,
    variables =dat2_removed_variables
  )
## Select features:
# Finally, we typically perform feature selection on the data. Feature selection is
#an expensive operation, so we usually want to train the feature selection model on
#a sample of the dataset. Here, we choose to aggregate the data instead of sampling
#it (i.e. collapse it to per-well aggregates)

#For combined data

aggregated <-
  cytominer::aggregate(
    population = transformed,
    variables = na_removed_variables,
    strata = "Wellsite"
  ) %>%
  dplyr::collect()

#For dataset1

dat1_aggregated <-
  cytominer::aggregate(
    population = dat1_transformed,
    variables = dat1_removed_variables,
    strata = "Wellsite"
  ) %>%
  dplyr::collect()
```

```
#For dataset2

dat2_aggregated <-
  cytominer::aggregate(
    population = dat2_transformed,
    variables = dat2_removed_variables,
    strata = "Wellsite"
  ) %>%
  dplyr::collect()

## write the aggreagated file to save a record
write.csv(aggregated, "image_aggregated.csv", row.names = FALSE)
write.csv(dat1_aggregated, "dat1_aggregated.csv", row.names = FALSE)
write.csv(dat2_aggregated, "dat2_aggregated.csv", row.names = FALSE)

# Then apply feature selection on the per-cell data. Here
#`correlation_threshold` - a method that reduces the redundancy of features -
#is used.

#For the combined data
selected <-
  cytominer::variable_select(
    population = transformed,
    variables = na_removed_variables,
    sample = aggregated,
    operation = "correlation_threshold"
  ) %>%
  dplyr::collect()

#For dataset1

dat1_selected <-
  cytominer::variable_select(
    population = dat1_transformed,
    variables = dat1_removed_variables,
    sample = dat1_aggregated,
    operation = "correlation_threshold"
  ) %>%
  dplyr::collect()

#For dataset 2

dat2_selected <-
  cytominer::variable_select(
    population = dat2_transformed,
    variables = dat2_removed_variables,
    sample = dat2_aggregated,
    operation = "correlation_threshold"
  ) %>%
  dplyr::collect()

#remove the variables of Eulernumber


t<-colnames(selected) %>% stringr::str_subset("Euler")
d2<- which (colnames(selected) %in% t)
selected<-selected[,-d2]

selected_variable<-names(selected)[-c(1:8)]
aggregated<-aggregate(
  population = selected,
  variables = selected_variable,
  strata = "Wellsite"
) %>%
  dplyr::collect()

#for dataset 1
```

```
t1 <-colnames(dat1_selected) %>% stringr::str_subset("Euler")
dt1<- which (colnames(dat1_selected) %in% t1)

#there is no "Euler" feature in dataset 1 anymore, so no need to remove it.

dat1_selected_variable<-names(dat1_selected)[-c(1:8)]
dat1_aggregated <- aggregate(
  population = dat1_selected,
  variables = dat1_selected_variable,
  strata = "Wellsite"
) %>%
  dplyr::collect()

#for dataset 2
t2 <-colnames(dat2_selected) %>% stringr::str_subset("Euler")
dt2<- which (colnames(dat2_selected) %in% t2)

#there is no "Euler" feature in dataset 2 anymore, so no need to remove it.

dat2_selected_variable<-names(dat2_selected)[-c(1:8)]
dat2_aggregated <- aggregate(
  population = dat2_selected,
  variables = dat2_selected_variable,
  strata = "Wellsite"
) %>%
  dplyr::collect()

## Perform PCA

# for the combined data
combined_pca <- prcomp(aggregated[,2:176], scale. = TRUE)

# for dataset 1
dat1_pca <- prcomp(dat1_aggregated[,2:9], scale. = TRUE)

# for dataset 2
dat2_pca <- prcomp(dat2_aggregated[,2:14], scale. = TRUE)

#load packages for plotting
library(ggbiplot)
library(factoextra)


#PCA plotting, separated by cell types
#For combined data
comb_samples <-aggregated$Wellsite
comb_gplot <- ggbiplot(combined_pca, obs.scale = 1, var.scale = 1, groups =
comb_samples, circle = TRUE)
comb_gplot <- comb_gplot + scale_color_discrete(names(''))
comb_gplot <- comb_gplot + theme(legend.direction = 'horizontal', legend.position =
'top')
print(comb_gplot)

#For dataset 1
dat1_samples <- dat1_aggregated$Wellsite
dat1_gplot <- ggbiplot(dat1_pca, obs.scale = 1, var.scale = 1, groups =
dat1_samples, circle = TRUE)
dat1_gplot<- dat1_gplot + scale_color_discrete(names(''))
dat1_gplot <- dat1_gplot + theme(legend.direction = 'horizontal', legend.position =
'top')
print(dat1_gplot)

#For dataset 2
dat2_samples <- dat2_aggregated$Wellsite
dat2_gplot <- ggbiplot(dat2_pca, obs.scale = 1, var.scale = 1, groups =
dat2_samples, circle = TRUE)
dat2_gplot<- dat2_gplot + scale_color_discrete(names(''))
```

```
dat2_gplot <- dat2_gplot + theme(legend.direction = 'horizontal', legend.position =
'top')
print(dat2_gplot)

#variance plotting/Scre Plot
#For combined data
fviz_eig(combined_pca)

#For dataset1
fviz_eig(dat1_pca)

#For dataset2
fviz_eig(dat2_pca)

#eigenvalues
#For combined data
eig.val_comb <- get_eigenvalue(combined_pca)
#for dataset1
eig.val_dat1 <- get_eigenvalue(dat1_pca)
#for dataset2
eig.val_dat2 <- get_eigenvalue(dat2_pca)

#results for variables: how much each variable (feature) contribute to each PC
#For combined data
comb_res.var <- get_pca_var(combined_pca)
#for dataset1
dat1_res.var <- get_pca_var(dat1_pca)
#for dataset2
dat2_res.var <- get_pca_var(dat2_pca)

#how does each variable correlate to each PC in terms of:
#For combined data
comb_res.var$coord          # Coordination with each PC
comb_res.var$contrib        # Contribution to each PC-which is used to determine
important features
comb_res.var$cos2           # Quality of representation in each PC

#For dataset 1
dat1_res.var$coord          # Coordination with each PC
dat1_res.var$contrib        # Contribution to each PC-which is used to determine
important features
dat1_res.var$cos2           # Quality of representation in each PC

#For dataset 2
dat2_res.var$coord          # Coordination with each PC
dat2_res.var$contrib        # Contribution to each PC-which is used to determine
important features
dat2_res.var$cos2           # Quality of representation in each PC

#Export the aggregated data
write.csv(aggregated,"combined_aggregated.csv", row.names = TRUE)
write.csv(dat1_aggregated,"dat1_aggregated.csv", row.names = TRUE)
write.csv(dat2_aggregated,"dat2_aggregated.csv", row.names = TRUE)

#Export the contribution values of each feature to the PCs
write.csv(comb_res.var$contrib,"combined_contrib.csv", row.names = TRUE)
write.csv(dat1_res.var$contrib,"dat1_contrib.csv", row.names = TRUE)
write.csv(dat2_res.var$contrib,"dat2_contrib.csv", row.names = TRUE)
```

Reference

. National Center for Biotechnology Information

https://pubchem.ncbi.nlm.nih.gov/compound/614 National Center for Biotechnology Information. Available: https://pubchem.ncbi.nlm.nih.gov/compound/614 [Accessed accessed Sept. 12, 2015].

.

ACAMPORA, D., DI GIOVANNANTONIO, L. G. & SIMEONE, A. 2013. Otx2 is an intrinsic determinant of the embryonic stem cell state and is required for transition to a stable epiblast stem cell condition. *Development,* 140**,** 43-55.

ADAMS, E. & FRANK, L. 1980. Metabolism of proline and the hydroxyprolines. *Annu Rev Biochem,* 49**,** 1005-61.

AGLEDAL, L., NIERE, M. & ZIEGLER, M. 2010. The phosphate makes a difference: cellular functions of NADP. *Redox Rep,* 15**,** 2-10.

ALONSO, E. & RUBIO, V. 1989. Participation of ornithine aminotransferase in the synthesis and catabolism of ornithine in mice. Studies using gabaculine and arginine deprivation. *Biochem J,* 259**,** 131-8.

ARENTSON, B. W., SANYAL, N. & BECKER, D. F. 2012. Substrate channeling in proline metabolism. *Front Biosci (Landmark Ed),* 17**,** 375-88.

ARMSTRONG, L., TILGNER, K., SARETZKI, G., ATKINSON, S. P., STOJKOVIC, M., MORENO, R., PRZYBORSKI, S. & LAKO, M. 2010. Human induced pluripotent stem cell lines show stress defense mechanisms and mitochondrial regulation similar to those of human embryonic stem cells. *Stem Cells,* 28**,** 661-73.

BALABAN, R. S., NEMOTO, S. & FINKEL, T. 2005. Mitochondria, oxidants, and aging. *Cell,* 120**,** 483-95.

BECKMAN, D. A., PUGARELLI, J. E., JENSEN, M., KOSZALKA, T. R., BRENT, R. L. & LLOYD, J. B. 1990. Sources of amino acids for protein synthesis during early organogenesis in the rat. I. Relative contributions of free amino acids and of proteins. *Placenta,* 11**,** 109-21.

BECKMAN, D. A., PUGARELLI, J. E., KOSZALKA, T. R., BRENT, R. L. & LLOYD, J. B. 1991. Sources of amino acids for protein synthesis during early organogenesis in the rat. 2. Exchange with amino acid and protein pools in embryo and yolk sac. *Placenta,* 12**,** 37-46.

BEDDINGTON, R. S. & ROBERTSON, E. J. 1989. An assessment of the developmental potential of embryonic stem cells in the midgestation mouse embryo. *Development,* 105**,** 733-7.

BINO, L., KUCERA, J., STEFKOVA, K., SVIHALKOVA SINDLEROVA, L., LANOVA, M., KUDOVA, J., KUBALA, L. & PACHERNIK, J. 2016. The stabilization of hypoxia inducible factor modulates differentiation status and inhibits the proliferation of mouse embryonic stem cells. *Chem Biol Interact,* 244**,** 204-14.

BIRKET, M. J., CASINI, S., KOSMIDIS, G., ELLIOTT, D. A., GERENCSER, A. A., BAARTSCHEER, A., SCHUMACHER, C., MASTROBERARDINO, P. G., ELEFANTY, A. G., STANLEY, E. G. & MUMMERY, C. L. 2013. PGC-1alpha and reactive oxygen species regulate human embryonic stem cell-derived cardiomyocyte function. *Stem Cell Reports,* 1**,** 560-74.

BIRKET, M. J., ORR, A. L., GERENCSER, A. A., MADDEN, D. T., VITELLI, C., SWISTOWSKI, A., BRAND, M. D. & ZENG, X. 2011. A reduction in ATP demand and mitochondrial activity with neural differentiation of human embryonic stem cells. *J Cell Sci,* 124**,** 348-58.

BLAKE, R. L., HALL, J. G. & RUSSELL, E. S. 1976. Mitochondrial proline dehydrogenase deficiency in hyperprolinemic PRO/Re mice: genetic and enzymatic analyses. *Biochem Genet,* 14**,** 739-57.

BORG, A. J., YONG, H. E., LAPPAS, M., DEGRELLE, S. A., KEOGH, R. J., DA SILVA-COSTA, F., FOURNIER, T., ABUMAREE, M., KEELAN, J. A., KALIONIS, B. & MURTHI, P. 2015. Decreased STAT3 in human idiopathic fetal growth restriction contributes to trophoblast dysfunction. *Reproduction,* 149**,** 523-32.

BOROVIAK, T., LOOS, R., BERTONE, P., SMITH, A. & NICHOLS, J. 2014. The ability of inner-cell-mass cells to self-renew as embryonic stem cells is acquired following epiblast specification. *Nat Cell Biol,* 16**,** 516-28.

BOUKOURIS, A. E., ZERVOPOULOS, S. D. & MICHELAKIS, E. D. 2016. Metabolic Enzymes Moonlighting in the Nucleus: Metabolic Regulation of Gene Transcription. *Trends Biochem Sci,* 41**,** 712-730.

BOUTROS, M., HEIGWER, F. & LAUFER, C. 2015. Microscopy-Based High-Content Screening. *Cell,* 163**,** 1314-25.

BRADLEY, A., EVANS, M., KAUFMAN, M. H. & ROBERTSON, E. 1984. Formation of germ-line chimaeras from embryo-derived teratocarcinoma cell lines. *Nature,* 309**,** 255-6.

BRAND, M. D. 2016. Mitochondrial generation of superoxide and hydrogen peroxide as the source of mitochondrial redox signaling. *Free Radic Biol Med,* 100**,** 14-31.

BRERETON, M. F., ROHM, M., SHIMOMURA, K., HOLLAND, C., TORNOVSKY-BABEAY, S., DADON, D., IBERL, M., CHIBALINA, M. V., LEE, S., GLASER, B., DOR, Y., RORSMAN, P., CLARK, A. & ASHCROFT, F. M. 2016. Hyperglycaemia induces metabolic dysfunction and glycogen accumulation in pancreatic beta-cells. *Nat Commun,* 7**,** 13496.

BROER, S. 2014. The SLC38 family of sodium-amino acid co-transporters. *Pflugers Arch,* 466**,** 155-72.

BRUNET, A., SWEENEY, L. B., STURGILL, J. F., CHUA, K. F., GREER, P. L., LIN, Y., TRAN, H., ROSS, S. E., MOSTOSLAVSKY, R., COHEN, H. Y., HU, L. S., CHENG, H. L., JEDRYCHOWSKI, M. P., GYGI, S. P., SINCLAIR, D. A., ALT, F. W. & GREENBERG, M. E. 2004. Stress-dependent regulation of FOXO transcription factors by the SIRT1 deacetylase. *Science,* 303**,** 2011-5.

BUKOWIECKI, R., ADJAYE, J. & PRIGIONE, A. 2014. Mitochondrial function in pluripotent stem cells and cellular reprogramming. *Gerontology,* 60**,** 174-82.

BUSZCZAK, M., SIGNER, R. A. & MORRISON, S. J. 2014. Cellular differences in protein synthesis regulate tissue homeostasis. *Cell,* 159**,** 242-51.

C, O. N. 2013. PI3-kinase/Akt/mTOR signaling: impaired on/off switches in aging, cognitive decline and Alzheimer's disease. *Exp Gerontol,* 48**,** 647-53.

CAI, Z. & YAN, L. J. 2013. Protein Oxidative Modifications: Beneficial Roles in Disease and Health. *J Biochem Pharmacol Res,* 1**,** 15-26.

CAICEDO, J. C., COOPER, S., HEIGWER, F., WARCHAL, S., QIU, P., MOLNAR, C., VASILEVICH, A. S., BARRY, J. D., BANSAL, H. S., KRAUS, O., WAWER, M., PAAVOLAINEN, L., HERRMANN, M. D., ROHBAN, M., HUNG, J., HENNIG, H., CONCANNON, J., SMITH, I., CLEMONS, P. A., SINGH, S., REES, P., HORVATH, P., LININGTON, R. G. & CARPENTER, A. E. 2017. Data-analysis strategies for image-based cell profiling. *Nat Methods,* 14**,** 849-863.

CAMPBELL, H. D., WEBB, G. C. & YOUNG, I. G. 1997. A human homologue of the Drosophila melanogaster sluggish-A (proline oxidase) gene maps to 22q11.2, and is a candidate gene for type-I hyperprolinaemia. *Hum Genet,* 101**,** 69-74.

CANTO, C., MENZIES, K. J. & AUWERX, J. 2015. NAD(+) Metabolism and the Control of Energy Homeostasis: A Balancing Act between Mitochondria and the Nucleus. *Cell Metab,* 22**,** 31-53.

CARBOGNIN, E., BETTO, R. M., SORIANO, M. E., SMITH, A. G. & MARTELLO, G. 2016. Stat3 promotes mitochondrial transcription and oxidative respiration during maintenance and induction of naive pluripotency. *Embo j,* 35**,** 618-34.

CAREY, B. W., FINLEY, L. W., CROSS, J. R., ALLIS, C. D. & THOMPSON, C. B. 2015. Intracellular alpha-ketoglutarate maintains the pluripotency of embryonic stem cells. *Nature,* 518**,** 413-6.

CASALINO, L., COMES, S., LAMBAZZI, G., DE STEFANO, B., FILOSA, S., DE FALCO, S., DE CESARE, D., MINCHIOTTI, G. & PATRIARCA, E. J. 2011. Control of embryonic stem cell metastability by L-proline catabolism. *J Mol Cell Biol,* 3**,** 108-22.

CASCONE, T., MCKENZIE, J. A., MBOFUNG, R. M., PUNT, S., WANG, Z., XU, C., WILLIAMS, L. J., WANG, Z., BRISTOW, C. A., CARUGO, A., PEOPLES, M. D., LI, L., KARPINETS, T., HUANG, L., MALU, S., CREASY, C., LEAHEY, S. E., CHEN, J., CHEN, Y., PELICANO, H., BERNATCHEZ, C., GOPAL, Y. N. V., HEFFERNAN, T. P., HU, J., WANG, J., AMARIA, R. N., GARRAWAY, L. A., HUANG, P., YANG, P., WISTUBA, II, WOODMAN, S. E., ROSZIK, J., DAVIS, R. E., DAVIES, M. A., HEYMACH, J. V., HWU,

P. & PENG, W. 2018. Increased Tumor Glycolysis Characterizes Immune Resistance to Adoptive T Cell Therapy. *Cell Metab,* 27**,** 977-987.e4.

CHAE, H. Z., KANG, S. W. & RHEE, S. G. 1999a. Isoforms of mammalian peroxiredoxin that reduce peroxides in presence of thioredoxin. *Methods Enzymol,* 300**,** 219-26.

CHAE, H. Z., KIM, H. J., KANG, S. W. & RHEE, S. G. 1999b. Characterization of three isoforms of mammalian peroxiredoxin that reduce peroxides in the presence of thioredoxin. *Diabetes Res Clin Pract,* 45**,** 101-12.

CHANTRANUPONG, L., WOLFSON, R. L. & SABATINI, D. M. 2015. Nutrient-sensing mechanisms across evolution. *Cell,* 161**,** 67-83.

CHEN, C. T., SHIH, Y. R., KUO, T. K., LEE, O. K. & WEI, Y. H. 2008. Coordinated changes of mitochondrial biogenesis and antioxidant enzymes during osteogenic differentiation of human mesenchymal stem cells. *Stem Cells,* 26**,** 960-8.

CHEN, T., UEDA, Y., DODGE, J. E., WANG, Z. & LI, E. 2003. Establishment and maintenance of genomic methylation patterns in mouse embryonic stem cells by Dnmt3a and Dnmt3b. *Mol Cell Biol,* 23**,** 5594-605.

CHO, Y. M., KWON, S., PAK, Y. K., SEOL, H. W., CHOI, Y. M., PARK, D. J., PARK, K. S. & LEE, H. K. 2006a. Dynamic changes in mitochondrial biogenesis and antioxidant enzymes during the spontaneous differentiation of human embryonic stem cells. *Biochem Biophys Res Commun,* 348**,** 1472-8.

CHO, Y. M., KWON, S., PAK, Y. K., SEOL, H. W., CHOI, Y. M., PARK DO, J., PARK, K. S. & LEE, H. K. 2006b. Dynamic changes in mitochondrial biogenesis and antioxidant enzymes during the spontaneous differentiation of human embryonic stem cells. *Biochem Biophys Res Commun,* 348**,** 1472-8.

CHOI, J., HUEBNER, A. J., CLEMENT, K., WALSH, R. M., SAVOL, A., LIN, K., GU, H., DI STEFANO, B., BRUMBAUGH, J., KIM, S. Y., SHARIF, J., ROSE, C. M., MOHAMMAD, A., ODAJIMA, J., CHARRON, J., SHIODA, T., GNIRKE, A., GYGI, S., KOSEKI, H., SADREYEV, R. I., XIAO, A., MEISSNER, A. & HOCHEDLINGER, K. 2017. Prolonged Mek1/2 suppression impairs the developmental potential of embryonic stem cells. *Nature,* 548**,** 219-223.

CHUNG, S., ARRELL, D. K., FAUSTINO, R. S., TERZIC, A. & DZEJA, P. P. 2010. Glycolytic network restructuring integral to the energetics of embryonic stem cell cardiac differentiation. *J Mol Cell Cardiol,* 48**,** 725-34.

CHUNG, S., DZEJA, P. P., FAUSTINO, R. S., PEREZ-TERZIC, C., BEHFAR, A. & TERZIC, A. 2007. Mitochondrial oxidative metabolism is required for the cardiac differentiation of stem cells. *Nat Clin Pract Cardiovasc Med,* 4 Suppl 1**,** S60-7.

CHUNG, S., DZEJA, P. P., FAUSTINO, R. S. & TERZIC, A. 2008. Developmental restructuring of the creatine kinase system integrates mitochondrial energetics with stem cell cardiogenesis. *Ann N Y Acad Sci,* 1147**,** 254-63.

COMES, S., GAGLIARDI, M., LAPRANO, N., FICO, A., CIMMINO, A., PALAMIDESSI, A., DE CESARE, D., DE FALCO, S., ANGELINI, C., SCITA, G., PATRIARCA, E. J., MATARAZZO, M. R. & MINCHIOTTI, G. 2013. L-Proline induces a mesenchymal-like invasive program in embryonic stem cells by remodeling H3K9 and H3K36 methylation. *Stem Cell Reports,* 1**,** 307-21.

CORONADO, D., GODET, M., BOURILLOT, P. Y., TAPPONNIER, Y., BERNAT, A., PETIT, M., AFANASSIEFF, M., MARKOSSIAN, S., MALASHICHEVA, A., IACONE, R., ANASTASSIADIS, K. & SAVATIER, P. 2013. A short G1 phase is an intrinsic determinant of naive embryonic stem cell pluripotency. *Stem Cell Res,* 10**,** 118-31.

COVARRUBIAS, L., HERNANDEZ-GARCIA, D., SCHNABEL, D., SALAS-VIDAL, E. & CASTRO-OBREGON, S. 2008. Function of reactive oxygen species during animal development: passive or active? *Dev Biol,* 320**,** 1-11.

CRESPO, F. L., SOBRADO, V. R., GOMEZ, L., CERVERA, A. M. & MCCREATH, K. J. 2010. Mitochondrial reactive oxygen species mediate cardiomyocyte formation from embryonic stem cells in high glucose. *Stem Cells,* 28**,** 1132-42.

CUNNANE, S., NUGENT, S., ROY, M., COURCHESNE-LOYER, A., CROTEAU, E., TREMBLAY, S., CASTELLANO, A., PIFFERI, F., BOCTI, C., PAQUET, N., BEGDOURI, H., BENTOURKIA, M., TURCOTTE, E., ALLARD, M., BARBERGER-GATEAU, P., FULOP, T. & RAPOPORT, S. I. 2011. Brain fuel metabolism, aging, and Alzheimer's disease. *Nutrition,* 27**,** 3-20.

D'ANIELLO, C., FICO, A., CASALINO, L., GUARDIOLA, O., DI NAPOLI, G., CERMOLA, F., DE CESARE, D., TATE, R., COBELLIS, G., PATRIARCA, E. J. & MINCHIOTTI, G. 2015. A novel autoregulatory loop between the Gcn2-Atf4 pathway and L-Proline metabolism controls stem cell identity. *Cell Death Differ,* 22**,** 1094-105.

D'ANIELLO, C., HABIBI, E., CERMOLA, F., PARIS, D., RUSSO, F., FIORENZANO, A., DI NAPOLI, G., MELCK, D. J., COBELLIS, G., ANGELINI, C., FICO, A., BLELLOCH, R., MOTTA, A., STUNNENBERG, H. G., DE CESARE, D., PATRIARCA, E. J. & MINCHIOTTI, G. 2017. Vitamin C and l-Proline Antagonistic Effects Capture Alternative States in the Pluripotency Continuum. *Stem Cell Reports,* 8**,** 1-10.

DAHERON, L., OPITZ, S. L., ZAEHRES, H., LENSCH, M. W., ANDREWS, P. W., ITSKOVITZ-ELDOR, J. & DALEY, G. Q. 2004. LIF/STAT3 signaling fails to maintain self-renewal of human embryonic stem cells. *Stem Cells,* 22**,** 770-8.

DANG, C. V. 2012. Links between metabolism and cancer. *Genes Dev,* 26**,** 877-90.

DAWSON, K. M. & BALTZ, J. M. 1997. Organic osmolytes and embryos: substrates of the Gly and beta transport systems protect mouse zygotes against the effects of raised osmolarity. *Biol Reprod,* 56**,** 1550-8.

DEBERARDINIS, R. J. & THOMPSON, C. B. 2012. Cellular metabolism and disease: what do metabolic outliers teach us? *Cell,* 148**,** 1132-44.

DIBBLE, C. C. & CANTLEY, L. C. 2015. Regulation of mTORC1 by PI3K signaling. *Trends Cell Biol,* 25**,** 545-55.

DIBBLE, C. C. & MANNING, B. D. 2013. Signal integration by mTORC1 coordinates nutrient input with biosynthetic output. *Nat Cell Biol,* 15**,** 555-64.

DING, L., LIANG, X. G., HU, Y., ZHU, D. Y. & LOU, Y. J. 2008. Involvement of p38MAPK and reactive oxygen species in icariin-induced cardiomyocyte differentiation of murine embryonic stem cells in vitro. *Stem Cells Dev,* 17**,** 751-60.

DOETSCHMAN, T. C., EISTETTER, H., KATZ, M., SCHMIDT, W. & KEMLER, R. 1985. The in vitro development of blastocyst-derived embryonic stem cell lines: formation of visceral yolk sac, blood islands and myocardium. *J Embryol Exp Morphol,* 87**,** 27-45.

DONALD, S. P., SUN, X. Y., HU, C. A., YU, J., MEI, J. M., VALLE, D. & PHANG, J. M. 2001. Proline oxidase, encoded by p53-induced gene-6, catalyzes the generation of proline-dependent reactive oxygen species. *Cancer Res,* 61**,** 1810-5.

ECHTAY, K. S. & BRAND, M. D. 2007. 4-hydroxy-2-nonenal and uncoupling proteins: an approach for regulation of mitochondrial ROS production. *Redox Rep,* 12**,** 26-9.

EFEYAN, A., COMB, W. C. & SABATINI, D. M. 2015. Nutrient-sensing mechanisms and pathways. *Nature,* 517**,** 302-10.

ELIA, I., BROEKAERT, D., CHRISTEN, S., BOON, R., RADAELLI, E., ORTH, M. F., VERFAILLIE, C., GRUNEWALD, T. G. P. & FENDT, S. M. 2017. Proline metabolism supports metastasis formation and could be inhibited to selectively target metastasizing cancer cells. *Nat Commun,* 8**,** 15267.

ENZO, E., SANTINON, G., POCATERRA, A., ARAGONA, M., BRESOLIN, S., FORCATO, M., GRIFONI, D., PESSION, A., ZANCONATO, F., GUZZO, G., BICCIATO, S. & DUPONT, S. 2015. Aerobic glycolysis tunes YAP/TAZ transcriptional activity. *Embo j,* 34**,** 1349-70.

EPSTEIN, T., GATENBY, R. A. & BROWN, J. S. 2017. The Warburg effect as an adaptation of cancer cells to rapid fluctuations in energy demand. *PLoS One,* 12**,** e0185085.

ESTEBAN, M. A., WANG, T., QIN, B., YANG, J., QIN, D., CAI, J., LI, W., WENG, Z., CHEN, J., NI, S., CHEN, K., LI, Y., LIU, X., XU, J., ZHANG, S., LI, F., HE, W., LABUDA, K., SONG, Y., PETERBAUER, A., WOLBANK, S., REDL, H., ZHONG, M., CAI, D., ZENG, L. & PEI, D. 2010. Vitamin C enhances the generation of mouse and human induced pluripotent stem cells. *Cell Stem Cell,* 6**,** 71-9.

EVANS, M. J. & KAUFMAN, M. H. 1981. Establishment in culture of pluripotential cells from mouse embryos. *Nature,* 292**,** 154-6.

FACUCHO-OLIVEIRA, J. M., ALDERSON, J., SPIKINGS, E. C., EGGINTON, S. & ST JOHN, J. C. 2007. Mitochondrial DNA replication during differentiation of murine embryonic stem cells. *J Cell Sci,* 120**,** 4025-34.

FARRANT, R. D., WALKER, V., MILLS, G. A., MELLOR, J. M. & LANGLEY, G. J. 2001. Pyridoxal phosphate de-activation by pyrroline-5-carboxylic acid. Increased risk of vitamin B6 deficiency and seizures in hyperprolinemia type II. *J Biol Chem,* 276**,** 15107-16.

FICZ, G., HORE, T. A., SANTOS, F., LEE, H. J., DEAN, W., ARAND, J., KRUEGER, F., OXLEY, D., PAUL, Y. L., WALTER, J., COOK, S. J., ANDREWS, S., BRANCO, M. R. & REIK, W. 2013. FGF signaling inhibition in ESCs drives rapid genome-wide demethylation to the epigenetic ground state of pluripotency. *Cell Stem Cell,* 13**,** 351-9.

FINKELSTEIN, J. D. 1990. Methionine metabolism in mammals. *J Nutr Biochem,* 1**,** 228-37.

FLEMING, G. A., HAGEDORN, C. H., GRANGER, A. S. & PHANG, J. M. 1984. Pyrroline-5-carboxylate in human plasma. *Metabolism,* 33**,** 739-42.

FOLMES, C. D., DZEJA, P. P., NELSON, T. J. & TERZIC, A. 2012. Metabolic plasticity in stem cell homeostasis and differentiation. *Cell Stem Cell,* 11**,** 596-606.

FOLMES, C. D., NELSON, T. J., MARTINEZ-FERNANDEZ, A., ARRELL, D. K., LINDOR, J. Z., DZEJA, P. P., IKEDA, Y., PEREZ-TERZIC, C. & TERZIC, A. 2011. Somatic oxidative bioenergetics transitions into pluripotency-dependent glycolysis to facilitate nuclear reprogramming. *Cell Metab,* 14**,** 264-71.

FORMAN, H. J., URSINI, F. & MAIORINO, M. 2014. An overview of mechanisms of redox signaling. *J Mol Cell Cardiol,* 73**,** 2-9.

FORNERIS, F., BINDA, C., VANONI, M. A., MATTEVI, A. & BATTAGLIOLI, E. 2005. Histone demethylation catalysed by LSD1 is a flavin-dependent oxidative process. *FEBS Lett,* 579**,** 2203-7.

FRIDOVICH, I. 1997. Superoxide anion radical (O2-.), superoxide dismutases, and related matters. *J Biol Chem,* 272**,** 18515-7.

GABUT, M., SAMAVARCHI-TEHRANI, P., WANG, X., SLOBODENIUC, V., O'HANLON, D., SUNG, H. K., ALVAREZ, M., TALUKDER, S., PAN, Q., MAZZONI, E. O., NEDELEC, S., WICHTERLE, H., WOLTJEN, K., HUGHES, T. R., ZANDSTRA, P. W., NAGY, A., WRANA, J. L. & BLENCOWE, B. J. 2011. An alternative splicing switch regulates embryonic stem cell pluripotency and reprogramming. *Cell,* 147**,** 132-46.

GALGANI, M., DE ROSA, V. & MATARESE, G. 2015. T cell metabolism and susceptibility to autoimmune diseases. *Mol Immunol,* 68**,** 558-63.

GALLUZZI, L., KEPP, O., VANDER HEIDEN, M. G. & KROEMER, G. 2013. Metabolic targets for cancer therapy. *Nat Rev Drug Discov,* 12**,** 829-46.

GIANNONI, E., BURICCHI, F., RAUGEI, G., RAMPONI, G. & CHIARUGI, P. 2005. Intracellular reactive oxygen species activate Src tyrosine kinase during cell adhesion and anchorage-dependent cell growth. *Mol Cell Biol,* 25**,** 6391-403.

GINGUAY, A., CYNOBER, L., CURIS, E. & NICOLIS, I. 2017. Ornithine Aminotransferase, an Important Glutamate-Metabolizing Enzyme at the Crossroads of Multiple Metabolic Pathways. *Biology (Basel),* 6.

GOBERDHAN, D. C., WILSON, C. & HARRIS, A. L. 2016. Amino Acid Sensing by mTORC1: Intracellular Transporters Mark the Spot. *Cell Metab,* 23**,** 580-9.

GODWIN, S., WARD, D., PEDONE, E., HOMER, M., FLETCHER, A. G. & MARUCCI, L. 2017. An extended model for culture-dependent heterogenous gene expression and proliferation dynamics in mouse embryonic stem cells. *NPJ Syst Biol Appl,* 3**,** 19.

GOGOS, J. A., SANTHA, M., TAKACS, Z., BECK, K. D., LUINE, V., LUCAS, L. R., NADLER, J. V. & KARAYIORGOU, M. 1999. The gene encoding proline dehydrogenase modulates sensorimotor gating in mice. *Nat Genet,* 21**,** 434-9.

GONCALVES, R. L., ROTHSCHILD, D. E., QUINLAN, C. L., SCOTT, G. K., BENZ, C. C. & BRAND, M. D. 2014. Sources of superoxide/H2O2 during mitochondrial proline oxidation. *Redox Biol,* 2**,** 901-9.

GONG, F. & MILLER, K. M. 2013. Mammalian DNA repair: HATs and HDACs make their mark through histone acetylation. *Mutat Res,* 750**,** 23-30.

GORRES, K. L. & RAINES, R. T. 2010. Prolyl 4-hydroxylase. *Crit Rev Biochem Mol Biol,* 45**,** 106-24.

GRAF, T. & STADTFELD, M. 2008. Heterogeneity of embryonic and adult stem cells. *Cell Stem Cell,* 3**,** 480-3.

GRIMSRUD, P. A., XIE, H., GRIFFIN, T. J. & BERNLOHR, D. A. 2008. Oxidative stress and covalent modification of protein with bioactive aldehydes. *J Biol Chem,* 283**,** 21837-41.

GU, W., GAETA, X., SAHAKYAN, A., CHAN, A. B., HONG, C. S., KIM, R., BRAAS, D., PLATH, K., LOWRY, W. E. & CHRISTOFK, H. R. 2016. Glycolytic Metabolism Plays a Functional Role in Regulating Human Pluripotent Stem Cell State. *Cell Stem Cell,* 19**,** 476-490.

GUO, G., VON MEYENN, F., SANTOS, F., CHEN, Y., REIK, W., BERTONE, P., SMITH, A. & NICHOLS, J. 2016. Naive Pluripotent Stem Cells Derived Directly from Isolated Cells of the Human Inner Cell Mass. *Stem Cell Reports,* 6**,** 437-46.

GUO, G., YANG, J., NICHOLS, J., HALL, J. S., EYRES, I., MANSFIELD, W. & SMITH, A. 2009. Klf4 reverts developmentally programmed restriction of ground state pluripotency. *Development,* 136**,** 1063-9.

GUO, Y., EINHORN, L., KELLEY, M., HIROTA, K., YODOI, J., REINBOLD, R., SCHOLER, H., RAMSEY, H. & HROMAS, R. 2004. Redox regulation of the embryonic stem cell transcription factor oct-4 by thioredoxin. *Stem Cells,* 22**,** 259-64.

GUSTAFSDOTTIR, S. M., LJOSA, V., SOKOLNICKI, K. L., ANTHONY WILSON, J., WALPITA, D., KEMP, M. M., PETRI SEILER, K., CARREL, H. A., GOLUB, T. R., SCHREIBER, S. L., CLEMONS, P. A., CARPENTER, A. E. & SHAMJI, A. F. 2013. Multiplex cytological profiling assay to measure diverse cellular states. *PLoS One,* 8**,** e80999.

HABIBI, E., BRINKMAN, A. B., ARAND, J., KROEZE, L. I., KERSTENS, H. H., MATARESE, F., LEPIKHOV, K., GUT, M., BRUN-HEATH, I., HUBNER, N. C., BENEDETTI, R., ALTUCCI, L., JANSEN, J. H., WALTER, J., GUT, I. G., MARKS, H. & STUNNENBERG, H. G. 2013. Whole-genome bisulfite sequencing of two distinct interconvertible DNA methylomes of mouse embryonic stem cells. *Cell Stem Cell,* 13**,** 360-9.

HAGEDORN, C. H. & PHANG, J. M. 1983. Transfer of reducing equivalents into mitochondria by the interconversions of proline and delta 1-pyrroline-5-carboxylate. *Arch Biochem Biophys,* 225**,** 95-101.

HAGEDORN, C. H. & PHANG, J. M. 1986. Catalytic transfer of hydride ions from NADPH to oxygen by the interconversions of proline and delta 1-pyrroline-5-carboxylate. *Arch Biochem Biophys,* 248**,** 166-74.

HAN, M. K., SONG, E. K., GUO, Y., OU, X., MANTEL, C. & BROXMEYER, H. E. 2008. SIRT1 regulates apoptosis and Nanog expression in mouse embryonic stem cells by controlling p53 subcellular localization. *Cell Stem Cell,* 2**,** 241-51.

HANCOCK, C. N., LIU, W., ALVORD, W. G. & PHANG, J. M. 2016. Co-regulation of mitochondrial respiration by proline dehydrogenase/oxidase and succinate. *Amino Acids,* 48**,** 859-72.

HANNA, J. H., SAHA, K. & JAENISCH, R. 2010. Pluripotency and cellular reprogramming: facts, hypotheses, unresolved issues. *Cell,* 143**,** 508-25.

HARA, K., YONEZAWA, K., WENG, Q. P., KOZLOWSKI, M. T., BELHAM, C. & AVRUCH, J. 1998. Amino acid sufficiency and mTOR regulate p70 S6 kinase and eIF-4E BP1 through a common effector mechanism. *J Biol Chem,* 273**,** 14484-94.

HARVEY, A., GIBSON, T., LONERGAN, T. & BRENNER, C. 2011. Dynamic regulation of mitochondrial function in preimplantation embryos and embryonic stem cells. *Mitochondrion,* 11**,** 829-38.

HAYASHI, K., LOPES, S. M., TANG, F. & SURANI, M. A. 2008. Dynamic equilibrium and heterogeneity of mouse pluripotent stem cells with distinct functional and epigenetic states. *Cell Stem Cell,* 3**,** 391-401.

HEO, H. J., KIM, H. K., YOUM, J. B., CHO, S. W., SONG, I. S., LEE, S. Y., KO, T. H., KIM, N., KO, K. S., RHEE, B. D. & HAN, J. 2016. Mitochondrial pyruvate dehydrogenase phosphatase 1 regulates the early differentiation of cardiomyocytes from mouse embryonic stem cells. *Exp Mol Med,* 48**,** e254.

HERBERG, M., GLAUCHE, I., ZERJATKE, T., WINZI, M., BUCHHOLZ, F. & ROEDER, I. 2016. Dissecting mechanisms of mouse embryonic stem cells heterogeneity through a model-based analysis of transcription factor dynamics. *J R Soc Interface,* 13.

HOLMSTROM, K. M. & FINKEL, T. 2014. Cellular mechanisms and physiological consequences of redox-dependent signalling. *Nat Rev Mol Cell Biol,* 15**,** 411-21.

HU, C. A., BART WILLIAMS, D., ZHAORIGETU, S., KHALIL, S., WAN, G. & VALLE, D. 2008. Functional genomics and SNP analysis of human genes encoding proline metabolic enzymes. *Amino Acids,* 35**,** 655-64.

HU, C. A., DONALD, S. P., YU, J., LIN, W. W., LIU, Z., STEEL, G., OBIE, C., VALLE, D. & PHANG, J. M. 2007. Overexpression of proline oxidase induces proline-dependent and mitochondria-mediated apoptosis. *Mol Cell Biochem,* 295**,** 85-92.

HU, C. A., LIN, W. W., OBIE, C. & VALLE, D. 1999. Molecular enzymology of mammalian Delta1-pyrroline-5-carboxylate synthase. Alternative splice donor utilization generates isoforms with different sensitivity to ornithine inhibition. *J Biol Chem,* 274**,** 6754-62.

HUANGYANG, P. & SIMON, M. C. 2018. Hidden features: exploring the non-canonical functions of metabolic enzymes. *Dis Model Mech,* 11.

HUGHES, J. N., DODGE, N., RATHJEN, P. D. & RATHJEN, J. 2009. A novel role for gamma-secretase in the formation of primitive streak-like intermediates from ES cells in culture. *Stem Cells,* 27**,** 2941-51.

HYDE, R., CWIKLINSKI, E. L., MACAULAY, K., TAYLOR, P. M. & HUNDAL, H. S. 2007. Distinct sensor pathways in the hierarchical control of SNAT2, a putative amino acid transceptor, by amino acid availability. *J Biol Chem,* 282**,** 19788-98.

ITO, K., HIRAO, A., ARAI, F., TAKUBO, K., MATSUOKA, S., MIYAMOTO, K., OHMURA, M., NAKA, K., HOSOKAWA, K., IKEDA, Y. & SUDA, T. 2006. Reactive oxygen species act through p38 MAPK to limit the lifespan of hematopoietic stem cells. *Nat Med,* 12**,** 446-51.

ITO, K. & SUDA, T. 2014. Metabolic requirements for the maintenance of self-renewing stem cells. *Nat Rev Mol Cell Biol,* 15**,** 243-56.

JEONG, A. Y., LEE, M. Y., LEE, S. H., PARK, J. H. & HAN, H. J. 2009. PPARdelta agonist-mediated ROS stimulates mouse embryonic stem cell proliferation through cooperation of p38 MAPK and Wnt/beta-catenin. *Cell Cycle,* 8**,** 611-9.

JEWELL, J. L. & GUAN, K. L. 2013. Nutrient signaling to mTOR and cell growth. *Trends Biochem Sci,* 38**,** 233-42.

JEWELL, J. L., KIM, Y. C., RUSSELL, R. C., YU, F. X., PARK, H. W., PLOUFFE, S. W., TAGLIABRACCI, V. S. & GUAN, K. L. 2015. Metabolism. Differential regulation of mTORC1 by leucine and glutamine. *Science,* 347**,** 194-8.

JI, A. R., KU, S. Y., CHO, M. S., KIM, Y. Y., KIM, Y. J., OH, S. K., KIM, S. H., MOON, S. Y. & CHOI, Y. M. 2010. Reactive oxygen species enhance differentiation of human embryonic stem cells into mesendodermal lineage. *Exp Mol Med,* 42**,** 175-86.

JI, J., SHARMA, V., QI, S., GUARCH, M. E., ZHAO, P., LUO, Z., FAN, W., WANG, Y., MBABAALI, F., NECULAI, D., ESTEBAN, M. A., MCPHERSON, J. D. & BATADA, N. N. 2014. Antioxidant supplementation reduces genomic aberrations in human induced pluripotent stem cells. *Stem Cell Reports,* 2**,** 44-51.

JIANG, Y., QIAN, X., SHEN, J., WANG, Y., LI, X., LIU, R., XIA, Y., CHEN, Q., PENG, G., LIN, S. Y. & LU, Z. 2015. Local generation of fumarate promotes DNA repair through inhibition of histone H3 demethylation. *Nat Cell Biol,* 17**,** 1158-68.

JONES, H. N., ASHWORTH, C. J., PAGE, K. R. & MCARDLE, H. J. 2006. Cortisol stimulates system A amino acid transport and SNAT2 expression in a human placental cell line (BeWo). *Am J Physiol Endocrinol Metab,* 291**,** E596-603.

JONES, H. N., JANSSON, T. & POWELL, T. L. 2009. IL-6 stimulates system A amino acid transporter activity in trophoblast cells through STAT3 and increased expression of SNAT2. *Am J Physiol Cell Physiol,* 297**,** C1228-35.

KAELIN, W. G., JR. 2011. Cancer and altered metabolism: potential importance of hypoxia-inducible factor and 2-oxoglutarate-dependent dioxygenases. *Cold Spring Harb Symp Quant Biol,* 76**,** 335-45.

KALKAN, T., OLOVA, N., ROODE, M., MULAS, C., LEE, H. J., NETT, I., MARKS, H., WALKER, R., STUNNENBERG, H. G., LILLEY, K. S., NICHOLS, J., REIK, W., BERTONE, P. & SMITH, A. 2017. Tracking the embryonic stem cell transition from ground state pluripotency. *Development,* 144**,** 1221-1234.

KAUFMAN, B. A., LI, C. & SOLEIMANPOUR, S. A. 2015. Mitochondrial regulation of beta-cell function: maintaining the momentum for insulin release. *Mol Aspects Med,* 42**,** 91-104.

KAUL, S., SHARMA, S. S. & MEHTA, I. K. 2008. Free radical scavenging potential of L-proline: evidence from in vitro assays. *Amino Acids,* 34**,** 315-20.

KERKAR, S. P. & RESTIFO, N. P. 2012. Cellular constituents of immune escape within the tumor microenvironment. *Cancer Res,* 72**,** 3125-30.

KERWAR, S. S. 1979. Regulation of collagen synthesis and maturation by 3,4-dehydroproline. *Arch Biol Med Exp (Santiago),* 12**,** 359-66.

KERWAR, S. S. & FELIX, A. M. 1976. Effect of L-3,4-dehydroproline on collagen synthesis and prolyl hydroxylase activity in mammalian cell cultures. *J Biol Chem,* 251**,** 503-9.

KILBERG, M. S., STEVENS, B. R. & NOVAK, D. A. 1993. Recent advances in mammalian amino acid transport. *Annu Rev Nutr,* 13**,** 137-65.

KILBERG, M. S., TERADA, N. & SHAN, J. 2016. Influence of Amino Acid Metabolism on Embryonic Stem Cell Function and Differentiation. *Adv Nutr,* 7**,** 780s-9s.

KILENS, S., MEISTERMANN, D., MORENO, D., CHARIAU, C., GAIGNERIE, A., REIGNIER, A., LELIEVRE, Y., CASANOVA, M., VALLOT, C., NEDELLEC, S., FLIPPE, L., FIRMIN, J., SONG, J., CHARPENTIER, E., LAMMERS, J., DONNART, A., MAREC, N., DEB, W., BIHOUEE, A., LE CAIGNEC, C., PECQUEUR, C., REDON, R., BARRIERE, P., BOURDON, J., PASQUE, V., SOUMILLON, M., MIKKELSEN, T. S., ROUGEULLE, C., FREOUR, T. & DAVID, L. 2018. Parallel derivation of isogenic human primed and naive induced pluripotent stem cells. *Nat Commun,* 9**,** 360.

KIM, E., GORAKSHA-HICKS, P., LI, L., NEUFELD, T. P. & GUAN, K. L. 2008. Regulation of TORC1 by Rag GTPases in nutrient response. *Nat Cell Biol,* 10**,** 935-45.

KOLODZIEJCZYK, A. A., KIM, J. K., TSANG, J. C., ILICIC, T., HENRIKSSON, J., NATARAJAN, K. N., TUCK, A. C., GAO, X., BUHLER, M., LIU, P., MARIONI, J. C. & TEICHMANN, S. A. 2015. Single Cell RNA-Sequencing of Pluripotent States Unlocks Modular Transcriptional Variation. *Cell Stem Cell,* 17**,** 471-85.

KONDOH, H., LLEONART, M. E., NAKASHIMA, Y., YOKODE, M., TANAKA, M., BERNARD, D., GIL, J. & BEACH, D. 2007. A high glycolytic flux supports the proliferative potential of murine embryonic stem cells. *Antioxid Redox Signal,* 9**,** 293-9.

KRISHNAN, N., DICKMAN, M. B. & BECKER, D. F. 2008. Proline modulates the intracellular redox environment and protects mammalian cells against oxidative stress. *Free Radic Biol Med,* 44**,** 671-81.

KUBLI, D. A. & SUSSMAN, M. A. 2017. Eat, breathe, ROS: controlling stem cell fate through metabolism. *Expert Rev Cardiovasc Ther,* 15**,** 345-356.

KUNATH, T. 2011. Primed for pluripotency. *Cell Stem Cell,* 8**,** 241-2.

KUNATH, T., SABA-EL-LEIL, M. K., ALMOUSAILLEAKH, M., WRAY, J., MELOCHE, S. & SMITH, A. 2007. FGF stimulation of the Erk1/2 signalling cascade triggers transition of pluripotent embryonic stem cells from self-renewal to lineage commitment. *Development,* 134**,** 2895-902.

KURODA, Y., MITSUI, T., KUNISHIGE, M., SHONO, M., AKAIKE, M., AZUMA, H. & MATSUMOTO, T. 2006. Parkin enhances mitochondrial biogenesis in proliferating cells. *Hum Mol Genet,* 15**,** 883-95.

KWON, H., SPENCER, T. E., BAZER, F. W. & WU, G. 2003. Developmental changes of amino acids in ovine fetal fluids. *Biol Reprod,* 68**,** 1813-20.

LAKE, J., RATHJEN, J., REMISZEWSKI, J. & RATHJEN, P. D. 2000. Reversible programming of pluripotent cell differentiation. *J Cell Sci,* 113 (Pt 3)**,** 555-66.

LAU, E., KLUGER, H., VARSANO, T., LEE, K., SCHEFFLER, I., RIMM, D. L., IDEKER, T. & RONAI, Z. A. 2012. PKCepsilon promotes oncogenic functions of ATF2 in the nucleus while blocking its apoptotic function at mitochondria. *Cell,* 148**,** 543-55.

LEE, J., KIM, H. K., HAN, Y. M. & KIM, J. 2008. Pyruvate kinase isozyme type M2 (PKM2) interacts and cooperates with Oct-4 in regulating transcription. *Int J Biochem Cell Biol,* 40**,** 1043-54.

LEE, Y. H., NADARAIA, S., GU, D., BECKER, D. F. & TANNER, J. J. 2003. Structure of the proline dehydrogenase domain of the multifunctional PutA flavoprotein. *Nat Struct Biol,* 10**,** 109-14.

LEES, J. G., GARDNER, D. K. & HARVEY, A. J. 2017. Pluripotent Stem Cell Metabolism and Mitochondria: Beyond ATP. *Stem Cells Int,* 2017**,** 2874283.

LI, D., HIRSILA, M., KOIVUNEN, P., BRENNER, M. C., XU, L., YANG, C., KIVIRIKKO, K. I. & MYLLYHARJU, J. 2004. Many amino acid substitutions in a hypoxia-inducible transcription factor (HIF)-1alpha-like peptide cause only minor changes in its hydroxylation by the HIF prolyl 4-hydroxylases: substitution of 3,4-dehydroproline or azetidine-2-carboxylic acid for the proline leads to a high rate of uncoupled 2-oxoglutarate decarboxylation. *J Biol Chem,* 279**,** 55051-9.

LI, T. S. & MARBAN, E. 2010. Physiological levels of reactive oxygen species are required to maintain genomic stability in stem cells. *Stem Cells,* 28**,** 1178-85.

LI, X., EGERVARI, G., WANG, Y., BERGER, S. L. & LU, Z. 2018. Regulation of chromatin and gene expression by metabolic enzymes and metabolites. *Nat Rev Mol Cell Biol*.

LIANG, Y., LIU, J. & FENG, Z. 2013. The regulation of cellular metabolism by tumor suppressor p53. *Cell Biosci,* 3**,** 9.

LIAO, J., KARNIK, R., GU, H., ZILLER, M. J., CLEMENT, K., TSANKOV, A. M., AKOPIAN, V., GIFFORD, C. A., DONAGHEY, J., GALONSKA, C., POP, R., REYON, D., TSAI, S. Q., MALLARD, W., JOUNG, J. K., RINN, J. L., GNIRKE, A. & MEISSNER, A. 2015. Targeted disruption of DNMT1, DNMT3A and DNMT3B in human embryonic stem cells. *Nat Genet,* 47**,** 469-78.

LIBERTI, M. V. & LOCASALE, J. W. 2016. The Warburg Effect: How Does it Benefit Cancer Cells? *Trends Biochem Sci,* 41**,** 211-218.

LISOWSKI, P., KANNAN, P., MLODY, B. & PRIGIONE, A. 2018. Mitochondria and the dynamic control of stem cell homeostasis. *EMBO Rep,* 19.

LIU, G., MAUNOURY, C., KAMOUN, P. & ARAL, B. 1996. Assignment of the human gene encoding the delta 1-pyrroline-5-carboxylate synthetase (P5CS) to 10q24.3 by in situ hybridization. *Genomics,* 37**,** 145-6.

LIU, J. W., HSU, Y. C., KAO, C. Y., SU, H. L. & CHIU, I. M. 2013. Leukemia inhibitory factor-induced Stat3 signaling suppresses fibroblast growth factor 1-induced Erk1/2 activation to inhibit the downstream differentiation in mouse embryonic stem cells. *Stem Cells Dev,* 22**,** 1190-7.

LIU, W., HANCOCK, C. N., FISCHER, J. W., HARMAN, M. & PHANG, J. M. 2015. Proline biosynthesis augments tumor cell growth and aerobic glycolysis: involvement of pyridine nucleotides. *Sci Rep,* 5**,** 17206.

LIU, W., LE, A., HANCOCK, C., LANE, A. N., DANG, C. V., FAN, T. W. & PHANG, J. M. 2012. Reprogramming of proline and glutamine metabolism contributes to the proliferative and metabolic responses regulated by oncogenic transcription factor c-MYC. *Proc Natl Acad Sci U S A,* 109**,** 8983-8.

LIU, W. & PHANG, J. M. 2012. Proline dehydrogenase (oxidase) in cancer. *Biofactors,* 38**,** 398-406.

LIU, Y., BORCHERT, G. L., DONALD, S. P., DIWAN, B. A., ANVER, M. & PHANG, J. M. 2009. Proline oxidase functions as a mitochondrial tumor suppressor in human cancers. *Cancer Res,* 69**,** 6414-22.

LIU, Y., BORCHERT, G. L., SURAZYNSKI, A., HU, C. A. & PHANG, J. M. 2006. Proline oxidase activates both intrinsic and extrinsic pathways for apoptosis: the role of ROS/superoxides, NFAT and MEK/ERK signaling. *Oncogene,* 25**,** 5640-7.

LUO, M., ARENTSON, B. W., SRIVASTAVA, D., BECKER, D. F. & TANNER, J. J. 2012. Crystal structures and kinetics of monofunctional proline dehydrogenase provide insight into substrate recognition and conformational changes associated with flavin reduction and product release. *Biochemistry,* 51**,** 10099-108.

LUSHCHAK, V. I. 2014. Free radicals, reactive oxygen species, oxidative stress and its classification. *Chem Biol Interact,* 224**,** 164-75.

LYUBLINSKAYA, O. G., IVANOVA, J. S., PUGOVKINA, N. A., KOZHUKHAROVA, I. V., KOVALEVA, Z. V., SHATROVA, A. N., AKSENOV, N. D., ZENIN, V. V., KAULIN, Y. A., GAMALEY, I. A. & NIKOLSKY, N. N. 2017. Redox environment in stem and differentiated cells: A quantitative approach. *Redox Biol,* 12**,** 758-769.

MACARTHUR, B. D., SEVILLA, A., LENZ, M., MULLER, F. J., SCHULDT, B. M., SCHUPPERT, A. A., RIDDEN, S. J., STUMPF, P. S., FIDALGO, M., MA'AYAN, A., WANG, J. & LEMISCHKA, I. R. 2012. Nanog-dependent feedback loops regulate murine embryonic stem cell heterogeneity. *Nat Cell Biol,* 14**,** 1139-47.

MANDAL, S., LINDGREN, A. G., SRIVASTAVA, A. S., CLARK, A. T. & BANERJEE, U. 2011. Mitochondrial function controls proliferation and early differentiation potential of embryonic stem cells. *Stem Cells,* 29**,** 486-95.

MARCO-MARIN, C., GIL-ORTIZ, F., PEREZ-ARELLANO, I., CERVERA, J., FITA, I. & RUBIO, V. 2007. A novel two-domain architecture within the amino acid kinase enzyme family revealed by the crystal structure of Escherichia coli glutamate 5-kinase. *J Mol Biol,* 367**,** 1431-46.

MARSBOOM, G., ZHANG, G. F., POHL-AVILA, N., ZHANG, Y., YUAN, Y., KANG, H., HAO, B., BRUNENGRABER, H., MALIK, A. B. & REHMAN, J. 2016. Glutamine Metabolism Regulates the Pluripotency Transcription Factor OCT4. *Cell Rep,* 16**,** 323-32.

MASON, E. F. & RATHMELL, J. C. 2011. Cell metabolism: an essential link between cell growth and apoptosis. *Biochim Biophys Acta,* 1813**,** 645-54.

MASUI, S., NAKATAKE, Y., TOYOOKA, Y., SHIMOSATO, D., YAGI, R., TAKAHASHI, K., OKOCHI, H., OKUDA, A., MATOBA, R., SHAROV, A. A., KO, M. S. & NIWA, H. 2007. Pluripotency governed by Sox2 via regulation of Oct3/4 expression in mouse embryonic stem cells. *Nat Cell Biol,* 9**,** 625-35.

MATHIEU, J. & RUOHOLA-BAKER, H. 2017. Metabolic remodeling during the loss and acquisition of pluripotency. *Development,* 144**,** 541-551.

MATSCHINSKY, F. M. 1990. Glucokinase as glucose sensor and metabolic signal generator in pancreatic beta-cells and hepatocytes. *Diabetes,* 39**,** 647-52.

MATSCHINSKY, F. M. 2002. Regulation of pancreatic beta-cell glucokinase: from basics to therapeutics. *Diabetes,* 51 Suppl 3**,** S394-404.

MAXWELL, S. A. & DAVIS, G. E. 2000. Differential gene expression in p53-mediated apoptosis-resistant vs. apoptosis-sensitive tumor cell lines. *Proc Natl Acad Sci U S A,* 97**,** 13009-14.

MEISSEN, J. K., YUEN, B. T., KIND, T., RIGGS, J. W., BARUPAL, D. K., KNOEPFLER, P. S. & FIEHN, O. 2012. Induced pluripotent stem cells show metabolomic differences to embryonic stem cells in polyunsaturated phosphatidylcholines and primary metabolism. *PLoS One,* 7**,** e46770.

MEISSNER, A., MIKKELSEN, T. S., GU, H., WERNIG, M., HANNA, J., SIVACHENKO, A., ZHANG, X., BERNSTEIN, B. E., NUSBAUM, C., JAFFE, D. B., GNIRKE, A., JAENISCH, R. & LANDER, E. S. 2008. Genome-scale DNA methylation maps of pluripotent and differentiated cells. *Nature,* 454**,** 766-70.

METALLO, C. M. & VANDER HEIDEN, M. G. 2013. Understanding metabolic regulation and its influence on cell physiology. *Mol Cell,* 49**,** 388-98.

MEYN, M. A., 3RD, SCHREINER, S. J., DUMITRESCU, T. P., NAU, G. J. & SMITHGALL, T. E. 2005. SRC family kinase activity is required for murine embryonic stem cell growth and differentiation. *Mol Pharmacol,* 68**,** 1320-30.

MEYN, M. A., 3RD & SMITHGALL, T. E. 2009. Chemical genetics identifies c-Src as an activator of primitive ectoderm formation in murine embryonic stem cells. *Sci Signal,* 2**,** ra64.

MICHALEK, R. D., GERRIETS, V. A., JACOBS, S. R., MACINTYRE, A. N., MACIVER, N. J., MASON, E. F., SULLIVAN, S. A., NICHOLS, A. G. & RATHMELL, J. C. 2011. Cutting edge: distinct glycolytic and lipid oxidative metabolic programs are essential for effector and regulatory CD4+ T cell subsets. *J Immunol,* 186**,** 3299-303.

MILLER, G., HONIG, A., STEIN, H., SUZUKI, N., MITTLER, R. & ZILBERSTEIN, A. 2009. Unraveling delta1-pyrroline-5-carboxylate-proline cycle in plants by uncoupled expression of proline oxidation enzymes. *J Biol Chem,* 284**,** 26482-92.

MITSUI, K., TOKUZAWA, Y., ITOH, H., SEGAWA, K., MURAKAMI, M., TAKAHASHI, K., MARUYAMA, M., MAEDA, M. & YAMANAKA, S. 2003. The homeoprotein Nanog is required for maintenance of pluripotency in mouse epiblast and ES cells. *Cell,* 113**,** 631-42.

MORGANI, S. M. & BRICKMAN, J. M. 2015. LIF supports primitive endoderm expansion during pre-implantation development. *Development,* 142**,** 3488-99.

MOUSSAIEFF, A., ROULEAU, M., KITSBERG, D., COHEN, M., LEVY, G., BARASCH, D., NEMIROVSKI, A., SHEN-ORR, S., LAEVSKY, I., AMIT, M., BOMZE, D., ELENA-HERRMANN, B., SCHERF, T., NISSIM-RAFINIA, M., KEMPA, S., ITSKOVITZ-ELDOR, J., MESHORER, E., ABERDAM, D. & NAHMIAS, Y. 2015. Glycolysis-mediated changes in acetyl-CoA and histone acetylation control the early differentiation of embryonic stem cells. *Cell Metab,* 21**,** 392-402.

MURPHY, M. P. 2009. How mitochondria produce reactive oxygen species. *Biochem J,* 417**,** 1-13.

MURPHY, M. P., HOLMGREN, A., LARSSON, N. G., HALLIWELL, B., CHANG, C. J., KALYANARAMAN, B., RHEE, S. G., THORNALLEY, P. J., PARTRIDGE, L., GEMS, D., NYSTROM, T., BELOUSOV, V., SCHUMACKER, P. T. & WINTERBOURN, C. C. 2011. Unraveling the biological roles of reactive oxygen species. *Cell Metab,* 13**,** 361-366.

MURRAY, T. V., SMYRNIAS, I., SHAH, A. M. & BREWER, A. C. 2013. NADPH oxidase 4 regulates cardiomyocyte differentiation via redox activation of c-Jun protein and the cis-regulation of GATA-4 gene transcription. *J Biol Chem,* 288**,** 15745-59.

MYLLYHARJU, J. 2008. Prolyl 4-hydroxylases, key enzymes in the synthesis of collagens and regulation of the response to hypoxia, and their roles as treatment targets. *Ann Med,* 40**,** 402-17.

MYLLYHARJU, J. 2013. Prolyl 4-hydroxylases, master regulators of the hypoxia response. *Acta Physiol (Oxf),* 208**,** 148-65.

NAIR, G., ABRANCHES, E., GUEDES, A. M., HENRIQUE, D. & RAJ, A. 2015. Heterogeneous lineage marker expression in naive embryonic stem cells is mostly due to spontaneous differentiation. *Sci Rep,* 5**,** 13339.

NAKAJIMA, H., KUBO, T., IHARA, H., HIKIDA, T., DANJO, T., NAKATSUJI, M., SHAHANI, N., ITAKURA, M., ONO, Y., AZUMA, Y. T., INUI, T., KAMIYA, A., SAWA, A. & TAKEUCHI, T. 2015. Nuclear-translocated Glyceraldehyde-3-phosphate Dehydrogenase Promotes Poly(ADP-ribose) Polymerase-1 Activation during Oxidative/Nitrosative Stress in Stroke. *J Biol Chem,* 290**,** 14493-503.

NATARAJAN, S. K., ZHU, W., LIANG, X., ZHANG, L., DEMERS, A. J., ZIMMERMAN, M. C., SIMPSON, M. A. & BECKER, D. F. 2012. Proline dehydrogenase is essential for proline protection against hydrogen peroxide-induced cell death. *Free Radic Biol Med,* 53**,** 1181-91.

NEUPANE, J., GHIMIRE, S., VANDEWOESTYNE, M., LU, Y., GERRIS, J., VAN COSTER, R., DEROO, T., DEFORCE, D., VANSTEELANDT, S., DE SUTTER, P. & HEINDRYCKX, B. 2015. Cellular Heterogeneity in the Level of mtDNA Heteroplasmy in Mouse Embryonic Stem Cells. *Cell Rep,* 13**,** 1304-1309.

NICHOLS, J. & SMITH, A. 2009. Naive and primed pluripotent states. *Cell Stem Cell,* 4**,** 487-92.

NICHOLS, J. & SMITH, A. 2012. Pluripotency in the embryo and in culture. *Cold Spring Harb Perspect Biol,* 4**,** a008128.

NICKLIN, P., BERGMAN, P., ZHANG, B., TRIANTAFELLOW, E., WANG, H., NYFELER, B., YANG, H., HILD, M., KUNG, C., WILSON, C., MYER, V. E., MACKEIGAN, J. P., PORTER, J. A., WANG, Y. K., CANTLEY,

L. C., FINAN, P. M. & MURPHY, L. O. 2009. Bidirectional transport of amino acids regulates mTOR and autophagy. *Cell,* 136**,** 521-34.

NISHIMURA, A., NASUNO, R. & TAKAGI, H. 2012. The proline metabolism intermediate Delta1-pyrroline-5-carboxylate directly inhibits the mitochondrial respiration in budding yeast. *FEBS Lett,* 586**,** 2411-6.

NOMURA, M. & TAKAGI, H. 2004. Role of the yeast acetyltransferase Mpr1 in oxidative stress: regulation of oxygen reactive species caused by a toxic proline catabolism intermediate. *Proc Natl Acad Sci U S A,* 101**,** 12616-21.

NORDBERG, J. & ARNER, E. S. 2001. Reactive oxygen species, antioxidants, and the mammalian thioredoxin system. *Free Radic Biol Med,* 31**,** 1287-312.

ONISHI, K., TONGE, P. D., NAGY, A. & ZANDSTRA, P. W. 2014. Local BMP-SMAD1 signaling increases LIF receptor-dependent STAT3 responsiveness and primed-to-naive mouse pluripotent stem cell conversion frequency. *Stem Cell Reports,* 3**,** 156-68.

ONISHI, K. & ZANDSTRA, P. W. 2015. LIF signaling in stem cells and development. *Development,* 142**,** 2230-6.

ONO, H. & TUBOI, S. 1986. Translocation of proteins into rat liver mitochondria. The precursor polypeptides of a large subunit of succinate dehydrogenase and ornithine aminotransferase and their imports into their own locations of mitochondria. *Eur J Biochem,* 155**,** 543-9.

OSORNO, R. & CHAMBERS, I. 2011. Transcription factor heterogeneity and epiblast pluripotency. *Philos Trans R Soc Lond B Biol Sci,* 366**,** 2230-7.

OSTRANDER, E. L., LARSON, J. D., SCHUERMANN, J. P. & TANNER, J. J. 2009. A conserved active site tyrosine residue of proline dehydrogenase helps enforce the preference for proline over hydroxyproline as the substrate. *Biochemistry,* 48**,** 951-9.

PALACIN, M., ESTEVEZ, R., BERTRAN, J. & ZORZANO, A. 1998. Molecular biology of mammalian plasma membrane amino acid transporters. *Physiol Rev,* 78**,** 969-1054.

PANDHARE, J., COOPER, S. K. & PHANG, J. M. 2006. Proline oxidase, a proapoptotic gene, is induced by troglitazone: evidence for both peroxisome proliferator-activated receptor gamma-dependent and -independent mechanisms. *J Biol Chem,* 281**,** 2044-52.

PANDHARE, J., DONALD, S. P., COOPER, S. K. & PHANG, J. M. 2009. Regulation and function of proline oxidase under nutrient stress. *J Cell Biochem,* 107**,** 759-68.

PANOPOULOS, A. D., YANES, O., RUIZ, S., KIDA, Y. S., DIEP, D., TAUTENHAHN, R., HERRERIAS, A., BATCHELDER, E. M., PLONGTHONGKUM, N., LUTZ, M., BERGGREN, W. T., ZHANG, K., EVANS, R. M., SIUZDAK, G. & IZPISUA BELMONTE, J. C. 2012. The metabolome of induced pluripotent stem cells reveals metabolic changes occurring in somatic cell reprogramming. *Cell Res,* 22**,** 168-77.

PARMAR, N. & TAMANOI, F. 2010. Rheb G-Proteins and the Activation of mTORC1. *Enzymes,* 27**,** 39-56.

PAVLOVA, N. N. & THOMPSON, C. B. 2016. The Emerging Hallmarks of Cancer Metabolism. *Cell Metab,* 23**,** 27-47.

PEARCE, E. L., WALSH, M. C., CEJAS, P. J., HARMS, G. M., SHEN, H., WANG, L. S., JONES, R. G. & CHOI, Y. 2009. Enhancing CD8 T-cell memory by modulating fatty acid metabolism. *Nature,* 460**,** 103-7.

PELTON, T. A., SHARMA, S., SCHULZ, T. C., RATHJEN, J. & RATHJEN, P. D. 2002. Transient pluripotent cell populations during primitive ectoderm formation: correlation of in vivo and in vitro pluripotent cell development. *J Cell Sci,* 115**,** 329-39.

PENDERGRASS, W., WOLF, N. & POOT, M. 2004. Efficacy of MitoTracker Green and CMXrosamine to measure changes in mitochondrial membrane potentials in living cells and tissues. *Cytometry A,* 61**,** 162-9.

PEREZ-ARELLANO, I., RUBIO, V. & CERVERA, J. 2006. Mapping active site residues in glutamate-5-kinase. The substrate glutamate and the feed-back inhibitor proline bind at overlapping sites. *FEBS Lett,* 580**,** 6247-53.

PHANG, J. M. 1985. The regulatory functions of proline and pyrroline-5-carboxylic acid. *Curr Top Cell Regul,* 25**,** 91-132.

PHANG, J. M., DONALD, S. P., PANDHARE, J. & LIU, Y. 2008a. The metabolism of proline, a stress substrate, modulates carcinogenic pathways. *Amino Acids,* 35**,** 681-90.

PHANG, J. M., LIU, W., HANCOCK, C. & CHRISTIAN, K. J. 2012. The proline regulatory axis and cancer. *Front Oncol,* 2**,** 60.

PHANG, J. M., LIU, W., HANCOCK, C. N. & FISCHER, J. W. 2015. Proline metabolism and cancer: emerging links to glutamine and collagen. *Curr Opin Clin Nutr Metab Care,* 18**,** 71-7.

PHANG, J. M., PANDHARE, J. & LIU, Y. 2008b. The metabolism of proline as microenvironmental stress substrate. *J Nutr,* 138**,** 2008s-2015s.

PINILLA, J., ALEDO, J. C., CWIKLINSKI, E., HYDE, R., TAYLOR, P. M. & HUNDAL, H. S. 2011. SNAT2 transceptor signalling via mTOR: a role in cell growth and proliferation? *Front Biosci (Elite Ed),* 3**,** 1289-99.

PLUSA, B. & HADJANTONAKIS, A. K. 2014. Embryonic stem cell identity grounded in the embryo. *Nat Cell Biol,* 16**,** 502-4.

POLLIZZI, K. N., SUN, I. H., PATEL, C. H., LO, Y. C., OH, M. H., WAICKMAN, A. T., TAM, A. J., BLOSSER, R. L., WEN, J., DELGOFFE, G. M. & POWELL, J. D. 2016. Asymmetric inheritance of mTORC1 kinase activity during division dictates CD8(+) T cell differentiation. *Nat Immunol,* 17**,** 704-11.

PRIGIONE, A. & ADJAYE, J. 2010. Modulation of mitochondrial biogenesis and bioenergetic metabolism upon in vitro and in vivo differentiation of human ES and iPS cells. *Int J Dev Biol,* 54**,** 1729-41.

PRIGIONE, A., FAULER, B., LURZ, R., LEHRACH, H. & ADJAYE, J. 2010. The senescence-related mitochondrial/oxidative stress pathway is repressed in human induced pluripotent stem cells. *Stem Cells,* 28**,** 721-33.

PRIGIONE, A., ROHWER, N., HOFFMANN, S., MLODY, B., DREWS, K., BUKOWIECKI, R., BLUMLEIN, K., WANKER, E. E., RALSER, M., CRAMER, T. & ADJAYE, J. 2014. HIF1alpha modulates cell fate reprogramming through early glycolytic shift and upregulation of PDK1-3 and PKM2. *Stem Cells,* 32**,** 364-76.

PROWSE, A. B., CHONG, F., ELLIOTT, D. A., ELEFANTY, A. G., STANLEY, E. G., GRAY, P. P., MUNRO, T. P. & OSBORNE, G. W. 2012. Analysis of mitochondrial function and localisation during human embryonic stem cell differentiation in vitro. *PLoS One,* 7**,** e52214.

PUZIO-KUTER, A. M. 2011. The Role of p53 in Metabolic Regulation. *Genes Cancer,* 2**,** 385-91.

QAMAR, A., MYSORE, K. S. & SENTHIL-KUMAR, M. 2015. Role of proline and pyrroline-5-carboxylate metabolism in plant defense against invading pathogens. *Front Plant Sci,* 6**,** 503.

RAMESH, V., CHENG, S. V., KOZAK, C. A., HERRON, B. J., SHIH, V. E., TAYLOR, B. A. & GUSELLA, J. F. 1992. Mapping of ornithine aminotransferase gene sequences to mouse chromosomes 7, X, and 3. *Mamm Genome,* 3**,** 17-22.

RATHJEN, J., LAKE, J. A., BETTESS, M. D., WASHINGTON, J. M., CHAPMAN, G. & RATHJEN, P. D. 1999. Formation of a primitive ectoderm like cell population, EPL cells, from ES cells in response to biologically derived factors. *J Cell Sci,* 112 (Pt 5)**,** 601-12.

RATHJEN, J. & RATHJEN, P. D. 2003. Lineage specific differentiation of mouse ES cells: formation and differentiation of early primitive ectoderm-like (EPL) cells. *Methods Enzymol,* 365**,** 3-25.

RATHJEN, J., WASHINGTON, J. M., BETTESS, M. D. & RATHJEN, P. D. 2003. Identification of a biological activity that supports maintenance and proliferation of pluripotent cells from the primitive ectoderm of the mouse. *Biol Reprod,* 69**,** 1863-71.

RATHJEN, J., YEO, C., YAP, C., TAN, B. S., RATHJEN, P. D. & GARDNER, D. K. 2014. Culture environment regulates amino acid turnover and glucose utilisation in human ES cells. *Reprod Fertil Dev,* 26**,** 703-16.

REBSAMEN, M., POCHINI, L., STASYK, T., DE ARAUJO, M. E., GALLUCCIO, M., KANDASAMY, R. K., SNIJDER, B., FAUSTER, A., RUDASHEVSKAYA, E. L., BRUCKNER, M., SCORZONI, S., FILIPEK, P. A., HUBER, K. V., BIGENZAHN, J. W., HEINZ, L. X., KRAFT, C., BENNETT, K. L., INDIVERI, C., HUBER,

L. A. & SUPERTI-FURGA, G. 2015. SLC38A9 is a component of the lysosomal amino acid sensing machinery that controls mTORC1. *Nature,* 519**,** 477-81.

REIMER, R. J., CHAUDHRY, F. A., GRAY, A. T. & EDWARDS, R. H. 2000. Amino acid transport system A resembles system N in sequence but differs in mechanism. *Proc Natl Acad Sci U S A,* 97**,** 7715-20.

RENAULT, V. M., RAFALSKI, V. A., MORGAN, A. A., SALIH, D. A., BRETT, J. O., WEBB, A. E., VILLEDA, S. A., THEKKAT, P. U., GUILLEREY, C., DENKO, N. C., PALMER, T. D., BUTTE, A. J. & BRUNET, A. 2009. FoxO3 regulates neural stem cell homeostasis. *Cell Stem Cell,* 5**,** 527-39.

RIVERA, A. & MAXWELL, S. A. 2005. The p53-induced gene-6 (proline oxidase) mediates apoptosis through a calcineurin-dependent pathway. *J Biol Chem,* 280**,** 29346-54.

RONN, R. E., GUIBENTIF, C., SAXENA, S. & WOODS, N. B. 2017. Reactive Oxygen Species Impair the Function of CD90(+) Hematopoietic Progenitors Generated from Human Pluripotent Stem Cells. *Stem Cells,* 35**,** 197-206.

RYALL, J. G. 2012. The role of sirtuins in the regulation of metabolic homeostasis in skeletal muscle. *Curr Opin Clin Nutr Metab Care,* 15**,** 561-6.

RYALL, J. G., DELL'ORSO, S., DERFOUL, A., JUAN, A., ZARE, H., FENG, X., CLERMONT, D., KOULNIS, M., GUTIERREZ-CRUZ, G., FULCO, M. & SARTORELLI, V. 2015. The NAD(+)-dependent SIRT1 deacetylase translates a metabolic switch into regulatory epigenetics in skeletal muscle stem cells. *Cell Stem Cell,* 16**,** 171-83.

RYU, J. M., LEE, H. J., JUNG, Y. H., LEE, K. H., KIM, D. I., KIM, J. Y., KO, S. H., CHOI, G. E., CHAI, II, SONG, E. J., OH, J. Y., LEE, S. J. & HAN, H. J. 2015. Regulation of Stem Cell Fate by ROS-mediated Alteration of Metabolism. *Int J Stem Cells,* 8**,** 24-35.

SAHU, N., DELA CRUZ, D., GAO, M., SANDOVAL, W., HAVERTY, P. M., LIU, J., STEPHAN, J. P., HALEY, B., CLASSON, M., HATZIVASSILIOU, G. & SETTLEMAN, J. 2016. Proline Starvation Induces Unresolved ER Stress and Hinders mTORC1-Dependent Tumorigenesis. *Cell Metab,* 24**,** 753-761.

SAMUDIO, I., HARMANCEY, R., FIEGL, M., KANTARJIAN, H., KONOPLEVA, M., KORCHIN, B., KALUARACHCHI, K., BORNMANN, W., DUVVURI, S., TAEGTMEYER, H. & ANDREEFF, M. 2010. Pharmacologic inhibition of fatty acid oxidation sensitizes human leukemia cells to apoptosis induction. *J Clin Invest,* 120**,** 142-56.

SARETZKI, G., WALTER, T., ATKINSON, S., PASSOS, J. F., BARETH, B., KEITH, W. N., STEWART, R., HOARE, S., STOJKOVIC, M., ARMSTRONG, L., VON ZGLINICKI, T. & LAKO, M. 2008. Downregulation of multiple stress defense mechanisms during differentiation of human embryonic stem cells. *Stem Cells,* 26**,** 455-64.

SART, S., SONG, L. & LI, Y. 2015. Controlling Redox Status for Stem Cell Survival, Expansion, and Differentiation. *Oxid Med Cell Longev,* 2015**,** 105135.

SATO, N., MEIJER, L., SKALTSOUNIS, L., GREENGARD, P. & BRIVANLOU, A. H. 2004. Maintenance of pluripotency in human and mouse embryonic stem cells through activation of Wnt signaling by a pharmacological GSK-3-specific inhibitor. *Nat Med,* 10**,** 55-63.

SAUER, H., RAHIMI, G., HESCHELER, J. & WARTENBERG, M. 2000. Role of reactive oxygen species and phosphatidylinositol 3-kinase in cardiomyocyte differentiation of embryonic stem cells. *FEBS Lett,* 476**,** 218-23.

SAVATIER, P., OSTEIL, P. & TAM, P. P. 2017. Pluripotency of embryo-derived stem cells from rodents, lagomorphs, and primates: Slippery slope, terrace and cliff. *Stem Cell Res,* 19**,** 104-112.

SCHIEKE, S. M., MA, M., CAO, L., MCCOY, J. P., JR., LIU, C., HENSEL, N. F., BARRETT, A. J., BOEHM, M. & FINKEL, T. 2008. Mitochondrial metabolism modulates differentiation and teratoma formation capacity in mouse embryonic stem cells. *J Biol Chem,* 283**,** 28506-12.

SCHMELTER, M., ATEGHANG, B., HELMIG, S., WARTENBERG, M. & SAUER, H. 2006. Embryonic stem cells utilize reactive oxygen species as transducers of mechanical strain-induced cardiovascular differentiation. *Faseb j,* 20**,** 1182-4.

SCHULTZ, G. A., KAYE, P. L., MCKAY, D. J. & JOHNSON, M. H. 1981. Endogenous amino acid pool sizes in mouse eggs and preimplantation embryos. *J Reprod Fertil,* 61**,** 387-93.

SCOGNAMIGLIO, R., CABEZAS-WALLSCHEID, N., THIER, M. C., ALTAMURA, S., REYES, A., PRENDERGAST, A. M., BAUMGARTNER, D., CARNEVALLI, L. S., ATZBERGER, A., HAAS, S., VON PALESKE, L., BOROVIAK, T., WORSDORFER, P., ESSERS, M. A., KLOZ, U., EISENMAN, R. N., EDENHOFER, F., BERTONE, P., HUBER, W., VAN DER HOEVEN, F., SMITH, A. & TRUMPP, A. 2016. Myc Depletion Induces a Pluripotent Dormant State Mimicking Diapause. *Cell,* 164**,** 668-80.

SHAN, J., HAMAZAKI, T., TANG, T. A., TERADA, N. & KILBERG, M. S. 2013. Activation of the amino acid response modulates lineage specification during differentiation of murine embryonic stem cells. *Am J Physiol Endocrinol Metab,* 305**,** E325-35.

SHERLEY, J. L., STADLER, P. B. & STADLER, J. S. 1995. A quantitative method for the analysis of mammalian cell proliferation in culture in terms of dividing and non-dividing cells. *Cell Prolif,* 28**,** 137-44.

SHI, Y., LAN, F., MATSON, C., MULLIGAN, P., WHETSTINE, J. R., COLE, P. A., CASERO, R. A. & SHI, Y. 2004. Histone demethylation mediated by the nuclear amine oxidase homolog LSD1. *Cell,* 119**,** 941-53.

SHIRAKI, N., SHIRAKI, Y., TSUYAMA, T., OBATA, F., MIURA, M., NAGAE, G., ABURATANI, H., KUME, K., ENDO, F. & KUME, S. 2014. Methionine metabolism regulates maintenance and differentiation of human pluripotent stem cells. *Cell Metab,* 19**,** 780-94.

SHYH-CHANG, N., LOCASALE, J. W., LYSSIOTIS, C. A., ZHENG, Y., TEO, R. Y., RATANASIRINTRAWOOT, S., ZHANG, J., ONDER, T., UNTERNAEHRER, J. J., ZHU, H., ASARA, J. M., DALEY, G. Q. & CANTLEY, L. C. 2013. Influence of threonine metabolism on S-adenosylmethionine and histone methylation. *Science,* 339**,** 222-6.

SICA, A., STRAUSS, L., CONSONNI, F. M., TRAVELLI, C., GENAZZANI, A. & PORTA, C. 2017. Metabolic regulation of suppressive myeloid cells in cancer. *Cytokine Growth Factor Rev,* 35**,** 27-35.

SIMON, P. 2003. Q-Gene: processing quantitative real-time RT-PCR data. *Bioinformatics,* 19**,** 1439-40.

SINGER, Z. S., YONG, J., TISCHLER, J., HACKETT, J. A., ALTINOK, A., SURANI, M. A., CAI, L. & ELOWITZ, M. B. 2014. Dynamic heterogeneity and DNA methylation in embryonic stem cells. *Mol Cell,* 55**,** 319-31.

SMITH, L. C., RAVEL, J. M., SKINNER, C. G. & SHIVE, W. 1962. 3,4-Dehydroproline, a proline antagonist. *Arch Biochem Biophys,* 99**,** 60-4.

SMITH, R. J., DOWNING, S. J., PHANG, J. M., LODATO, R. F. & AOKI, T. T. 1980. Pyrroline-5-carboxylate synthase activity in mammalian cells. *Proc Natl Acad Sci U S A,* 77**,** 5221-5.

SMITH, Z. D., CHAN, M. M., MIKKELSEN, T. S., GU, H., GNIRKE, A., REGEV, A. & MEISSNER, A. 2012. A unique regulatory phase of DNA methylation in the early mammalian embryo. *Nature,* 484**,** 339-44.

SNAEBJORNSSON, M. T. & SCHULZE, A. 2018. Non-canonical functions of enzymes facilitate cross-talk between cell metabolic and regulatory pathways. *Exp Mol Med,* 50**,** 34.

SONG, S. H., KIM, K., PARK, J. J., MIN, K. H. & SUH, W. 2014. Reactive oxygen species regulate the quiescence of CD34-positive cells derived from human embryonic stem cells. *Cardiovasc Res,* 103**,** 147-55.

SOPHOS, N. A. & VASILIOU, V. 2003. Aldehyde dehydrogenase gene superfamily: the 2002 update. *Chem Biol Interact,* 143-144**,** 5-22.

SPERBER, H., MATHIEU, J., WANG, Y., FERRECCIO, A., HESSON, J., XU, Z., FISCHER, K. A., DEVI, A., DETRAUX, D., GU, H., BATTLE, S. L., SHOWALTER, M., VALENSISI, C., BIELAS, J. H., ERICSON, N. G., MARGARETHA, L., ROBITAILLE, A. M., MARGINEANTU, D., FIEHN, O., HOCKENBERY, D., BLAU, C. A., RAFTERY, D., MARGOLIN, A. A., HAWKINS, R. D., MOON, R. T., WARE, C. B. & RUOHOLA-BAKER, H. 2015. The metabolome regulates the epigenetic landscape during naive-to-primed human embryonic stem cell transition. *Nat Cell Biol,* 17**,** 1523-35.

SRIVASTAVA, M. K., SINHA, P., CLEMENTS, V. K., RODRIGUEZ, P. & OSTRAND-ROSENBERG, S. 2010. Myeloid-derived suppressor cells inhibit T-cell activation by depleting cystine and cysteine. *Cancer Res,* 70**,** 68-77.

STORZ, P. 2011. Forkhead homeobox type O transcription factors in the responses to oxidative stress. *Antioxid Redox Signal,* 14**,** 593-605.

SUGAWARA, M., NAKANISHI, T., FEI, Y. J., HUANG, W., GANAPATHY, M. E., LEIBACH, F. H. & GANAPATHY, V. 2000. Cloning of an amino acid transporter with functional characteristics and tissue expression pattern identical to that of system A. *J Biol Chem,* 275**,** 16473-7.

SUHR, S. T., CHANG, E. A., TJONG, J., ALCASID, N., PERKINS, G. A., GOISSIS, M. D., ELLISMAN, M. H., PEREZ, G. I. & CIBELLI, J. B. 2010. Mitochondrial rejuvenation after induced pluripotency. *PLoS One,* 5**,** e14095.

SUKUMAR, M., KISHTON, R. J. & RESTIFO, N. P. 2017. Metabolic reprograming of anti-tumor immunity. *Curr Opin Immunol,* 46**,** 14-22.

TAKAHASHI, K. & YAMANAKA, S. 2006. Induction of pluripotent stem cells from mouse embryonic and adult fibroblast cultures by defined factors. *Cell,* 126**,** 663-76.

TAKAHASHI, S., KOBAYASHI, S. & HIRATANI, I. 2018. Epigenetic differences between naive and primed pluripotent stem cells. *Cell Mol Life Sci,* 75**,** 1191-1203.

TAKASHIMA, Y., GUO, G., LOOS, R., NICHOLS, J., FICZ, G., KRUEGER, F., OXLEY, D., SANTOS, F., CLARKE, J., MANSFIELD, W., REIK, W., BERTONE, P. & SMITH, A. 2014. Resetting transcription factor control circuitry toward ground-state pluripotency in human. *Cell,* 158**,** 1254-1269.

TALEAHMAD, S., MIRZAEI, M., PARKER, L. M., HASSANI, S. N., MOLLAMOHAMMADI, S., SHARIFI-ZARCHI, A., HAYNES, P. A., BAHARVAND, H. & SALEKDEH, G. H. 2015. Proteome Analysis of Ground State Pluripotency. *Sci Rep,* 5**,** 17985.

TAN, B. S., KWEK, J., WONG, C. K., SANER, N. J., YAP, C., FELQUER, F., MORRIS, M. B., GARDNER, D. K., RATHJEN, P. D. & RATHJEN, J. 2016a. Src Family Kinases and p38 Mitogen-Activated Protein Kinases Regulate Pluripotent Cell Differentiation in Culture. *PLoS One,* 11**,** e0163244.

TAN, B. S., RATHJEN, P. D., HARVEY, A. J., GARDNER, D. K. & RATHJEN, J. 2016b. Regulation of amino acid transporters in pluripotent cell populations in the embryo and in culture; novel roles for sodium-coupled neutral amino acid transporters. *Mech Dev,* 141**,** 32-9.

TAN, B. S. N., LONIC, A., MORRIS, M. B., RATHJEN, P. D. & RATHJEN, J. 2011. *The amino acid transporter SNAT2 mediates l-proline-induced differentiation of ES cells*.

TANAKA, T. S. 2009. Transcriptional heterogeneity in mouse embryonic stem cells. *Reprod Fertil Dev,* 21**,** 67-75.

TANG, F., BARBACIORU, C., BAO, S., LEE, C., NORDMAN, E., WANG, X., LAO, K. & SURANI, M. A. 2010. Tracing the derivation of embryonic stem cells from the inner cell mass by single-cell RNA-Seq analysis. *Cell Stem Cell,* 6**,** 468-78.

TANG, Y., LUO, Y., JIANG, Z., MA, Y., LIN, C. J., KIM, C., CARTER, M. G., AMANO, T., PARK, J., KISH, S. & TIAN, X. C. 2012. Jak/Stat3 signaling promotes somatic cell reprogramming by epigenetic regulation. *Stem Cells,* 30**,** 2645-56.

TANNER, J. J. 2008. Structural biology of proline catabolism. *Amino Acids,* 35**,** 719-30.

TANZER, F., FIRAT, M., ALAGOZ, M. & ERDOGAN, H. 2011. Gyrate atrophy of the choroid and retina with hyperornithinemia, cystinuria and lysinuria responsive to vitamin B6. *BMJ Case Rep,* 2011.

TATAPUDY, S., ALOISIO, F., BARBER, D. & NYSTUL, T. 2017. Cell fate decisions: emerging roles for metabolic signals and cell morphology. *EMBO Rep,* 18**,** 2105-2118.

TAYLOR, P. M. 2014. Role of amino acid transporters in amino acid sensing. *Am J Clin Nutr,* 99**,** 223s-230s.

THORENS, B. 2015. GLUT2, glucose sensing and glucose homeostasis. *Diabetologia,* 58**,** 221-32.

TOTHOVA, Z. & GILLILAND, D. G. 2007. FoxO transcription factors and stem cell homeostasis: insights from the hematopoietic system. *Cell Stem Cell,* 1**,** 140-52.

TSUKADA, Y., FANG, J., ERDJUMENT-BROMAGE, H., WARREN, M. E., BORCHERS, C. H., TEMPST, P. & ZHANG, Y. 2006. Histone demethylation by a family of JmjC domain-containing proteins. *Nature,* 439**,** 811-6.

TURCO, M. Y., FURIA, L., DIETZE, A., FERNANDEZ DIAZ, L., RONZONI, S., SCIULLO, A., SIMEONE, A., CONSTAM, D., FARETTA, M. & LANFRANCONE, L. 2012. Cellular heterogeneity during embryonic stem cell differentiation to epiblast stem cells is revealed by the ShcD/RaLP adaptor protein. *Stem Cells,* 30**,** 2423-36.

VALDECANTOS, M. P., PEREZ-MATUTE, P., QUINTERO, P. & MARTINEZ, J. A. 2010. Vitamin C, resveratrol and lipoic acid actions on isolated rat liver mitochondria: all antioxidants but different. *Redox Rep,* 15**,** 207-16.

VAN DER KNAAP, J. A. & VERRIJZER, C. P. 2016. Undercover: gene control by metabolites and metabolic enzymes. *Genes Dev,* 30**,** 2345-2369.

VAN DER VOS, K. E. & COFFER, P. J. 2012. Glutamine metabolism links growth factor signaling to the regulation of autophagy. *Autophagy,* 8**,** 1862-4.

VAN OOSTEN, A. L., COSTA, Y., SMITH, A. & SILVA, J. C. 2012. JAK/STAT3 signalling is sufficient and dominant over antagonistic cues for the establishment of naive pluripotency. *Nat Commun,* 3**,** 817.

VAN WINKLE, L. J. 2001. Amino acid transport regulation and early embryo development. *Biol Reprod,* 64**,** 1-12.

VAN WINKLE, L. J. & DICKINSON, H. R. 1995. Differences in amino acid content of preimplantation mouse embryos that develop in vitro versus in vivo: in vitro effects of five amino acids that are abundant in oviductal secretions. *Biol Reprod,* 52**,** 96-104.

VARUM, S., MOMCILOVIC, O., CASTRO, C., BEN-YEHUDAH, A., RAMALHO-SANTOS, J. & NAVARA, C. S. 2009. Enhancement of human embryonic stem cell pluripotency through inhibition of the mitochondrial respiratory chain. *Stem Cell Res,* 3**,** 142-56.

VARUM, S., RODRIGUES, A. S., MOURA, M. B., MOMCILOVIC, O., EASLEY, C. A. T., RAMALHO-SANTOS, J., VAN HOUTEN, B. & SCHATTEN, G. 2011. Energy metabolism in human pluripotent stem cells and their differentiated counterparts. *PLoS One,* 6**,** e20914.

VASSENA, R., BOUE, S., GONZALEZ-ROCA, E., ARAN, B., AUER, H., VEIGA, A. & IZPISUA BELMONTE, J. C. 2011. Waves of early transcriptional activation and pluripotency program initiation during human preimplantation development. *Development,* 138**,** 3699-709.

VELAZQUEZ-VILLEGAS, L. A., ORTIZ, V., STROM, A., TORRES, N., ENGLER, D. A., MATSUNAMI, R., ORDAZ-ROSADO, D., GARCIA-BECERRA, R., LOPEZ-BARRADAS, A. M., LARREA, F., GUSTAFSSON, J. A. & TOVAR, A. R. 2014. Transcriptional regulation of the sodium-coupled neutral amino acid transporter (SNAT2) by 17beta-estradiol. *Proc Natl Acad Sci U S A,* 111**,** 11443-8.

WANG, H., ZHANG, K., LIU, Y., FU, Y., GAO, S., GONG, P., WANG, H., ZHOU, Z., ZENG, M., WU, Z., SUN, Y., CHEN, T., LI, S. & LIU, L. 2017. Telomere heterogeneity linked to metabolism and pluripotency state revealed by simultaneous analysis of telomere length and RNA-seq in the same human embryonic stem cell. *BMC Biol,* 15**,** 114.

WANG, J., ALEXANDER, P., WU, L., HAMMER, R., CLEAVER, O. & MCKNIGHT, S. L. 2009. Dependence of mouse embryonic stem cells on threonine catabolism. *Science,* 325**,** 435-9.

WANG, K., ZHANG, T., DONG, Q., NICE, E. C., HUANG, C. & WEI, Y. 2013. Redox homeostasis: the linchpin in stem cell self-renewal and differentiation. *Cell Death Dis,* 4**,** e537.

WANG, L., LI, J. J., GUO, L. Y., LI, P., ZHAO, Z., ZHOU, H. & DI, L. J. 2018. Molecular link between glucose and glutamine consumption in cancer cells mediated by CtBP and SIRT4. *Oncogenesis,* 7**,** 26.

WANG, R., DILLON, C. P., SHI, L. Z., MILASTA, S., CARTER, R., FINKELSTEIN, D., MCCORMICK, L. L., FITZGERALD, P., CHI, H., MUNGER, J. & GREEN, D. R. 2011. The transcription factor Myc controls metabolic reprogramming upon T lymphocyte activation. *Immunity,* 35**,** 871-82.

WARBURG, O. 1956. On the origin of cancer cells. *Science,* 123**,** 309-14.

WASHINGTON, J. M., RATHJEN, J., FELQUER, F., LONIC, A., BETTESS, M. D., HAMRA, N., SEMENDRIC, L., TAN, B. S., LAKE, J. A., KEOUGH, R. A., MORRIS, M. B. & RATHJEN, P. D. 2010. L-Proline induces differentiation of ES cells: a novel role for an amino acid in the regulation of pluripotent cells in culture. *Am J Physiol Cell Physiol,* 298**,** C982-92.

WHITE, T. A., JOHNSON, W. H., JR., WHITMAN, C. P. & TANNER, J. J. 2008. Structural basis for the inactivation of Thermus thermophilus proline dehydrogenase by N-propargylglycine. *Biochemistry,* 47**,** 5573-80.

WOLLHEIM, C. B. & MAECHLER, P. 2002. Beta-cell mitochondria and insulin secretion: messenger role of nucleotides and metabolites. *Diabetes,* 51 Suppl 1**,** S37-42.

WU, G., BAZER, F. W., BURGHARDT, R. C., JOHNSON, G. A., KIM, S. W., KNABE, D. A., LI, P., LI, X., MCKNIGHT, J. R., SATTERFIELD, M. C. & SPENCER, T. E. 2011. Proline and hydroxyproline metabolism: implications for animal and human nutrition. *Amino Acids,* 40**,** 1053-63.

WU, G., BAZER, F. W., DATTA, S., JOHNSON, G. A., LI, P., SATTERFIELD, M. C. & SPENCER, T. E. 2008. Proline metabolism in the conceptus: implications for fetal growth and development. *Amino Acids,* 35**,** 691-702.

WU, J. & IZPISUA BELMONTE, J. C. 2015. Metabolic exit from naive pluripotency. *Nat Cell Biol,* 17**,** 1519-21.

XIAO, B., DENG, X., ZHOU, W. & TAN, E. K. 2016. Flow Cytometry-Based Assessment of Mitophagy Using MitoTracker. *Front Cell Neurosci,* 10**,** 76.

XIAO, Q., LUO, Z., PEPE, A. E., MARGARITI, A., ZENG, L. & XU, Q. 2009. Embryonic stem cell differentiation into smooth muscle cells is mediated by Nox4-produced H2O2. *Am J Physiol Cell Physiol,* 296**,** C711-23.

XIAO, W., WANG, R. S., HANDY, D. E. & LOSCALZO, J. 2018. NAD(H) and NADP(H) Redox Couples and Cellular Energy Metabolism. *Antioxid Redox Signal,* 28**,** 251-272.

YANES, O., CLARK, J., WONG, D. M., PATTI, G. J., SANCHEZ-RUIZ, A., BENTON, H. P., TRAUGER, S. A., DESPONTS, C., DING, S. & SIUZDAK, G. 2010. Metabolic oxidation regulates embryonic stem cell differentiation. *Nat Chem Biol,* 6**,** P411-7.

YANG, H., LIN, H., XU, H., ZHANG, L., CHENG, L., WEN, B., SHOU, J., GUAN, K., XIONG, Y. & YE, D. 2014. TET-catalyzed 5-methylcytosine hydroxylation is dynamically regulated by metabolites. *Cell Res,* 24**,** 1017-20.

YAO, D., MACKENZIE, B., MING, H., VAROQUI, H., ZHU, H., HEDIGER, M. A. & ERICKSON, J. D. 2000. A novel system A isoform mediating Na+/neutral amino acid cotransport. *J Biol Chem,* 275**,** 22790-7.

YEO, H., LYSSIOTIS, C. A., ZHANG, Y., YING, H., ASARA, J. M., CANTLEY, L. C. & PAIK, J. H. 2013. FoxO3 coordinates metabolic pathways to maintain redox balance in neural stem cells. *Embo j,* 32**,** 2589-602.

YIN, F., SANCHETI, H., PATIL, I. & CADENAS, E. 2016. Energy metabolism and inflammation in brain aging and Alzheimer's disease. *Free Radic Biol Med,* 100**,** 108-122.

YING, Q. L., WRAY, J., NICHOLS, J., BATLLE-MORERA, L., DOBLE, B., WOODGETT, J., COHEN, P. & SMITH, A. 2008. The ground state of embryonic stem cell self-renewal. *Nature,* 453**,** 519-23.

YOON, K. A., NAKAMURA, Y. & ARAKAWA, H. 2004. Identification of ALDH4 as a p53-inducible gene and its protective role in cellular stresses. *J Hum Genet,* 49**,** 134-40.

YUAN, H. X., XIONG, Y. & GUAN, K. L. 2013. Nutrient sensing, metabolism, and cell growth control. *Mol Cell,* 49**,** 379-87.

ZHANG, H., BADUR, M. G., DIVAKARUNI, A. S., PARKER, S. J., JAGER, C., HILLER, K., MURPHY, A. N. & METALLO, C. M. 2016. Distinct Metabolic States Can Support Self-Renewal and Lipogenesis in Human Pluripotent Stem Cells under Different Culture Conditions. *Cell Rep,* 16**,** 1536-1547.

ZHANG, J., KHVOROSTOV, I., HONG, J. S., OKTAY, Y., VERGNES, L., NUEBEL, E., WAHJUDI, P. N., SETOGUCHI, K., WANG, G., DO, A., JUNG, H. J., MCCAFFERY, J. M., KURLAND, I. J., REUE, K., LEE, W. N., KOEHLER, C. M. & TEITELL, M. A. 2011a. UCP2 regulates energy metabolism and differentiation potential of human pluripotent stem cells. *Embo j,* 30**,** 4860-73.

ZHANG, M., WHITE, T. A., SCHUERMANN, J. P., BABAN, B. A., BECKER, D. F. & TANNER, J. J. 2004. Structures of the Escherichia coli PutA proline dehydrogenase domain in complex with competitive inhibitors. *Biochemistry,* 43**,** 12539-48.

ZHANG, X., YALCIN, S., LEE, D. F., YEH, T. Y., LEE, S. M., SU, J., MUNGAMURI, S. K., RIMMELE, P., KENNEDY, M., SELLERS, R., LANDTHALER, M., TUSCHL, T., CHI, N. W., LEMISCHKA, I., KELLER, G. & GHAFFARI, S. 2011b. FOXO1 is an essential regulator of pluripotency in human embryonic stem cells. *Nat Cell Biol,* 13**,** 1092-9.

ZHANG, Z., ZANDER, C. B. & GREWER, C. 2011c. The C-terminal domain of the neutral amino acid transporter SNAT2 regulates transport activity through voltage-dependent processes. *Biochem J,* 434**,** 287-96.

ZHOU, G., MENG, S., LI, Y., GHEBRE, Y. T. & COOKE, J. P. 2016. Optimal ROS Signaling Is Critical for Nuclear Reprogramming. *Cell Rep,* 15**,** 919-25.

ZHOU, W., CHOI, M., MARGINEANTU, D., MARGARETHA, L., HESSON, J., CAVANAUGH, C., BLAU, C. A., HORWITZ, M. S., HOCKENBERY, D., WARE, C. & RUOHOLA-BAKER, H. 2012. HIF1alpha induced switch from bivalent to exclusively glycolytic metabolism during ESC-to-EpiSC/hESC transition. *Embo j,* 31**,** 2103-16.

ZHU, W., GINCHERMAN, Y., DOCHERTY, P., SPILLING, C. D. & BECKER, D. F. 2002. Effects of proline analog binding on the spectroscopic and redox properties of PutA. *Arch Biochem Biophys,* 408**,** 131-6.

ZOU, G. M., LUO, M. H., REED, A., KELLEY, M. R. & YODER, M. C. 2007. Ape1 regulates hematopoietic differentiation of embryonic stem cells through its redox functional domain. *Blood,* 109**,** 1917-22.